Synthesis and investigation of novel mono- and bifunctional vinyl cyclopropane derivatives - fast curing and low shrinking polymers

---

DISSERTATION

zur Erlangung des akademischen Grades eines Doktors
der Naturwissenschaften (Dr. rer. nat.)
in der Bayreuther Graduiertenschule für Mathematik und
Naturwissenschaften
(BayNAT)
der Universität Bayreuth

vorgelegt von
Sören Schumacher
aus *Heilbronn*
Bayreuth, 2026

Die vorliegende Arbeit wurde in der Zeit von *Juli/2018* bis *Februar/2026* in Bayreuth am Lehrstuhl *Makromolekulare Chemie II* unter Betreuung von Frau Professorin Dr. *Seema Agarwal* angefertigt.

Vollständiger Abdruck der von der Bayreutehr Graduiertenschule für Mathematik und Naturwissenschaften (BayNAT) der Universität Bayreuth genehmigten Dissertation zur Erlangung des akademischen grades eines Doktors der Naturwissenschaften (Dr. rer. nat.).

Form der Dissertation: Monographie
Dissertation eingereicht am: 11.02.2026
Zulassung durch das Leistungsgremium: 19.02.2026
Wissenschaftliches Kolloquium: 02.07.2026

Amtierender Direktor: Prof. Dr. Jürgen Senker

Prüfungsausschuss:

Prof. Dr. Seema Agarwal (Erstgutachter)
Prof. Dr. Shoubhik Das (Zweitgutachter)
Prof. Dr. Johannes Brendel (Vorsitz)
Prof.Dr. Stephan Gekle

Die vorliegende Arbeit ist als Monographie verfasst.

Teile der Arbeit sind bereits in den folgenden Publikationen erschienen:

Theoretical and Experimental Study of Monofunctional Vinyl Cyclopropanes Bearing Hydrogen Bond Enabling Side Chains
S. Schumacher; S. Pantawane; S. Gekle; S. Agarwal. *Macromolecules*, **2021**, 54, 11–21.
DOI: 10.1021/acs.macromol.0c02490
Diese Publikation ist in der vorliegenden Arbeit mit der Literaturstelle[1] zitiert.

The Effect of Hydrogen Bonding on Polymerization Behavior of Monofunctional Vinyl Cyclopropane-Amides with Different Side Chains.
S. Schumacher; S. Pantawane; S. Gekle; S. Agarwal. *Macromolecular Chemistry and Physics*, **2022**, 223, 2200155.
DOI: 10.1002/macp.202200155
Diese Publikation ist in der vorliegenden Arbeit mit der Literaturstelle[2] zitiert.

List of abbreviations

AIBN	azobisisobutyronitrile
APT	attached proton test
AROP	anionic ring-opening polymerization
ATR	attenuated total reflection
BPO	benzophenone
C	carbon
CDI	1,1'-carbonyldiimidazole
COSY	correlation spectroscopy
CQ	camphorquinone
CROP	cationic ring-opening polymerization
DBPO	dibenzoyl peroxide
DCC	N,N'-dicyclohexylcarbodiimide
DCM	methylene chloride
DMAP	4-dimethylaminopyridine
DMF	N,N-dimethylformamide
DMSO	dimethyl sulfoxide
DSC	differential scanning calorimetry
ECHA	European Chemicals Agency
EDMAB	ethyl 4-dimethylaminobenzoate
ESI	electrospray ionization
EtOAc	ethyl acetate

FT-IR	fourier transform infrared spectroscopy
GC	gas chromatography
GPC	gel permeation chromatography
h	hour
H	hydrogen
HMBC	heteronuclear multiple bond correlation
HOBt-Cl	6-chloro-1-hydroxy-benzotriazole
HRMS	high resolution mass spectrometry
HSQC	heteronuclear single quantum coherence
IPDA	isophorone diamine
ISC	intersystem crossing
J	coupling constant
K	kelvin
LD_{50}	median lethal dose
LED	light emitting diode
LC-MS	liquid chromatography–mass spectrometry
M	molar
MMA	methyl methacrylate
NMR	nuclear magnetic resonance
PE	polyethylene
PMMA	poly(methyl methacrylate)
PP	polypropylene
ppm	parts per million
PVC	polyvinyl chloride
PS	polystyrene
PTFE	polytetrafluorethylene
PPS	poly(phenylene sulfide)
PEEK	poly(ether ether ketone)

REACH	Registration, Evaluation, Authorization and Restriction of Chemicals
$\mathbf{R_p}$	Initial rate of polymerization
rt	room temperature
ROP	ring-opening polymerization
ROMP	ring-opening metathesis polymerization
RROP	radical ring-opening polymerization
rt	room temperature
VCP	vinyl cyclopropane
VdW	Van-der-Waals
$\mathbf{T_g}$	glass transition temperature
TGA	thermogravimetric analysis
THF	tetrahydrofuran
$\mathbf{T_m}$	melting temperature
UDMA	urethane dimethacrylate
UCST	upper critical solution temperature
UV	ultra violet

Contents

1 Introduction **5**

1.1 Volume shrinkage of polymeric materials 6

1.1.1 Theoretical background of the effect of volume shrinkage 6

1.1.2 Strategies to reduce volume shrinkage in materials 7

1.2 ring-opening polymerization 9

1.2.1 radical ring-opening polymerization (RROP) 11

1.3 vinyl cyclopropane (VCP) 13

1.3.1 VCPs in synthetic chemistry 13

1.3.2 VCPs as low shrinking monomers and resins 19

1.4 Photopolymerization 23

1.5 Further research on VCPs as monomeric platforms in polymer chemistry 26

2 Aim of the work **29**

3 Results and discussion **33**

3.1 Investigation of novel monofunctional VCP esters 33

3.1.1 Chemical synthesis of VCP derivatives 34

3.1.2 Alcohols 35

3.1.3 Chemical synthesis of monofunctional VCP esters 36

3.1.4 Preorganization of monofunctional VCP esters 40

3.1.5 Photopolymerization of monofunctional VCP esters 44

3.1.6 Polymer characterization of monofunctional VCP esters 47

3.2 Investigation of novel monofunctional VCP amides 50

3.2.1 Chemical synthesis of novel monofunctional VCP amides 53

3.2.2 Preorganization of monofunctional VCP amides 57

3.2.3 Photo polymerization of monofunctional VCP amides 59

3.2.4 Polymer characterization of monofunctional VCP amides 62

3.3 Investigation of novel bifunctional VCPs 63

3.3.1 Chemical synthesis of bifunctional VCPs 64

3.3.2 Cytotoxicity tests . . . 69
3.3.3 Photopolymerization of sterically hindered bifunctional VCP amides 70
3.3.4 Polymer characterization of bifunctional VCP amides . . . 72
3.3.5 Determination of volume shrinkage . . . 73
3.4 Conclusion . . . 75
3.5 Outlook . . . 76

4 Materials and methods 79
4.1 Analytical methods . . . 79
4.2 Chemical synthesis . . . 80
4.2.1 General remarks . . . 80
4.2.2 Synthesis of 1-(ethoxycarbonyl)-2-vinylcycloporpane-carboxylic acid 80
4.2.3 Synthesis of Monofunctional VCP esters . . . 83
4.2.4 Synthesis of Monofunctional VCP amides . . . 105
4.2.5 Synthesis of Bifunctional VCPs . . . 129
4.2.6 Unsuccessful synthesis of new bi functional monomers . . . 163
4.3 Monomer characterization . . . 173
4.3.1 nuclear magnetic resonance spectroscopy . . . 173
4.3.2 temperature variable nuclear magnetic resonance (NMR) . . . 173
4.4 Photo-polymerization . . . 177
4.4.1 Kinetic measurements . . . 177
4.4.2 Photo-Rheology . . . 178
4.5 Polymer characterization . . . 178
4.5.1 gel permeation chromatography . . . 178
4.5.2 differential scanning calorimetry . . . 180
4.5.3 Thermal stability . . . 181
4.5.4 Volume shrinkage . . . 183

Bibliography 185

5 Acknowledgment 203

6 Eidesstattliche Erklärung 205

Summary

Vinyl cyclopropanes VCPs, undergoing radical ring-opening polymerization (RROP), have been studied for potential applications in polymer chemistry. RROP can reduce the volume shrinkage, crucial for dental applications or solvent-free coatings where volume shrinkage causes unwanted gaps. Modifying the side groups can produce mono- and bifunctional VCPs with less shrinkage or even volume increase in some cases. However, one drawback is the slow and incomplete conversion of VCPs, which can be addressed by introducing VCP-amides. While the preorganization of the VCP-amide via hydrogen bonding was suspected to cause this behavior, a systematic study remains to be conducted, mainly due to the difficulty of investigating bifunctional systems leading to cross-linked structures. Therefore, this work explored the synthesis, characterization and properties of VCPs (both VCP-esters and VCP-amides) to better understand the effect of VCP structure on polymerization behavior, and polymer properties.

In the first part of the study, four monofunctional VCPs-esters were synthesized, each with different functional groups in the side chain, including urea, urethane, amide, and carbonate. These functional groups were selected to create VCPs esters with varying hydrogen-bonding capabilities, potentially influencing the preorganization of these VCPs monomers. This, in turn, could affect the polymerization rate and the resulting polymer properties. All monomers were fully characterized using NMR and fourier transform infrared spectroscopy (FT-IR) experiments. Solid-state NMR experiments at different temperatures were performed to compare the hydrogen bonding capability of different VCPs-monomers. Among the monomers, the urea side chain exhibited the most substantial interaction, attributed to its involvement with two hydrogen bond donors, resulting in a robust interaction. Urethane and amide showed strong linkages with their single hydrogen bond donor, with urethane exhibiting slightly stronger interactions. The monomers were polymerized under visible light in the presence of a light-sensitive initiator, and their conversion was monitored over time. The urea-containing monomer demonstrated the fastest initial polymerization rate, followed by urethane, amide, and carbonate. However, after 30 minutes, the polymerization rate of

the urea derivative slowed, leading to a lower overall conversion compared to the urethane and amide derivatives. Similar behavior was observed in their viscosity changes during photorheology experiments. Structural analysis of the polymers showed that preorganized monomers showed reduced backbiting and are expected to show reduced volume shrinkage.

In the next part, monofunctional VCP-amides were synthesized and fully characterized in order to study the effect of ester spacer in comparison to the amide. Apart from the carbonate-bearing VCP, all monomers were solid; thus, polymerization was conducted in solution. Rapid and complete polymerization was observed in all cases, with an increase in overall conversion compared to the VCP esters. An exception is the VCP-amide with additionals amide functionality in the side-chain, which only showed a minor difference compared to ester. The H-bond strength was most substantial for urea, followed by urethane, amide, and carbonate.

In the final part, sterically hindered bifunctional VCP diamines were synthesized; however only two out of the seven synthesized VCPs were liquid. For all bifunctional systems, cytotoxicity was tested to determine their suitability for medical applications. Linear monomers showed lower toxicity than cyclic linkers, and urethane dimethacrylate (UDMA), a commonly used monomer matrix in dental fillings. Polymerization was conducted in solution. All systems polymerized rapidly, and complete conversion was achieved. Structural differences in the investigated monomers explained the differences in the polymerization rate, underlining the importance of considering the overall structural properties. The resulting polymers showed high thermal stability and glass transition temperatures (T_gs) above 80 °C , making them suitable for dental restoration applications.
Another critical factor investigated was volume shrinkage. While all monomers showed reduced shrinkage compared to that observed during polymerization of, for example, poly(methyl methacrylate) (PMMA) or polystyrene, the difference in shrinkage was less dependent on the polymerization rate but by the steric hindrance of the monomers, even leading, in one case, to volume expansion on polymerization.

Zusammenfassung

In dieser Arbeit wurden VCP auf ihre Anwendung in der Polymerchemie untersucht. Diese sollten mittels RROP polymerisiert werden, um einen möglichst geringen Volumenschrumpf vorzuweisen, wichtig vor allem in der Anwendung im Dentalbereich. Es ist bekannt, dass der Schrumpf sowohl in mono- als auch bifunktionellen VCPs durch die richtige Auswahl der Seitengruppe drastisch, bis hin zu einer Volumenzunahme reduziert werden kann. Die geringe Reaktivität und unvollständige Aushärtung, eines der großen Probleme von VCPs konnte in der Vergangenheit gelöst werden, indem anstelle eines VCP-Ester ein -Amid generiert wurde. Hierbei steht die Hypothese im Raum, dass die Wasserstoffbrückenbindungen und die daraus resultierende Anordnung der Moleküle, Grund für diese Verbesserung sind. Was bisher jedoch fehlt ist eine systematische Untersuchung, da dies für die bisherigen bifunktionellen Systeme nur schwer möglich ist, da diese verzweigte Polymernetzwerke ausbilden. Dies wurde in der vorliegenden Arbeit nachgeholt um ein besseres Verständnis im Hinblick auf zukünftige Anwendungen zu erhalten.
Hierzu wurden im ersten Schritt vier VCPs mit unterschiedlichen Seitenketten synthetisiert. Diese Seitenketten, Carbonat, Urethan, Harnstoff und Amid sind in unterschiedlichem Maße in der Lage Wasserstoffbrücken auszubilden. Da der Effekt der Seitenkette geringer ist, als eine mögliche Präorganisation nahe des aktiven Zentrums, wurden VCP-Ester und keine Amide ausgewählt. Alle Moleküle wurden vollständig charakterisiert und die Stärke der Wasserstoffbrückenbindung wurde Mithilfe von Festkörper NMR untersucht, wo eine Schwächung der Wasserstoffbrücke mit steigender Temperatur zu sehen ist. Hier zeigte Harnstoff die stärkste Interaktion, bei der beide Stickstoffpositionen beitrugen, gefolgt von Urethan und Amid.
Die Monomere wurden bei Raumtemperatur photopolymerisiert und der Umsatz über die Zeit verfolgt. Hier konnte für das Harnstoffderivat die schnellste anfängliche Polymerisationsrate beobachtet werden, gefolgt von Urethan, Amid und Carbonat. Nach ca. 30 min kam es im Falle von Harnstoff zu einer Verlangsamung der Polymerisation, was zu einem geringeren Gesamtumsatz gegenüber der beiden anderen präorganisierten Derivate, Urethan und Amid, führte. Dieses Phänomen wurde mit Hilfe von

Photo-Rheology untersucht, wo das gleich Verhalten erkennbar war. Zudem zeigt das Harnstoffderivat eine weitaus höhere Viskosität, was den Schluss einer eingeschränkten Molekularbewegung zulässt.
Im nächsten Schritt wurden monofuktionelle VCP-Amide synthetisiert und charakterisiert. Außer das Carbonat-Derivat wurden alle Monomere in dem ungewünschten festen Aggregatszustand erhalten, was eine Polymerisation in Lösung notwendig machte. hierbei wurde, trotz Lösungsmittel, mit Ausnahme des Amid-Derivats, eine deutliche Steigerung der Polymerisationsgeschwindigkeit sowie des Gesamtumsatzes beobachtet. Die Stärke der Wasserstoffbrückenbindung wies dieselbe wie bereits für die VCP-Ester gefundene Reihenfolge auf.
Im letzten Teil sollten sterisch gehinderte bifunktionelle VCPs synthetisiert werden. Ziel waren flüssige Monomere, was jedoch nur in zwei von sieben Fällen gelang. Es wurden hierbei sowohl linear-verzweigte als auch cyclische Seitenketten eingesetzt. Die Monomere wurden auf ihre Toxizität untersucht, wo die linearen Systeme eine geringere Toxizität gegenüber der cyclischen sowie UDMA, einem bereits in der Praxis eingesetzten Monomer, auswiesen.
Auch in diesem Fall war eine Polymerisation in Lösung notwendig, welche in allen Fällen eine schnelle und vollständige Polymerisation zur Folge hatte. Unterschiede in der Geschwindigkeit können auf strukturelle Unterschiede der Moleküle, beispielsweise Taktizitäten, zurückgeführt werden, was die Wichtigkeit einer gesamtheitlichen Betrachtung der Monomer-Matrizen unterstreichen. Alle Systeme zeigten einen hohen T_g.Der Volumenschrumpf wurde ebenfalls untersucht, was eine stark verringerte Schrumpfung gegenüber anderen Polymeren, zum Beispiel PMMA oder Polystyrol aufwies und sich im Bereich bereits bekannter VCPs bewegt. In einem Fall war sogar eine Volumenzunahme erkennbar. Diese Ergebnisse korrelieren hierbei nicht mit der Polymerisationsgeschwindigkeit, sondern können alleine durch die Struktur und sterische Hinderung der Monomere erklärt werden.
Zusammenfassend konnte die klare Beziehung zwischen Stärke der Wasserstoffbrückenbindung verschiedener funktioneller Gruppen und deren Aushärtegeschwindigkeit betrachtet werden. Zudem wurde gezeigt, dass sterische Hinderung diese nicht maßgeblich beeinträchtigen, die Volumenabnahme jedoch verringert werden kann. Zusammen mit der geringen Toxizität und der schnellen Aushärtung konnte das große Potential von VCPs für den Einsatz, zum Beispiel im Dentalbereich, aufgezeigt werden.

1 Introduction

Polymers play a considerable role in every aspect of our modern society. most of these products are produced from polyethylene (PE), polypropylene (PP), polyvinyl chloride (PVC), and polystyrene (PS). These are the so-called commodity polymers, which are cheap and easily accessible and comprise approximately two-thirds of the polymers produced worldwide. On the other side are high-performance polymers. These show exceptional properties, but their production is difficult and expensive. Therefore, they are only used on a small scale for specific applications. Examples of commercially used high-performance polymers are polytetrafluorethylene (PTFE), poly(phenylene sulfide) (PPS), and poly(ether ether ketone) (PEEK).
The work presented here shows the development of new materials in the class of low shrinkage polymers, one type of high-performance polymer. Fast polymerization, complete monomer conversion, and low-to-no volume shrinkage are essential characteristics for photo-cross-linkable resins used in dental applications, electronic coatings, and more. VCP derivatives are particularly attractive monomers in this context, as they undergo rapid and quantitative RROP with significantly less shrinkage compared to other vinyl monomers, such as methacrylates. Previous research from Prof. Seema Agarwal's group has demonstrated that certain bifunctional VCP amides exhibit a promising combination of these properties. It was suggested that the exceptionally high polymerization rate was due to the preorganization of monomers through hydrogen bonding between amide units, which brought the reactive polymerizable vinyl groups into close proximity, thus enhancing the polymerization rate. The goal of the present work was to gain a deeper understanding of how substituents affect the ring-opening polymerization behavior of VCPs by synthesizing VCP derivatives with various substituents connected by spacers, such as amides, urethanes, urea and esters. These groups form hydrogen bonds to different extents, which influences the degree of preorganization. With this knowledge, the aim was to identify new bifunctional VCPs with improved properties compared to those already known, targeting applications in medical 3D printing or dental fillings.

In the following sections, the concept of material volume shrinkage and strategies to mitigate it are discussed for comprehensive understanding. Additionally, the role of preorganization, different polymerization techniques, and the latest findings on vinyl cyclopropanes are presented.

1.1 Volume shrinkage of polymeric materials

The volume of each material depends on different factors. One is the molecular size and orientation. Molecular size can be approximated by the use of atomic size, bond lengths and bond angles. While the orientation is irrelevant for small molecules, larger molecules can bend and twist, reducing their required volume.
The density and volume of the whole material are influenced by repulsive and attractive interactions between the different molecules, determining the distance between them. This distance, the Van-der-Waals distance, is reduced on polymerization as covalent bonds are formed, which are shorter than the Van-der-Waals (VdW) distance. If the resulting polymers are processed afterward, shrinkage can be neglected. For liquid, polyfunctional monomers, polymerized in situ, volume shrinkage is a big issue. This process can be divided into two parts: pre- and post-gel curing. During the pre-gel contraction, the polymer chains still flow in the material, allowing the whole sample to shrink.[3] In post-gel curing, the scaffold of the materials is fixed, and shrinking occurs only in minor domains. Consequently, a porous material is created.[4,5] The following section presents, a theoretical background on volume shrinkage.

1.1.1 Theoretical background of the effect of volume shrinkage

As mentioned in the previous paragraph, volume shrinkage can be seen as an effect of difference in monomer and polymer density. The density of a material, on a molecular level, depends on repulsive and attractive interactions. Repulsive interactions are described by the Pauli-principle. This states that two identical particles cannot simultaneously occupy the same quantum state. Consequently, electrons showing the same spin orientation repel each other when their orbitals overlap. As a result, a distance requiring no orbital overlap, is favored.[6] Therefore, this energy decreases drastically as the distance between molecules increases. As attractive interactions, VdW- and dipole-dipole-interactions and hydrogen and ionic bonds, whereby the latter plays no role in organic substances, are possible. The VdW interactions, being the weakest, are only present at a short distance and a low temperature with minimal molecular movement.

This attraction is due to a permanent and introduced dipole. With very short distances between molecules, this attractive interaction changes to a repulsive force, with the shortest distance being the VdW distance.[7–10] A particular form of VdW interaction is the so-called π-π stacking. Recent studies question the need for an aromatic system, claiming this interaction generally being the quadrupole interaction of π-systems.[11,12] The dipole-dipole interaction is present between two permanent dipoles. As with the VdW-interaction, it depends on the distances of the different molecules but also the orientation of the dipoles. Hydrogen bonding is among the most common ways to guide the orientation of a molecule. Here, an electronegative free electron pair attracts the hydrogen proton of an electropositive hydrogen.[13] Typical hydrogen donors are NH groups of amine, amide, urethane, or urea groups. However, sulfur or oxygen and sometimes carbon-based donors are also possible. The free electron pairs of nitrogen, sulfur, halogens, esters, and ethers, especially carbonyl groups, can be acceptors.[14,15] For polymeric materials, additional factors must be considered, one being temperature. Generally, the density is decreased with increasing temperature, as atom movement increases with rising temperature and attractive interactions such as hydrogen bonds weaken. Additionally, density changes drastically at temperatures below and above T_g and above the melting temperature (T_m) for semicrystalline polymers.[16,17] A second factor, influencing polymer density is pressure, as represented by the *Tait equation*, but its effect is much lower. A significant effect is the density difference between semicrystalline and amorphous polymers. Since crystalline regions are packed much more closely, semicrystalline polymers generally show a higher density with a higher degree of crystallinity.[18] Another factor is the chain length. It is reported that polymer density increases with chain length until it reaches a specific limit.[19] Additionally, elements used in the polymer influence the molecular density. While light elements such as hydrogen and carbon show a relatively low density, heavy elements such as halogens increase the density significantly.[20]

1.1.2 Strategies to reduce volume shrinkage in materials

Two different strategies are possible to reduce volume shrinkage. Since volume reduction depends on the difference between the monomer and polymer volume, one can reduce the VdW distance of the monomer system used. As mentioned above, attractive and repulsive interactions exist even at this distance. The introduction of ionic molecules can produce a much higher density. However, this alters the molecular properties considerably since a permanent charge is required. With only a partial shift in

charge, hydrogen (H)-bonding is a widely used attractive interaction.[21–23] While it is mainly used to form a specific structure, for example, in proteins, it also leads to a higher density in the resulting material.
As a second possibility, the polymer density can be increased. In the first step, linear polymers are favored over crosslinked systems, since every additional bond formed, increases volume shrinkage. Section 1.1.1 shows that a higher crystallinity leads to a higher polymer density. Since crystallinity is a result of organized polymer chains, polymers with less and smaller substituents have a higher tendency to form crystalline domains. Therefore, highly branched monomers, who have a higher tendency to form amorphous polymers, are advantageous for a lower density. Since stereoregular polymers promote crystallinity, stereoirregularity is an excellent strategy to ensure a higer level of amorphousness.[24] Preorganization promotes crystallinity and increases polymer density as it increases monomer density.
Besides the general molecular design, volume shrinkage depends on the experimental setup. The transition from a VdW distance to a covalent bond inevitably leads to a volume reduction. When composites are used, the percentage of new bonds in the overall material volume, since monomers comprise only a fraction of the whole material, can be reduced,decreasing shrinkage.[25] With this, the significance of the bond formation can be lowered. The same effect can be obtained by adding reactive diluents with a low density[26,27] or using pre-monomers.[25,28] Pre-monomers are macromolecules with reactive sites, which can be crosslinked afterwards. Here, the percentage of covalent bonds based on the total molecular size is reduced. Additionally, with this strategy the gel formation point can be altered, which is another factor of volume shrinkage. The mechanical properties also depend on the crosslinking density. Therefore, reducing the number of functional groups per molecule is only sometimes ideal.[25]

Another versatile strategy is ring-opening polymerization. While the concept is long known, when polysaccharides were introduced,[29] their purpose was not initially to reduce volume shrinkage. Since then, many aspects of cyclic monomers have been investigated, such as their free volume, ring strain, or polymerization kinetics. It was shown that, generally, two rings must be opened for one newly formed bond to successfully reduce volume shrinkage. Nevertheless, even without this, the shrinkage could be significantly reduced, as *Barley et al.* showed when comparing ethylene and ethylene oxide.[30] Here, the shrinkage was reduced by 17% due to the ring opening mechanism of the epoxide, making ring-opening polymerization (ROP) an excellent and convenient technique to reduce volume shrinkage.

1.2 ring-opening polymerization

ring-opening polymerization of cyclic monomers is one of the important ways to create new polymer systems. This is mainly due to the extensive range of monomers and the numerous, controllable, and specific properties that can be obtained. For example, currently very important, biodegradable polyesters are often synthesized by ROP.[31–33] Many of the hereby introduced functionalities are impossible to obtain by other polymerization techniques. In contrast to vinyl polymerization, the volume shrinkage during ROP is significantly less or sometimes even there is an increase in volume. The reactivity of cyclic monomers is mainly influenced by the ring strain, which is observed for rings with ring sizes of 3–8, except the six-membered ring which often does not polymerize.[34,35] In this range, the ring strain decreases with increasing ring size, for example, from oxiranes, with a strain of 116 kJ mol^{-1} [36] to six and seven-membered lactones and lactams with a ring strain of approximately 6 J mol^{-1}.[37] When heteroatoms such as sulfur, silicon, or oxygen are introduced, the rotation freedom of rings is reduced, usually leading to higher reactivity.[38]
However, when volume shrinkage should be reduced, larger ring sizes are favorable. The volume loss from bond formation can be counteracted on polymerization by creating a longer molecule chain from the ring opening. Table 1.1 shows the shrinkage for polymerization with different ring sizes. It is evident that the shrinkage decreases drastically with ring size, emphasizing that the ring size is close to the actual VdW radius of the resulting polymer chain for larger rings. The overall molecular volume does not increase significantly, especially for larger rings, while the resulting polymer is lengthened. Therefore, larger ring sizes generally lead to less volume shrinkage.[30]

Although, ROP, in general provides low volume shrinkage, the slow rate of polymerizations and incomplete monomer conversions are disadvantageous. While reactivity and shrinkage function in opposite directions, by selecting the appropriate reaction parameters, a fast reaction with low volume shrinkages is obtainable.[39] Depending on the starting material, different ROP types are possible: anionic ring-opening polymerization (AROP), cationic ring-opening polymerization (CROP), ring-opening metathesis polymerization (ROMP), and radical ring-opening polymerization. Figure 1 shows the different mechanisms.

Table 1.1: Calculated volume shrinkage of different carbocycles with different ring sizes.[30]

Monomer	Shrinkage [%]
Ethylene oxide	23
Cyclobutene	18
Cyclopentene	15
Cyclopentane	12
Cyclohexane	9
Cycloheptane	5
Cyclooctene	5
Cyclooctane	2
Cyclooctadiene	3

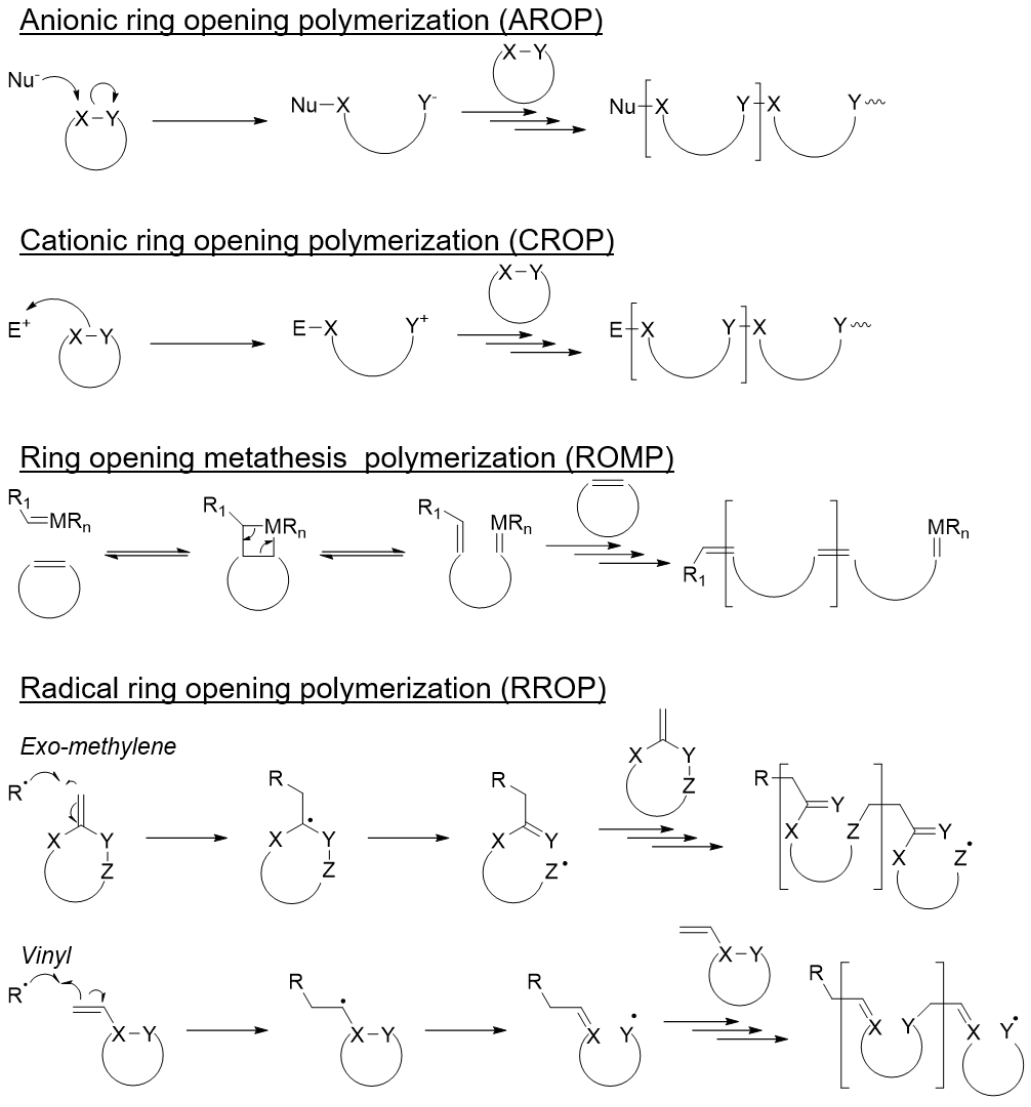

Figure 1: Different possible ring-opening polymerization reactions to form polymers from cyclic monomers. X, Y, and Z show heteroatoms and/or carbon atoms for ROP. Nu^- is a nucleophile, E^+ is an electrophile, and R is a radical. For RROP, vinylic and exo-methylene groups have been selected as an example, since they are the predominant species used.

Depending on the functional groups and ring sizes, different ROP reactions are possible. While anhydrides and carbonates are exclusively opened via AROP, cationic and anionic ROP is possible for lactones and lactams. Double bonds inside the ring are polymerized via ROMP, while vinylic or exo-unsaturated carbon bonds react predominantly via RROP.[38]

1.2.1 RROP

While the first and most used ROP techniques were AROP[39] and ROMP, RROP has also entered polymer chemistry with multiple examples. As a difference to the above mentioned AROP and CROP, RROP does not need high ring strain for a successful polymerization. Additionally, ring-opening can be promoted by a distorted ring structure. Since in RROP a radical is used, a radical acceptor, usually a carbon-carbon double bond, and a stabilized radical is required after ring-opening.[40] The more stable ring-opened structure is the driving force for RROP.[28] An additional isomerization might take place to get to the thermodynamically stable end product. The main advantage of RROP is its easiness, with a limited controllable reaction by the design of monomers, as mentioned above. Additionally, tolerance to different functional groups is higher than with other ROP techniques. This is underlined by the number of monomers usable for RROP, as shown in scheme 1.
Of these, especially cyclic ketene acetals and VCPs have attracted much interest for implementing as commercial products, as their synthesis has proven relatively easy, with great potential for polymer modifications by copolymerization with wide variety of vinyl monomers.[41–43] They were also among the first monomers investigated for use as RROP material.[44]
An additional advantage of RROP is the possible copolymerization of vinylic and cyclic monomers.[28,45] On the example of the copolymerization of VCP together with methyl methacrylate (MMA) the concept of a controllable RROP can be shown. While the predominated product in a free RROP is the cyclic polymer, by addition of a copper catalyst, a linear chain was obtained (Scheme 2).[46] This way, although using the same starting material, different products can be obtained.

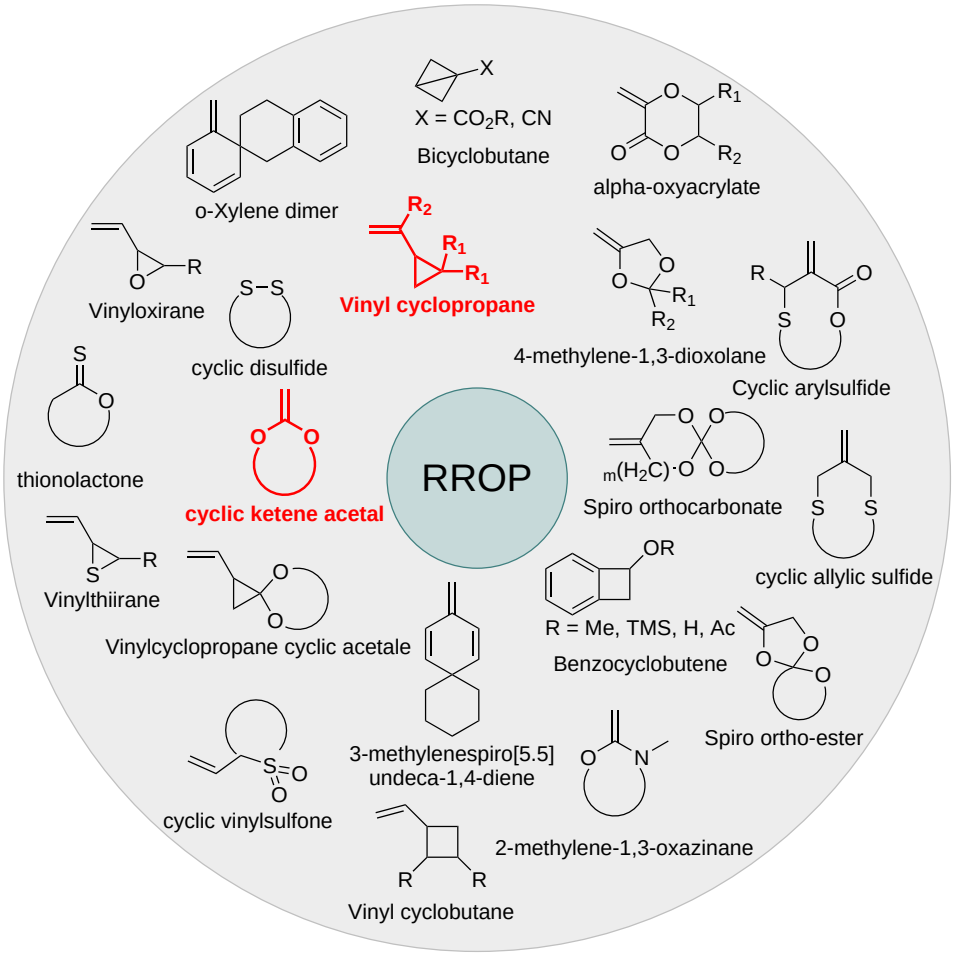

Scheme 1: Different monomeric platforms usable for RROP. The two red-marked monomers are the most investigated among these. Unless specifically mentioned, the R, R_1 and R_2 positions can comprise heteroatoms or other functional groups, for example electron-withdrawing groups of R_1 and R_2 for VCP.

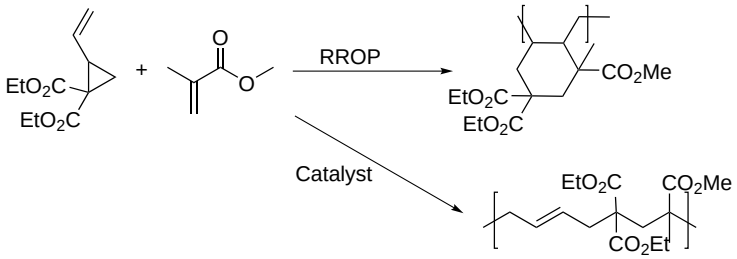

Scheme 2: Copolymerization of VCP with MMA. In an RROP, cyclic units are mainly formed, while the addition of a Cu catalyst leads to a linear structure.[46]

Other monomers, such as maleic anhydride or substituted ethylene, can be copolymerized as well, proving the versatility of VCP.[47–49] For example, branched systems can be

synthesized,[50] which is impossible with ROP. Therefore, in the next section, different aspects of VCP chemistry will be discussed.

1.3 VCP

As mentioned in section 1.2.1, VCPs were among the first molecules investigated as natural ring-openable monomers because the highly strained cyclopropane ring has a high tendency to be opened.[44] Nevertheless, the chemistry of VCPs is not only limited to ROP. This section describes the general chemistry of VCPs, as well as their use in polymer science.

1.3.1 VCPs in synthetic chemistry

One challenge in organic chemistry is the synthesis of cyclopentane rings. Six membered carbocycles can be easily synthesized via a Diels Alder reaction. For five membered rings, the corresponding [3+2] usually involves at least one heteroatom. Thus, furanes or pyrroles can be synthesized but not carbocycles. This is due to the Woodward-Hoffmann rule and the lack of odd-membered synthons to enable such reactions.[51] When VCPs are used, this limitation can be overcome. As first reported in 1959, the rearrangements of 1,1-dichloro-2-vinylcyclopropane, lead to cyclopentane (scheme 3).[52] Since then, many techniques have been reported to optimize and further the scope of VCP rearrangements.

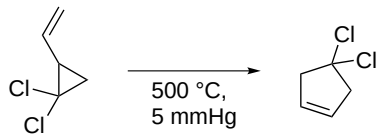

Scheme 3: Rearrangement reaction of 1,1-dichloro-2-vinylcyclopropane to 4,4-dichlorocyclopent-1-ene, the first reported reaction of VCP.

Therefore, VCPs are often used in organic synthesis. Besides rearrangement reactions, different ring sizes and molecular structures can be formed using cycloaddition reactions.

1.3.1.1 VCP synthesis

The synthesis of VCP has been the object of a massive field of research due to its highly versatile nature. Demjanov and Dojarenke reported the first successful synthe-

sis in 1922, where 1-cyclopropylethan-1-one oxime was methylated to form the vinylic double bond(scheme 4, **1**).[53] Since then, several alternative routes have been found to obtain VCP (scheme 4).[54–65]

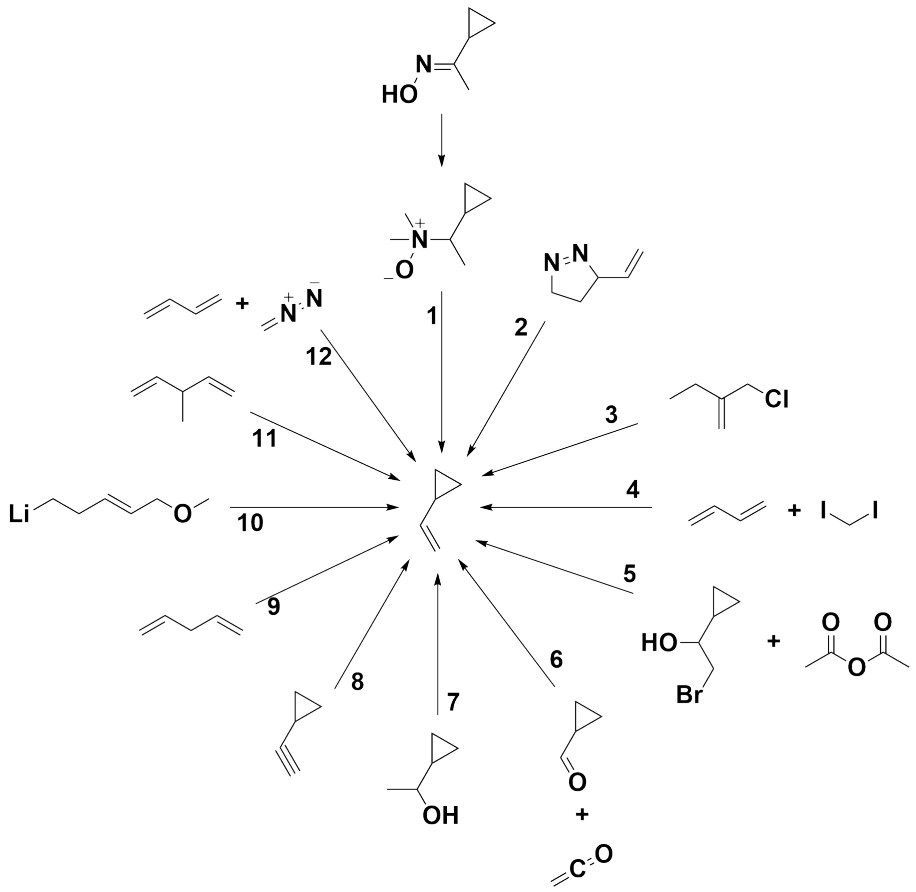

Scheme 4: Chemical reactions known in the literature to form unsubstituted VCPs. The first reported successful synthesis is shown in **1**; **2–12** shows other approaches leading to VCP. The starting materials from which VCP is formed are shown. Prior reaction steps are not considered if these starting materials are synthesized beforehand.

While the synthesis of VCP is of academic interest, substituted VCPs can be used for many applications, depending on the substituting group(s). Currently, the cyclopropane unit is mainly substituted. When electron-withdrawing groups are introduced, the electron density at the vinylic moiety is reduced, leading to a electrophilic VCP. This way it will readily react with nucleophiles at the vinylic moiety. Nucleophilic properties can be consequently obtained if an electron donor at the cyclopropane is synthesized, prone to react with electrophils under suitable conditions. A third class of reaction is radical propagation. Here, a radical is needed to start the reaction. This

can be favored when the substitutes stabilize the formed radical.[66,67]
Several pathways are known for the synthesis of substituted VCPs. The most used approach is the reaction of an unsaturated bihalogenide, for example, trans-1,4-dibromo-2-butene, with a good nucleophile, such as malonic esters, dicyanides, and others (scheme 5). This route is favored for its simplicity in inserting different substituents in the cyclopropane moiety and for its excellent yield.

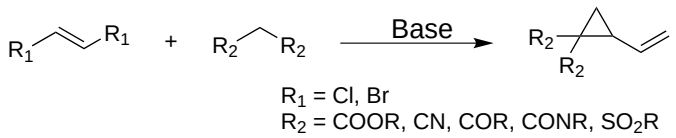

Scheme 5: Chemical synthesis of VCP starting from a halogenated butene and a very electrophilic carbon, due to electron-withdrawing groups attached.

A complete reaction is ensured by restricting the stereochemistry of the halogen to almost exclusively the trans product, enabling good overlap of the corresponding orbitals to form the cyclopropane ring. Only one example is known in the case of the cis-stereoisomer, leading to the desired cyclopropane in low yields. Here, using less active malonate increases the cyclopropane formation, while for more CH-acidic malonates, cyclopentane formation was favored, being the competing reaction product.[68]

Alternatively, carbene chemistry can be used. Here, chloro, bromo, or fluorocyclopropanes can be obtained using the corresponding di- tri- or tetrahalogenide, while using iodine leads to unsubstituted VCP (see scheme 4, **4**). The carbene reacts with butadiene or other diene compounds, enabling the insertion of additional groups into the cyclopropane(scheme 6).[69–72] Such bihalogenated VCPs are advantageous in RROPs, as the halogens act as radical stabilizing groups.[73]

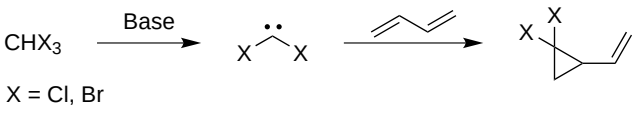

Scheme 6: Carbene chemistry to synthesize VCP. The chemistry is not restricted to butadiene. With iodine, unsubstituted VCPs can be obtained.

Diazo- and Grignard reagents and multi-step synthesis have been developed to further widen the scope of possible VCP derivatives.[74–76] The latter especially enables the

insertion of complex substituents, essentially synthesizing natural products or other difficult-to-synthesize molecules.[74,77]

With this, the substantial possibilities originating from VCP are becoming relatively straightforward. The following section describes reactions starting from different VCPs.

1.3.1.2 Rearrangement reactions

Rearrangement reactions are kinetically driven by ring strain or, if the formed bonds are thermodynamically favored, by the formation of a more stable structure after rearrangement. Thus, otherwise difficult-to-realize molecule synthesis can be used, for example, five-membered carbocycles. While Diels-Alder can easily create six-membered rings, five-membered rings cannot be synthesized since, in a similar reaction, both reaction partners would need the same charge, according to Evans' law. Therefore, heteroatoms are required to enable the reaction.
In 1959, the rearrangement of 1,1-dichloro-2-vinylcyclopropane to 1,1-dichlorocyclopent-4-ene was reported, marking the beginning of the now well-known vinylcyclopropane-cyclopentene rearrangement and the first opportunity to form five-membered carbocycles (scheme 3). One year later, the rearrangement of an unsubstituted VCP was developed independently by *Vogel*[78] and *Overberger et al.*[79].
Generally, two mechanisms are discussed to describe the rearrangement reaction: a biradical and a concerted mechanism, both being probable depending on the concrete reaction conditions and substituents (scheme 7).[80]

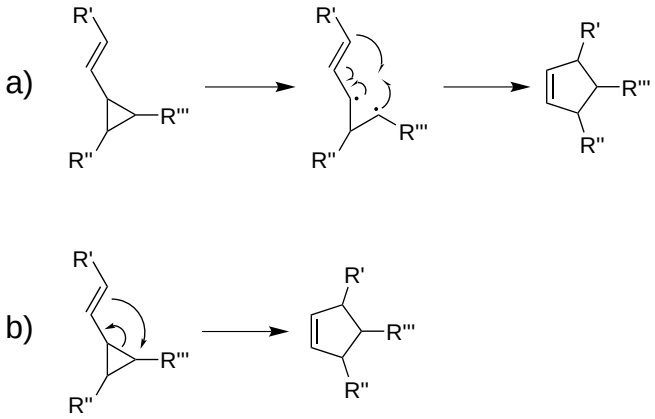

Scheme 7: The two rearrangement mechanisms discussed in the literature: a biradical reaction path (a) and a concerted mechanism (b).

While rearrangements were initially conducted using high temperatures or photoinitiation, later research focused on milder conditions via odd-electron-promoted isomerization. Milder conditions widened the scope of these reactions, and the need for active substrates resulted in additional synthetic steps.[81–83] Using a transition metal as a catalyst was also investigated. It has been postulated that a highly reduced metal, where the electron density at the metal center is high, should work well with unsubstituted VCP since its high nucleophilicity enables the attack of the olefinic site of the VCP. Ligands stabilizing the positively charged intermediate metal also benefit the reaction.[84]

Rearrangement reactions of VCPs are mainly used to synthesize natural products with complex structures. For example, the stereoselective synthesis of 2-oxindole derivatives, substrates of several natural products, was conducted from VCP rearrangement reactions and a [3+2] cycloaddition (Scheme 8).[85]

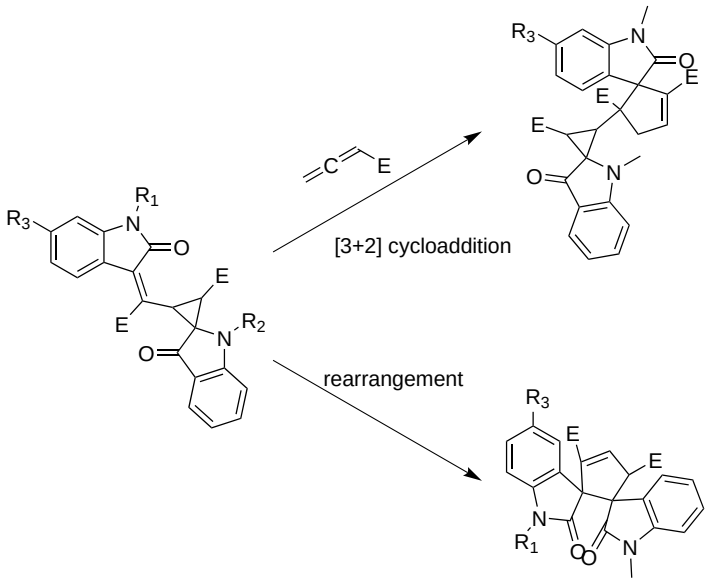

Scheme 8: Ring strain of carbocycles with a ring size of three to nine carbon atoms and the VCP synthon.

1.3.1.3 Cycloaddition

As shown in the previous example, VCPs undergo rearrangement reactions and can be used in various cycloadditions.

In cycloaddition reactions, two or more unsaturated systems react with each other to form a cyclic system. One of the best-known cycloadditions is the Diels-Alder reaction, a [4+2] cycloaddition. Heat, light, Lewis acids, and transition metals can mediate cy-

cloadditions. Metal induces cycloadditions, and often a C-C cleavage occurs. Due the high energy required in this process, highly strained rings such as VCP are good candidates for such reactions, since the energy from the strain release makes the cleavage energetically favorable.[86] Scheme 9 shows the ring strain of different ring sizes.

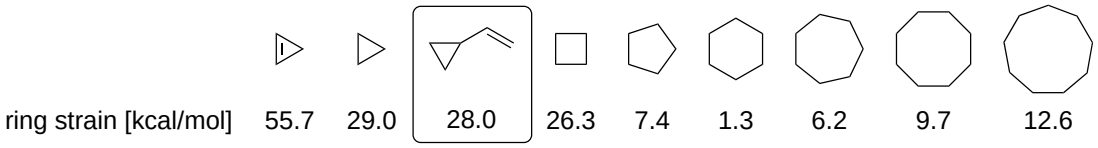

Scheme 9: Ring strain of carbocycles with ring sizes of three to nine carbon atoms and the VCP synthon. The values shown here comprise Baeyer and Pitzer strains.

VCPs can undergo various cycloaddition reactions, namely [5+1], [5+2], [5+2+1], and [5+1+2] when five carbon atoms participate in the reaction, or as a three-carbon synthon in [3+2] and [3+2+1] cycloadditions.[87] In many cases, donor-acceptor systems are used, where the vinylic double bond acts as an electron donor and the electron-withdrawing substituents in the cyclopropane ring as acceptors.[88] Thus, the ring-opening is further facilitated; only a few examples of intramolecular cycloadditions are reported for activated VCPs[89–91] (Scheme 10), while most of the reactions are intermolecular cycloadditions with various transition metals used as catalysts (fig. 2).

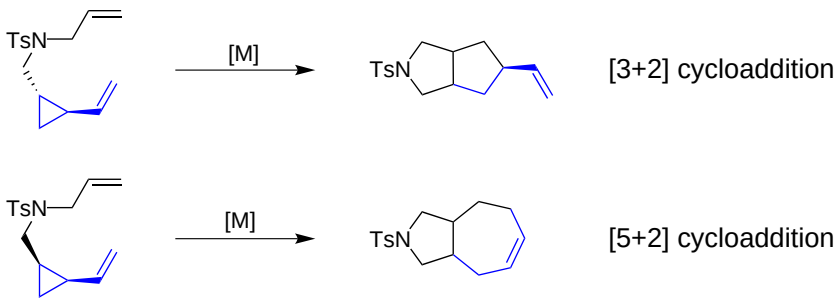

Scheme 10: Intramolecular [3+2] and [5+2] cycloadditions of substituted VCPs are two examples of cycloaddition reactions in which VCPs can participate.[92]

For non-activated VCPs, intramolecular and intermolecular reactions are common. The main difference from activated systems is the absence of a dipole and, therefore, a different reaction pattern, mainly via oxidative addition of the metal followed by the cycloaddition.[93–98] As for activated systems, intramolecular reactions require a more complex structure, enabling the cycloaddition.

One possible application of cycloadditions from VCPs is the synthesis of natural products.[99,100] Here, almost no reports are known for activated systems, while non-activated systems play a more prominent role due to seven-membered rings in many natural molecules.

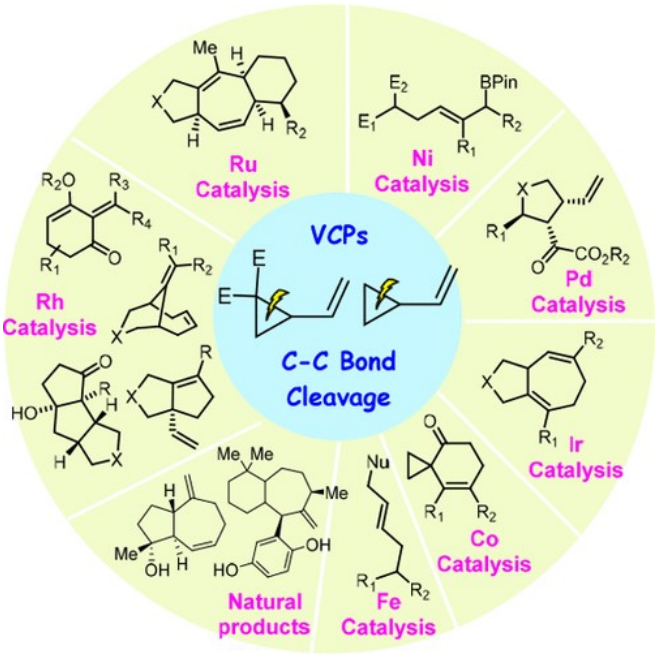

Figure 2: Metal catalyzed cycloaddition reactions of activated and non activated VCPs involving a C-C bond cleavage, showing the vast versatility of VCP in cycloaddition reactions. Reprinted with permission.[101] Copyright 2023 American Chemical Society

1.3.2 VCPs as low shrinking monomers and resins

While the first reports of VCP used all concerned organic synthesis, polymer scientists discovered the potential of VCPs 30 years ago when seeking new materials with low volume shrinkage. This research was mainly driven by the groups of *Endo et. al.* and *Moszner et al.* , who introduced VCPs as polymerizable monomers.[102–105] The growing interest over the last decades is also observed in publications about VCPs in polymer science. Figure 3 shows the number of publications in polymer science. Over the past decade, the work on VCPs used as monomers grew significantly and in 2021 comprised over half of all the work conducted on VCPs. The concept and reason for shrinkage and strategies to work against it are described in section 1.1 and section 1.2. In this section, VCP is described within this concept.

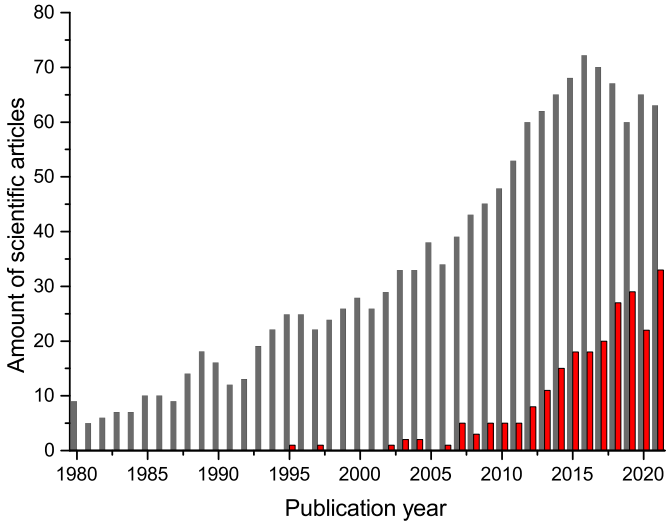

Figure 3: The number of publications from 1980 to 2021 regarding VCPs and VCP in polymer chemistry. The search was conducted on the Web of Science database using the keywords "vinyl cyclopropane" (gray) or "vinyl cyclopropane" AND "polymer" (red) in the title or abstract field.

As mentioned in section 1.2.1, VCPs polymerize via RROP, which *Takahashi* and *Yamashita* first described.[106] Cationically induced and Ziegler-Natta-catalyzed polymerizations are also known to mainly result in a 1,2-type polymerization, leaving the cyclopropane ring untouched.[107,108] The approach to anionically polymerizing VCPs resulted in a 3,5-polymer, leaving the vinyl group untouched.[109] For low volume shrinkage, 1,5-type reactions are required, mainly by radical polymerization. Scheme 11 shows the polymerization mechanism.[110]

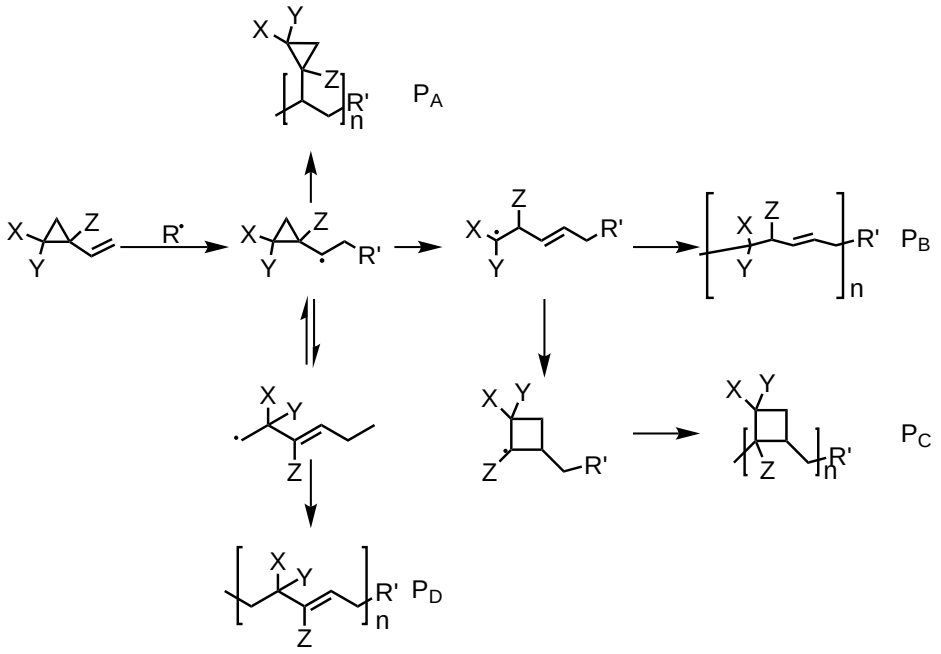

Scheme 11: Polymerization mechanism and different possible polymeric structures of VCP. P_B and P_D are the linear, predominant species formed, depending on the substituents and the preference of the ring-opening at position CZ−CH_2 or CZ−CX. P_A and P_C are additional possibilities, contributing to higher volume shrinkage.

Formation of a linear chain is desired to obtain low-volume shrinkage. The radical attack occurs at the vinylic end, which opens the cyclopropane ring or polymerizes in a 1,2-type reaction. The radical formed from the ring-opening can attack the next VCP unit in a propagation reaction or the unsaturated backbone to form a cyclobutane unit in the backbiting reaction. Backbiting must be avoided if low shrinkage is required. It has been reported that sterically hindered substituents can significantly lower the volume shrinkage. With an adamantyl VCP ester, even an expanding system could be obtained despite only opening one cycle per newly formed bond.[111] Despite this remarkable property, such systems never entered actual application due to the crystalline nature of adamantyl-containing monomers.

When examining the potential of VCPs, they are consistently compared with the highly accepted methacrylates, especially in the dental industry. Acrylates show high shrinkage (for MMA, shrinkage is reported to be 21%; for UDMA, the shrinkage is around 9%), but the resulting polymer shows good mechanical properties, complete monomer conversion, and reasonably rapid polymerization kinetics. Low polymerization speed and restricted monomer conversion have long been proven challenges in replacing currently used (meth)acrylate based systems with VCP derivatives. Researchers focused

on the development of new VCP-ester derivatives since the use of malonic ester is a convenient means to obtain the VCP-esters, by adding different alcohols, di- or polyols in a Steglich esterification. This way a huge variety of new compounds was formed but only showed low reactivity.[25,105,112–115]

Prof. Seema Agarwal's group introduced amines to form VCP amides.[116] They undergo faster and more complete polymerization and exhibit low volume shrinkage (fig. 4). The preorganization via hydrogen bonding has been identified as a possible reason for the difference from previously reported VCP-ester systems. Since then, new molecules have been reported following the same concept, and additional functional groups, such as urethane, which can form hydrogen bonds, have been introduced.[117–119]

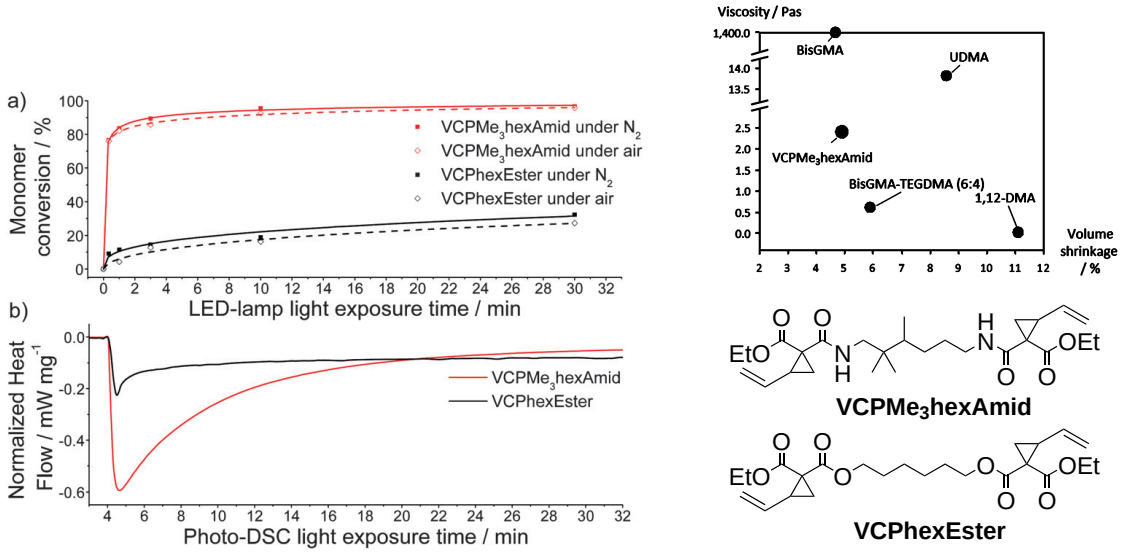

Figure 4: Comparison of polymerization rates of a VCP ester and a similar VCP amide (left) and the viscosity and volume shrinkage of the VCP-amide compared to commercially used monomer matrixxes in dental applications (right). The vast improvement in changing the functional group is evident, with VCP amide comparable or even superior to methacrylate-based monomers. Reprinted with permission[116].

RROP of VCPs was traditionally conducted using thermal radical initiators. The first publications on this topic observed the significant influence of temperature on volume shrinkage.[110] A widely accepted and regularly used initiator is azobisisobutyronitrile (AIBN), whose decomposition temperature is 65 °C . When used at 60 °C almost exclusively the linear 1,5-ring-opened product was observed, while polymerization at 80 °C , using dibenzoyl peroxide (DBPO) as radical initiator, yielded a second product, later identified as the cyclobutane-containing polymer.[110]

A second, much milder polymerization method, also used for VCPs, is described in the next section: photopolymerization.

1.4 Photopolymerization

Besides thermal energy, light exists to form radicals and, therefore, enable radical polymerization. The main advantage is that local heat can be avoided. Additionally, a much more controlled reaction path is possible with the appropriate intensity and choice of exposure area. Furthermore, photopolymerization is usually much faster, than thermally induced polymerization, can be performed without solvents, and is more cost-effective.[120,121]. The general reaction path is shown as follows.

$$PI \xrightarrow{hv} PI^*$$

The photoinitiator absorbs the emitted light if its absorption band overlaps with the light source's wavelength and is raised to an excited state (PI*).

$$PI \longleftarrow PI^* \longrightarrow I^+ \text{ or } I^\bullet$$

While this excited state has only a short life span, a decay back to its original state (PI) is possible, with the absorbed energy emitted by light or heat, or a chemical reaction to a reactive intermediate (I* or I^+) occuring.

$$RI \xleftarrow{R^\bullet} I^\bullet \xrightarrow{M} \text{polymer}$$

The reactive intermediate may then react with another radical or the monomer, forming a polymer.

O_2 can inhibit the reaction by reacting with the excited initiator or another free radical.Consequently, the formed peroxy radical must usually be sufficiently reactive to effectively initiate the polymerization.

$$PI^* \xrightarrow{O_2} PI{+}O_2^*$$

and

$$I^\bullet \xrightarrow[M]{O_2} IO_2^\bullet$$

Therefore, the reaction conditions in a vacuum or an inert atmosphere are often preferred. While peroxides or azides are predominant in thermally induced radical polymerization, the mechanism of light-induced excitation, and therefore the choice of initiators, is different.

Two types of photoinitiators exist: *type I* and *type II*. *Type I* Initiators are cleaved into two radicals when irradiated with light (α-cleavage) (fig. 5). These radicals directly initiate the polymerization; consequently, the photoinitiator is incorporated into the

polymer matrix. Commonly used *type I* photoinitiators are benzylic ketones bearing an α-hydroxy or α-alkyl group. These are cleaved into aldehyde and the corresponding alkyl or phosphinoxide radical (fig. 5).

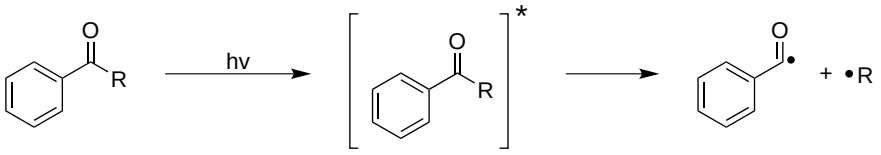

Figure 5: Activation of a *Type I* photoinitiator.

Recent research also reported using tin or germanium-based photoinitiators, with the latter being introduced as a highly efficient photoinitiator activated by irradiation with visible light. This is especially useful in dental applications, where visible light and low initiator concentrations are required.[122]

Type II Initiators, however, require a hydrogen from a donor as co initiator. Here, the photoinitiator is excited by light and abstracts a hydrogen donor, to form a diradical. This can then initiate the polymerization reaction. Due to its low cost and efficiency, the industry's most used *type II* initiator is benzophenone (BPO).[123,124] It cannot initiate any polymerization without an additional co initiator, since the formed ketyl radical is stabilized by delocalization and steric hindrance .[125]

Alcohols, ethers, and ternary amines can be used as hydrogen donors. The advantage of a ternary amine is its higher tolerance to oxygen; it is, therefore, the preferred system in dental and biological applications. One example of a *type II* photoinitiator is camphorquinone (CQ), the initiator selected in this work. It is often used in dental composites, as its absorption maximum is at 467 nm, enabling it to initiate the reaction with visible light. A light emitting diode (LED) can be used; this is a cost-effective light source that does not emit heat, which is one reason for its popularity. As a co-initiator, CQ is used with ethyl 4-dimethylaminobenzoate (EDMAB). Scheme 12 shows the typical *type II* mechanism.[126]

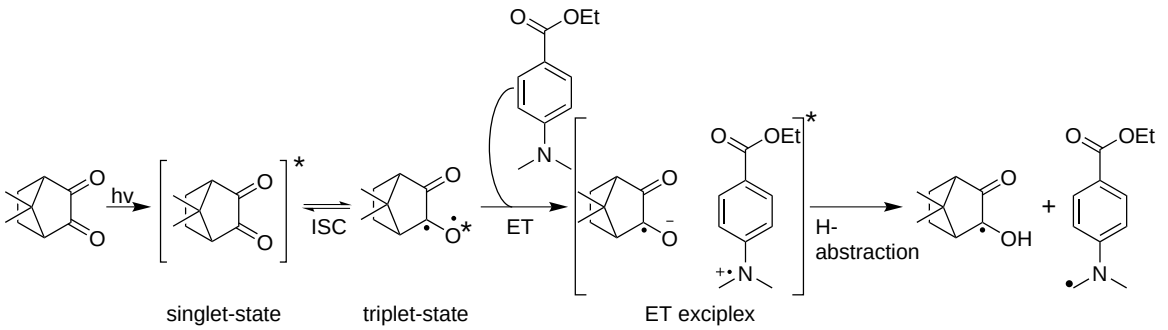

Scheme 12: Initiation of CQ, a *type II* photoinitiator with EDMAB as co-initiator. On irradiation, CQ is transferred to an excited singlet state. A diradical is formed via intersystem crossing (ISC) (triplet state). Subsequently, EDMAB transfers an electron to CQ to form an exciplex. After an H-proton transfer, an inactivated ketyl radical and EDMAB are formed, the latter being able to initiate photopolymerization.

Besides radical photopolymerization, ionic photoinitiators are known. Here, similar to *type I* photoinitiators ,homogeneous cleavage occurs on light exposure. The radicals then react with a Lewis acid, which can then initiate the polymerization. The advantages of this polymerization are the absence of oxygen inhibition and lower shrinkage stress of the cured materials. Moreover, because the initiation step can be viewed as a nucleophilic attack of the initiator on the monomer, a more selective polymerization is possible, tolerating functional groups that would be polymerized in a radical-induced polymerization, as shown by *Al-Doaiss et al.* , who investigated the cation-induced polymerization of a VCP- dioxolane co-monomer, where the VCP unit did not react under the conditions used.[127] A low level of toxicity, due to the absence of acrylates, common in radical polymerization, is another advantage of the cationic reaction path. It was also shown, that cationic photopolymerization reduces the volume shrinkage, otherwise observed for the polymerization of epoxy, improving the adhesion properties.[128] The most important advantage is the *dark reaction* of a cationic photopolymerization. In contrast to radicals, which are extinguished quickly after termination of irradiation, cationic polymerization can continue for some time, even when the light source is absent.[129] Commonly used initiators are onium salts, in which an organic cation is paired with an inorganic anion. While the cation, as a light-absorbing unit, determines the quantum yield of such initiators, the reactivity is related to the nucleophilicity of the anion. While the cation absorbs the light, it is not the actual initiator, but reacts with a proton-donating species to form a Brønsted acid, the primary initiator.
Onium salts can also improve radical photopolymerization if used as a ternary initiator. With CQ and EDMAB, for example, an increase in the polymerization and overall

conversion rate was visible, while only the radical reaction could be observed.[130] Another possibility is hybrid systems, where, different functional groups are present in the monomer. Only certain groups are polymerized by choosing the reaction conditions; consequently, the material properties can be selectively tuned.[131,132]

1.5 Further research on VCPs as monomeric platforms in polymer chemistry

Although the main property of VCPs scientists focus on is their low volume shrinkage, the versatility of this molecule makes it a good platform for various high-end applications.

One challenge is the spatiotemporal polymerization control, which enables a precise reaction that is crucial for various applications. *Zhang et al.* used VCP as a platform. These were modified after polymerization to create a redox-sensitive polymers.[133]

Post-polymerization modification is a widely used technique for using VCPs in different fields of high-performance applications. *Seuyep et al.* reported synthesizing an amphiphilic polymer using the two ester groups. Simultaneously, using a different approach, they showed an upper critical solution temperature (UCST) transition in ethanol and an ethanol-water mixture with different substituents .[134,135]

The formed double bond of the linear polymer chain is inactive but can also be modified by epoxidation, bromination or thiol-ene addition under the appropriate reaction conditions.[136](scheme 13).

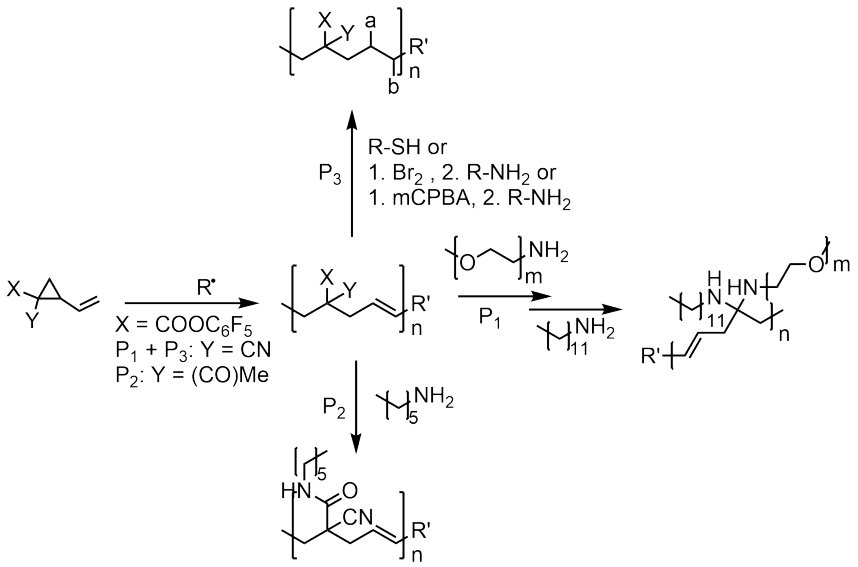

Scheme 13: Post polymerization modification of VCPs. in P_1 synthesis of an amphiphilic polymer is shown while the example of P_2 shows the formation of a polymer with an UCST transition in ethanol. P_3 shows the concept of a modification of the resulting backbone double bond.

2 Aim of the work

The advantage of vinyl cyclopropane (VCP)-esters in polymerization with reduced volume shrinkage is well documented in the literature. However, their incomplete conversion and slow reaction kinetics calls for alternative approaches. Bifunctional VCP-amides, first reported by the Agarwal group, were introduced as a promising alternative. The presence of hydrogen-bonding amide groups in the VCP structure is presumed to promote preorganization of the VCP-amide monomers, resulting in extremely fast polymerization with high monomer conversions.
Since bifunctional VCP-amides were employed in the pioneering work of Agarwal group, a systematic investigation has yet to be conducted, mainly due to the challenges associated with characterizing the cross-linked structures formed during RROP by spectroscopic methods.
Therefore, the aim of the present work was to explore the synthesis, characterization, and properties of VCP derivatives (VCP-amides in comparison to VCP-esters) in order to better understand how VCP structure and the potential preorganization of VCP monomers influence polymerization behavior and polymer properties.

To achieve this aim, the following working strategies were adopted:

1. Comparison of VCP-esters:
Monofunctional VCP-esters bearing different functional groups in the side chain, capable of hydrogen bonding, were synthesized, including urea, urethane, and amide functionalities. A reference VCP-ester containing a carbonate side chain, incapable of hydrogen bonding, was also synthesized. All four monomers possess distinct functional groups in the side chain but share an ester linkage to the VCP ring. (For structures, please see scheme 14)

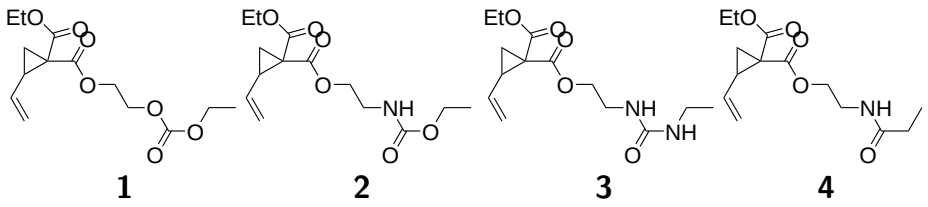

Scheme 14: VCP ester investigated in this work.

Here, the effect of the different side chains on conversion, reaction rate and monomer/polymer - properties were investigated.

2. Comparison of VCP-amides:

Analogous, monofunctional VCP-amides with various side-chain functionalities (urea, urethane, and amide) were synthesized, alongside a reference carbonate-functionalized VCP-amide that cannot engage in hydrogen bonding through side-chian. All four monomers feature different hydrogen-bonding capabilities in the side chain but are connected to the VCP ring via an amide linkage, a second position with possible hydrogen bonding. This comparison aimed to determine the impact of the position of the hydrogen-bonding unit within the VCP structure on polymerization behavior. (For structures, please see scheme 15)

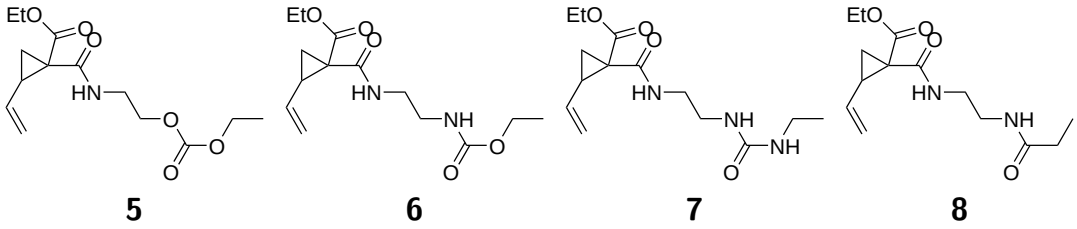

Scheme 15: Structure of synthesized VCP amides, bearing carbonate, urethane, urea, and amide side chains.

3. Comparison of mono- vs. bifunctional VCP-amides:

To further investigate structure–reactivity relationships, the behavior of monofunctional VCP-amides were implemented in the design of of bifunctional VCP-amides. Seven different bifunctional VCP-amides were synthesized and characterized. (For structures, please see scheme 16)

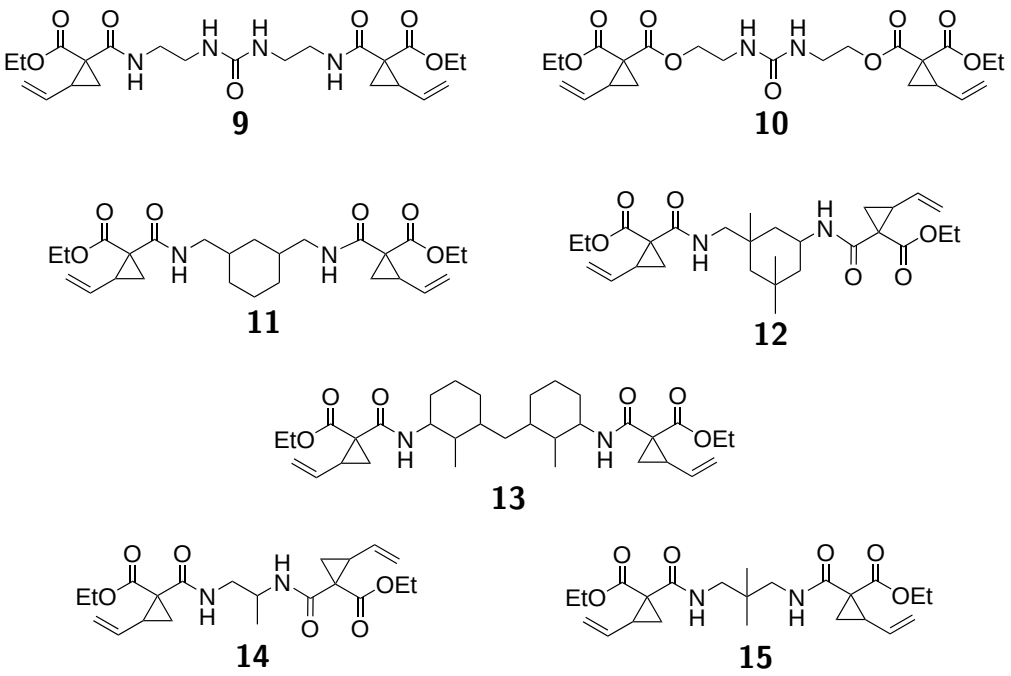

Scheme 16: Structures of linear and sterically hindered bifunctional VCPs.

The aim was to obtain a fast polymerizable system with a complete conversion, low volume shrinkage and low monomer toxicity.

Throughout the study, the primary focus was on elucidating the influence of monomer structure on polymerization rate and volume shrinkage.

3 Results and discussion

Parts of this work have already been published as two journal articles. These articles are cited in the present thesis as references [1,2]. Parts of the following chapters are found within these articles. Figures from these publications that are reproduced in this thesis are appropriately cited.

3.1 Investigation of novel monofunctional VCP esters

Previous work reported the synthesis of new bifunctional VCPs. [116] These systems show exceptional properties, such as rapid polymerization, low volume shrinkage, good mechanical properties, and low toxicity, and can replace established mathacrylate based polymers in different fields. [113,115–117] Since bifunctional VCPs provide a cross-linked polymer upon photopolymerization, a deeper understanding of the effect of substituents on photopolymerization rate, polymer structure, and other properties is not straight forward. Crosslinked polymeric networks are impossible to be dissolved in solvent and therefore, NMR and other analysis techniques, providing information on the polymerization behavior, are not straight forward. Thus, the synthesis of monofunctional VCPs was targeted. In the first part, four monofunctional VCP derivatives differing in the side-chain- functional groups were prepared to study the effect of functional groups on the polymerization rate. The working hypothesis was that the polymerization rate is affected by the monomer organization by H-bonding through the side chain. The side-chain functional groups selected were carbonate, which cannot form H-bonds; urethane and amide, forming one H-bond; and urea, with two H-bond sites. Scheme 17 shows the H-bonding possibilities in the four different functional groups in the side-chain.

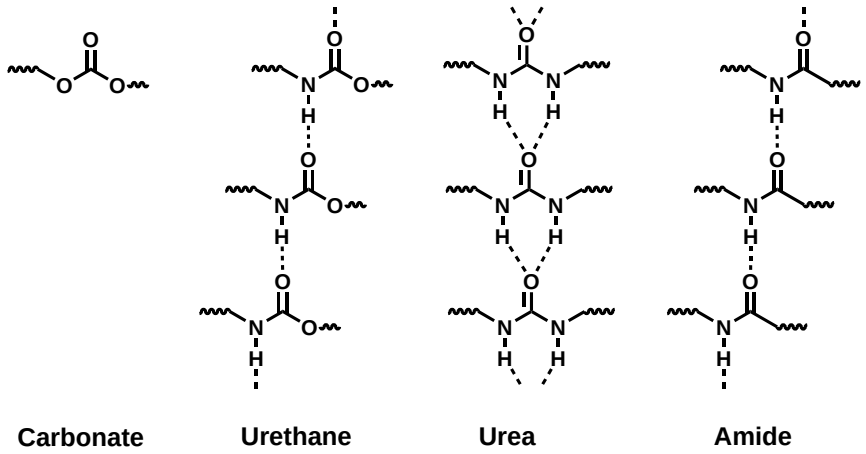

Scheme 17: Hydrogen bonding of the investigated side chains.[1]

3.1.1 Chemical synthesis of VCP derivatives

The VCP derivatives were prepared by the reaction of 1,4-dibromobut-2-ene with malonic acid diethyl ester, to form the VCP diester. By addition of one equivalent KOH, hydrolysis of one of the ester groups is achieved, which can be reacted with different alcohols in an Steglich esterification, to obtain different VCP derivatives (Scheme 18).

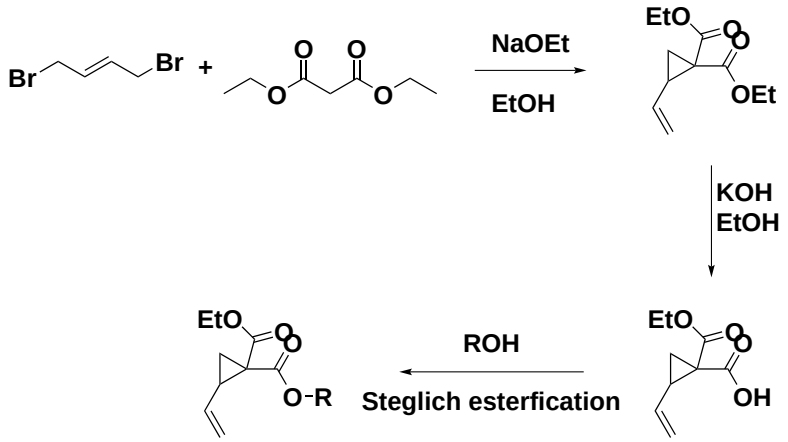

Scheme 18: General synthetic route for the synthesis of VCP-esters.

At each stage of synthesis the products were characterized by NMR. The ^{1}H NMRs of the respective products are given in section 3.1.2 and section 3.1.3 or in the Materials and Methods section 4.2.2 and fig. 29.[116]

3.1.2 Alcohols

As a second building block, alcohols containing the above-mentioned functional groups were synthesized. Scheme 19 shows the synthesized alcohols. A close proximity between the alcohol and the functionality was aimed at, to see the effect of each substituent, since the impact on the polymerization increases with a the proximity between reactive site and point of preorganization.

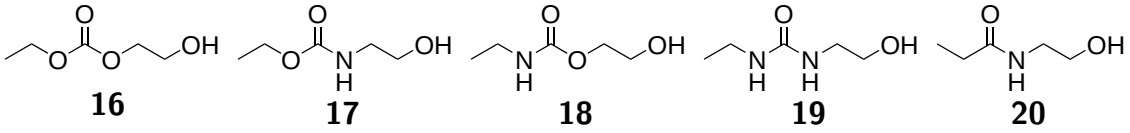

Scheme 19: Synthesized alcohols for the syntheses of VCP monoesters.

The Syntheses of all the molecules were performed by modified literature procedures (Scheme 20).[137–140] The presence of the desired products was confirmed by ^{1}H NMR experiments. The corresponding ^{1}H NMRs are given with peak assignments as section 3.1.2 below and figs. 30, 31, 43, 50 and 57 on pages 84, 85, 94, 99 and 104.

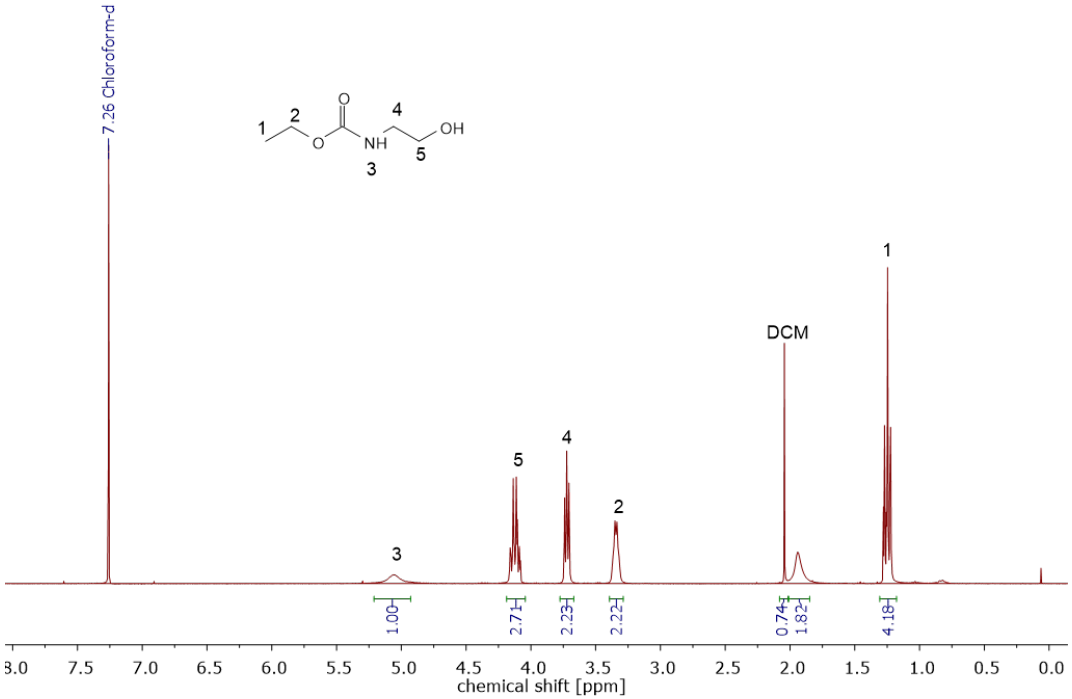

Figure 6: ^{1}H NMR of alcohol **17** as respective example.

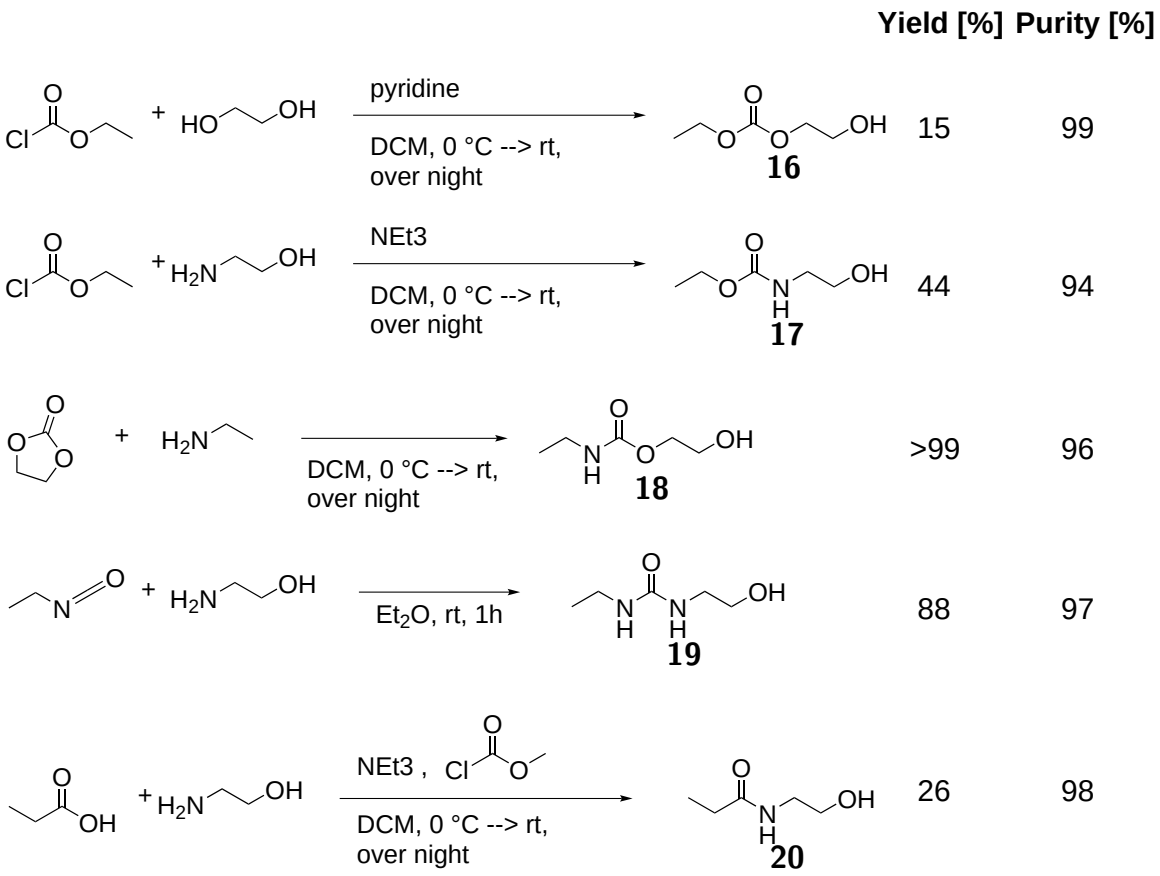

Scheme 20: Synthesis of the corresponding alcohols **21**. All are synthesized according to literature procedures and synthetic routes are described in details in section 4.2.3 on pages 83, 84, 88, 93, 98 and 103.

Depending on the reaction, yield and purity differed a lot. While for alcohol **19** almost quantitative yield was possible, in case of alcohol **16** a yield of only 15% was achieved. The crude mixture is purified by flash chromatography, yielding in a completely pure product. For alcohol **19** nevertheless, no side reaction is observed therefore, no purification was needed. Alcohol **20** was obtained with a good yield of 88%, alcohol **17** with a yield of 44%, while alcohol **18** could be synthesized with a yield of only 26%. Purity was determined using gas chromatography (GC) and showed high purities in all cases. Alcohols **21** were reacted with the VCP monoester to obtain VCP esters.

3.1.3 Chemical synthesis of monofunctional VCP esters

As mentioned, the esterification to obtain the desired monomers was conducted with self-synthesized alcohols and the VCP monoacid. A straight forward reaction is not possible, as the ester group of the VCP would react primarily, not yielding the de-

sired product. To prevent this a Steglich esterification was performed. Here, the acid is activated by N,N'-dicyclohexylcarbodiimide (DCC), enabling selective synthesis of monofunctional VCP esters. The reaction conditions were applied from previous published work[116]. In addition to DCC, 4-dimethylaminopyridine (DMAP) needs to be added, in order to prevent undesired side reactions between DCC and the acid. In this reaction DCC is converted into an urea, binding the released water from the esterification. The urea is insoluble in the used solvent and can therefore, be removed by filtration. By purification of the crude mixture via flash chromatography the esters are obtained in good purities. Scheme 21 shows the structures of the five monomers.

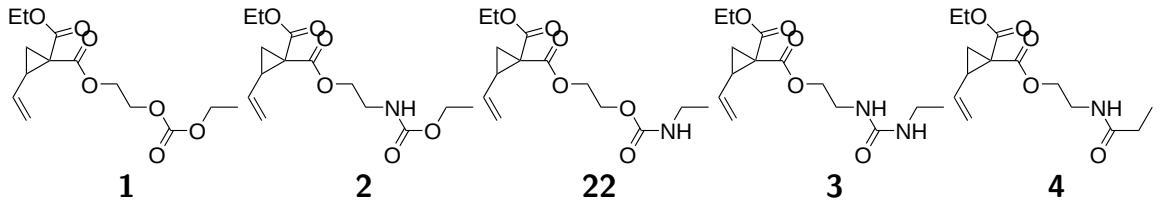

Scheme 21: VCP ester investigated in this section.

The chemical structure of the new VCP monomers was confirmed using various NMR techniques. As an example for all five monomers, the characterization of monomer **1** is described here. The ^{1}H and ^{13}C attached proton test (APT) NMR spectrum of monomer **1** is given in fig. 7 with peak assignments. Figure 8 presents the 2D heteronuclear single quantum coherence (HSQC) and heteronuclear multiple bond correlation (HMBC) spectra with the corresponding ^{1}H and ^{13}C experiments. For CH_3s 8 and 10, an overlapping double triplet is observed in ^{1}H NMR. Between 4.14 and 4.41, ppm $-O-CH_2-$ protons 5, 6, 7, and 9 are found but are indistinguishable. The other signals can be identified. The identification of primary, secondary, tertiary, and quaternary carbon (C) is enabled by a ^{13}C APT experiment. While secondary and quaternary protons have positive peaks, primary and tertiary protons show negative peaks (for spectrum of VCP **1** see fig. 34).

Based on the ^{1}J cross-coupling of peaks in the HSQC spectrum, ^{13}C-peak assignments were conducted (Figure 8a). The peaks could be easily correlated to ^{13}C NMR peaks by ^{1}J coupling. The $-O-CH_2-$ protons 5, 6, 7, and 9 showed an overlapping broad cross-peak, marked as **"A"** in fig. 8a. Moreover, based on the HSQC spectrum, ^{13}C signals of $-CH_3$ carbons could not be assigned individually. The ^{13}C NMR shows three different carbonyl carbons in the range of 150–170 Parts per million (ppm), as expected from the monomer **1** structure, but correct peak assignments are impossible based on

1D NMR and 2D HSQC. The HMBC experiment, which shows signals with coupling J > 1, was employed to identify the missing signals and fully resolve the monomer structure. The cross-peaks (7, 8) and (9, 10) in the HMBC spectrum (Figure 8b) confirmed that the peaks at 4.14–4.25 ppm belonged to protons 7 and 9. Protons 5 and 6 at 4.30-4.41 ppm showed cross-peaks with carbonyl carbons 12 and 13, respectively, confirming the peak positions of these two carbonyl carbons in ^{13}C NMR. Carbonyl carbon 12 is assigned by the observed cross-peak with proton 4.

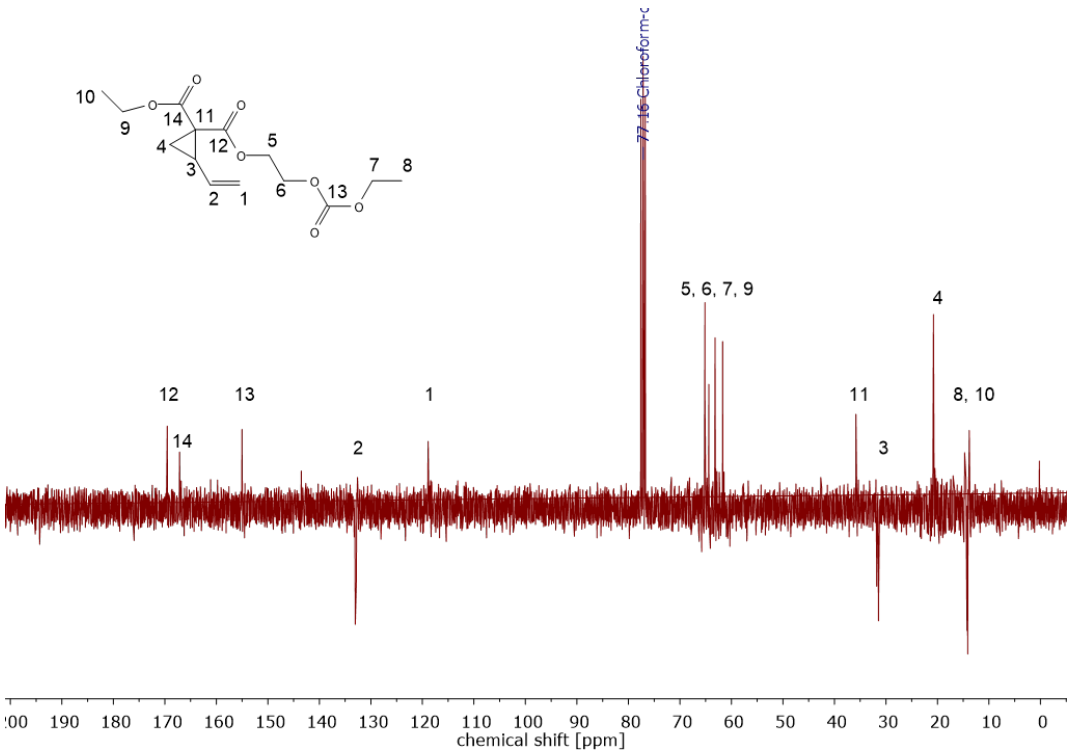

Figure 7: ^{13}C APT NMR of VCP **1**.

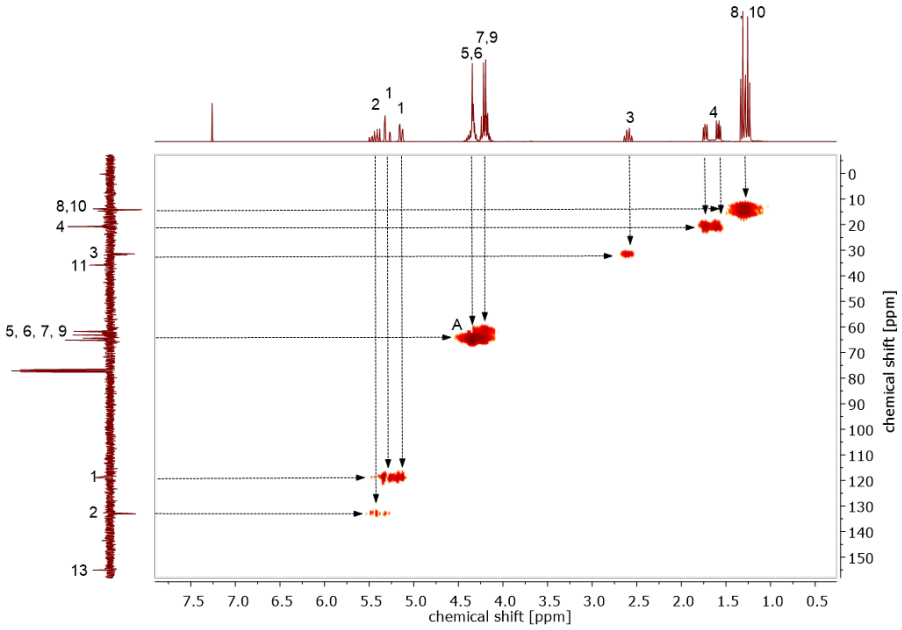

(a) HSQC NMR spectrum of monomer **1**

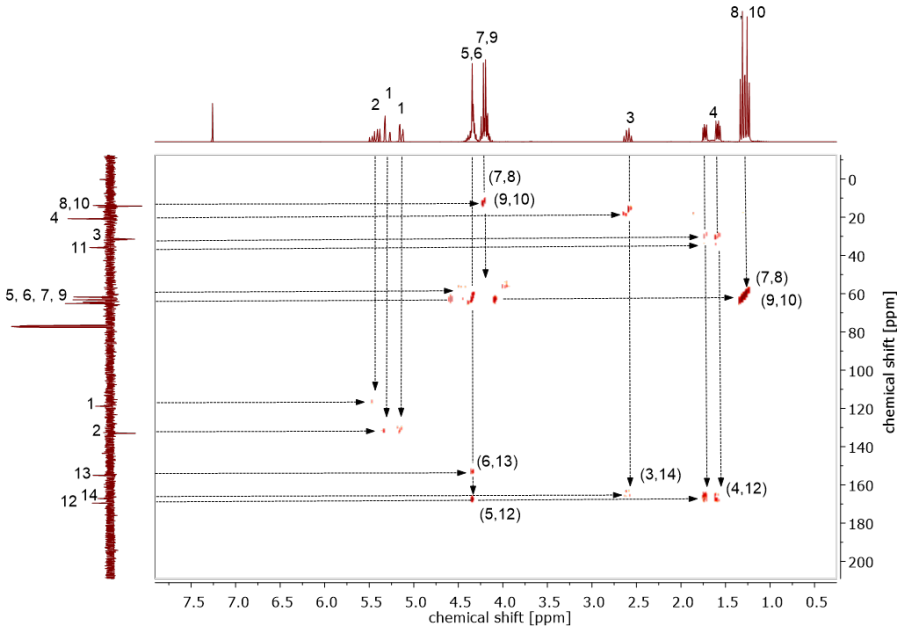

(b) HMBC NMR spectrum of monomer **1**

Figure 8: ^{1}H NMR (a) and ^{13}C NMR (b) spectra of monomer **1**

A similar method was used for the structural clarification and peak assignments in NMR for monomers **2**, **3**, and **4**, shown in section 4.2.3 Together with their respective synthesis procedures.

FT-IR was used to confirm the present of functional groups (see figs. 35, 42, 49 and 56). All monomers except monomer **22** were obtained as a liquid. Since bulk polymerization

is impossible with a solid monomer, monomer **22** is not investigated further in the following sections.

3.1.4 Preorganization of monofunctional VCP esters

As mentioned in section 1.3.2, the rapid rate of polymerization of VCPs-amides is expected to be influenced by preorganization via H-bonding.Via the H-bond, monomers are linked together and the distance between reactive sites is reduced. (Figure 9). In the not preorganized case, some monomers might polymerize, while many monomers need to move randomly in the bulk in order to find a reactive site close by.

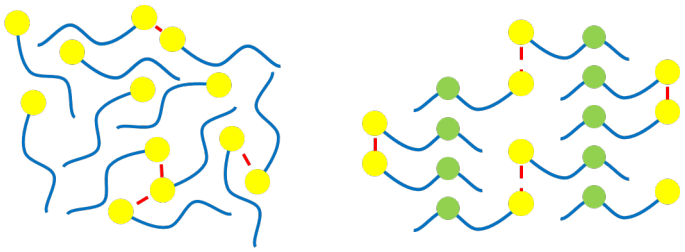

Figure 9: Representative picture of a not-preorganized monomer mixture (left) and a preorganization via the green sights (right). The reactive sides are depicted as yellow and the possible reaction links are shown as red.

Therefore, a strong hydrogen bond between the different monomers is desired. The NH protons work as H-bond donors, while the carbonyl groups in the side chain and all ester oxygens can act as acceptors.[14] By using variable-temperature solid-state NMR, the H-bond strength can be determined. Due to weaker H-bonding at higher temperatures, higher deshielding can be observed. The evaluation of the amine proton signals' at 6.0 - 7.7 ppm temperature dependency shows a shift to a higher field with increased temperature (Figures 10a and 10b and section 4.3.2). Figure 11 shows the difference of chemical shifts for the 3 monomers. The carbonate containing monomer VCP**1** was not investigated here, since there is no hydrogen bonding moiety present. The chemical shift at 25 °C is set at 0 and the peak shift plotted. This way, the strength of hydrogen bonding can be quantified.

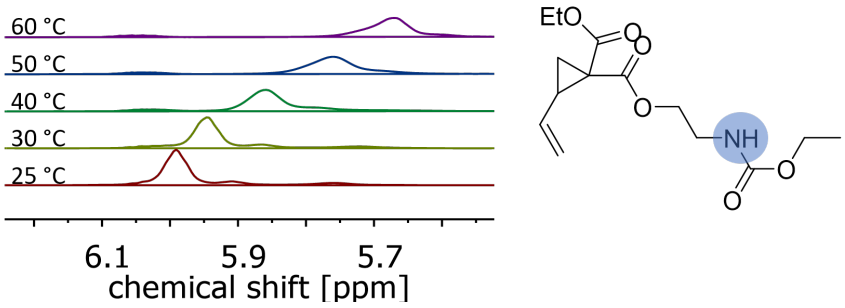

(a) Chemical shift of NH proton in correlation to temperature for monomer **2**.

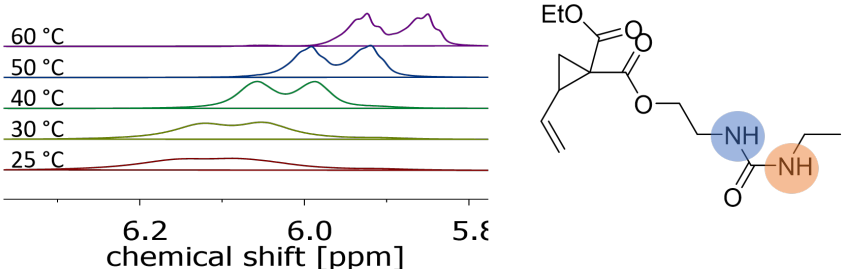

(b) Chemical shift of NH proton in correlation to temperature for monomer **3**. Both NH sites participate in H-bonding and are therefore descripted by **3**a and **3**b below.

Figure 10: Chemical shifts of at different temperatures **2** and **3**

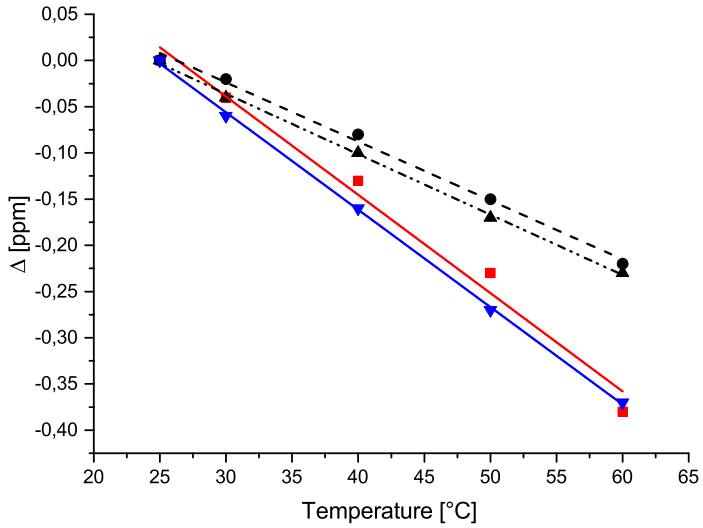

Figure 11: Change in chemical shift with temperature for monomers **2** (red), **3** (black), and **4** (blue). For **3**, both NH groups form hydrogen bonds are shown as **3a** and **3b**.[1]

For monomer **3**, both nitrogen protons form H-bonds. In temperature-dependent NMR at higher temperatures, two signals are formed. Further investigation in solution con-

firmed that these belong to the two distinctive NH- protons. While in chloroform, the nitrogen protons' signals are not visible, the NMR experiment in dimethyl sulfoxide (DMSO) showed two triplets at 5.9 ppm at room temperature, confirming no sole effect of temperature existed (Figure 12) but they are in fact a result of both nitrogens protons showing a slight difference in chemical shift, being able to quantify the contribution of both nitrogens to the overall preorganization.

The strength of the hydrogen bonds can be correlated to the slope of the change in chemical shift with temperature. The slope was determined by a linear fit for each NH-signal in the ss-NMR measurement. Slopes of 0.009 ppm/K for monomer **2**, -0.007 and -0.006 ppm/K for monomer **3**,and -0.010 ppm/K for monomer **4** were observed. With two H-bond donors, the overall strength for monomer **3** was expected to be highest, followed by monomers **2**, **4**, and **1** which have no H-bond donors (Figure 11). The following section investigates a correlation between preorganization via H-bonding and the polymerization rate.

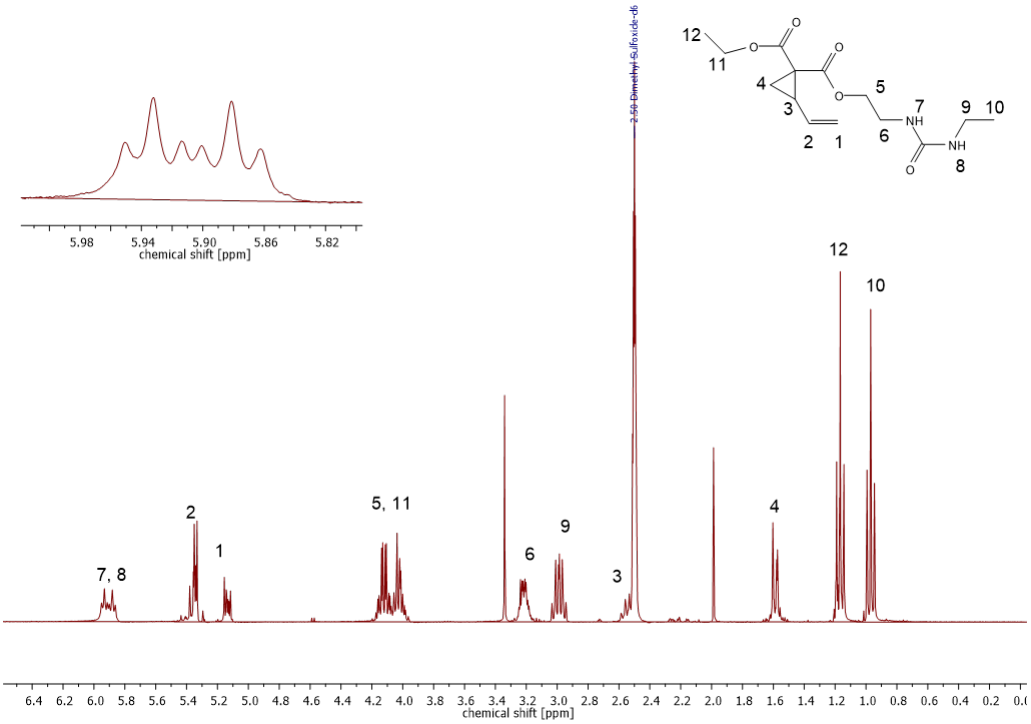

Figure 12: ^{1}H NMR of **3** in DMSO. As postulated, the formation of two separate triplets for the corresponding NH protons confirms the contribution of both hydrogens as hydrogen donors.

Solvent effect on the preorganization of monofunctional VCP esters

The previous section investigated the preorganization of the four liquid monomers. Since monomer **22** was obtained as a solid, it was excluded from the study for this thesis. Nevertheless, the need to dissolve this monomer was considered by studying the effect of preorganization in solution. Thus, **22** was polymerized in N,N-dimethylformamide (DMF), a solvent known to break hydrogen bonds at a specific concentration,[141] and anisole, which is the favored solvent for future solution-based radical polymerization due to its benign nature and high compatibility with many different systems.
AIBN was used as an initiator at 70 °C . Figure 13 shows the change in conversion over time in both cases. The measurement was performed only once, so no error was determined. The points were fitted, using a Hill fit with no weighting.

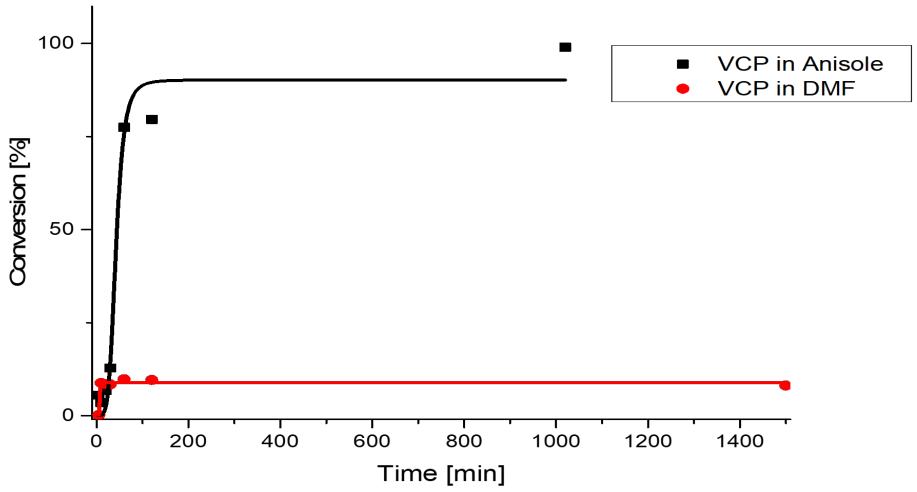

Figure 13: Polymerization of monomer **22** in anisole with AIBN as radical initiator. The conversion was determined by GC and fitting performed using a Hill fit.

The polymerization conversion in DMF remained below 20 %, while when using anisole, almost complete conversion was obtained after 24 h. VCP ester tends to have a low conversion,[116] so its polymerization behavior should be improved via preorganization. Therefore, it can be suspected that anisole allows and probably even supports building hydrogen bonds with VCPs (compare fig. 13). Notably, thermally induced polymerization tends to have a higher volume shrinkage at elevated temperatures.[110] Thus, the following section only discusses photopolymerization.

3.1.5 Photopolymerization of monofunctional VCP esters

Photoinduced radical polymerization is the technique of choice for VCP polymerization reactions. Reason is the possibility to use room temperature and therefore, reduce volume shrinking via backbiting. In addition, possible applications like the usage in dental fillings require polymerization at room temperature, too. The polymerization of monomers **1**, **2**, **3**, and **4** was conducted with CQ as a free-radical photoinitiator and EDMAB (1:2 mol%) as co-initiator. The optimal ratio between CQ and EDMAB has been investigated before and is applied here.[130] The free-radical polymerization of VCP derivatives mainly leads to 1,5 ring-opened units with a double bond in the polymer backbone. The rearrangement of the growing radical by adding to the double bond formed by the ring-opening of the VCP might also lead to the ring-closed cyclobutene ring in the backbone (Scheme 22). The ratio between these mainly determines the volume shrinkage of VCPs.

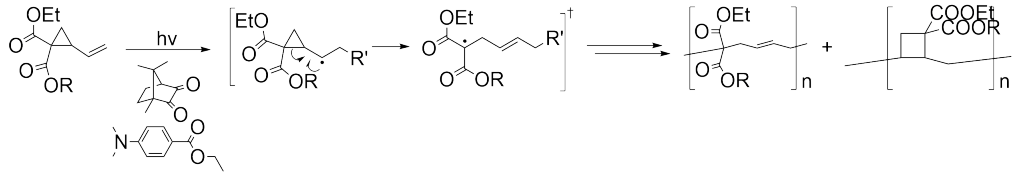

Scheme 22: General scheme for forming a linear or cyclobutane-containing polymer from VCP via photoinduced RROP.[1]

Kinetic measurements of RROP

Kinetic measurements were conducted to study the polymerization rate by following the monomer conversion with time. Small samples of monomer and initiator were irradiated with the light from a blue LED. After a given time, the sample was removed and polymerization was terminated by immersing the mixture in liquid nitrogen. The monomer was then extracted with a certain amount of a suitable solvent, dissolving the monomer but not the polymer. An internal standard, which was phenol in this study was used. Each measurement was repeated three times. The amount of unreacted monomer was obtained by measuring the signal integral in GC (see also section 4.4). The fastest polymerization was expected for monomer **3** due to the most robust hydrogen bonding shown in section 3.1.4 . Figure 14 presents time plots of the monomer conversion.

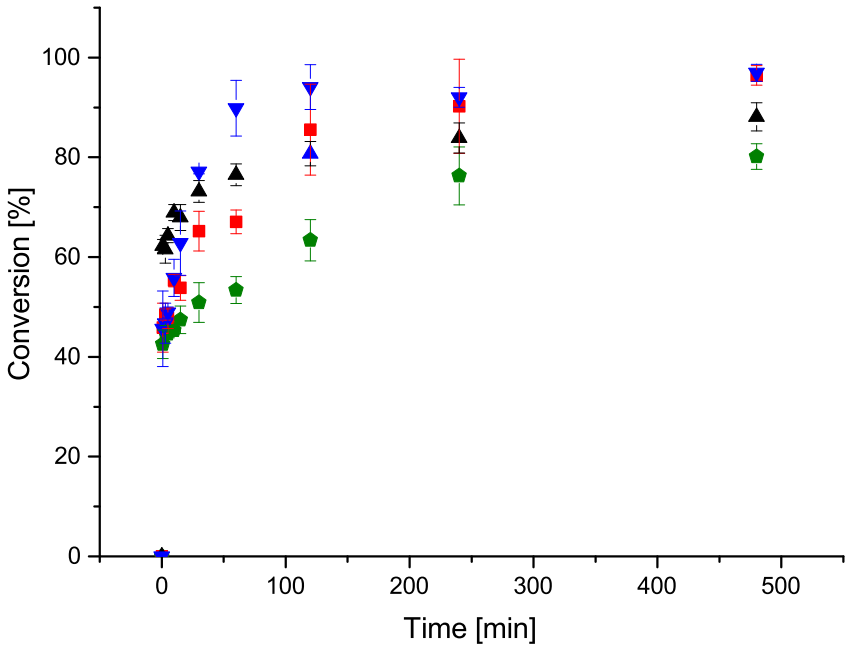

Figure 14: Conversion over time for the photoinduced polymerization of monomers **1** (green), **2** (red), **3** (black), and **4** (blue). Each signal represents a different sample irradiated with visible light and analyzed via GC.

Table 3.1 shows the overall conversion and Initial rate of polymerization (R_p).

Table 3.1: Initial polymerization rate and the overall conversion of the photopolymerization of monomers **1**, **2**, **3**, and **4**.

Monomer	R_p [%/min]	Overall conversion [%]
1	17.8 ± 5.8	80.2 ± 2.6
2	19.1 ± 6.3	96.4 ± 2.0
3	24.7 ± 8.9	88.1 ± 2.8
4	18.6 ± 6.4	97.0 ± 1.7

The R_p was calculated by the average slope of the first three points; the overall conversion was determined after an irradiation time of 24 h. The highest R_p was observed for monomer **3**, with $24.7\%/min$. This matches the findings in section 3.1.4, where twice the number of hydrogen bonds was observed for monomer **3**. With this higher preorganization, faster polymerization can be expected. This expectation was confirmed by monomer **1**, which showed the lowest R_p. Nevertheless, the differences were

less significant than expected for preorganized monomers. Interestingly, for monomer **3**, the polymerization rate changed after the first minutes, leading to a lower overall conversion. One explanation could be the sample's high viscosity disabling molecular movement. This hypothesis was verified with rheometric measurements during photoinduced polymerization. Here, the change in viscosity was investigated and is discussed in the next section.

Photorheology

A correlation between viscosity and R_p was drawn by in-situ rheometric measurements for all four monomers. Measurement was performed using a cone plate rheometer with a glass plate, allowing constant irradiation with light from below. Viscosity was determined by rotating measurement and a fixed shearing rate. Monomer **3** showed the fastest increase in viscosity before this slowed significantly. Surprisingly, the second fastest increase in viscosity was observed for monomer **1**, although no H-bonds could be formed here. One explanation is the low T_g of polymer **23** of 9 °C (see table 3.2). Additionally, the initial viscosity of monomer **1** was the lowest, enabling better molecular movement initially. The slowest growth in viscosity was found for monomer **2**, with a slightly more significant increase for monomer **4**. For monomers **1** and **3**, after 3 and 2 hours, respectively, a temporary loss of adhesion between the sample and glass plate or sample and stamp was observed. Consequently, a viscosity fluctuation was determined, as observed in fig. 15. Nevertheless, no further conditions were tested for the two monomers. Photorheology could not support the total result of previously obtained kinetic measurements but could explain the decrease in the rate of polymerization for monomer **3**. In addition, the previously found similarity of the rate of polymerization between monomers **1** and **4** could be supported as well.

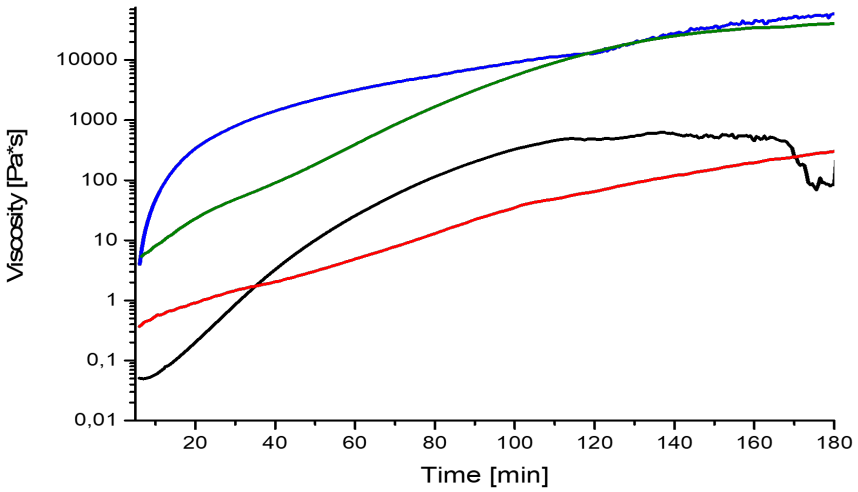

Figure 15: Change in viscosity over time for the photoinduced polymerization of monomers **1** (black), **2** (red), **3** (blue), and **4** (green). The samples were constantly irradiated with light while measuring the viscosity.

3.1.6 Polymer characterization of monofunctional VCP esters

In addition to the rate of polymerization, low volume shrinkage is an important property of VCPs. As mentioned in section 3.1.5, VCPs can form a linear structure or, via backbiting, cyclobutane units. The ratio between these depends on the reaction conditions, for example, temperature. A key feature of using VCPs is their ring-opening mechanism, which produces a longer repeating unit than its monomer structure and, therefore, counters the natural volume shrinkage occurring in polymerization reactions. Therefore, the ratio of cyclobutane to the linear structure is crucial. The structural characterization of the photopolymerized polymers was performed with ^{1}H NMR. Figure 16 shows the representative ^{1}H NMR spectra of polymers **1, 2, 3**, and **4**.

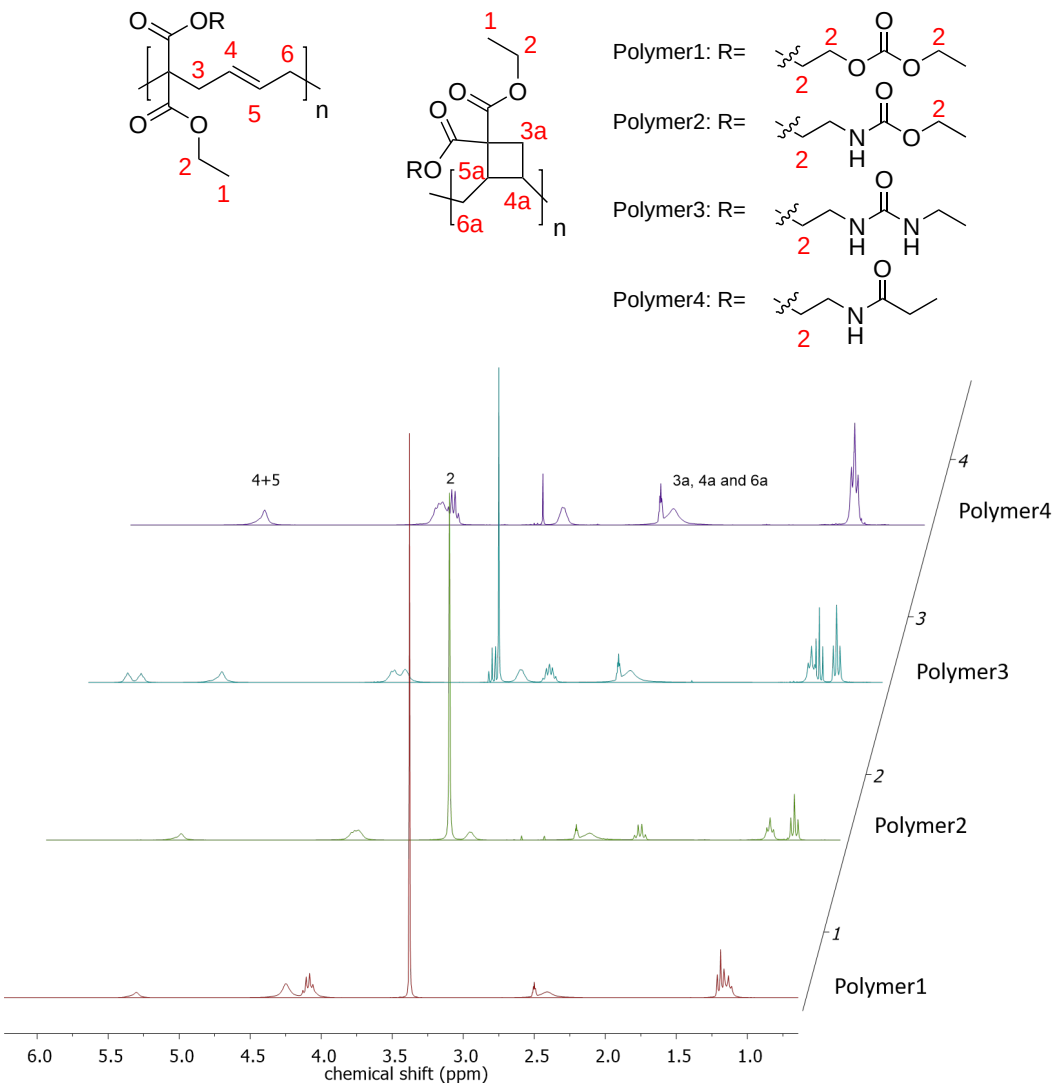

Figure 16: ^{1}H NMR of polymers **1, 2, 3**, and **4**. Position 4+5 corresponds to the formed linear structure, 3a, 4a, and 5a to the cyclobutane ring, while position 2 is found in both cases. The number of cyclobutane units can be calculated from the ratio between these signals.[1]

The double bond of the open structure is observable as a clear peak at 5.3 ppm, while the cyclobutane unit is observed as a broad signal between 1.5 and 2.5 ppm.[110] The combined signal of $-C(O)OCH_2$- protons of the ring-opened and ring-closed cyclobutene units is observed at 4.1 ppm, and secondary protons 3 and 6 are located at 2.5 ppm. Table 3.2 shows the percentage of the open-ring structure. The number of protons located beside oxygens (eight for polymer **1**, six for polymer **2**, and four for polymers **3** and **4**), signal 2 of fig. 16, is used to normalize the spectra. The ratio of open-ring and cyclobutene units, x, can be directly followed using the integral of olefinic protons 4 and 5. For x = 2, only linear units are present; for x = 0, 100% of all units are

cyclobutenes; and for x < 2, the analyzed NMR indicates a mixture of both. All polymers, except for polymer **1**, show a high degree ring-opened units. One reason is the slower polymerization of monomer **1** favoring intramolecular reactions. Almost no cyclobutane units are expected if the polymerization ratio is faster than the backbiting reaction. This ratio correlated directly to the volume shrinkage, and a lower volume shrinkage was expected, comparable to previous findings.[130]

gel permeation chromatography (GPC) was used to further characterize the polymers for molar mass. Unimodal GPC curves were obtained for all low to medium molar mass polymers (for curves, see section 4.5.1). The thermal stability was determined by thermogravimetric analysis (TGA) (for curves, see section 4.5.3). Polymers **3** and **4** showed stability up to 200 °C , while a higher number of oxygen atoms in the polymer increased the stability to 268 °C for polymer **2** and 333 °C for polymer **4** (Table 3.2). The polymer properties were further investigated with differential scanning calorimetry (DSC) (for curves, see section 4.5.2). Since no melting peak was visible in the observed temperature range, amorphous polymers were expected. The T_g shows an opposite trend to the polymer stability. Polymer **1**, unable to form hydrogen bonds, has a T_g at 9 °C , while the T_g increases from polymer **2** (27 °C) to polymer **4** (34 °C) to polymer **3** (46 °C). The higher T_g of polymer **3** is due to an additional hydrogen bond. While the electron pulling effect of the urethane' oxygen in polymer **2** does not affect the strength of the hydrogen bond, as shown previously (Figure 11), it leads to a reduced T_g in comparison to polymer **4** bearing an amide group.

Table 3.2: Ratio of open- versus closed-ring polymeric structure, molecular weight, thermal stability, and glass transition temperature of the corresponding polymers for monomers **1**, **2**, **3**, and **4**.

Polymer	Open-ring structure[a] [%]	$\bar{M}_n$[b]	$Đ_M$	T_g[d] [°C]	$T_{5\%}$[e] [°C]
1	61	$3.6 \cdot 10^4$	1.4	9	333
2	91	$2.6 \cdot 10^4$	2.8	27	268
3	93	$8.5 \cdot 10^3$ [c]	1.6	46	194
4	87	$1.3 \cdot 10^4$ [c]	1.9	34	204

[a] determined by ^{1}H NMR.
[b] GPC ($CHCl_3$, PS standard). [c] GPC (DMF)
[d] determined by DSC from -30 to 150 °C with a heating rate of 20 K/min. T_{Onset}
[e] temperature, where 95% of the original mass is still detectable.
Determined under a nitrogen atmosphere, measured from 20 to 600 °C with a heating rate of 10 K/min.

Polymer characteristics show that, depending on the field of application, different functional groups might be favorable. In dental and medical applications, the average temperature is at the body temperature of 37 °C . A T_g above that and a high degree of open ring structure and therefore a low volume shrinkage is preferable. Monofunctional VCP-derivatives will never be used all alone for dental or coating applications due to their linear structure. The systematic study, shown in this section, is an important step forward in this field of research to make some rule of thumbs for future reactions with the bifunctional VCP-derivatives. It helps understanding the polymerization behavior of VCP-derivatives.

3.2 Investigation of novel monofunctional VCP amides

Further work was done for understanding the effect of the position of H-bonding units in VCP-derivatives. Therefore, section 3.2 investigated VCP-derivatives in which the side-chains were attached to the VCP ring by amide bond instead of an ester unit. These new monomers are in general designated as VCP-amides. Previous work reported that the R_p and conversion significantly increase on using bifunctional VCP-amides rather than VCP-esters.[116] This section aimed to use this information and synthesize new monofunctional VCP-amides for making a structure-property correlation. The VCP-amides were prepared according to the following reaction scheme.

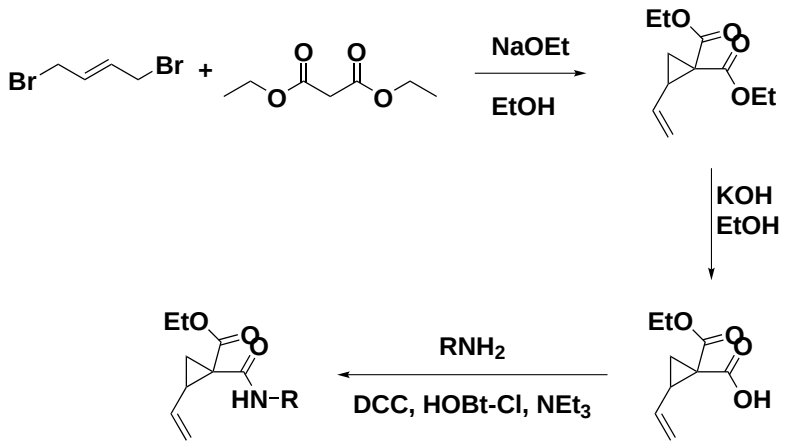

Scheme 23: General synthetic route for the synthesis of VCP-amides.

The first steps of formation of VCP-diester and VCP-ester-acid remained the same by reacting 1,4-dibromobut-2-ene with malonic acid diethyl ester followed by hydrolysis of one of the ester groups. In the final step VCP-amides were prepared by the reaction

of VCP-ester-acid with different amines having urethane, urea, and amide functional groups (Scheme 24. As a reference, amine with carbonate functional group was also prepared. The reaction scheme for the synthesis of these amines is given in scheme 26.

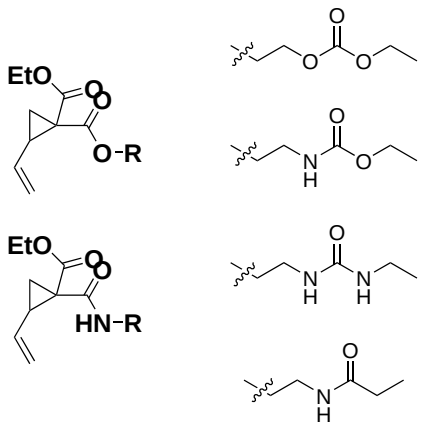

Scheme 24: Chemical structures of the VCP-esters, investigated in the last section and their corresponding VCP-amides.

The amines were synthesized according to the literature procedures.[142–145].

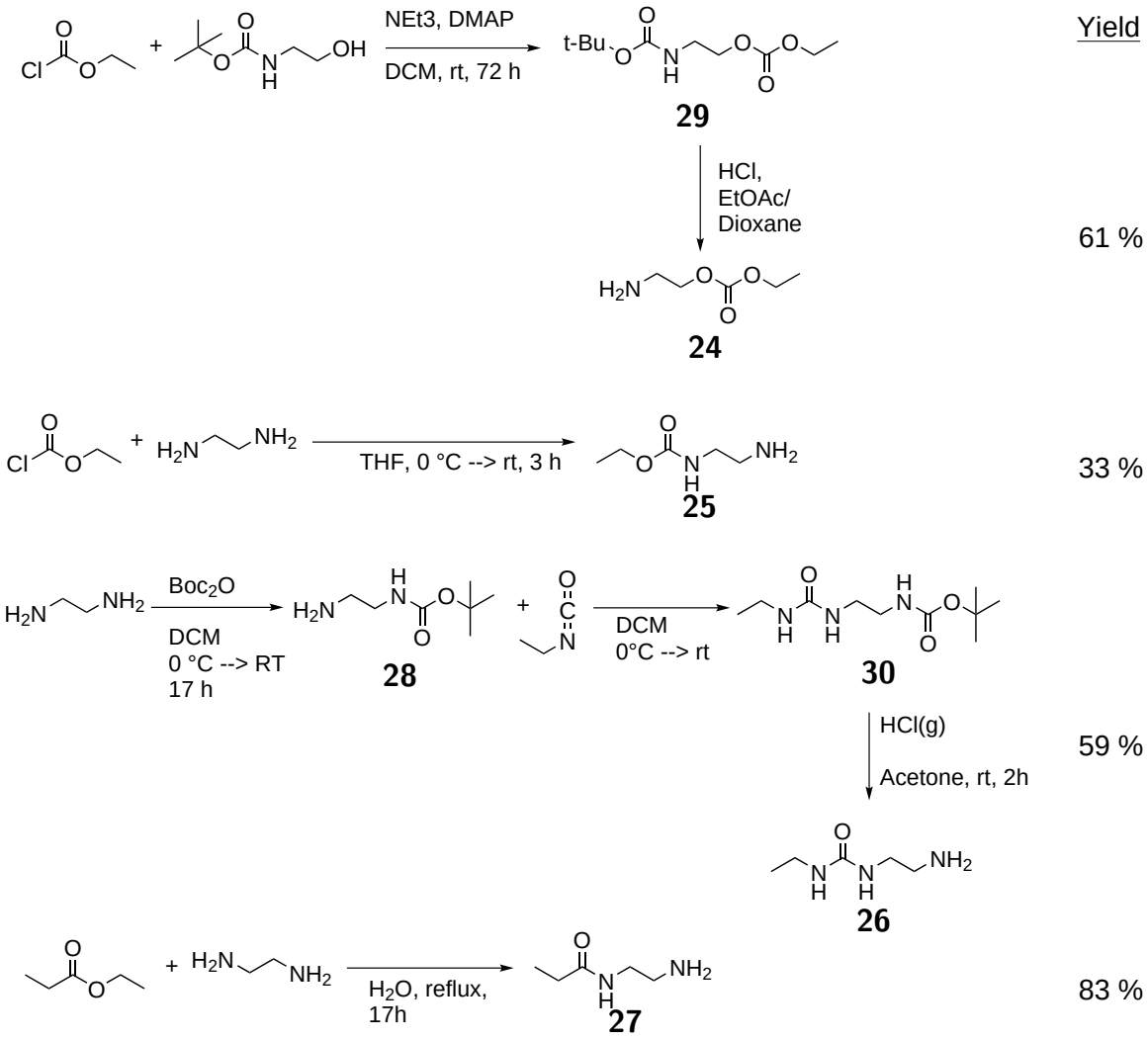

Scheme 25: Synthesized amines for synthesizing VCP amides.

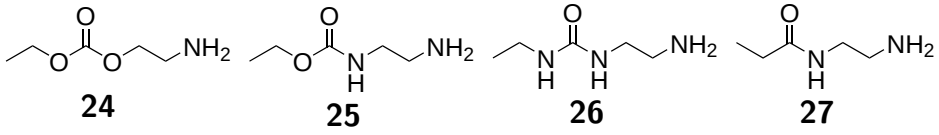

Scheme 26: Synthesized amines for synthesizing VCP amides.

For the synthesis of amines **25** and **27** no protection-deprotection chemistry was used. In contrast, amines **24** and **26** required the usage of protective groups. The reason is the higher nucleophilicity of amines in comparison to alcohols in the synthesis of amine **24**. For amine **26** the high reactivity of the isocyanate would result in an undesired product even when a huge excess of the diamine is used. The overall yields of the

multi-step synthesis are 61% and 59%, respectively, while the direct synthesis of amine **25** resulted in a yield of 33%. The reason is the possible side reaction of the relatively reactive acidic chloride. When a less reactive ester is used, the reaction performed at a much higher temperature showed good yield of 83%, resulting in amine **26**. All four amines were characterized by NMR spectroscopic methods. The ^{1}H NMR of amines with peak assignments are given in figs. 59, 65, 75 and 83 on pages 106, 111, 118 and 124.

3.2.1 Chemical synthesis of novel monofunctional VCP amides

As in section 3.1, VCP amides were synthesized by the reaction of the VCP monoacid and self- synthesized amines. Since OH is a poor leaving group, activation with DCC is necessary. Additionally, following previous work,[116] 6-chloro-1-hydroxy-benzotriazole (HOBt-Cl) was added to further activate the free amine. Thus, four new monomers could be synthesized, bearing carbonate, urethane, urea, and amide side chains (for general reaction scheme, see scheme 23). Scheme 27 shows the structures of the four monomers.

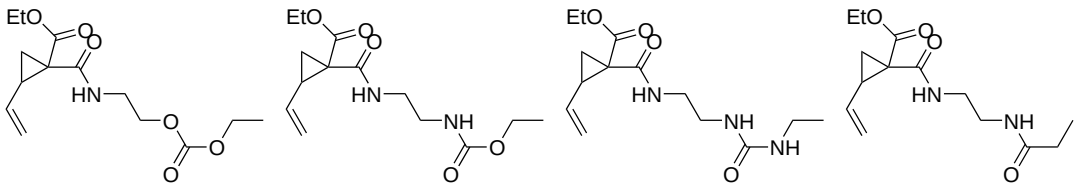

Scheme 27: Structure of synthesized VCP amides, bearing carbonate, urethane, urea, and amide side chains.

The new monofunctional VCP-amide derivatives were structurally analyzed using different NMR techniques (compare section 3.1.3). For monomer **5**, the ^{1}H and ^{13}C spectra with peak assignments are shown in fig. 17 as a representative example.

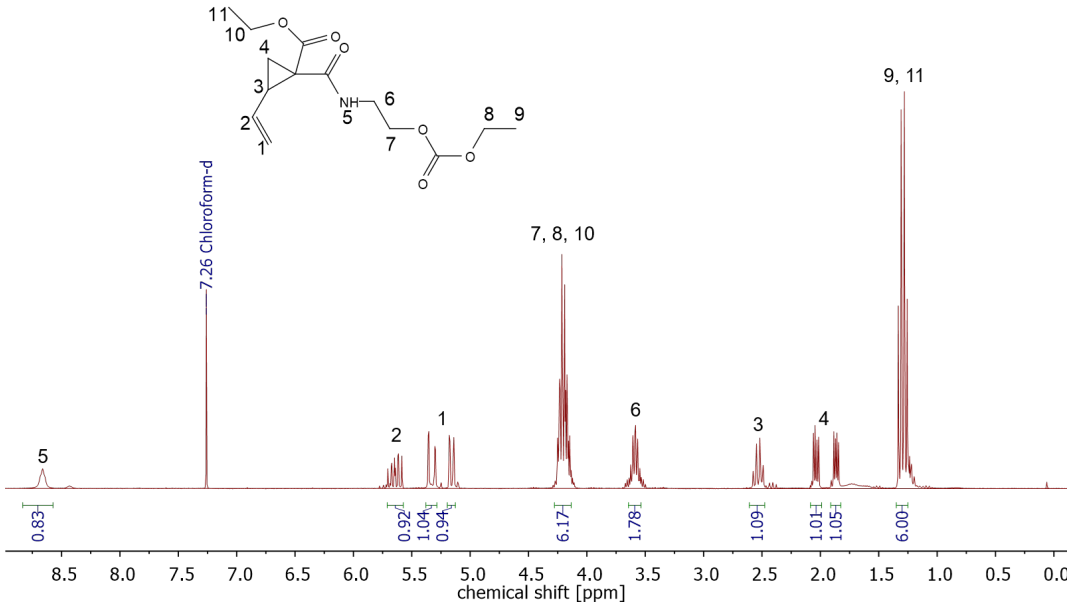

(a) ^{1}H NMR spectrum of monomer **5**

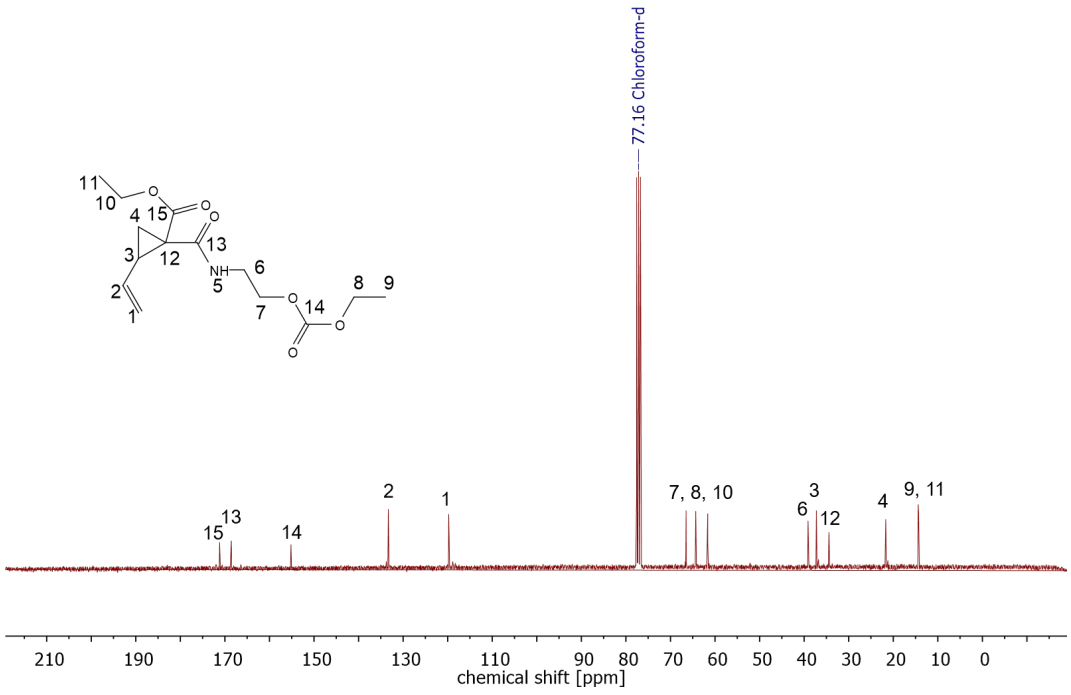

(b) ^{13}C NMR spectrum of monomer **5**

Figure 17: ^{1}H NMR (a) and ^{13}C NMR (b) spectra of monomer **5**

Although some of the protons, such as CH_3 protons (9, 11) at 1.25 ppm and $-O-CH_2$ protons 7, 8, and 10 with peaks between 4.15 and 4.25 ppm show overlapping signals in ^1H NMR and are indistinguishable, the integrated peak area agrees excellently with the monomer structure. Full characterization is possible with ^{13}C NMR as well as 2D-experiments (Figure 18).

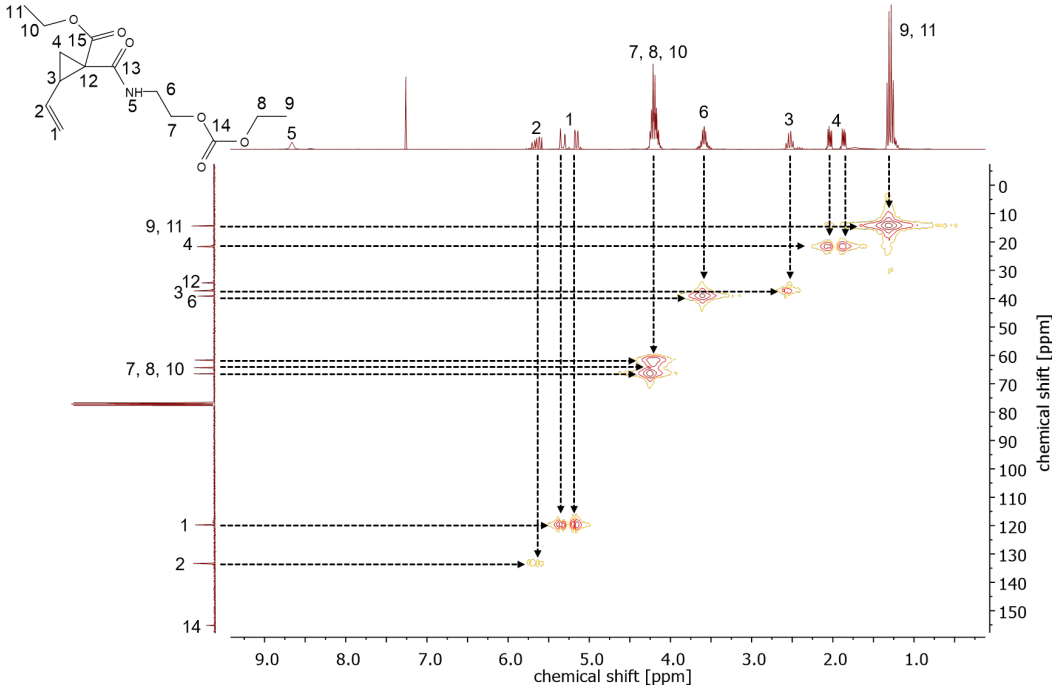

(a) 2D HSQC NMR spectrum of monomer **5**

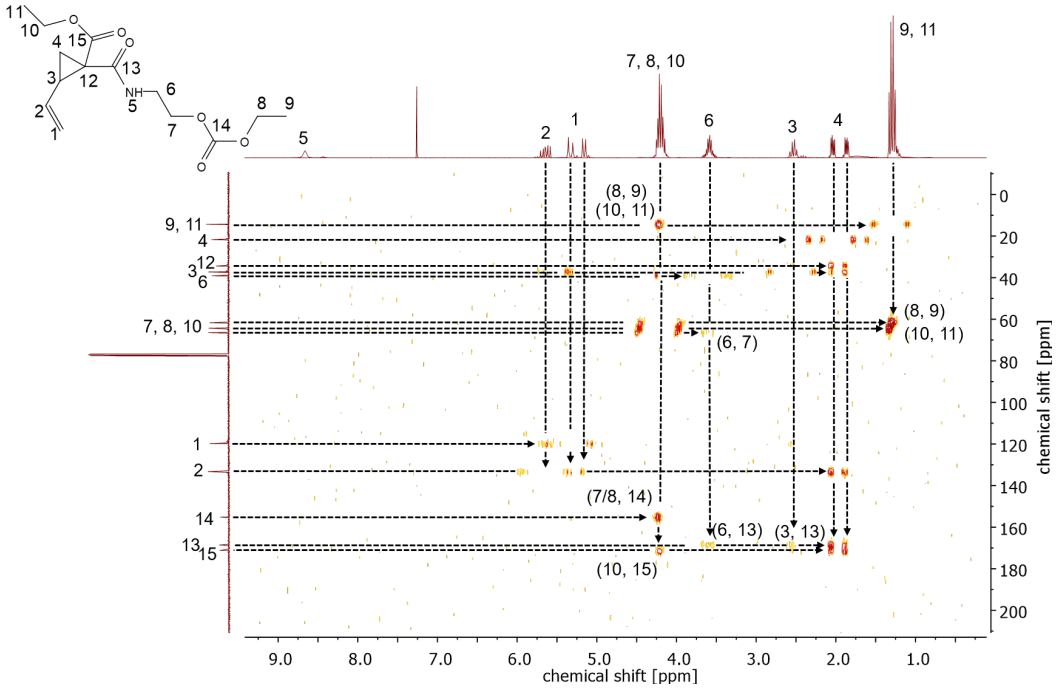

(b) 2D HMBC NMR spectrum of monomer **5**

Figure 18: HSQC (a) and HMBC (b) spectra of monomer **5**

The quaternary carbon at the cyclopropane ring (position 12) can be identified with cross-peaks (3, 4) and (4, 12). Conversely, the three carbonyl carbon peaks can be

assigned based on their coupling to different ^{1}H signals. Here, coupling the overlapping peaks of 7, 8, and 10 helped assign the C_{14}; distinctions between C_{13} and C_{15} were possible due to the cross-peaks (6, 13) and (10, 15). NH proton 5 could be identified with correlation spectroscopy (COSY) (for the spectra of monomer **5**, see figs. 60 to 63 on pages 108 to 109).
The structure of monomers **6**, **7**, and **8** was clarified using the same technique for peak assignments (please refer to figs. 66 to 71, figs. 76 to 81 and figs. 84 to 89 on pages 112 to 115, pages 120 to 122 and pages 125 to 128). FT-IR spectra were obtained to confirm the presence of the corresponding functionalities (figs. 64, 72, 82 and 90 on pages 110, 115, 123 and 128).

3.2.2 Preorganization of monofunctional VCP amides

As in section 3.1.4, temperature-dependent solid-state NMR was used to observe the hydrogen bond strength of VCP amides. The NH units of the side-chain functional groups, urethane, urea, and amide, and those of the NH units connecting the side chain to the VCP ring, were investigated and distinguished. Generally, signals of the side-chain NH units can be observed at a much higher field than the amide linked to the VCP ring. The H-bonds are weakened as the temperature rises, and a shift to a higher field can be observed. The strength of each hydrogen bond can be estimated from the slope of this shift.

For **5**, only one amide proton signal beside the VCP unit is visible, with a slope of $-4.34 \cdot 10^{-3}$ ppm/K, as it has no other H-bonding units in the side chain. For **6**, the VCP C(O)NH proton (proton of amide group directly attached to the VCP ring) shows a slope of $-6.70 \cdot 10^{-3}$ and a side chain amide of $-8.35 \cdot 10^{-3}$ ppm/K; **7** shows two signals for both nitrogen protons in the side chain with slopes of $-6.00 \cdot 10^{-3}$ and $-5.70 \cdot 10^{-3}$ in addition to $-3.77 \cdot 10^{-3}$ ppm/K for the VCP C(O)NH proton. For **8**, the VCP C(O)NH proton has a slope of $-4.54 \cdot 10^{-3}$ and the side chain $-7.87 \cdot 10^{-3}$ ppm/K. Variable-temperature solid-state ^{1}H NMR measurements of **6** from 25–60 °C are shown in fig. 19 and the change in chemical shifts with the temperature of the different NH signals in fig. 20. Variable-temperature ^{1}H NMR measurements of **5** and **31** and the complete spectrum of **6** are presented in section 4.3.2 section 4.3.2. Since the measurement was performed only once, no standard deviation was possible.

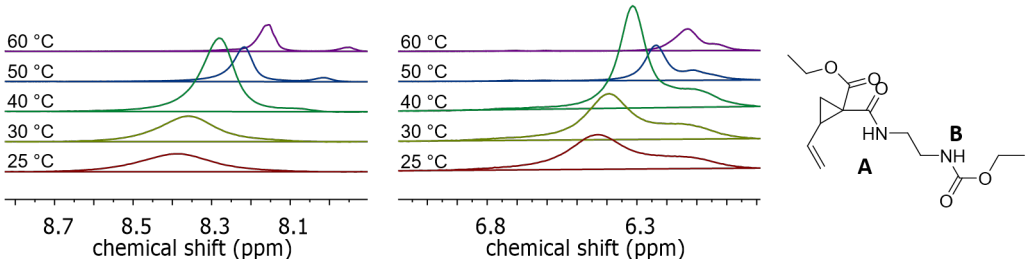

Figure 19: Change in chemical shift of monomer **6** with increasing temperature. Left, shift of signal **A**, right of signal **B**

Chemical shifts of side-chain amide protons are more significant, probably due to reduced steric hindrance, allowing a stronger bond than the amide protons directly attached to the VCP ring. Of the four monomers, **6** show the most significant shift, while the other three shows similar chemical shift behavior for the amides directly attached to the VCP ring. Urethane has a higher electron density and is therefore the better hydrogen acceptor. This results in a stronger hydrogen bond between the VCP amide and the side chain, contributing to this higher chemical shift. For the side-chain signals, urea hydrogen contributes to good preorganization but with less strength than the single NH-protons from monomers **6** and **8**, which show similar behavior. Correlating the H-bond strength to preorganization and, therefore, R_p, the fastest reaction is expected for monomer **6**. Monomer **5** due to only one site of preorganization should show the lowest rate. Monomer **7** is expected to react rapidly as well, as three NHs contribute to H-bonding, while monomer **8** is prone to show a slower reaction. The following section discusses the polymerization behavior of monomers **5**, **6**, **7**, and **8**.

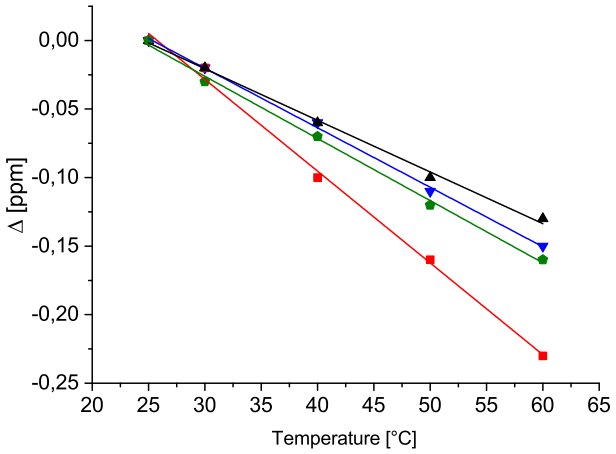

(a)

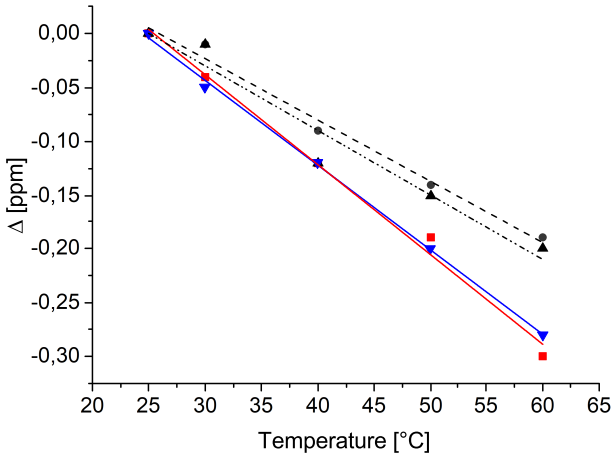

(b)

Figure 20: Change in chemical shifts with temperature for monomers **5** (green), **6** (red), **7** (black), and**8** (blue). a) shows the change in the hydrogen proton beside the VCPunit, while b) shows the change in the respective side-chain hydrogens.

3.2.3 Photo polymerization of monofunctional VCP amides

Section 3.1.5 describes the effect of different side chains on R_p.
In this section, the polymerization rate of VCP amides, where an additional hydrogen donor is introduced near the VCP backbone, is investigated. Figure 21 shows the kinetic measurement of the photopolymerization of monomers **5**, **6**, **7**, and **8** carried out at room temperature by a white LED-light.

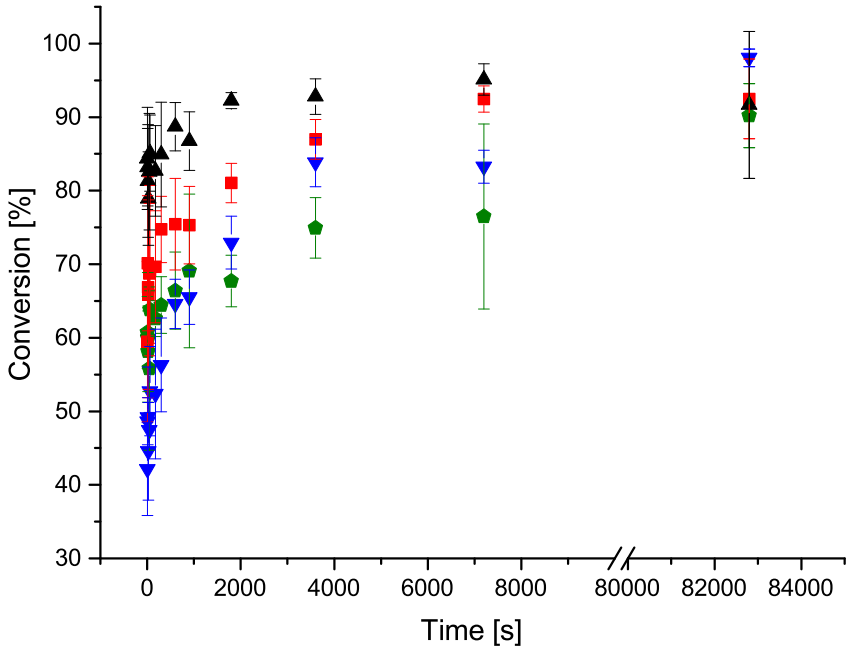

Figure 21: Light polymerization of monomers **5** (green), **6** (red), **7** (black), and **8** (blue). Change in conversion over time. Each signal represents a different sample irradiated with visible light and analyzed via GC.

With an initial R_p of 2.35 %/s, monomers **7** was the fastest, followed by monomer **6** (1.99 %/s), **5** (1.62 %/s), and **8** with 1.35 %/s. After 30 min, monomer **7** showed almost complete conversion, while the other monomers showed a much slower increase in conversion. At 6 hours, the conversion of **8** (∼83%) surpassed **5** (∼76%), although the high fluctuation of results in the case of **5** might have led to this result, and the actual conversion of **5** was higher. It is known in the literature that the N−H groups of urea exhibit a stronger H-bond than other functional groups, such as urethane,[146] which explains the faster polymerization behavior of monomer **7**. *Mattia et al.* investigated the hydrogen bonds of different functional groups. Their calculation was performed in bulk, however, while polymerization was performed in solution. Anisole was used as a solvent, as it does not prevent hydrogen bonding (see section 3.1.4). Nevertheless, the solvent effect must be considered when evaluating these results. Its ether group might act as a hydrogen bond donor, supporting the preorganization of hydrogen donor-containing monomers.[147] Table 3.3 shows an overview of the overall conversion and R_p.

Table 3.3: Initial polymerization rate and the overall conversion of the photopolymerization of monomers **5**, **6**, **7**, and **8**.

Monomer	R_p[a] [%/s]	Overall conversion[b] [%]
5	1.62 ± 0.71	90.2 ± 4.3
6	1.99 ± 0.70	92.5 ± 1.8
7	2.35 ± 0.98	95.1 ± 2.1
8	1.35 ± 0.51	98.7 ± 1.9

[a] calculated by the average slope of the first three points.
[b] conversion after 24 h.

Figure 22 shows the photopolymerization of VCP esters and corresponding VCP amides. VCP esters show a lower polymerization rate, despite polymerization being performed in bulk. This comparison shows the immense influence of preorganization via H-bonding on the polymerization behavior. In all cases, the only difference between VCP esters and VCP amides was the additional N−H group of VCP amides, rather than −C(O)− in the case of VCP esters, enabling the formation of an additional hydrogen bond beside the VCP unit. A comparison of monomers **1** and **5** showed this amide linker's effect on the polymerization rate since no preorganisation occurs in case of **1**. In comparison, **5** shows the effect of a preorganization near the reactive site. This effect is enhanced in terms of the rate of polymerization and monomer conversions when the side chain also contains functional groups capable of forming H–bonds.
The expected effect is not observed for monomers **4** and **8**, displaying an amide functionality. While a synergistic effect of the position of H-bonding sites might also play a role, other factors such as steric hindrance, conformation, or dipole effects could also explain this behavior.[148] Furthermore, section 3.1.5 showed the high initial rate of polymerization in the case of monomer **4** in comparison to other VCP esters. This supports the reduced effect of an additional hydrogen bond donor. A more detailed investigation of the mentioned effects will be part of future studies.

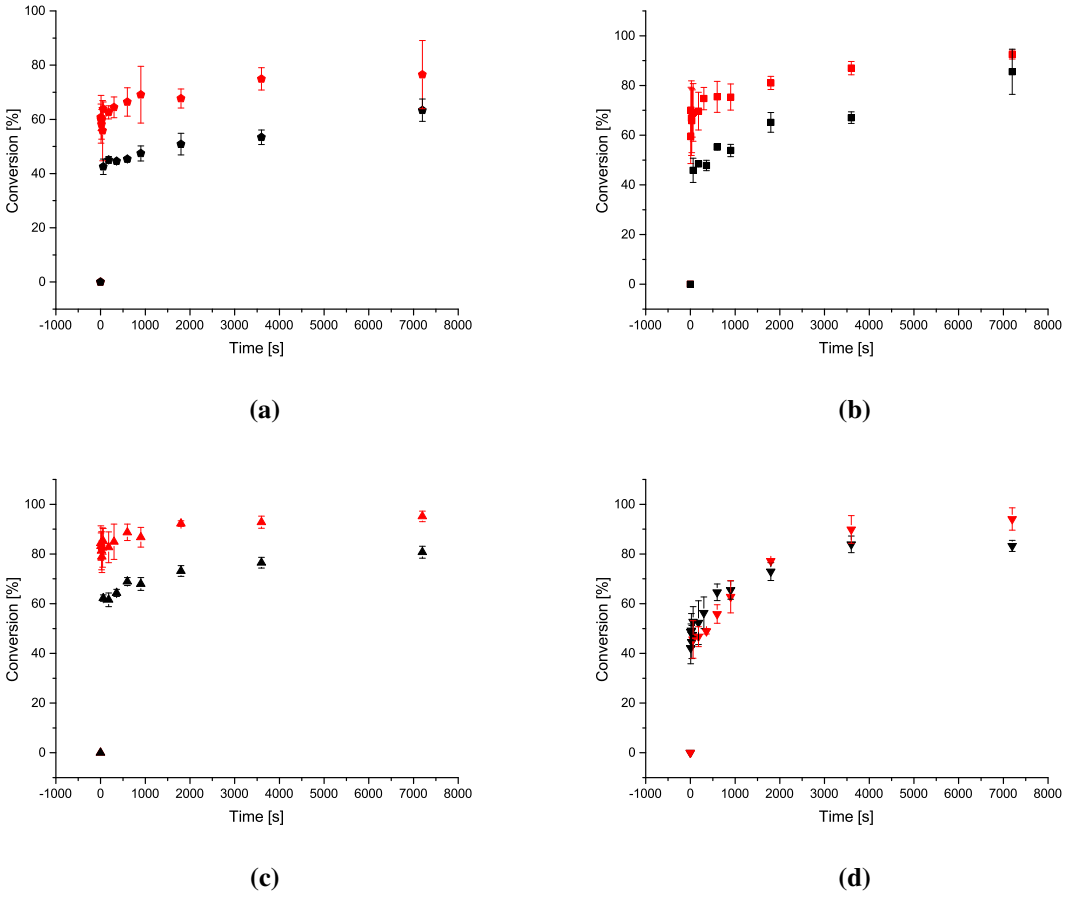

Figure 22: Comparison of conversion over time for the VCP amides and their corresponding esters. While the VCP esters were polymerized in bulk, polymerization of VCP amides was conducted in solution, with anisole as solvent. a) Monomer **1** (black) and monomer **5** (red). b) Monomer **2**(black) and monomer **6**(red). c) Monomer **3** (black) and monomer **7** (red). d) Monomer **4** (black) and monomer **8** (red).

3.2.4 Polymer characterization of monofunctional VCP amides

Polymer properties were characterized using GPC, TGA, and DSC analysis (Table 3.5). All polymers showed unimodal GPC curves with a low–medium molar mass. For the urea bearing polymer, the lowest thermal stability of up to 220 °C was obtained, while changing the sidechain to urethane or amide led to an increase in stability of 100 K. None of the investigated polymers showed a melting peak in DSC analysis, so amorphous polymers could be assumed. The T_g ranges from 32 °C for polymer **32** to 89 °C for the urea-containing polymer. The higher T_g can be explained by the degree of polymerization in the polymer and, therefore, reduced polymer chain mobility. For curves, see sections 4.5.1 to 4.5.3.

Table 3.4: Initial polymerization rate and the overall conversion of the photopolymerization of monomers **5**, **6**, **7**, and **8**.

Polymer	$\bar{M}_n$ [a]	$Đ_M$	T_g [b] [°C]	$T_{5\%}$ [c] [°C]
5	$6.9 \cdot 10^3$	1.4	32	275
6	$1.6 \cdot 10^4$	2.8	55	324
7	$1.1 \cdot 10^4$	1.6	89	221
8	$4.6 \cdot 10^4$	-	69	323

[a] GPC (DMF, PS standard).
[b] Determined by DSC from -60 to 150 °C
with a heating rate of 20 K/min. T_{Onset}
[c] Temperature, where 95% of the original mass is still detectable.
Determined under a nitrogen atmosphere,
measured in a range of 20 to 600 °C
with a heating rate of 10 K/min.

3.3 Investigation of novel bifunctional VCPs

Based on the results obtained in previous sections, urea functional group in the side chain of VCP-amide and VCP-esters appears to be more promising in enhancing the R_p in comparison to the other H-bonding functional groups. Therefore, synthesis of novel bi-functional VCPs with urea in the spacer group connecting the two polymerizable VCP- rings was targeted. Bifunctional monomers, on polymerization, form a stable network, which cannot be dissolved without breaking polymerization down the polymer chains. For any application where the stability of the polymer is essential, these systems are preferably used (see fig. 23).

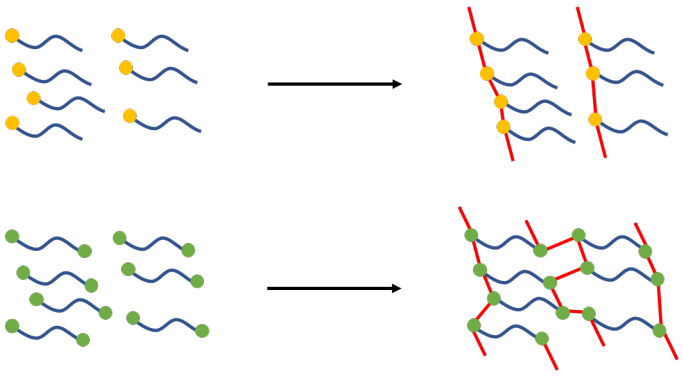

Figure 23: Representative polymer chain formation from monofunctional monomers (up) and bifunctional systems (below). While the monofunctional chains can be separated with the penetration of, e.g., solvents, in bifunctional systems, the crosslinking prevents such behavior.

The polymerization behavior and properties of new bifunctional urea group containing VCP-derivatives were investigated in this section with an aim to obtain versatile fast polymerizing alternatives for dental and coating applications The targeted properties are low shrinking, low viscosity, low toxicity, and rapid polymerization. Rapid polymerization and low volume shrinkage are crucial to outperform currently used methacrylate based materials in dental applications and also for a new class of coating material. A liquid monomer is required in both cases to enable solvent-free polymerization. For medical applications, only non-toxic materials can be used. The following section describes the synthesis of bifunctional VCPs.

3.3.1 Chemical synthesis of bifunctional VCPs

In section 3.1 and section 3.2, urea was the side chain identified to boost the initial R_p. Therefore, the synthesis of bifunctional VCPs bearing an intervening urea unit was targeted. Although the importance of a VCP amide in which amide group links the side chain to the VCP ring in enhancing the rate of polymerization could be confirmed in previous sections, the bifunctional VCP derivatives were prepared using both amide (bifunctional VCP-amide) and ester (bifunctional VCP-ester) linking functionalities (Structures **9** and **10**). Bifunctional VCP ester (**10**) was synthesized as reference material. Aditionally, a side chain with oxalyl diamine was identified as an additional monomer (structure **33**). Here, an additional H-bond acceptor could be introduced, leading to even stronger preorganization. The additional acceptor might increase the viscosity of the resulting monomer since the molecules are more prone to being fixed into a particular position. Conversely, it should simultaneously increase the polymer-

ization rate. Scheme 28 shows the structure of the desired linear bifunctional monomers **9**, **10**, and **33**.

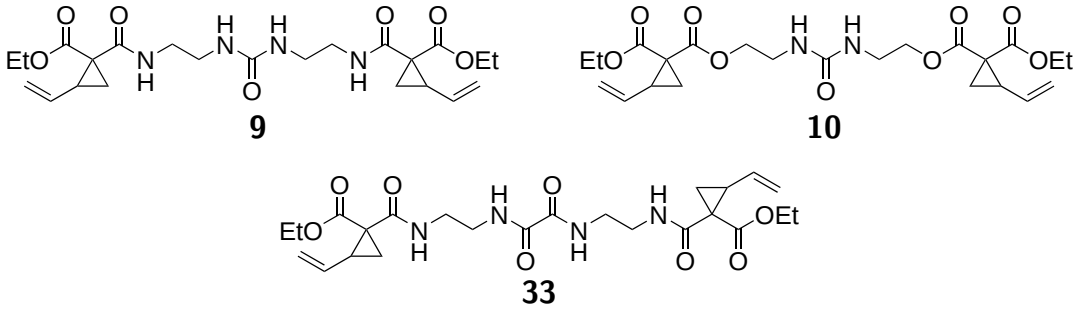

Scheme 28: Linear bifunctional VCP investigated in this section.

Bifunctional VCP derivatives were prepared by the reaction of VCP monoacid with the corresponding diamines or diols (For reaction schemes see page 131 and page 136). The diol and diamine were synthesized according to known literature procedures as shown on pages 130 and 136.[149,150] In case of the diol **34**, with nitrogen being the better nucleophile, a direct synthesis is possible. In case of the diamine **35**, the protected ethylene diamine was used, similar to section 3.2.1. Both products were obtained in a moderate yield and high purity after recrystallization for **34** and precipitation in the case of **35**. Esterification and amidation reactions were used from the same sources as previously described. The presence of monomer **9** and **10** intermediate and final products was confirmed using NMR experiments (for spectra, see section 4.2.5 and figs. 92 to 98 and 100 to 105 on pages 130 to 135 and pages 137 to 140. For FT-IR spectra, see figs. 99 and 106 on pages 135 and 140

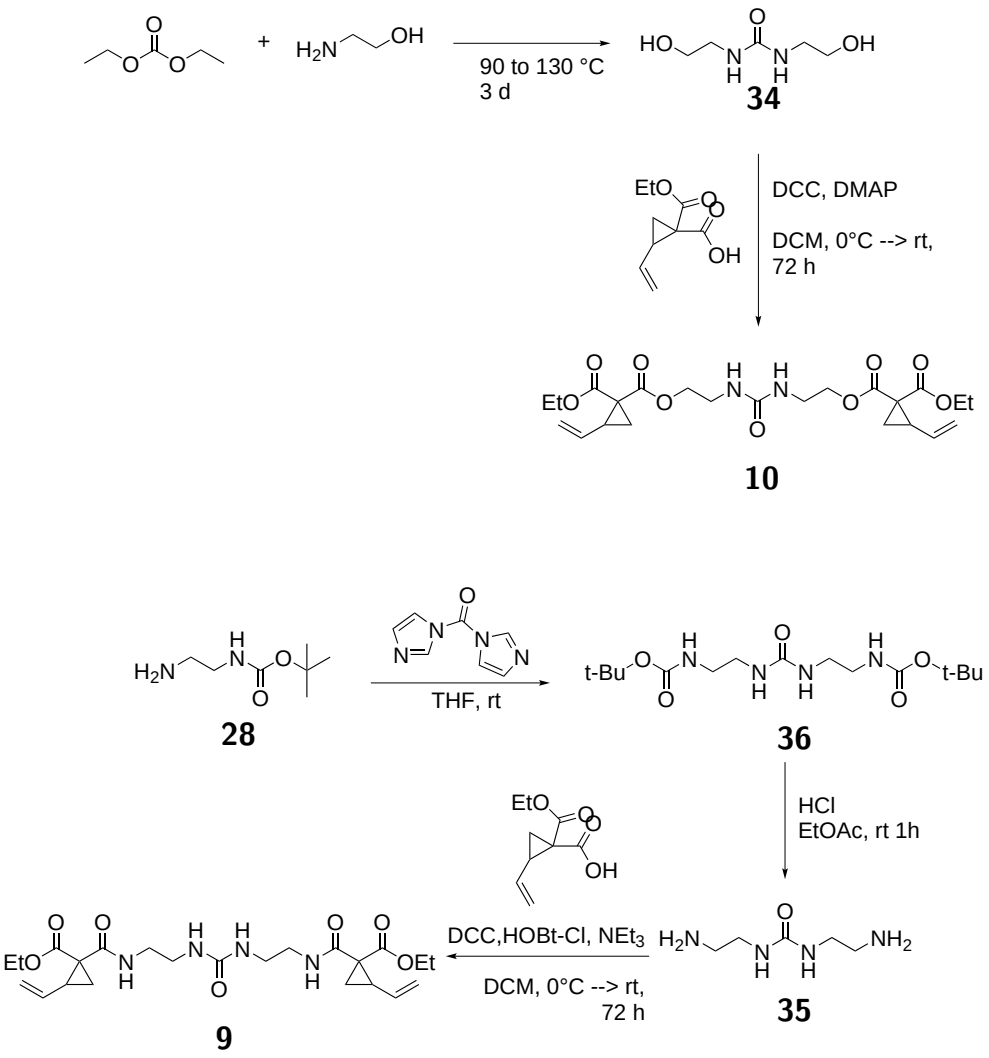

Scheme 29: Synthesis scheme of monomers **9** and**10**

While the bifunctional VCP of the two isomers 2,4,4-trimethylhexane-1,6-diamine and 2,2,4-trimethylhexane-1,6-diamine, which was synthesiszed in Agarwal group by Dr. Pineda[116] and has since been established as benchmark material, was described as a low viscosity monomer, the bifunctional VCP-derivatives obtained in this work were solid. This reason is probably due to the higher degree of preorganization resulting from the urea unit and linear spacer structure, which allows dense packing of the different molecules, which can be confirmed by density measurements of the monomers (Table 3.5).

Table 3.5: Density of monomers **9** and **10** measured by gas pycnometry.

Monomer	Monomer density [g/cm]
9	1.184 ± 0.019
10	1.179 ± 0.011

A second reason might be the lack of different isomers, which prevented high-density molecular stacking.

Synthesis of the oxalyl diamine is also already known in the literature but could not be repeated here. While the first steps (scheme 30, and section 4.2.6) were successful and could be confirmed with NMR experiments, after the deprotection, the obtained solid was insoluble in all of the solvents used, namely acetone, ethyl acetate, methanol, toluene, tetrahydrofuran (THF), methylene chloride (DCM), anisole, DMF, and DMSO, and therefore, could not be analyzed. A small trial reaction was performed to determine whether a reactive amine was present, but synthesis of targeted monomer **33** was unsuccessful. Since no confirmation of the correct product was possible, the synthesis of monomer **33** was not pursued further.

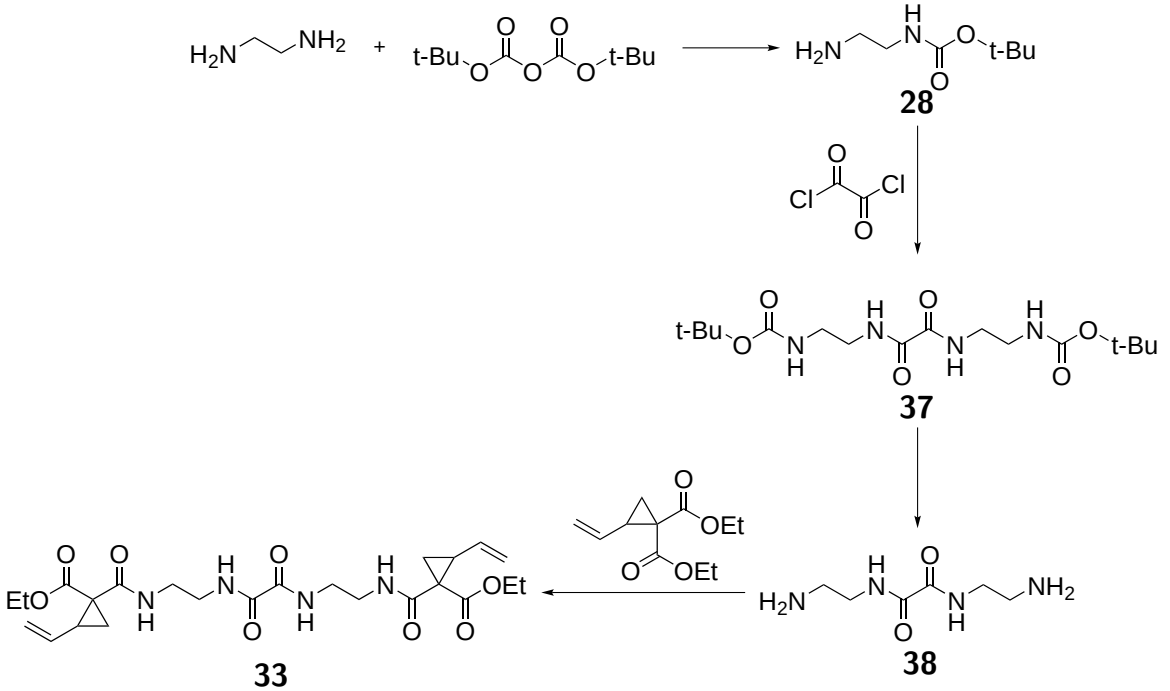

Scheme 30: Synthesis scheme of monomer **33**

Since monomers **9** and **10** showed a high density which leads to a high volume shrinkage, sterically hindered groups should be introduced. Thus, a strong preorganization but less dense packaging is targeted in the next step.

3.3.1.1 Sterically hindered bifunctional VCP amides

Commercially available diamines were used to synthesize novel bifunctional VCPs. Thus, easy access to new material was ensured since the synthesis of the diamines is a multiple-step process and, therefore, is costly and time-consuming. All the amines used are produced in large quantities, registered at the European Chemicals Agency (ECHA) database and, REACH compliant. This and cost-effective production are crucial for transitioning from academia to industrial application. Scheme 31 shows the commercially used diamines and their resulting monomers.

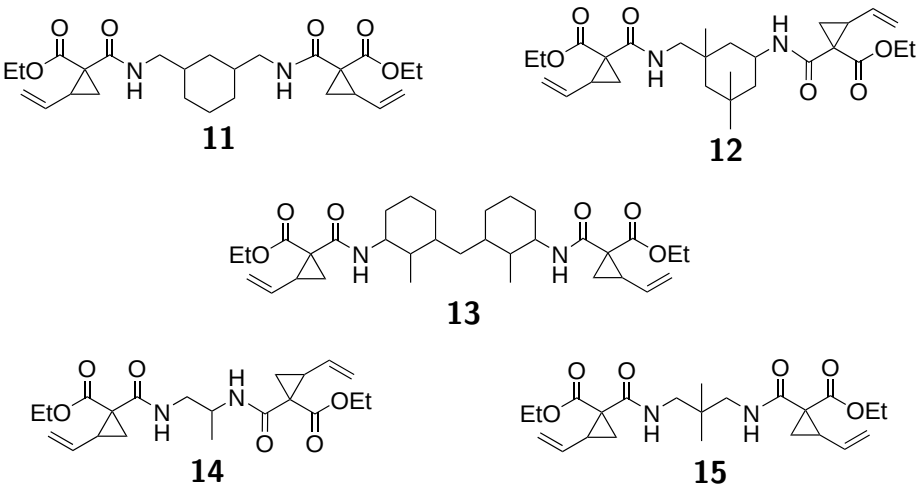

Scheme 31: Structures of sterically hindered VCP amides investigated in this section.

Synthesis , under the same conditions as in section 3.2.1, of all five bifunctional monomers was successful, with yields ranging from 15% for monomer **14** to 68% for monomer **13**. The correct structure was confirmed by different NMR experiments (for spectra see figs. 107 to 112, 114 to 119, 121 to 126, 128 to 133 and 135 to 140. NMR analysis proved difficult for various reasons. For monomers **11** and **13**, the diamine was used in two stereoisomers, leading to several overlapping signals. For monomer **12**, traces of the unreacted diamines remained after purification, so the NMR spectrum was complex to evaluate, underlining the importance of a secondary analysis method to confirm the successful reaction of the desired monomers. Section 4.2.5 presents the NMR spectra with peak assignments of all monomers. The evaluation was conducted as described

in section 3.1.3. Of the synthesized monomers, only monomers **14** and **15** were liquid, while the remainder were obtained as solids. One factor affecting the melting point is the molecule's molar mass.[151] However, preorganization must also be considered since hydrogen bonds can be formed, influencing the physical properties of different molecules. The proportions of the two effects were not investigated in this work.

3.3.2 Cytotoxicity tests

As mentioned above, toxicity measurements are essential in medical applications. Thus, all seven monomers were investigated in a standard assay performed by Matthias Völkl of Prof. Freitag's group, where different concentrations of the DMSO-dissolved monomers, diluted with water, were added to L929 cells and the number of viable cells measured after 24 h. Figure 24 shows the concentration dependencies of the different monomers.

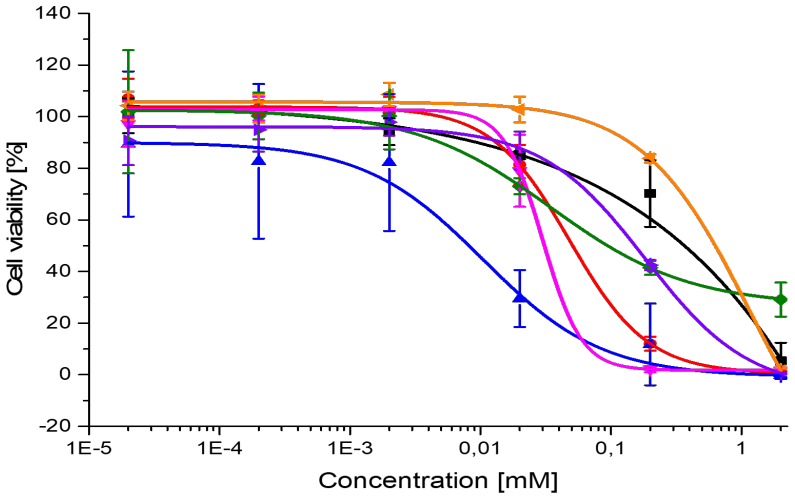

Figure 24: Cell viability with different concentrations of **9** (black), **10** (red), **11** (blue), **12** (pink), **13** (green), **14** (orange), and **15** (purple).

The median lethal dose (LD_{50}), the value at which half of the cells remain alive, is given in table 3.6:

Table 3.6: LD_{50} values of self-synthesized bifunctional VCPs. Tests were conducted with L929 cells over 24 hours.

Monomer	LD_{50} [mM]
9	0.356 ± 0.022
10	0.048 ± 0.003
11	0.010 ± 0.004
12	0.030 ± 0.004
13	0.035 ± 0.004
14	0.632 ± 0.035
15	0.184 ± 0.015

While all cyclohexane-containing monomers show relatively high toxicity, monomer **14** was the least toxic. All monomers were dissolved in DMSO, which is slightly cytotoxic. At the highest concentration of 10 mM after 24 h, 86 ± 12 % of all cells remained alive, meaning the obtained values should have been slightly higher had no solvent been used. However, this effect is lower for a more diluted sample. In previous work, the cytotoxicity of VCPs was investigated and compared to UDMA, a widely used dental filling material.[152,153] In this test, UDMA showed an LD_{50} value of 0.071 ± 0.009 mM, making it three times more toxic than monomer **9**, twice as toxic as monomer **15**, and eight times as toxic as monomer **14** in this study. Based on these measurements, it appears that linear systems are far more favorable. Another observation is the higher toxicity of the VCP ester compared to the amide. Additionally, VCP esters were generelly shown to polymerize much slower. Toxicity tests were performed for 24 hours, while materials remain in the human body for much longer. Therefore, long-term cytotoxicity tests are necessary.

3.3.3 Photopolymerization of sterically hindered bifunctional VCP amides

Kinetic measurements

As in section 3.1.5 and section 3.2.3, monomer conversion was followed over time while irradiating the monomers with light. Since only a fraction of all the monomers obtained were liquid, polymerization was performed in solution with anisole as solvent. The conversion was analyzed using GC for monomers **39** and **40** and NMR for the remaining synthesized monomers. Figure 25 shows the conversion over time.

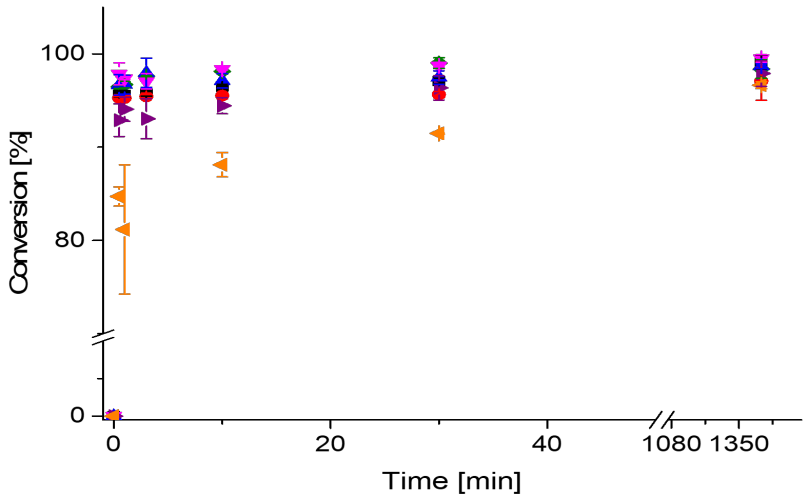

Figure 25: Change in conversion over time for the light-induced RROP of monomers **9** (black), **10** (red), **11** (blue), **12** (pink), **13** (green), **14** (orange), and **15** (purple).

It is evident that all monomers show a high R_p and almost complete conversion after 24 hours (table 3.7). A minor exception is **14**, which has a relatively slow increase in conversion in comparison. The unsymmetric monomeric structure leads to a less degree of preorganisation. As a result, a slower polymerization can be observed.
The highest R_p is observed for **12**, closely followed by **11** and **13**. The bulky cyclohexane rings do not affect the polymerization behavior. All three diamines were supplied as stereoisomers with an unknown ratio. While this should reduce the degree of preorganization, nothing is observable from the polymerization rate.

With **10** showing a slightly slower polymerization behavior than the amide equivalent **9**, the effect of the additional H-bond is demonstrated again. However, the urea group might have helped minimize the difference. Nevertheless, both sterically hindered linear systems show the lowest R_p, with **15** being the fastest, probably due to the above-mentioned reason. This study underlines the importance of considering the functional groups and the overall structure.

Table 3.7: Overall conversion and R_p for monomers **9**, **10**, **11**, **12**, **13**, **14**, and **15**.

Monomer	Overall conversion [%]	R_p [%/s]
9	99.13 ±0.74	1.85 ± 0.58
10	97.09 ±2.06	1.87 ± 0.61
11	98.69 ±0.25	1.96 ± 0.47
12	99.51 ±0.41	2.84 ± 0.51
13	99.02 ±0.57	1.78 ± 0.50
14	96.65 ± 0.37	1.41 ± 0.19
15	97.90 ±1.39	1.96 ± 0.47

3.3.4 Polymer characterization of bifunctional VCP amides

Since bifunctional systems form a network, determination of the molecular mass via GPC is impossible. The thermal stability of monomers **9**, **10**, **11**, **12**, **13**, **14**, and **15** was analyzed by TGA. TGA curves and $T_{5\%}$ values are shown in section 4.5.3 and table 3.8.

The most significant difference is observed between urea-linked, linear systems which showed much lower stability than more hindered and rigid structures for the remaining polymers. Their degradation temperature is in the same range found for polycarbonates and slightly higher than that found for monofunctional VCP amides (Table 3.8).

Table 3.8: Thermal stability and glass transition temperature of the corresponding polymers to monomers **9**, **10**, **11**, **12**, **13**, **14**, and **15**.

Polymer of monomer	T_g[a] [°C]	$T_{5\%}$[d] [°C]
9	112	236
10	84	224
11	143[b]	329
12	164[c]	340
13	158[c]	343
14	97	329
15	83	335

[a] Determined by DSC from -40 to 150 °C with a heating rate of 20 K/min;
[b] -40 to 180 °C with a heating rate of 20 K/min; [c] -40 to 200 °C at 20 K/min;
[d] Temperature, where 95% of the original mass is still detectable.
determined under a nitrogen atmosphere, measured in a range of 20 to 600 °C with a heating rate of 10 K/min.

3.3.5 Determination of volume shrinkage

Low volume shrinkage is one reason for using VCPs in polymer chemistry. Steric hindrance is reported as a tool to work against shrinkage and obtain even volume-expanding VCPs.[116,154] A second factor is rapid polymerization. Both favor the inter- rather than the intramolecular attack. As mentioned in section 3.1.6, the intramolecular attack leads to a cyclobutane structure responsible for the volume shrinkage. A more direct method of measuring volume shrinkage is the change in density from monomer to polymer. The monomer density was determined with a gas pycnometer, since it enables the exact measurement of liquid and solid samples. Air encapsulations, which cannot be reached with helium gas, are a drawback of this technique. Therefore, an alternative method was selected for less porous structures with a fixed geometry, as for precipitated polymer samples. The Archimedes method was used for polymer samples, where density is measured based on the weight change between the sample in air and in a liquid with a known density, in this case, water. Figure 26 and table 3.9 show the volume shrinkage of bifunctional VCP.

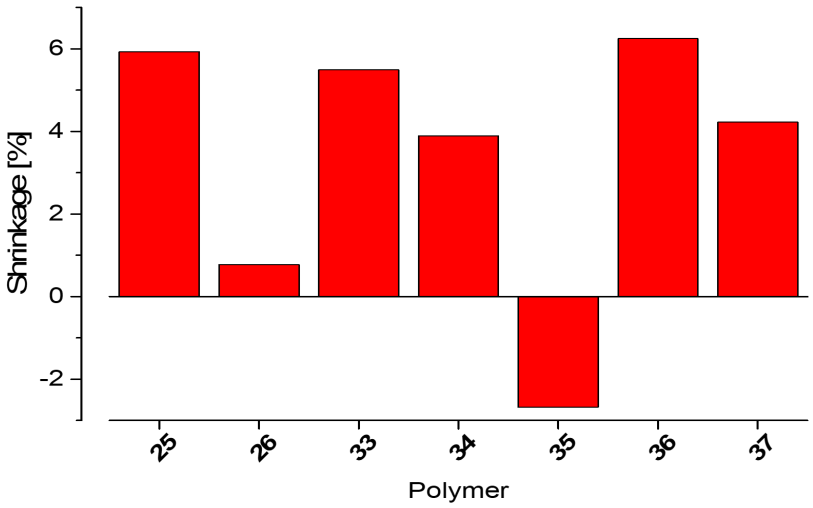

Figure 26: Volume shrinkages of bifunctional polymers **9**, **10**, **11**, **12**, **13**, **14**, and **15**, determined by the difference in density between monomer and polymer.

All investigated monomers show a shrinkage of 4–6%, all in the range of commonly used dental matrixes, and the VCP previously presented by the Agarwal group benchmark molecule[116] with two exceptions: monomer **10** with a shrinkage of 0.8% and **13**, which even shows an expansion of 2.8%. The only known example of a volume-expanding VCP containing monomer, with an expansion of 6.1%, contains adamantane units to

induce this effect (scheme 32).[154] Monomer **13**, due to a much more straightforward approach, is a good alternative for this known system.

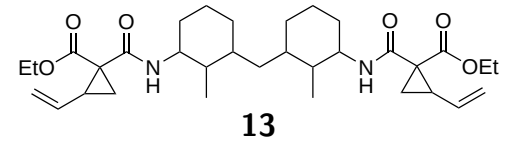

13

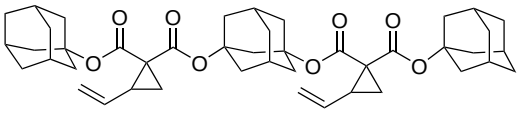

41

Scheme 32: Volume-expanding VCP amide **13** and the already known expanding adamantyl VCP monomer **41**.

Since a rapid ring opening polymerization should lead to low volume shrinkage,[116] the lowest shrinkage is expected for monomers **12**, **11**, and **13**, while monomers **14** and **15** should show the highest shrinkage. In the obtained results, monomer **13** showed the lowest shrinkage, followed by monomer **10**, which is inconsistent with the kinetic measurements.

As mentioned above, steric hindrance is also a significant factor. In the case of monomer **13**, the VCP amide has a direct connection to the cyclohexane ring. Therefore, molecular mobility is reduced and backbiting is less likely. This also explains the high shrinkage of monomer **11**, despite the rapid polymerization, where, due to the more flexible $-CH_2-$cyclohexane connection, more molecular movement is possible. The linear and less sterically hindered structures also show relatively high shrinkage, with VCP amide **9** having the highest shrinkage.

The high shrinkage of **14** is probably explainable due to its asymmetric nature, less orientated monomer structure, and slower polymerization. This differs for **15**, where the reduced molecular mobility causes less backbiting and, consequently, much lower shrinkage. The same applies to **12**, where the direct connection to the cyclohexane ring on the one side and the additional methyl substituent on the other lead to reduced shrinkage.

Table 3.9: Monomer and polymer density of monomers **9**, **10**, **11**, **12**, **13**, **14**, and **15** and calculated volume shrinkage.

Monomer	Monomer density[a] $[g/cm^3]$	Polymer density[b] $[g/cm^3]$	Volume shrinkage [%]
9	1.184	1.259	5.9
10	1.179	1.188	0.8
11	1.069	1.131	5.5
12	1.058	1.101	3.9
13	1.066	1.038	-2.7
14	1.080	1.152	6.2
15	1.058	1.105	4.2

[a] determined by gas pycnometry.
[b] determined by the Archimedes method in H_2O.

3.4 Conclusion

This work shows the successful synthesis of nine new monofunctional and seven new bifunctional VCPs. All molecules were fully characterized.
The first set of five monomers, all monofunctional VCP esters with different functional groups in the side chain, showed the highest strength of hydrogen bonds in the case of urea, followed by urethane, amide, and finally, carbonate not capable of forming hydrogen bonds. This behavior could also be observed on the initial rate of polymerization; however, viscosity, increased by a high degree of preorganization, countered the effect to a certain extent, which was analyzed using photorheology. As a result, the amide containing VCP was identified to show the best overall behavior.
On changing from VCP esters to VCP amides, the following four monofunctional monomers, led to completely solid monomers and much faster polymerization, although solvent use was necessary. As similar trend, as observed for VCP esters, could be observed with the urea containing VCP showing the highest rate of polymerization, followed by urethane. The carbonate bearing VCP showed a much increased rate of polymerization but remains the slowest of the investigated monomers.

For bifunctional VCP, new aspects of these systems could be shown, one being the lower toxicity of linear structures, compared to cyclohexane-containing VCPs and the higher toxicity of ester functional groups compared to the amide-bearing equivalent. Differences in the polymerization rate could be correlated with structural differences, one

being the uneven effect of monomer **14**, where the two hydrogen donor point in differen directions, leading to a less ordered macrostructure and, consequently, a slower polymerization. However, the bulkiness of the substituents did not lead to slower polymerization. This bulkiness, implemented to reduce volume shrinkage, prohibits backbiting, the most significant cause of volume shrinkage for VCPs, especially when intramolecular mobility is restrained. Thus, volume expansion of **13** was possible. Generally, the impact of VCPs on volume shrinkage could be demonstrated, with shrinkage being roughly 4–6% compared to 21% for PMMA. While dental applications were targeted in this work, low toxicity and shrinkage are also significant in other applications such as medical 3D printing, indicating the same materials might be usable in both cases. While several new materials were synthesized and their basic properties investigated, mechanical properties are also necessary for the application, which could not be obtained in this work due to unsuccessful specimen preparation and the ultimate lack of material. Of the seven VCPs, only two were liquid (monomers **14** and **15**) and, therefore, usable as such. For the others, additives or solvents would be necessary to convert them into a liquid. This, as well as the formulation of the exact composition of new systems, is the task of future researchers.

3.5 Outlook

The high versatility of VCPs has been shown by various groups over the past years, with dental fillings being only a tiny proportion.

A growing field where different techniques and materials have been intensively investigated is 3D printing.[155] The most common technique is fused deposition modeling, where a continuous flow of melted filament is produced and printed in the desired shape. While structures otherwise impossible to form can thus be built, its relatively low precision limits the field of application. Therefore, other techniques are preferred in medical 3D printing.

The most commonly used method is powder sintering, where a material is exposed to a laser beam and thereby selectively cured.[156] While this is already implemented to build implants and models of the patient's anatomy for better surgery planning, this technique is expensive due to its complexity and the machines required.[157] Using a liquid platform and light to cure the desired form selectively enables faster, easier, and cheaper specimen production for crafting very fine and complex structures.[158] VCPs would be a suitable platform for this type of 3D printing due to their rapid polymer-

ization and low shrinkage, both essential properties for a highly effective process.
As the spacer between the VCP units can be easily modified, antimicrobial or water-soluble monomers are likely. Thus, the formation of hydrogels, for example, in tissue engineering, is feasible. Different photoinitiators might be necessary, to ensure good crosslinking and rapid polymerization in an aqueous solution.

Since sustainability is becoming an increasingly critical part of society, investigating bio-based linkers would be of interest. These can be naturally occurring amines or molecules that can be easily converted into them.

Functional groups in bio-based molecules can be reacted to form amines, the most common being alcohols via ammonolysis[159] and unsaturated carbons via hydroamination reactions.[160,161] Acids, for example, in fatty acids, might be either reacted to form epoxides, standard products in the epoxy industry, which can then react with aqueous ammonia to form amines[162] or transformed into aldehydes or alcohols which can also be reacted to form amines.[163,164]
Several molecules are also available from the enzymatic fermentation of biomass, such as 1,3-propanediol and 1,4-butanediol.

Another aspect is reevaluating the synthesis of VCPs to use bio-based resources and reduce waste throughout the process (Figure 27).

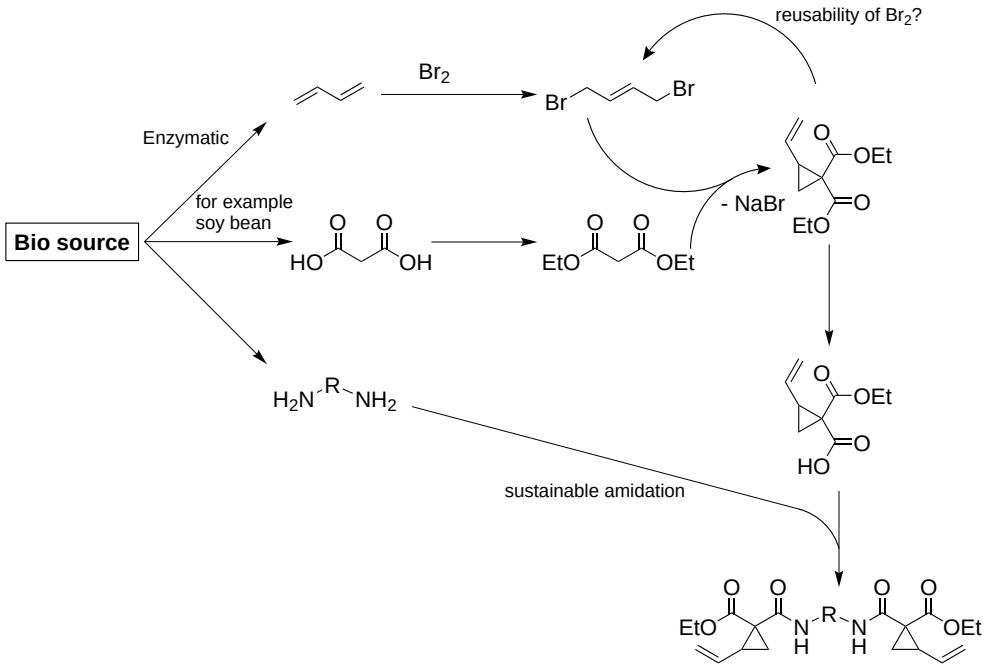

Figure 27: Possible bio-based and sustainable synthesis of bifunctional VCP amides.

Various publications exist on the bio- or chemical synthesis from a bio source of butadiene[165,166] as well as malonic acid.[167,168] Malonic acid is also known to be present in plants such as legumes.[169,170] Recyclability is another factor in a sustainable synthesis. Bromine can be used to convert butadiene into the desired dibromide. This is then eliminated in the next step, forming NaBr. Therefore, bromide recycling is an important step in reducing waste. Additionally, a more sustainable bromination can be considered. Much research has been conducted in this field, although *Sabuzi et al.* showed in their review that not all processes declared sustainable adhere to all the principles of green chemistry.[171] Another focus is on an alternative amidation reaction.[172,173] DCC enables a mild amidation reaction and increases the yield, as the water formed is removed by forming an insoluble urea compound. From a sustainability viewpoint, this process could be improved due to its poor atomic economy. Therefore, alternative amidation reactions should be considered.

4 Materials and methods

4.1 Analytical methods

^{1}H- (300 MHz) and ^{13}C-NMR spectra (75 MHz) were recorded on a Bruker Ultrashied-300 spectrometer at room temperature. To distinguish between primary and tertiary or secondary and quarterly carbons, ^{13}C APT was conducted. The two-dimensional NMR heteronuclear single quantum coherence experiments were performed to observe ^{1}J coupling and heteronuclear multiple bond correlation experiments for coupling J>1. Solid-state NMR (2.0 kHz) was recorded on a Bruker Advance III HD NMR 400 (field strength 9,4 T) with a 3.2 mm sample carrier. Variable ^{1}H temperature experiments have been performed from 25 °C to 60 °C .

GPC was performed using an SDV XL gel column (particle size = 5μm with a separation range of 100 - 3 000 000 Da)and a refractive index detector (1200 series, Agilent Technologies). Chloroform or DMF was used as the solvent and eluant with a flow rate of 0.5 ml min^{-1}.The calibration was performed with a narrowly distributed polystyrene homopolymer (PSS calibration kit). Before measurement, the sample was dissolved in chloroform/ DMF and filtered with a 0.22 μm PTFE filter. The injection volume was 20 μl. Toluene served as the internal standard

DSC measurements were performed on a NETZSCH DSC 204 F1 Phoenix under a nitrogen atmosphere with a 20 ml /min flow.

TGA was performed in alumina pans with sample masses of around 5 mg and a flow rate of 20 ml per minute on a NETZSCH Libra F1 device.

Photo rheology measurements were performed on an Anton Paar MCR 302 rheometer. Rotational tests were performed between a glass plate with Peltier temperature control and a cone with a diameter of 25mm and an angle of 2° with a frequency of 1 Hz. The sample was irradiated with an Omnicure S2000 light source and an intensity of 2W/cm^{2} at the light source. All rheology measurements were performed under nitrogen gas using a Peltier temperature-controlled hood and a constant gas flow of 200 L/h.

Cytotoxicity tests were performed in the group of Prof. Freitag by Matthias Völkl as a

standard L929 essay.
Density measurements by gas pycnometer were measured on an AccuPyc 1330 gas pycnometer (Micromeritics) with helium used as measuring gas.

4.2 Chemical synthesis

4.2.1 General remarks

1,4-Dibromo-2-butene, diethyl malonate, sodium, ethanolamine, methyl chloroformate, ethylamine, ethylenediamine, *tert*-butyl dicarbonate, oxalyl chloride, $LiAlH_4$ powder, isophorone diamine, 2,2-dimethylpropane-1,3-diamine, valinamid-hydrochloride, 2-chloropropane, and CQ were supplied by Aldrich and used without further purification. Ethylene glycol, DMAP, and EDMAB (Fluka) were used without further purification. Ethyl isocyanate, ethyl chloroformate, N-Boc-ethanolamine, ethylenediamine, DCC, 1,1'-carbonyldiimidazole (CDI), and ethylene carbonate were supplied by Alfa Aesar and used without further purification. Diethyl carbonate, 6-Chlor-1-hydroxy-1H-benzotriazole, nitromethane, malononitrile, boron trifluoride - ethyl ether complex, and propane-1,2-diamine were supplied by TCI and used without further purification. Sodium bicarbonate, a cis and trans mixture of 1,3-cyclohexanebis(methylamine) and 3,3'-methylenebis(2-methylcyclohexan-1-amine), tert-Butylchloride, and $AlCl_3$ (Fisher chemical) was used without further purification. Potassium hydroxide (Carl Roth), propionic acid, and triethylamine (Güssing) were used without further purification. Sulfuric acid and ammonium chloride were supplied by VWR and used without further purification. All solvents were distilled before use.

4.2.2 Synthesis of 1-(ethoxycarbonyl)-2-vinylcycloporpane-carboxylic acid

2-vinylcyclopropane-1,1-dicarboxylate

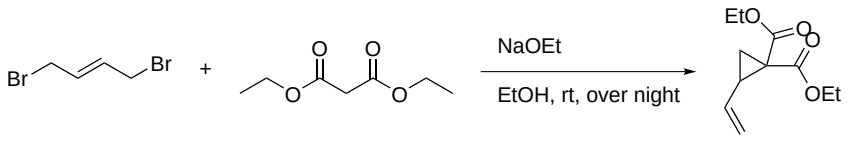

42

The synthesis was performed as reported before[110]. Under argon, trans-1,4-dibromobutene-2 (12.0 g, 56 mmol) and malonic acid diethyl ester (1 eq, 9.0 g, 56 mmol) were dissolved in 40 ml of predried absolute ethanol. At room temperature freshly prepared sodium ethanolate (2.2 eq, 68 ml, 67.3 mmol) was added slowly. The reaction mixture was stirred at room temperature over night and conversion was monitored via GC-analysis. The reaction mixture was filtered, washed with ethanol and the solvent was removed under reduced pressure. The remaining product was filtered again and washed with diethylether. The organic phase was washed with water, saturated sodium chloride solution, dried over Mg_2SO_4 and the solvent was removed under reduced pressure. After purification via flash chromatography (Cylcohexane:EtOAc 10:1) the purified product **42** was obtained as colorless liquid in a yield of 90 % (10.7 g, 50.2 mmol).

^{1}H NMR (300 MHz, $CDCl_3$, 293K):

δ [ppm] = 5.41 (m, 1H), 5.31 (dd, 1H), 5.12 (dd, 1H), 4.19 (m, 4H), 2.58 (q, 1H), 1.68 (q, 1H), 1.55 (q, 1H), 1.27 (t, 6H) ppm.

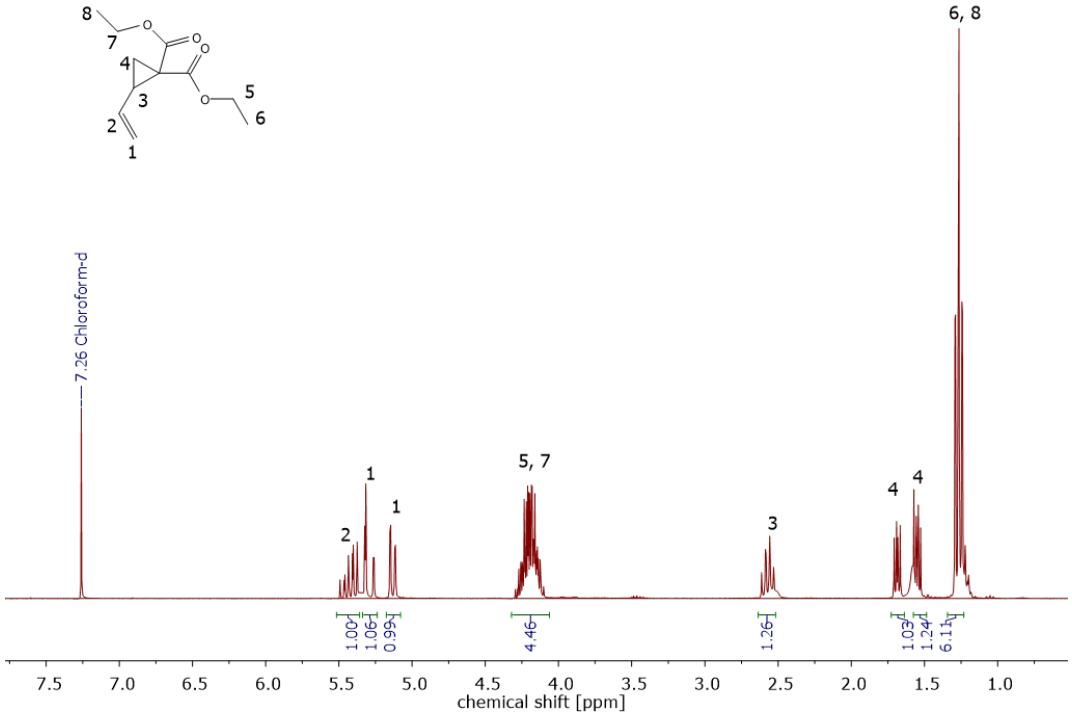

Figure 28: ^{1}H NMR of **42**.

1-(ethoxycarbonyl)-2-vinylcycloporpane-carboxylic acid

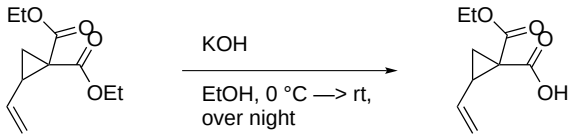

42 **43**

The synthesis was performed as reported before[102]. Under argon, at -5 °C in 40 ml predried ethanol dissolved KOH (5.5 g, 98.9 mmol, 1.05 eq) was slowly added to a solution of **42** (20.0 g, 94.2 mmol), dissolved in 10 ml predried ethanol. Temperature should not surpass 5 °C . The mixture was stirred at room temperature over night. The solvent was evaporated under reduced pressure, and the crude product was dissolved in 100 ml of water with pH=9. The solution was washed three times with Et_2O, acidified to pH=2 and extracted with Et_2O. After washing with saturated NaCl solution and evaporating the solvent, the product **43** was obtained as a colourless liquid in a yield of 54% (9.24 g, 50.2 mmol).

^{1}H NMR (300 MHz, $CDCl_3$, 293K):

δ [ppm] = 5.66 (m, 1H), 5.40 (dd, 1H), 5.25 (dd, 1H), 4.29 (m, 2H), 2.76 (q, 1H), 2.15 (dd, 1H), 2.00 (dd, 1H). 1.32 (t, 3H) ppm.

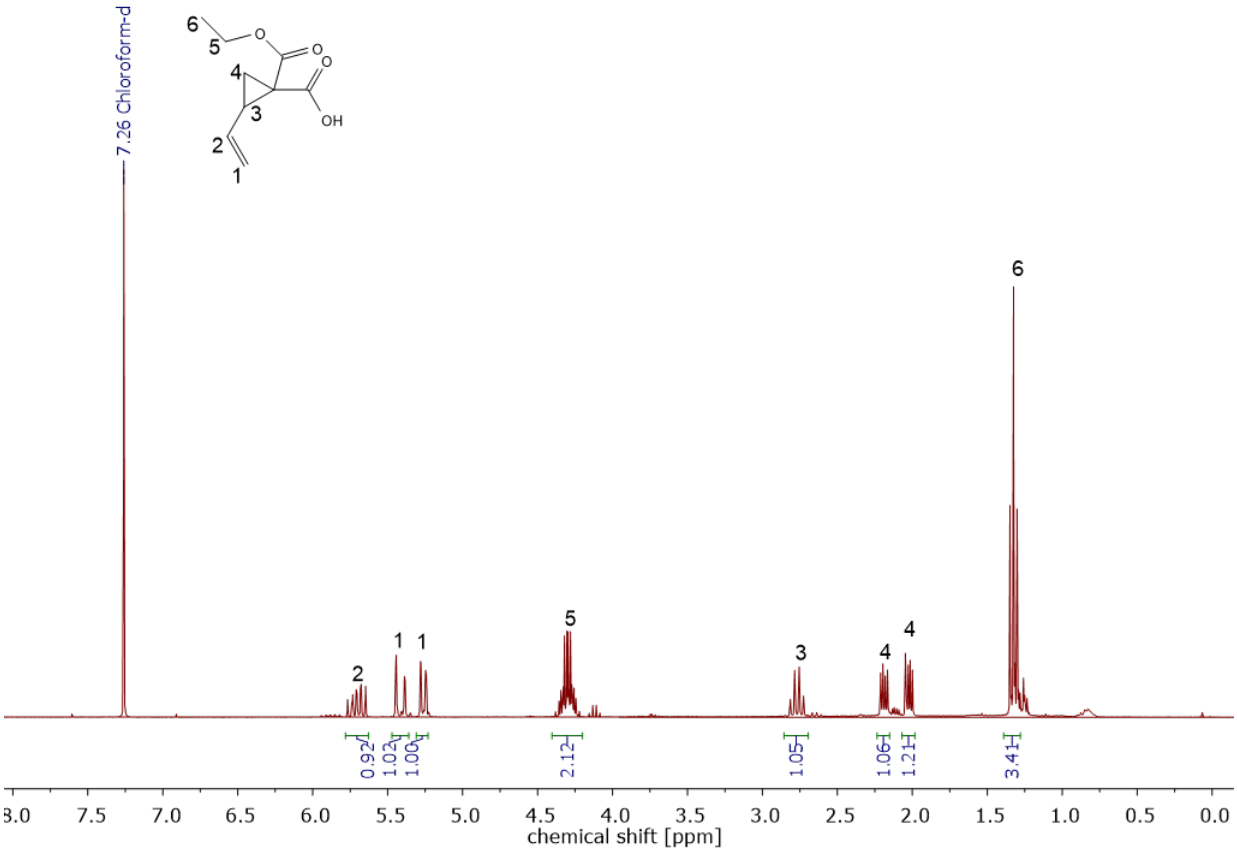

Figure 29: ^{1}H NMR of **43**.

4.2.3 Synthesis of Monofunctional VCP esters

Ethyl (2-hydroxyethyl) carbonate

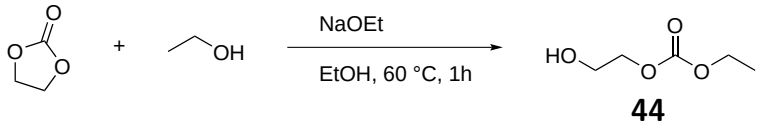

44

Under argon, NaOEt (0.03 eq, 235 µl, 3 mmol) was added slowly to in 35 ml of predried ethanol dissolved ethylencarbonate (8.81 g, 100 mmol). The mixture was stirred at 60 °C for 1 h. The reaction was quenched by adding water and the mixture was extracted with DCM. the organic phase was dried over Mg_2SO_4, filtered and the solvent was removed under reduced pressure. After purification by flash chromatographie (Cylcohexane:Ethylactetate 7:3) the product **44** was obtained as yellow liquid in a yield of 11 % (1.44 g, 10.7 mmol).

^{1}H NMR (300 MHz, $CDCl_3$, 293K):

δ [ppm] = 4.23 (m, 2), 4.20 (m, 2H), 3.85 (t, 2H), 1.32 (t, 3H) ppm.

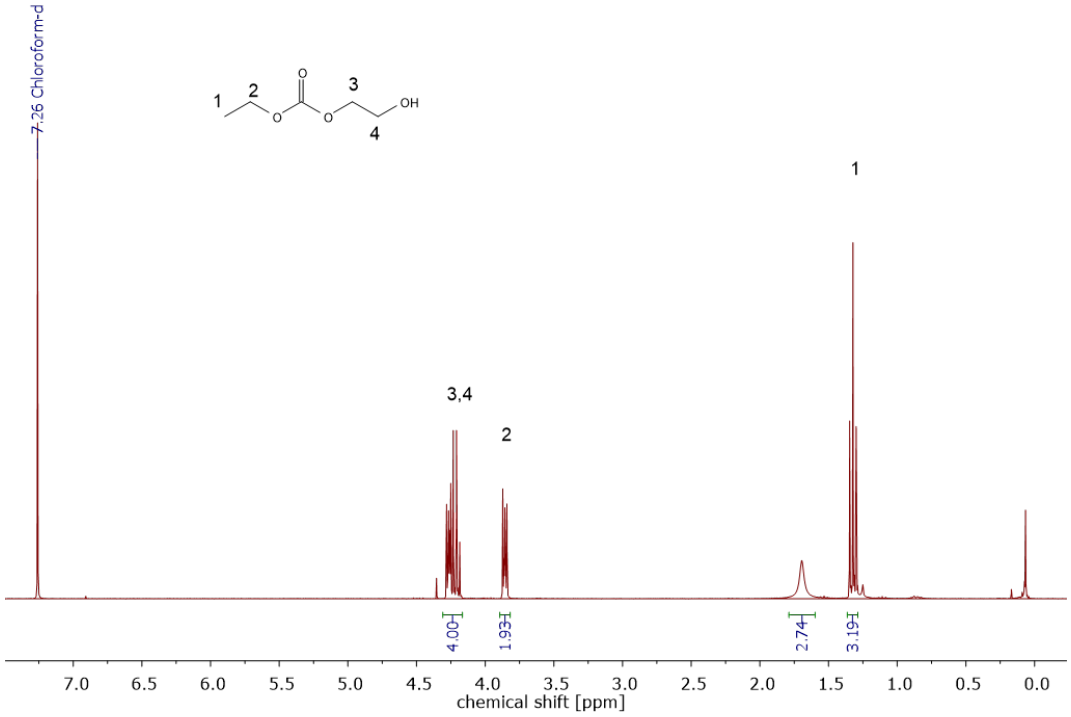

Figure 30: ^{1}H NMR of **44**.

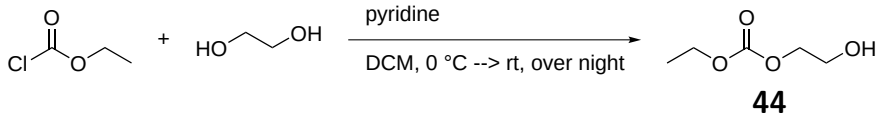

This compound was synthesized as reported before[138]. Under argon ethyl chloroformate (10 g, 81.6 mmol) was dissolved in 50 ml dry DCM. At 0 °C pyridine (3 eq, 19.8 ml, 244.8 mmol) and ethylene glycol (3 eq, 16.9 ml, 244.8 mmol) were slowly added. The reaction was stirred at room temperature for 20 h. The solvent was removed under reduced pressure and the product **44** was obtained as a colourless oil in a yield of 15 % (1.63 g, 12.2 mmol).

^{1}H NMR (300 MHz, $CDCl_3$, 293K):

δ [ppm] = 4.32 – 4.14 (m, 4H), 3.88 – 3.82 (m, 2H), 1.32 (t, J = 7.1 Hz, 3H) ppm.

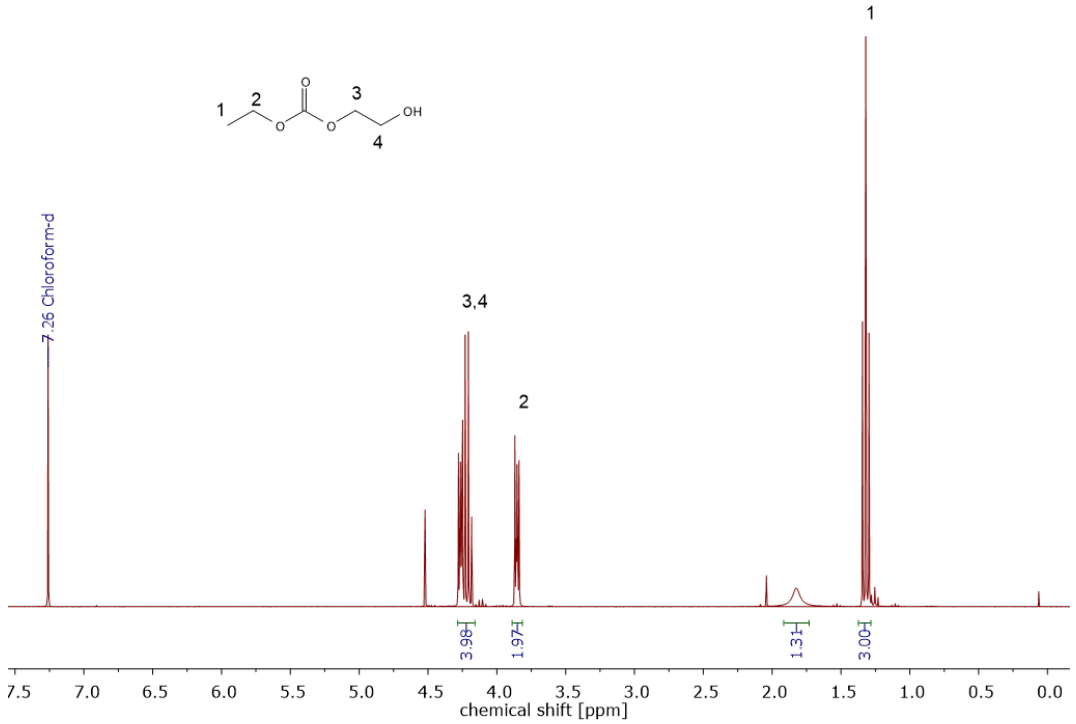

Figure 31: ^{1}H NMR of **44** second synthesis path.

1-(2-((Ethoxycarbonyl)oxy)ethyl) 1-Ethyl 2-vinylcyclopropane-1,1-dicarboxylate

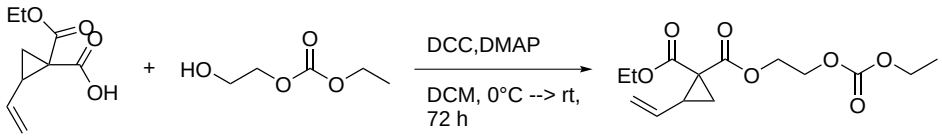

43 **44** **1**

Under argon 4.07 g of **43** (22.0 mmol), DMAP (0.11 eq, 268 mg, 2.2 mmol)), and **44** (1.1 eq, 3.68 g, 24.0 mmol) were dissolved in 50 ml dry DCM. At 0 °C in 30 ml dry DCM, dissolved DCC (1.1 eq, 5.02 g, 24.0 mmol) was slowly added. The reaction was stirred at 0 °C for one hour and at room temperature for 17 h. The reaction mixture was filtered, and the filtrate was washed three times with 0.5 M HCl, saturated $NaHCO_3$, and saturated NaCl solution, respectively. The organic phase was dried over $MgSO_4$, and the solvent was removed under reduced pressure. The product **1**was obtained after purification using flash chromatography (Cylcohexane:EtOAc 95:5) as a slightly yellow liquid in a yield of 40 % (2.64 g, 8.8 mmol).

^{1}H NMR (300 MHz, $CDCl_3$, 293K):

δ [ppm] = 5.52 – 5.34 (m, 1H), 5.30 (dd, J = 17.2, 1.8 Hz, 1H), 5.18 – 5.08 (m, 1H),

4.48 – 4.27 (m, 4H), 4.27 – 4.09 (m, 4H), 2.60 (dd, J = 16.8, 7.9 Hz, 1H), 2.04 (s, 1H), 1.74 (dd, J = 7.6, 5.0 Hz, 1H), 1.58 (s, 3H), 1.31 (t, J = 7.1 Hz, 3H), 1.26 (t, J = 7.1 Hz, 3H).

^{13}C NMR (75 MHz, $CDCl_3$, 293K):

δ [ppm] = 169.6, 167.2, 155.0, 133.0, 118.9, 65.2, 64.4, 63.2, 61.7, 35.8, 31.5, 20.8, 14.3.

FT-IR (ATR mode): 2986, 1724, 1639, 1446, 1394, 1373, 1319, 1278, 1247, 1196, 1130, 1027, 990, 960, 917, 863, 789, 747, 710, 666 cm-1.

HRMS (ESI, pos.) m/z calculated for $C_{14}H_{20}NaO_7$ $[M + Na]^+$ 323.1107, found 323.1099

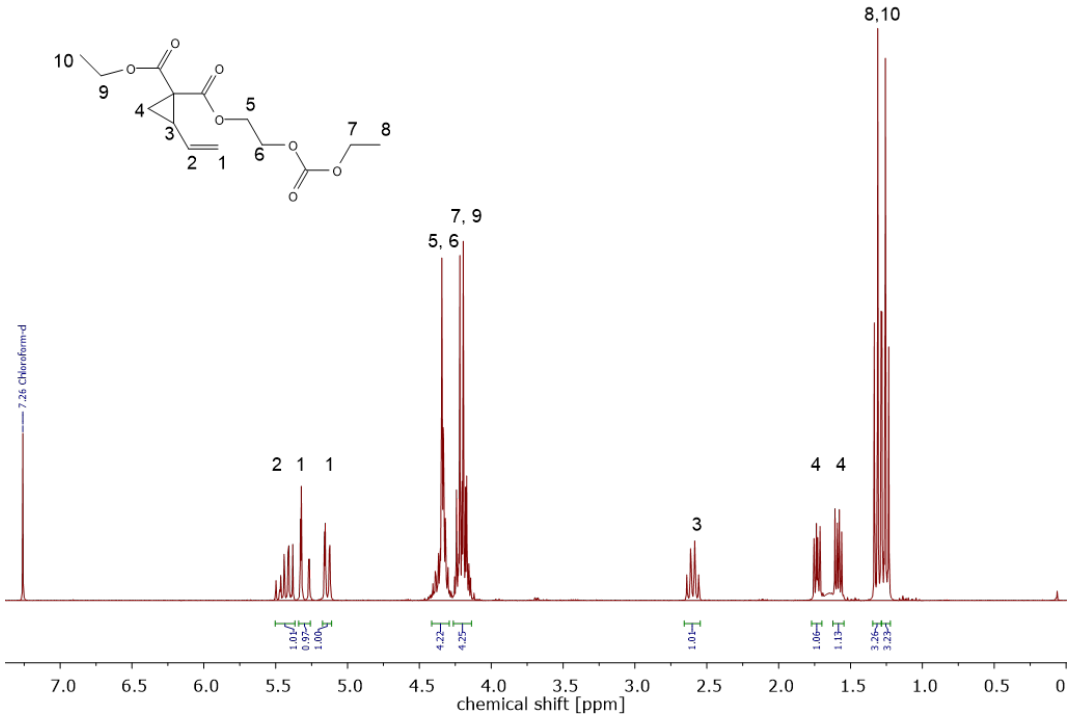

Figure 32: ^{1}H NMR of VCP **1**.

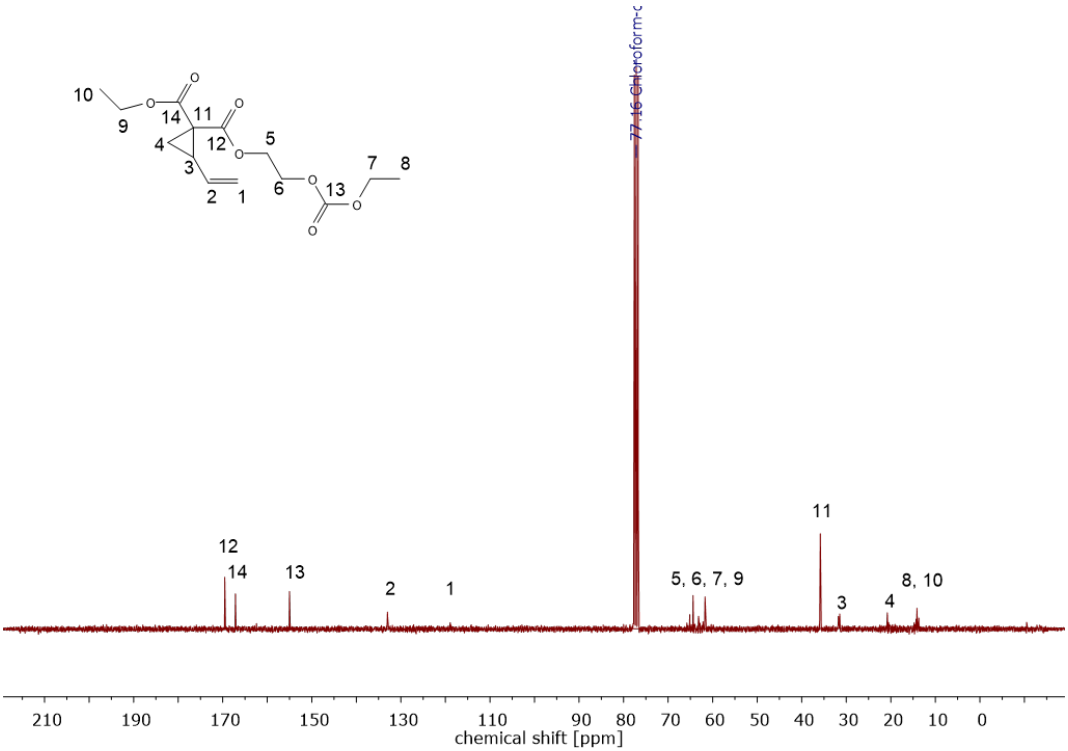

Figure 33: ^{13}C NMR of VCP **1**.

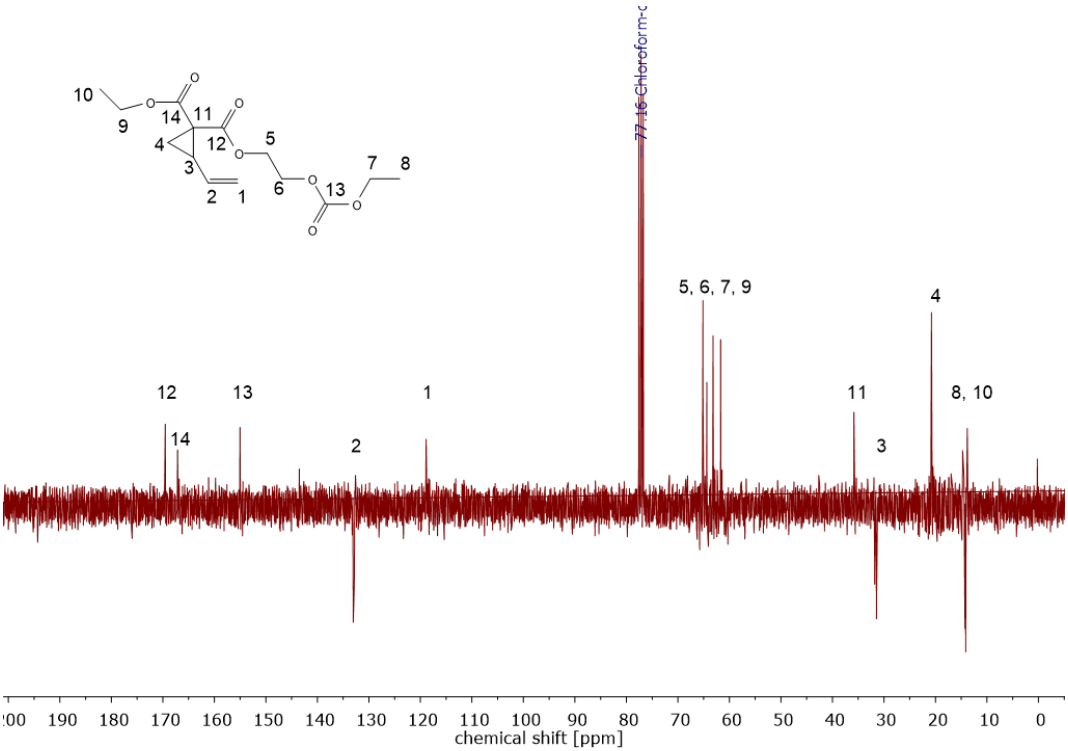

Figure 34: ^{13}C APT NMR of VCP **1**.

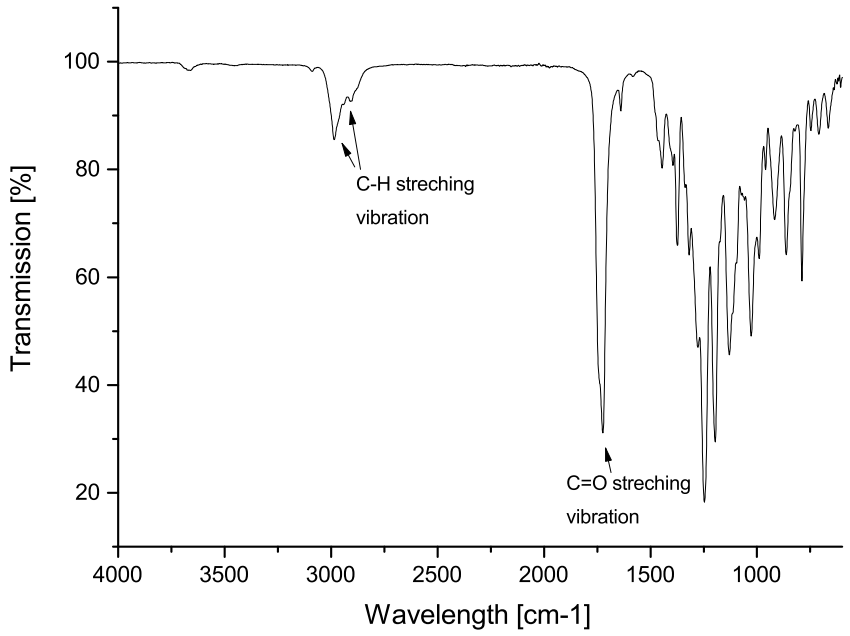

Figure 35: FT-IR of **1**.

Ethyl (2-hydroxyethyl)carbamate

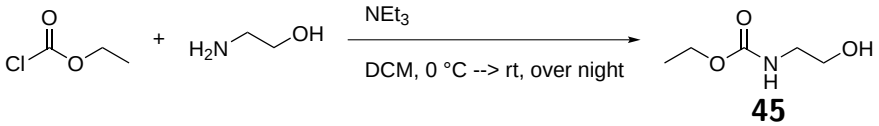

45

Under argon, ethanolamine (1.2 g, 20.0 mmol) was dissolved in 40 ml dry DCM. At 0 °C , 3.3 ml NEt_3 was added, and ethyl chloroformate (1.2 eq, 2.6 g, 24 mmol) was added dropwise. The reaction mixture was stirred at 0 °C for one hour and room temperature overnight. The solvent was removed under reduced pressure, the mixture dissolved in ethyl acetate (EtOAc), and filtered. After removing the solvent under reduced pressure, the mixture was purified via flash chromatography (Cylcohexane:EtOAc 2:8). The product **45** was obtained in a yield of 44% (1.2 g, 8.8 mmol).

^{1}H NMR (300 MHz, $CDCl_3$, 293K):

δ [ppm] = 5.06 (s, 1H), 4.21 – 4.06 (m, 2H), 3.77 – 3.67 (m, 2H), 3.34 (d, J = 4.7 Hz, 2H), 1.25 (dd, J = 8.4, 5.9 Hz, 3H).

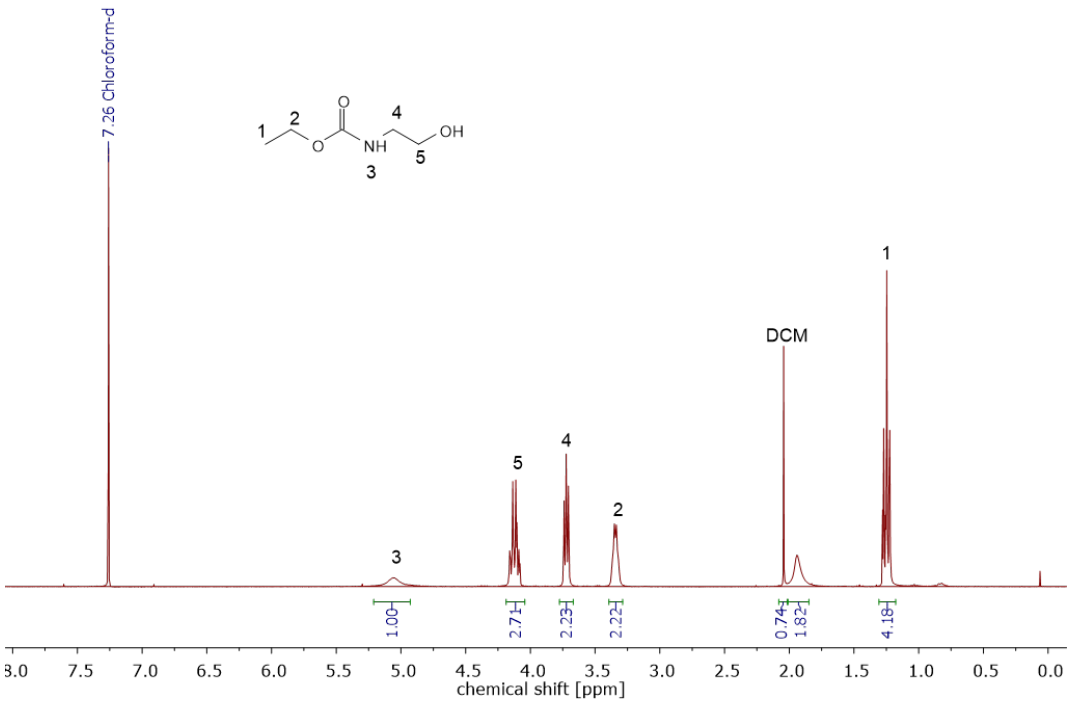

Figure 36: ^{1}H NMR of **45**.

1-ethyl 1-(2-propionamidoethyl) 2-vinylcyclopropane-1,1-dicarboxylate

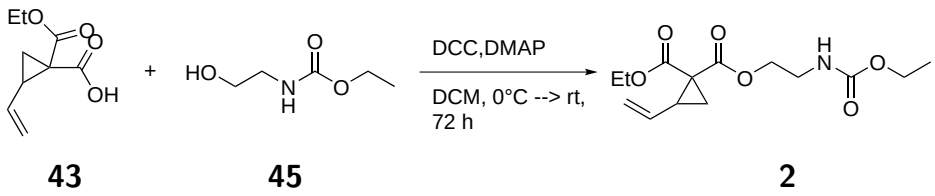

43 **45** **2**

Under argon 3.68 g of **43** (20.0 mmol), DMAP (0.11 eq, 268 mg, 2.2 mmol)), and **45** (1.1 eq, 2.93 g, 22.0 mmol) were dissolved in 50 ml dry DCM. At 0 °C in 30 ml dry DCM, dissolved DCC (1.1 eq, 4.54 g, 22.0 mmol) was slowly added. The reaction was stirred at 0 °C for one hour and at room temperature for 17 h. The reaction mixture was filtered, and the filtrate was washed three times with 0.5 M HCl, saturated $NaHCO_3$, and saturated NaCl solution, respectively. The organic phase was dried over $MgSO_4$, and the solvent was removed under reduced pressure. The product **2** was obtained after purification using flash chromatography (Cylcohexane:EtOAc 9:1) as a yellow oil in a yield of 55 % (3.19 g, 11.0 mmol).

^{1}H NMR (300 MHz, $CDCl_3$, 293K):

δ [ppm] = 5.97 (s, 1H), 5.53 – 5.39 (m, 1H), 5.31 (dd, J = 17.0, 1.9 Hz, 1H), 5.19 – 5.13 (m, 1H), 4.33 (ddd, J = 11.1, 6.6, 4.2 Hz, 1H), 4.25 – 4.06 (m, 3H), 3.63 – 3.46 (m, 2H), 2.60 (dd, J = 16.7, 8.0 Hz, 1H), 2.24 (d, J = 7.6 Hz, 2H), 1.76 (dd, J = 7.7, 5.0 Hz, 1H), 1.57 (dd, J = 9.1, 4.9 Hz, 1H), 1.25 (t, J = 7.1 Hz, 3H), 1.15 (t, J = 7.6 Hz, 3H).

^{13}C NMR (75 MHz, $CDCl_3$, 293K):

δ [ppm] = 169.7, 167.4, 156.6, 132.8, 119.1, 64.8, 61.8, 61.1, 39.9, 35.8, 31.7, 21.0, 14.7, 14.3.

FT-IR (ATR mode)): 3382, 2982, 2118, 1716, 1638, 1525, 1446, 1372, 1319, 1255, 1197, 1172, 1130, 1036, 991, 959, 917, 863, 836, 778, 747, 707, 664 cm-1.

HRMS (ESI, pos.) m/z calculated for $C_{14}H_{21}NNaO_5$ $[M + Na]^+$ 306.1317, found 306.1310

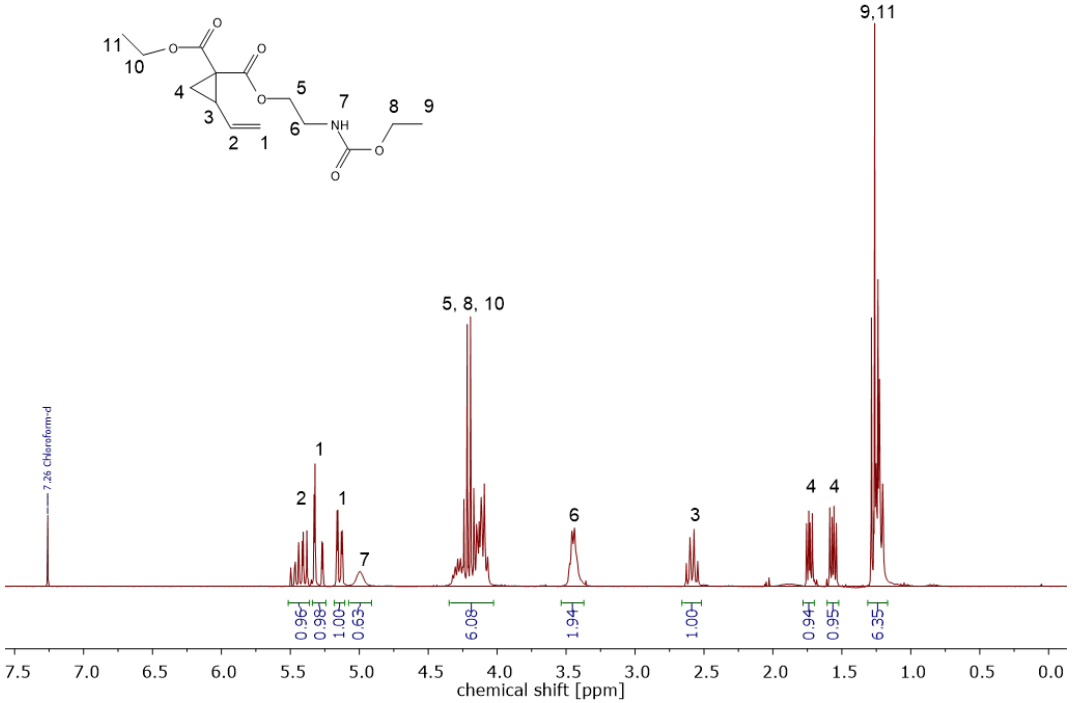

Figure 37: ^{1}H NMR of **2**.

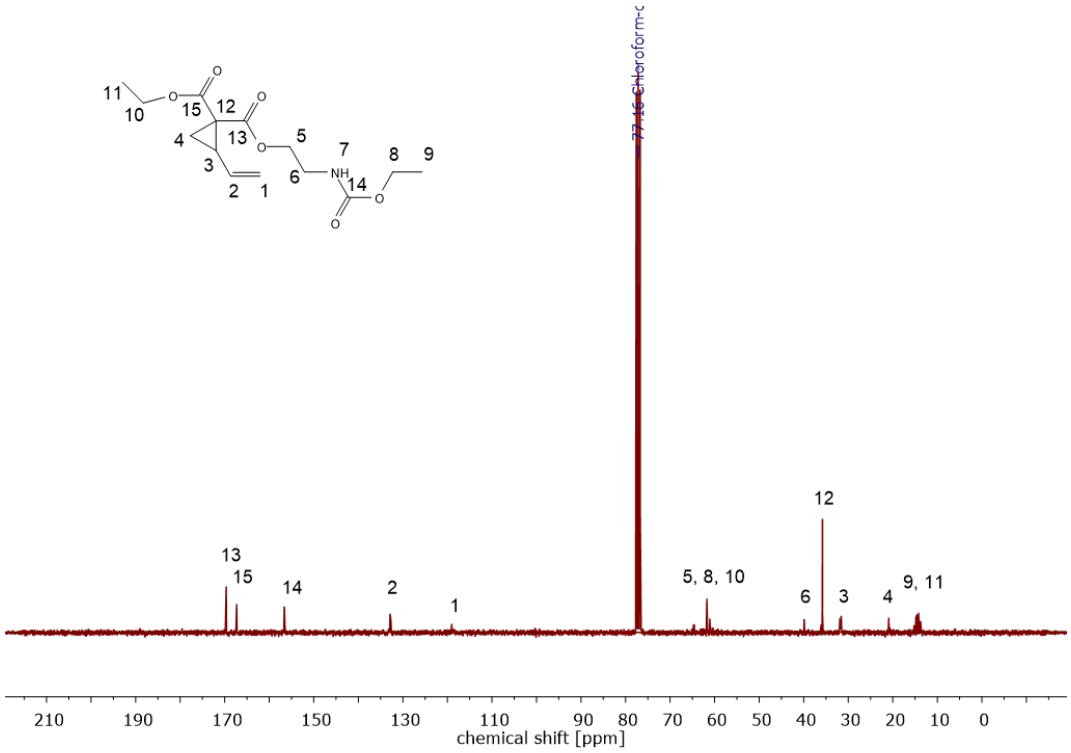

Figure 38: ^{13}C NMR of **2**.

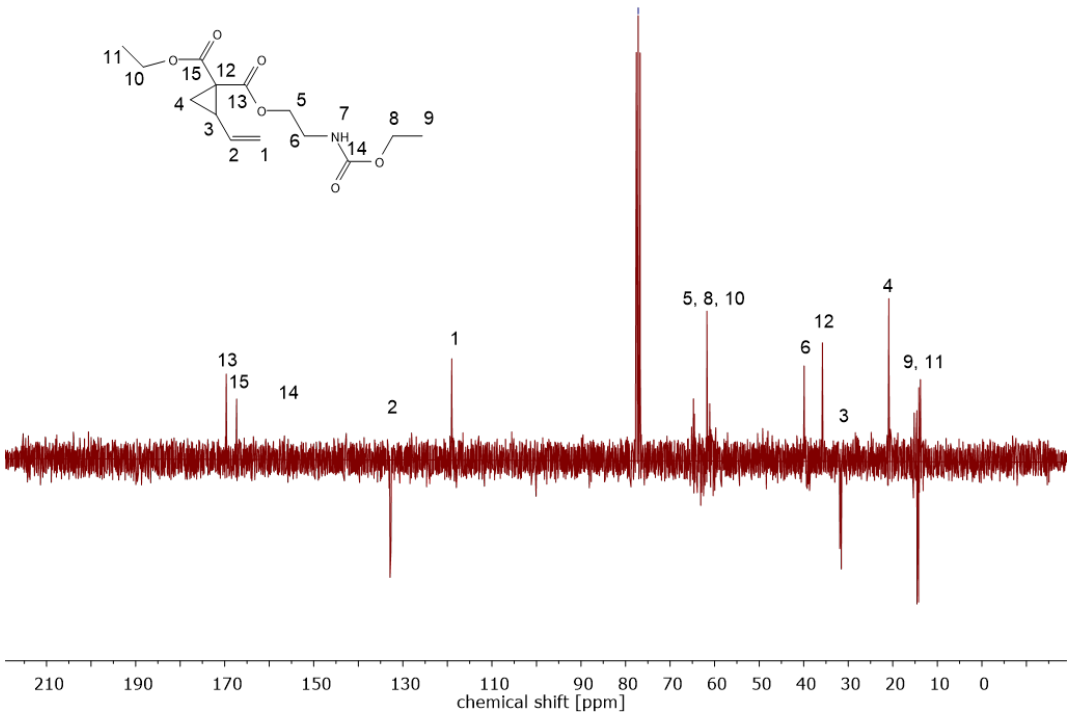

Figure 39: ^{13}C APT NMR of **2**.

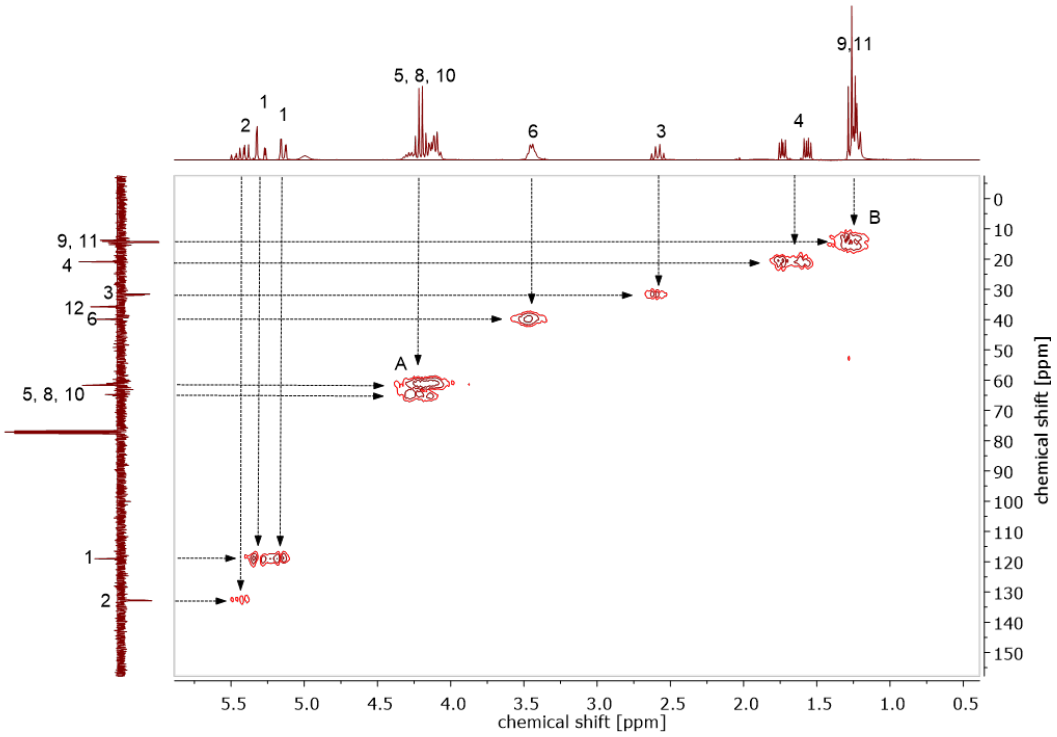

Figure 40: HSQC 2D NMR of **2**.

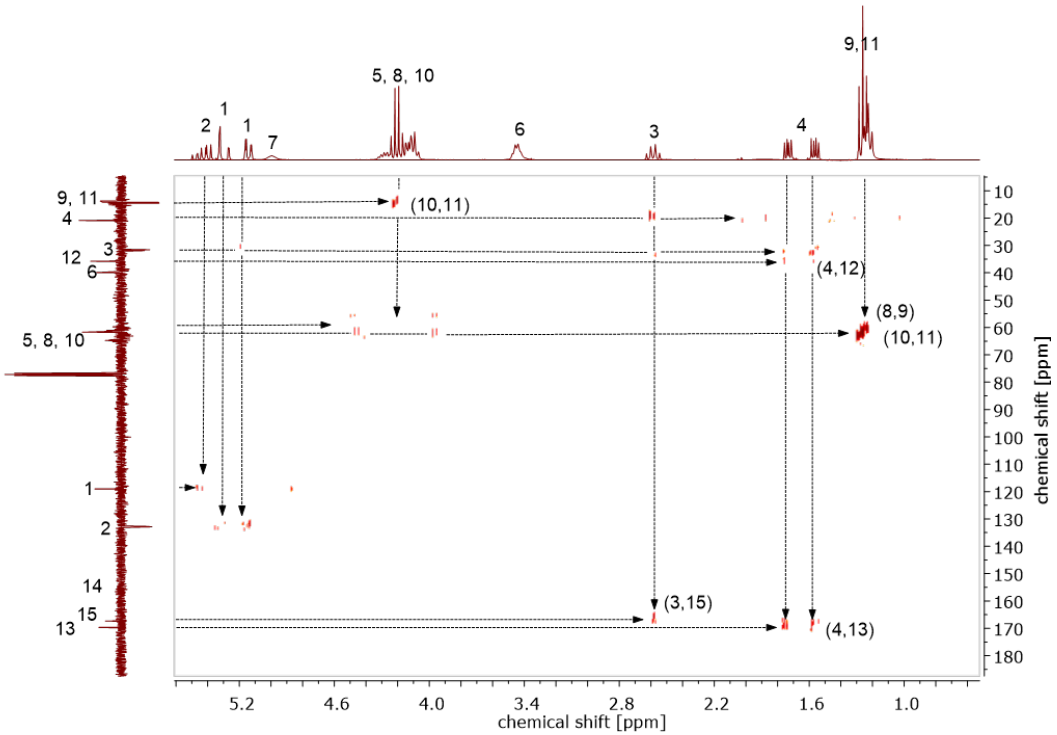

Figure 41: HMBC 2D NMR of **2**.

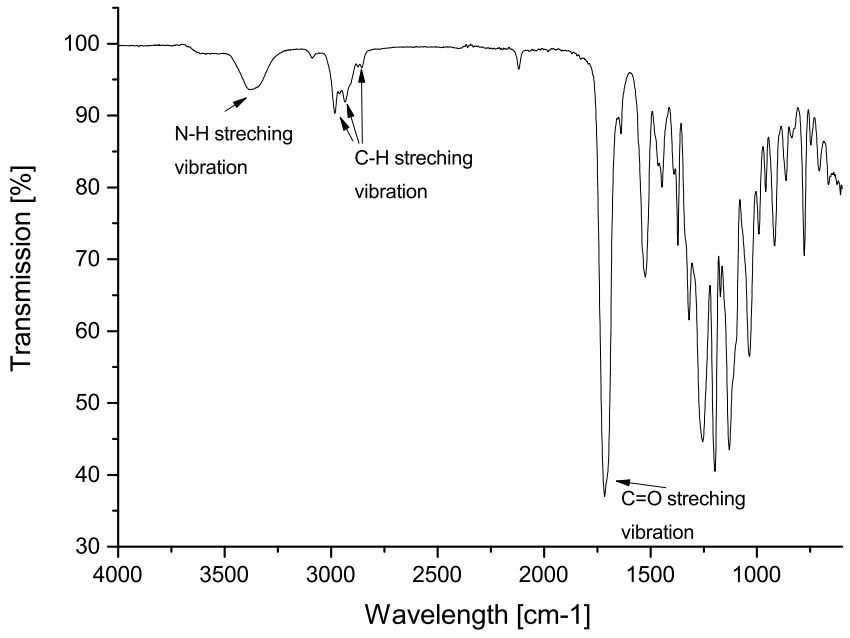

Figure 42: FT-IR of **2**.

1-ethyl-3-(2-hydroxyethyl)urea

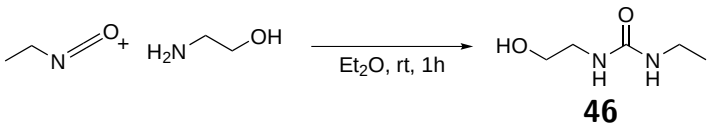

46

The synthesis was performed as reported before[140]. Under argon, at room temperature, ethylisocyanate (2.52 g, 35.3 mmol) was added drop wise to a solution of ethanolamin (1 eq, 2.16 g, 35.3 mmol) in 17 ml dry Et_2O. The reaction was stirred at room temperature for 1 h, till GC-analysis showed complete conversion. The mixture was filtered, washed with Et_2O and the solvent was removed under reduced pressure. The product **46** was obtained after recrystallization in 95% ethanol as a white solid.

^{1}H NMR (300 MHz, $CDCl_3$, 293K):

δ [ppm] = 4.42 (t, 1H), 4.06 (t, 1H), 3.72 (q, 4H), 1.24 (t, 3H) ppm.

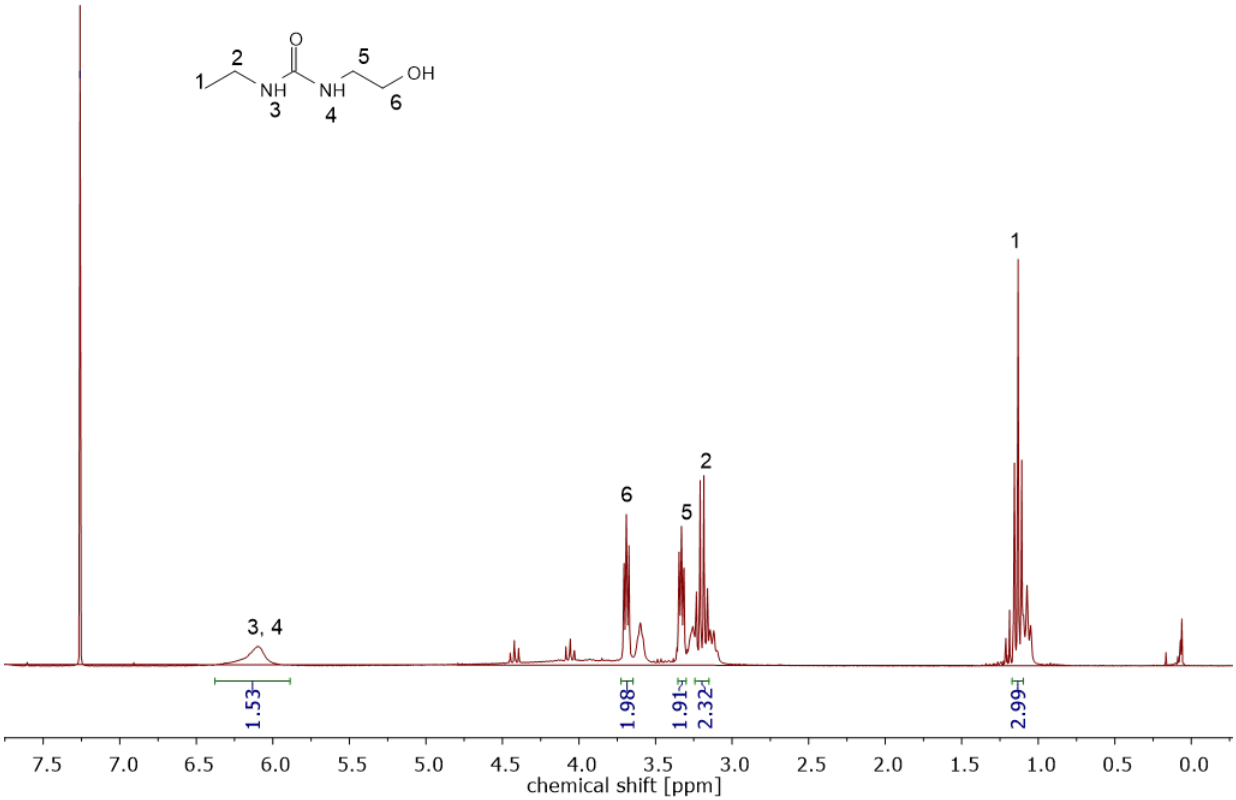

Figure 43: ^{1}H NMR of **46**.

1-ethyl 1-(2-(3-ethylureido)ethyl) 2-vinylcyclopropane-1,1-dicarboxylate

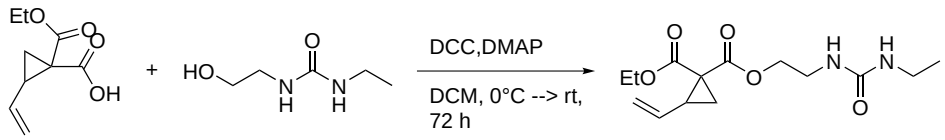

43 **46** **3**

Under argon 3.10 g of **43** (16.8 mmol), DMAP (0.11 eq, 226 mg, 1.9 mmol)), and **46** (1.1 eq, 2.44 g, 18.5 mmol) were dissolved in 45 ml dry DCM. At 0 °C in 25 ml dry DCM, dissolved DCC (1.1 eq, 3.82 g, 18.5 mmol) was slowly added. The reaction was stirred at 0 °C for one hour and at room temperature for 17 h. The reaction mixture was filtered, and the filtrate was washed three times with 0.5 M HCl, saturated $NaHCO_3$, and saturated NaCl solution, respectively. The organic phase was dried over $MgSO_4$, and the solvent was removed under reduced pressure. The product **3** was obtained after purification using flash chromatography (DCM:EtOAc 9:1 → 7:3) as a light yellow oil

in a yield of 65 % (3.26 g, 10.9 mmol).

^{1}H NMR (300 MHz, $CDCl_3$, 293K):

δ [ppm] = 5.53 – 5.39 (m, 1H), 5.36 – 5.27 (m, 1H), 5.20 – 5.13 (m, 1H), 4.80 (s, 1H), 4.38 – 4.07 (m, 4H), 3.48 (dd, J = 10.5, 4.8 Hz, 2H), 3.20 (q, J = 7.2 Hz, 2H), 2.61 (dd, J = 16.8, 8.0 Hz, 1H), 1.76 (dd, J = 7.6, 5.0 Hz, 1H), 1.59 (dd, J = 9.1, 4.9 Hz, 1H), 1.27 (t, J = 7.1 Hz, 3H), 1.13 (t, J = 7.2 Hz, 3H).

^{13}C NMR (75 MHz, $CDCl_3$, 293K):

δ [ppm] = 169.8, 167.6, 158.1, 132.8, 119.1, 65.3, 61.7, 39.3, 35.8, 35.5, 31.9, 20.9, 15.6, 14.4 ppm.

FT-IR (ATR mode):

3335, 2979, 1723, 1634, 1566, 1446, 1371, 1318, 1262, 1196, 1129, 1033, 991, 959, 317, 862, 843, 775, 747, 635 cm-1.

HRMS (ESI, pos.) m/z calculated for $C_{14}H_{22}N_2NaO_5$ $[M + Na]^+$ 321.1426, found 321.1419

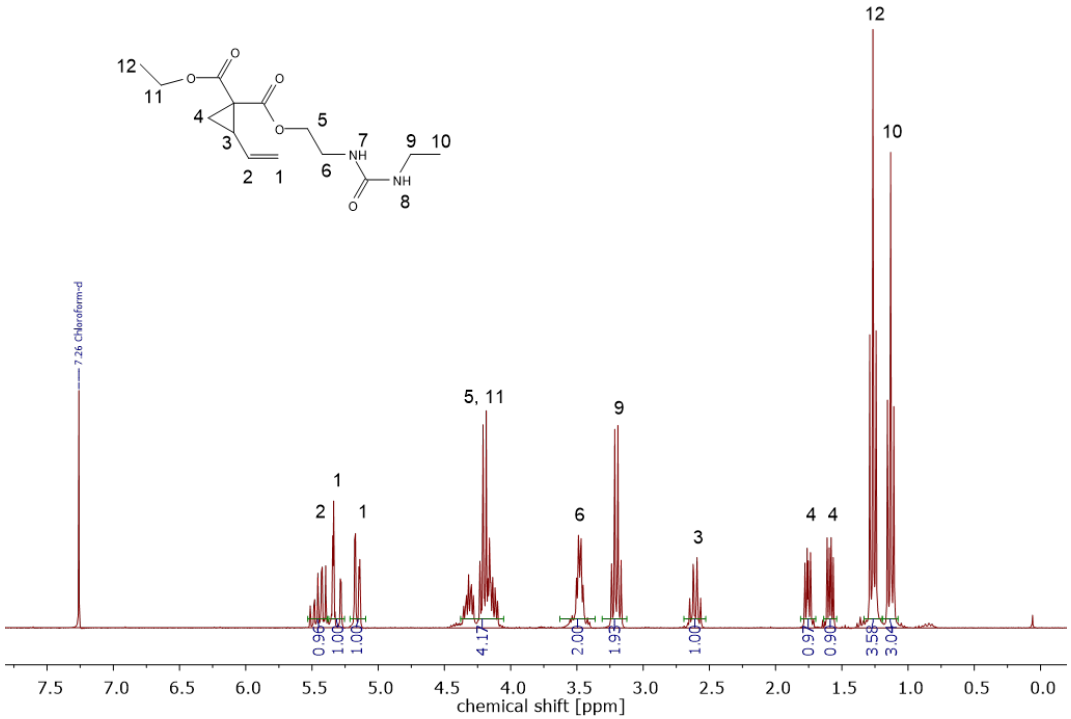

Figure 44: ^{1}H NMR of **3**.

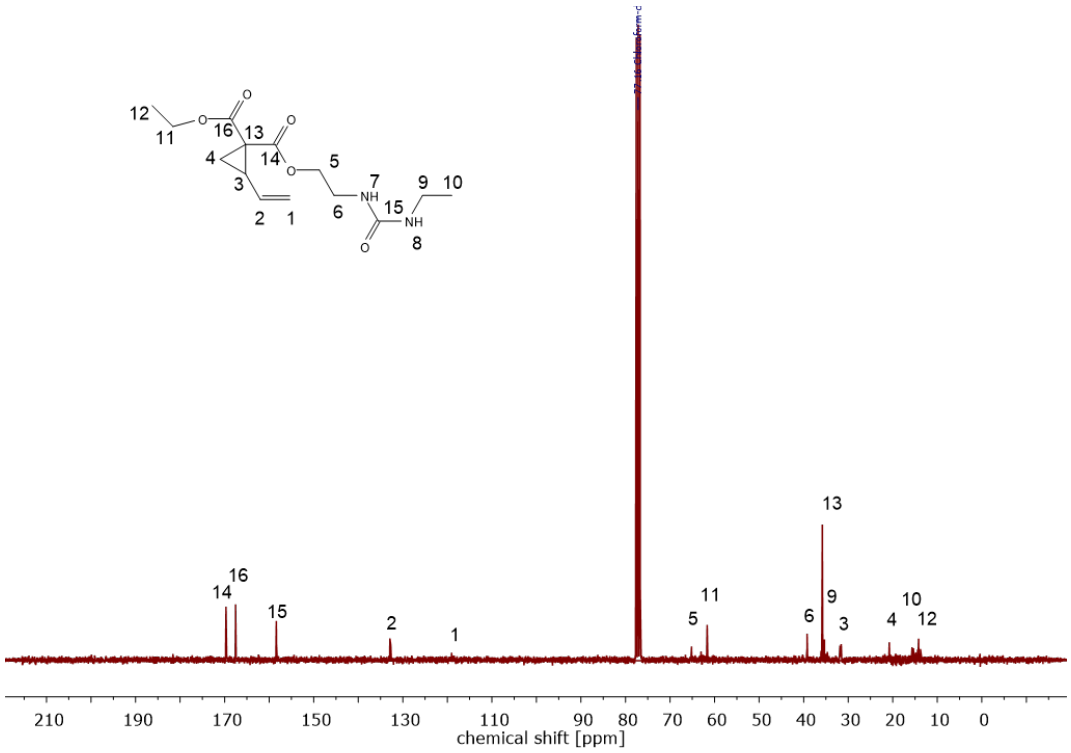

Figure 45: ^{13}C NMR of **3**.

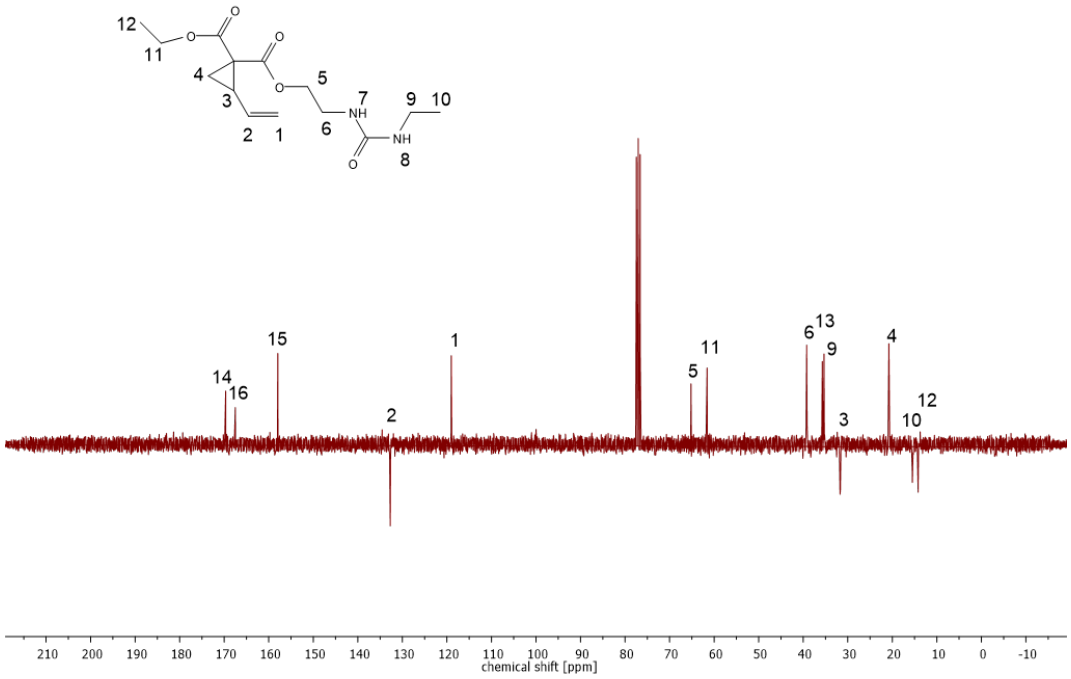

Figure 46: ^{13}C APT NMR of **2**.

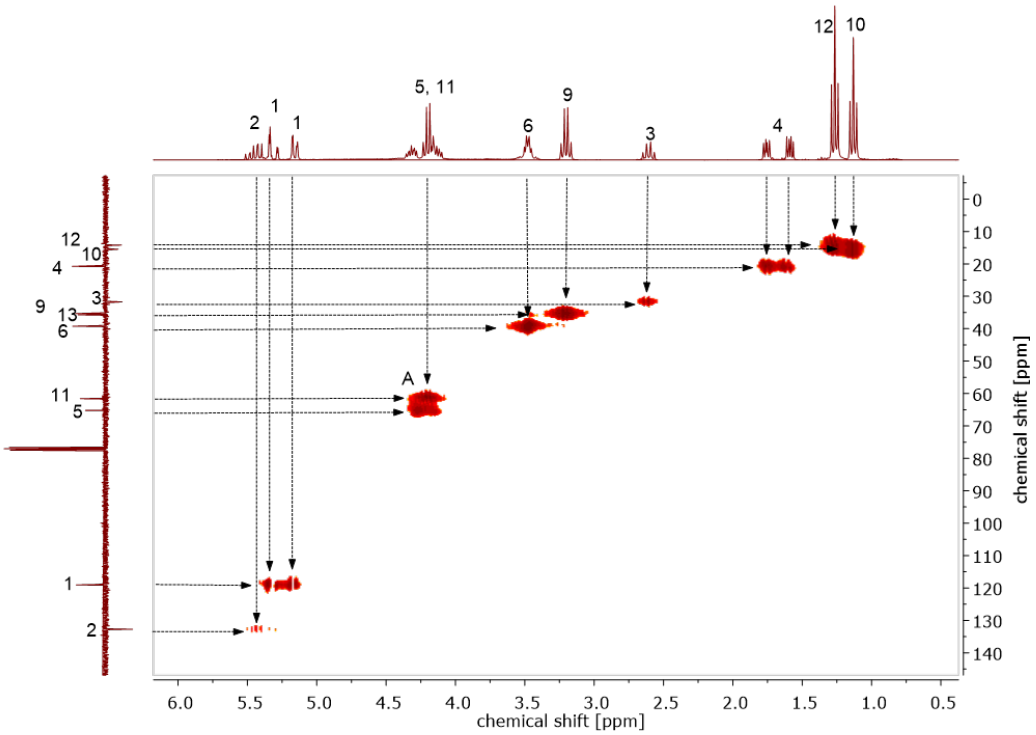

Figure 47: HSQC 2D NMR of **3**.

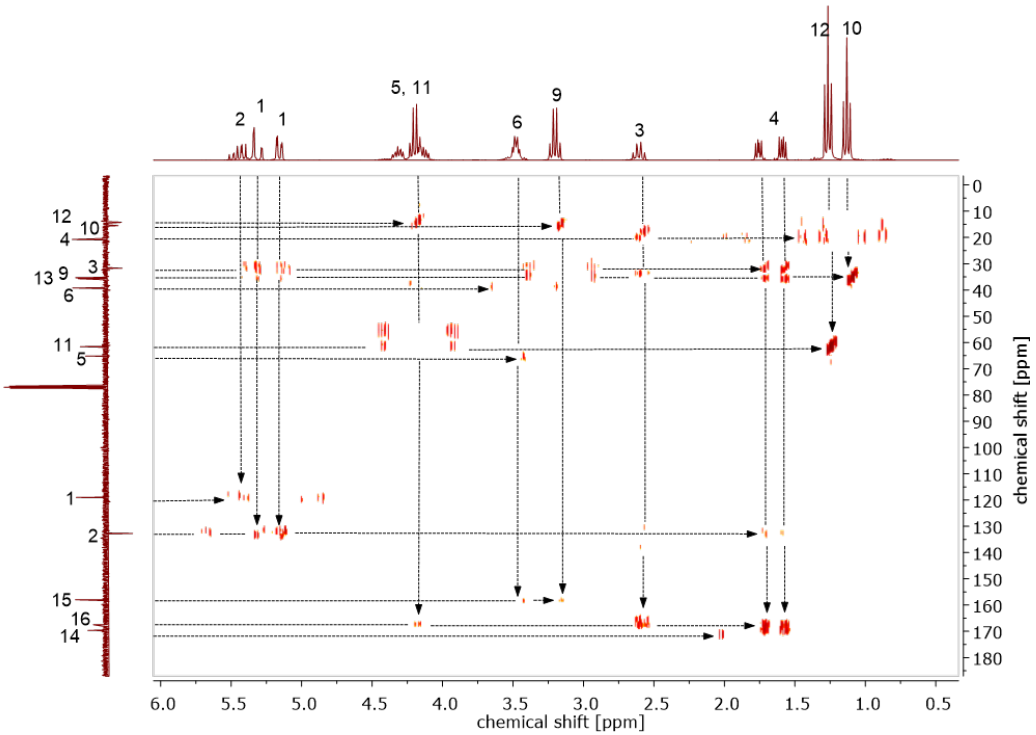

Figure 48: HMBC 2D NMR of **3**.

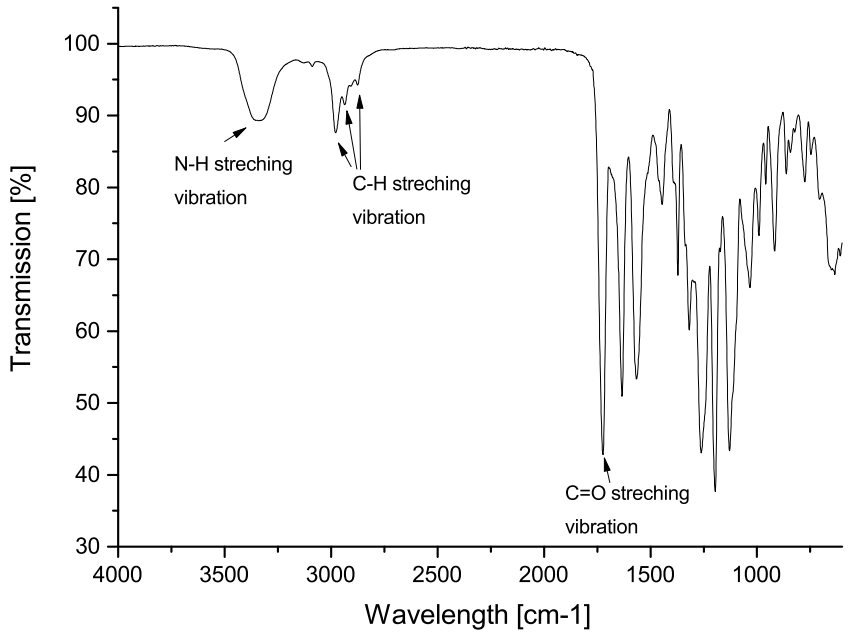

Figure 49: FT-IR of **3**.

N-(2-hydroxyethyl)propionamide

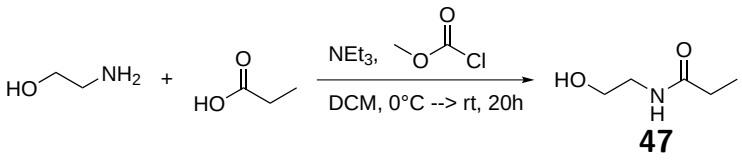

47

The alcohol **47** was prepared by a modified literature procedure[139]. Propionic acid (3.7 g, 50 mmol) was dissolved in 50 ml DCM. At 0 °C , triethylamine (2 eq, 13.9 ml, 100 mmol) was added, and methyl chloroformate (2 eq, 9.45 g, 100 mmol) was slowly added. The reaction mixture was stirred at room temperature for two h. At 0 °C , ethanolamine (2 eq, 6.1 g, 100 mmol) was added dropwise. The reaction was stirred at room temperature over night. The solvent was removed under reduced pressure, and the product **47** was obtained after purification via flash chromatography (EtOAc: EtOH 85:15) in a yield of 26% (1.53 g, 13 mmol).

^{1}H NMR (300 MHz, $CDCl_3$, 293K):

δ [ppm] = 6.20 (s, 1H), 3.77 – 3.69 (m, 2H), 3.42 (dd, J = 10.2, 5.4 Hz, 2H), 2.25 (q, J = 7.6 Hz, 2H), 1.16 (t, J = 7.6 Hz, 3H).

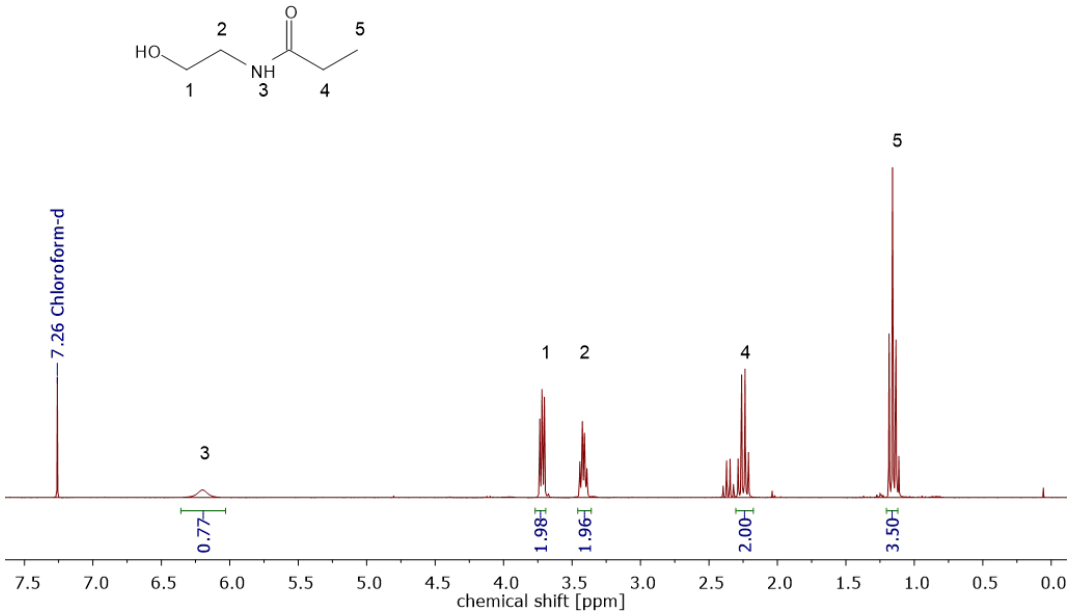

Figure 50: ^{1}H NMR of **47**.

1-(2-((ethoxycarbonyl)amino)ethyl) 1-ethyl 2-vinylcyclopropane-1,1-dicarboxylate

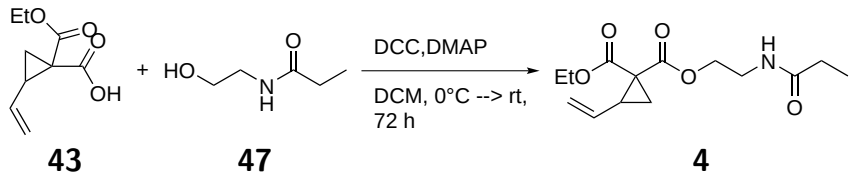

43 **47** **4**

Under argon 3.13 g of **43** (17.0 mmol), DMAP (0.11 eq, 228 mg, 1.9 mmol)), and **24** (1.1 eq, 2.19 g, 18.7 mmol) were dissolved in 50 ml dry DCM. At 0 °C in 30 ml dry DCM, dissolved DCC (1.1 eq, 3.86 g, 18.7 mmol) was slowly added. The reaction was stirred at 0 °C for one hour and at room temperature for 17 h. The reaction mixture was filtered, and the filtrate was washed three times with 0.5 M HCl, saturated $NaHCO_3$, and saturated NaCl solution, respectively. The organic phase was dried over $MgSO_4$, and the solvent was removed under reduced pressure. The product **4** was obtained after purification using flash chromatography (Cylcohexane:EtOAc 100:0 → 7:3) as a light yellow oil in a yield of 65 % (3.13 g, 11.1 mmol).

^{1}H NMR (300 MHz, $CDCl_3$, 293K):

δ [ppm] = 5.52 – 5.38 (m, 1H), 5.31 (dd, J = 17.1, 1.8 Hz, 1H), 5.19 – 5.13 (m, 1H), 4.96 (s, 1H), 4.37 – 4.05 (m, 6H), 3.55 – 3.39 (m, 2H), 2.60 (dd, J = 16.8, 7.9 Hz, 1H), 1.75 (dd, J = 7.6, 4.9 Hz, 1H), 1.58 (dd, J = 9.1, 4.9 Hz, 1H), 1.26 (dt, J = 10.4, 7.1 Hz, 6H).

^{13}C NMR (75 MHz, $CDCl_3$, 293K):

δ [ppm] = 174.1, 169.8, 167.5, 132.7, 119.1, 64.6, 61.7, 38.4, 35.7, 31.7, 29.7, 20.9, 14.3, 9.8.

FT-IR (ATR mode): 3304, 3087, 2981, 1723, 1647, 1538, 1464, 1446, 1371, 1319, 1267, 1196, 1127, 1058, 1032, 991, 359, 916, 862, 822, 779, 746, 706, 665 cm-1.

HRMS (ESI, pos.) m/z calculated for $C_{14}H_{21}NNaO_6$ $[M + Na]^+$ 322.1267, found 322.1259

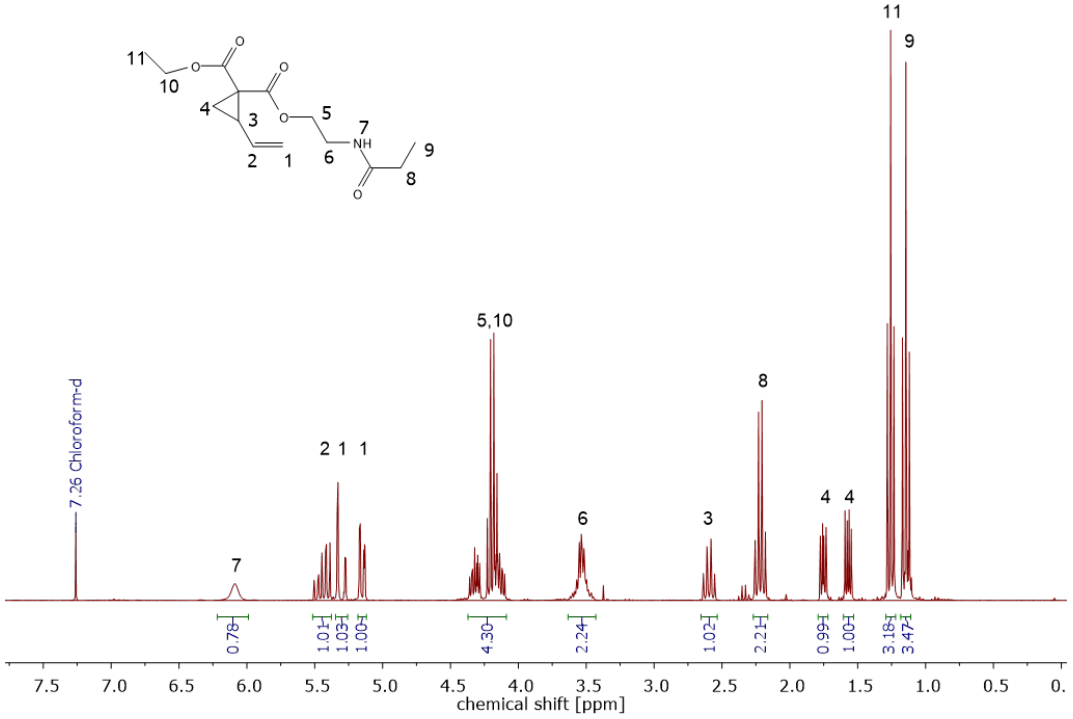

Figure 51: ^{1}H NMR of **4**.

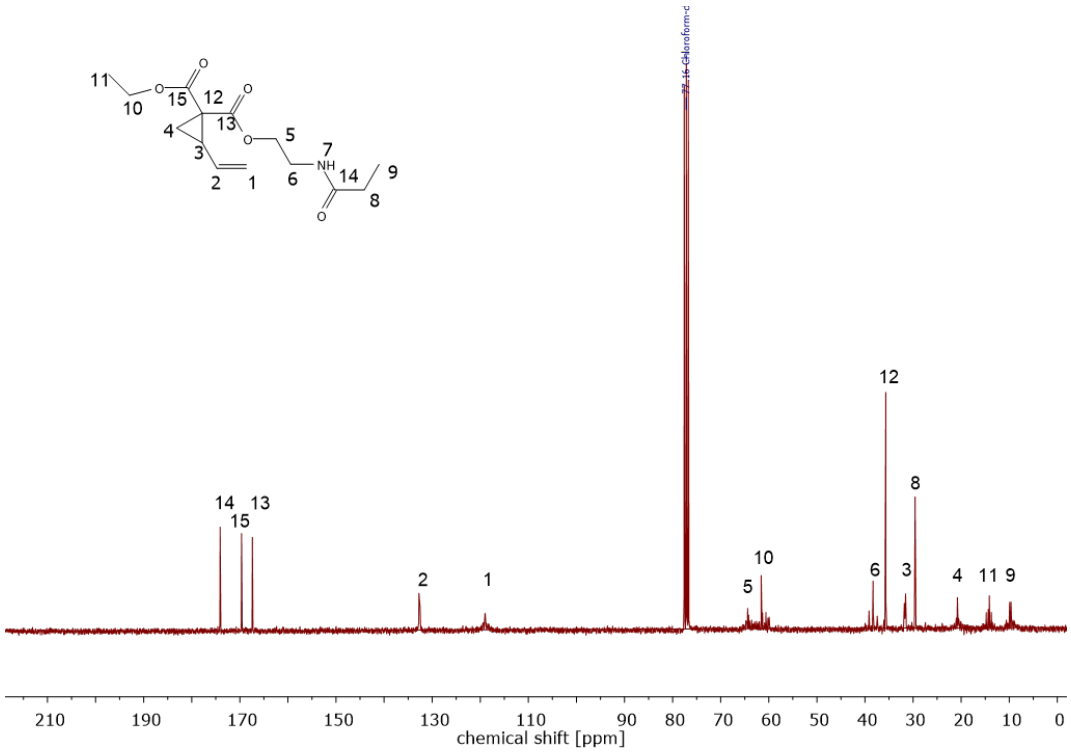

Figure 52: ^{13}C NMR of **4**.

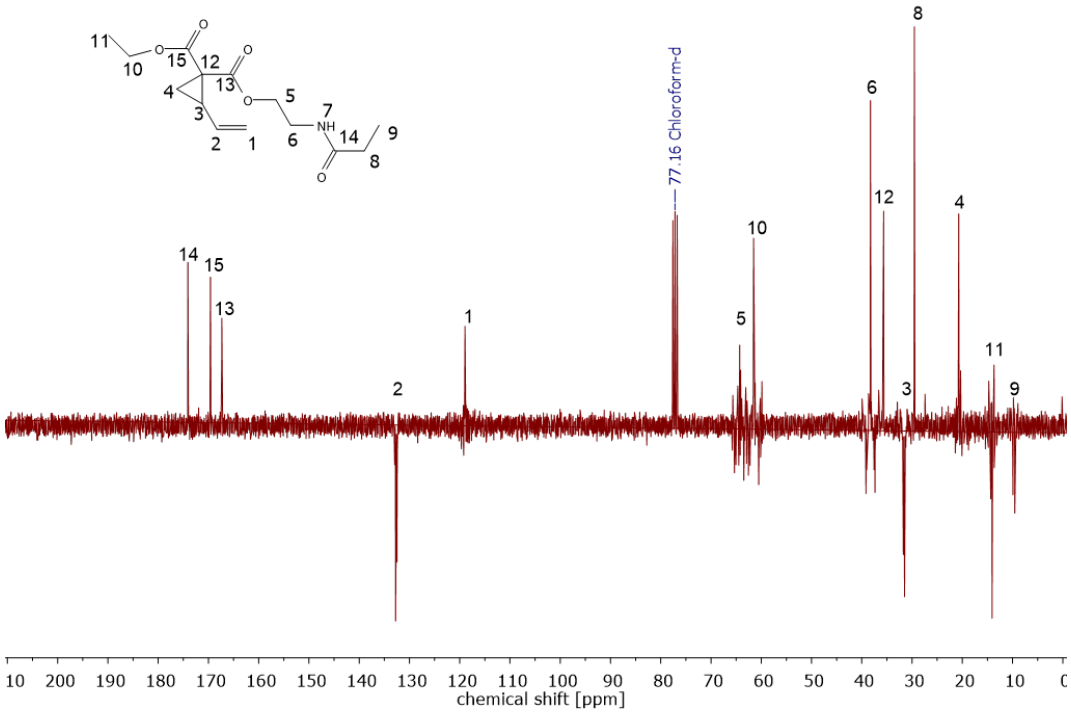

Figure 53: ^{13}CAPT NMR of **4**.

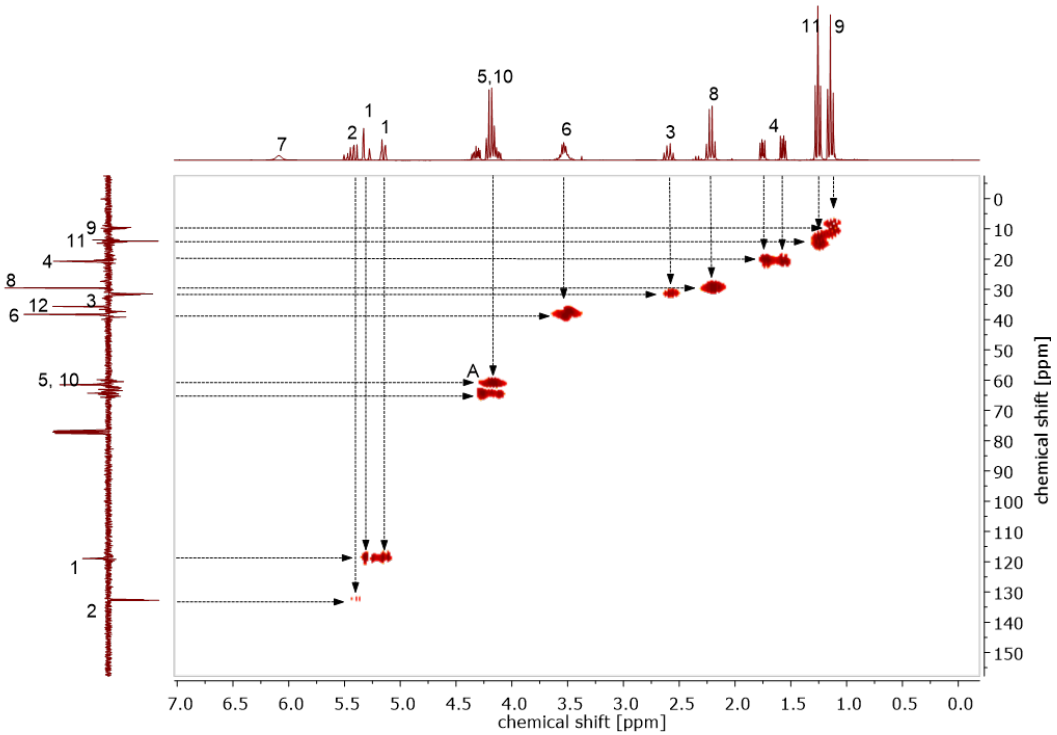

Figure 54: HSQC 2D NMR of **4**.

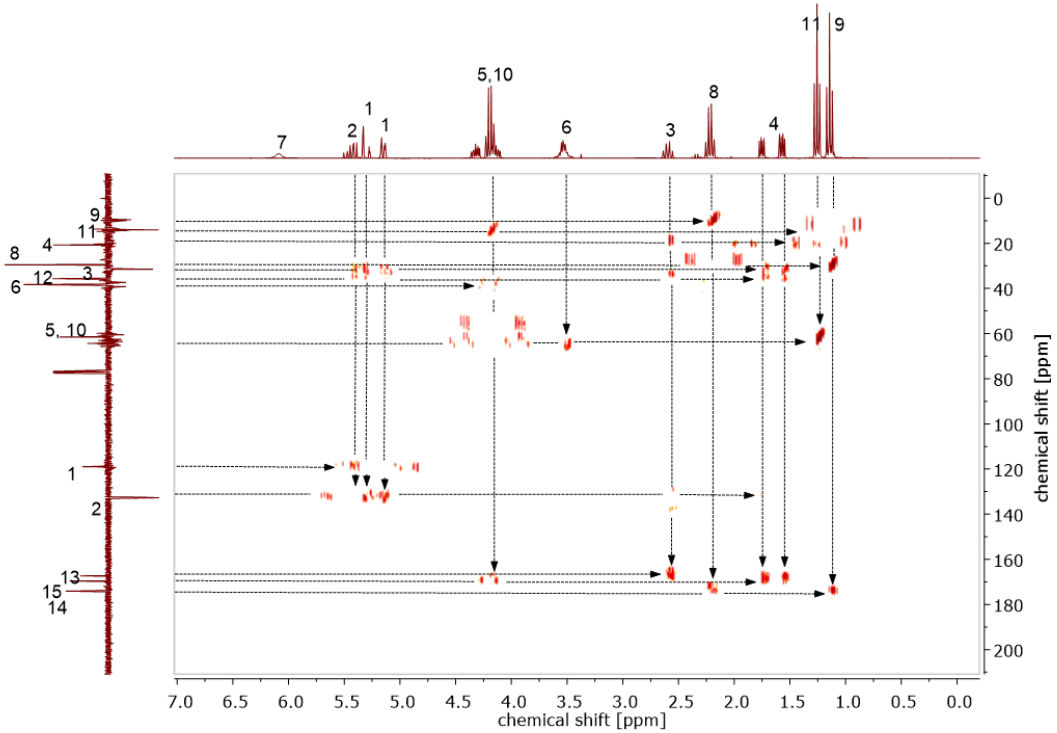

Figure 55: HMBC 2D NMR of **4**.

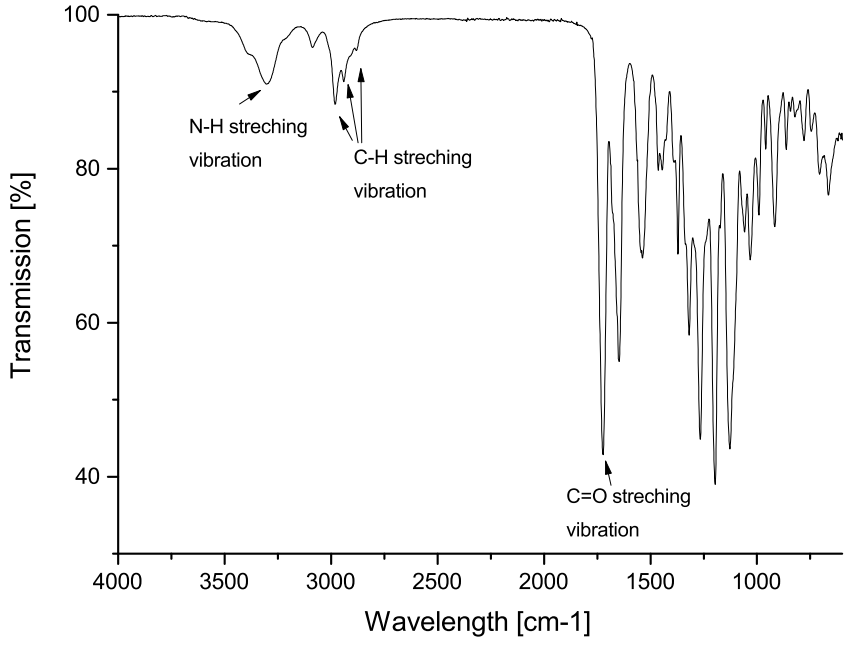

Figure 56: FT-IR of **4**.

2-hydroxyethyl ethylcarbamate

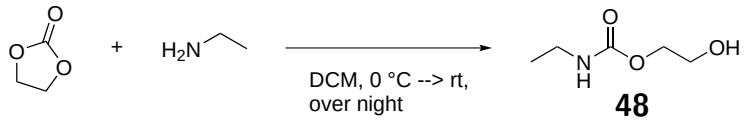

The alcohol **48** was prepared by a modified literature procedure[].Ehylencarbonate (10.0 g, 114 mmol) was dissolved in 100 ml DCM. At 0 °C ,ethylamin (1.1 eq, 5.6 g, 125 mmol) was added dropwise. The reaction mixture was stirred at room temperature for 2 h and at room temperature over night. The solvent was removed under reduced pressure, and the product **48** was obtainedas white solid in a yield of 84% (12.9 g, 97 mmol).

^{1}H NMR (300 MHz, $CDCl_3$, 293K):
δ [ppm] = 4.84 (s, 1H), 4.35 – 4.14 (m, 2H), 3.88 – 3.75 (m, 2H), 3.30 – 3.13 (m, 2H), 1.14 (t, J = 7.3 Hz, 3H).

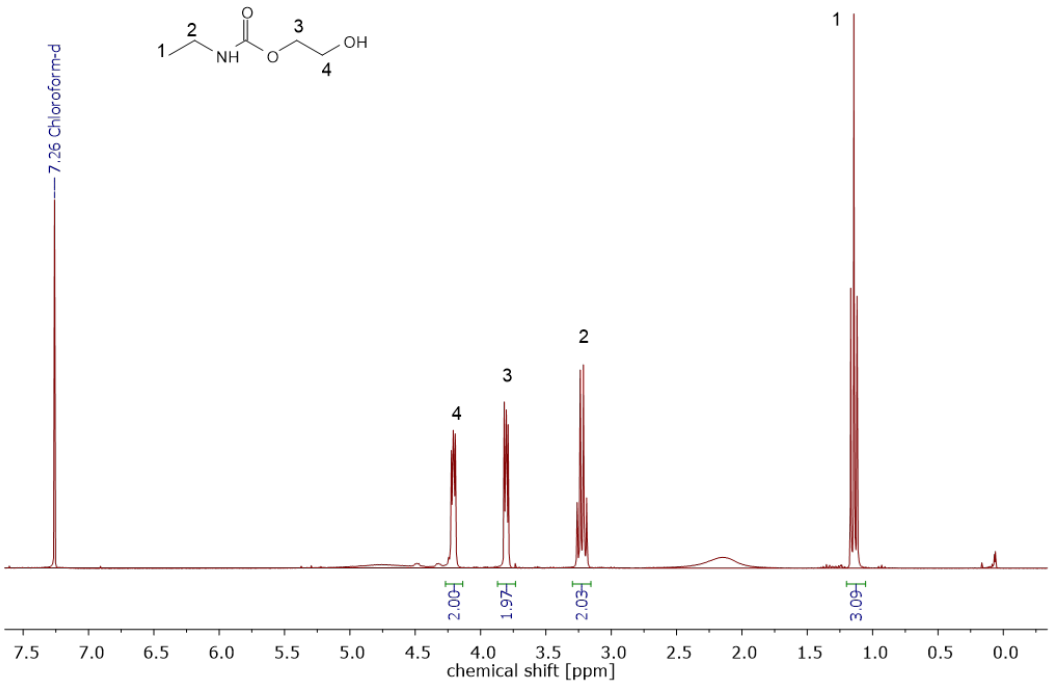

Figure 57: ^{1}H NMR of **48**.

1-ethyl 1-(2-((ethylcarbamoyl)oxy)ethyl) 2-vinylcyclopropane-1,1-dicarboxylate

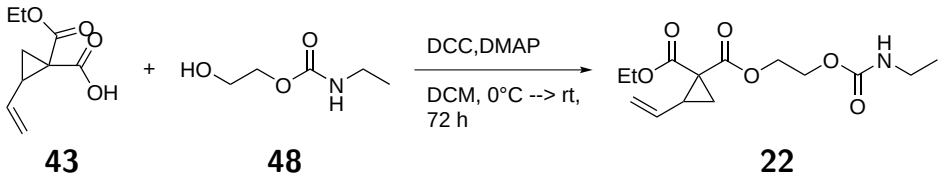

Under argon 3.68 g of **43** (20.0 mmol), DMAP (0.11 eq, 270 mg, 2.2 mmol)), and **48** (1.1 eq, 2.92 g, 22.0 mmol) were dissolved in 40 ml dry DCM. At 0 °C in 30 ml dry DCM, dissolved DCC (1.1 eq, 4.54 g, 22.0 mmol) was slowly added. The reaction was stirred at 0 °C for one hour and at room temperature for 17 h. The reaction mixture was filtered, and the filtrate was washed three times with 0.5 M HCl, saturated $NaHCO_3$, and saturated NaCl solution, respectively. The organic phase was dried over $MgSO_4$, and the solvent was removed under reduced pressure. The product **22**was obtained**^{1}H NMR (300 MHz, $CDCl_3$, 293K):**

δ [ppm] = 5.54 – 5.35 (m, 1H), 5.30 (dd, J = 17.1, 1.8 Hz, 1H), 5.20 – 5.09 (m, 1H), 4.69 (s, 1H), 4.45 – 4.07 (m, 6H), 3.30 – 3.13 (m, 2H), 2.60 (dt, J = 15.8, 7.9 Hz, 1H),

1.72 (dt, J = 8.5, 4.3 Hz, 1H), 1.64 – 1.55 (m, 1H), 1.26 (td, J = 7.1, 1.9 Hz, 3H), 1.14 (t, J = 7.2 Hz, 3H).

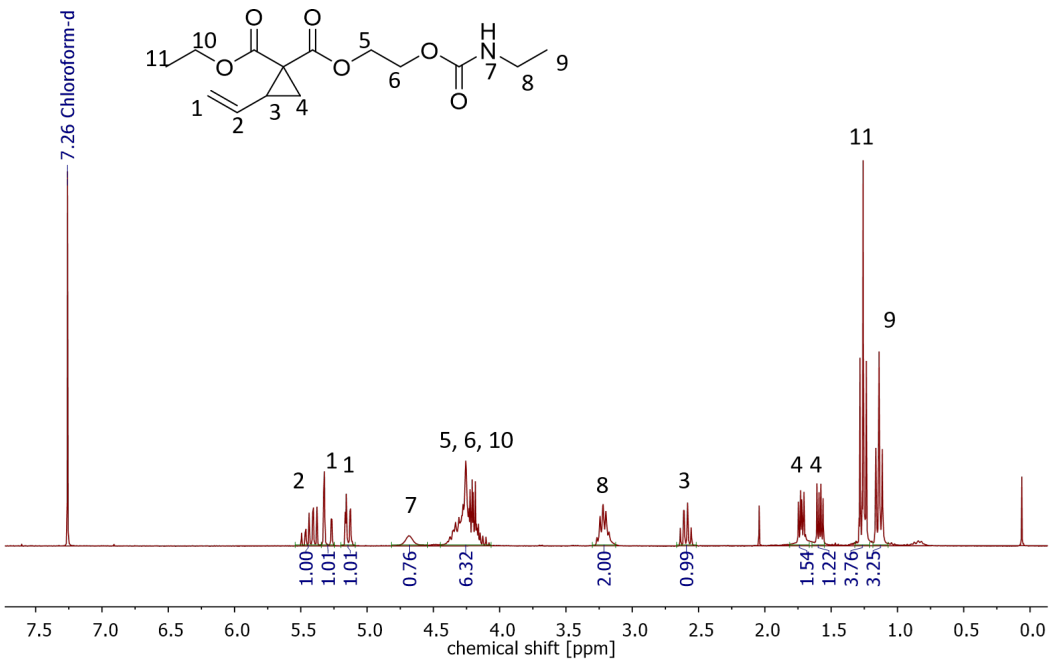

Figure 58: ^{1}H NMR of **22**.

4.2.4 Synthesis of Monofunctional VCP amides

2-aminoethyl ethyl carbonate

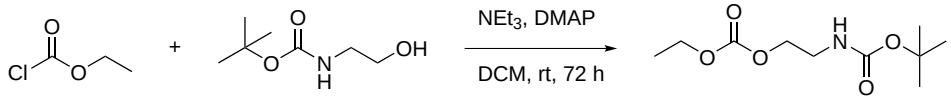

29

Under argon, 5.00 g *tert*-butyl (2-hydroxyethyl)carbamate (31.0 mmol) was dissolved in 200 ml DCM. At room temperature NEt_3 (1.1 eq, 3.45 g, 34.1 mmol) and DMAP (0.1 eq, 378 mg, 3.1 mmol) was added. At 0 °C , ethyl chloroformate (1.1 eq, 5.60 g, 34.1 mmol) was slowly added. The mixture was stirred at room temperature overnight. The crude mixture was washed three times with citric acid, saturated NaHCO3 solution and dried over $MgSO_4$. After removing the solvent, the product **29** was obtained without further purification in a yield of 92% (6.62 g, 28.4 mmol).

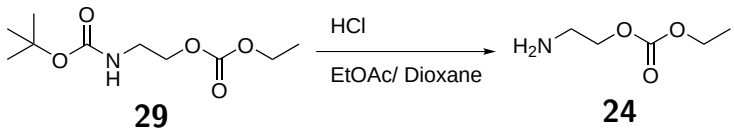

29 **24**

49 (6.60 g, 28.3 mmol) was dissolved in 140 ml ethyl acetate. At room temperature, 84 ml of a 4 M solution of HCl in Dioxane was added and the mixture was stirred at room temperature for 5 h. The solvent was removed under reduced pressure and the product **24** used without further purification. **^{1}H NMR (300 MHz, $CDCl_3$, 293K):**
δ [ppm] = 8.24 (s, 3H), 4.32 – 4.22 (m, 2H), 4.15 (q, J = 7.1 Hz, 2H), 3.14 – 3.01 (m, 2H), 1.22 (t, J = 7.1 Hz, 3H).

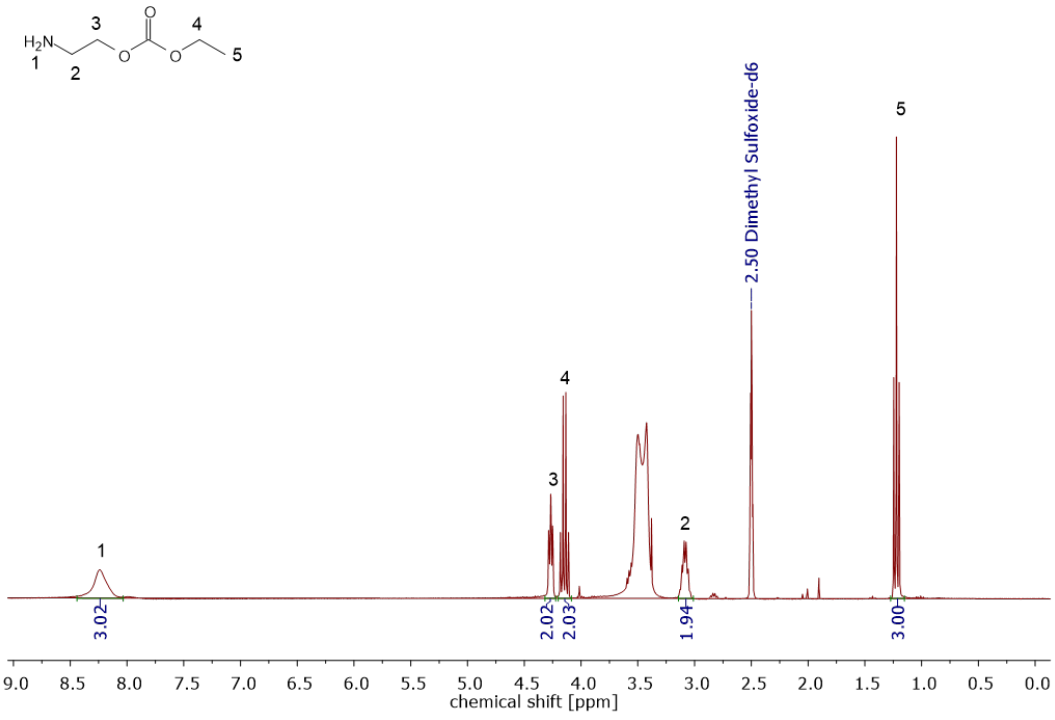

Figure 59: ^{1}H NMR of **24**.

ethyl
1-((2-((ethoxycarbonyl)oxy)ethyl)carbamoyl)-2-vinylcyclopropane-1-carboxylate

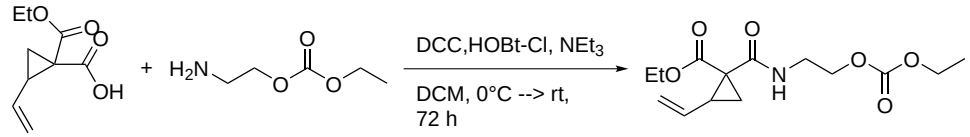

43 **24** **5**

Under argon, 4.17 g **43** (1.1 eq, 22.6 mmol), HOBt-Cl (1.25 eq, 4.05 g, 23.9 mmol), and **24** (2.51 g, 18.9 mmol) were dissolved in 30 ml dry DCM. At 0 °C , NEt_3 (2.1 eq, 4.02 g, 5.5 ml, 39.7 mmol) was added, and the reaction stirred for 15 min. At °C in 50 dry DCM, dissolved DCC (1.05 eq, 4.09 g, 19.8 mmol) was slowly added. The reaction was stirred at 0 °C for one hour and at room temperature for 17 h. The reaction mixture was filtered, and the filtrate was washed three times with 0.5 M HCl, saturated $NaHCO_3$, and saturated NaCl solution, respectively. The organic phase was dried over $MgSO_4$, and the solvent was removed under reduced pressure. The product **5** was obtained after purification using flash chromatography (Cylcohexane:EtOAc 9:1 → 7:3). White solid, yield 66 % (3.73 g, 12.4 mmol).

^{1}H NMR (300 MHz, $CDCl_3$, 293K):

δ [ppm] = 8.66 (s, 1H), 5.71 – 5.57 (m, 1H), 5.33 (dd, J = 17.1, 1.5 Hz, 1H), 5.16 (dd, J = 10.2, 1.5 Hz, 1H), 4.28 – 4.13 (m, 6H), 3.64 – 3.54 (m, 2H), 2.53 (dd, J = 17.1, 8.7 Hz, 1H), 2.08 – 1.99 (m, 1H), 1.91 – 1.83 (m, 1H), 1.29 (dt, J = 8.5, 7.1 Hz, 6H).

^{13}C NMR (75 MHz, $CDCl_3$, 293K):

δ [ppm] = 171.2, 168.6, 155.2, 133.3, 119.8, 66.5, 64.3, 61.6, 39.1, 37.3, 34.4, 21.7, 14.4, 14.3 ppm.

FT-IR (ATR mode):

3361, 2384, 2938, 1744, 1704, 1657, 1528, 1466, 1447, 1371, 1250, 1142, 1019, 917, 866, 790,741, 626 cm-1.

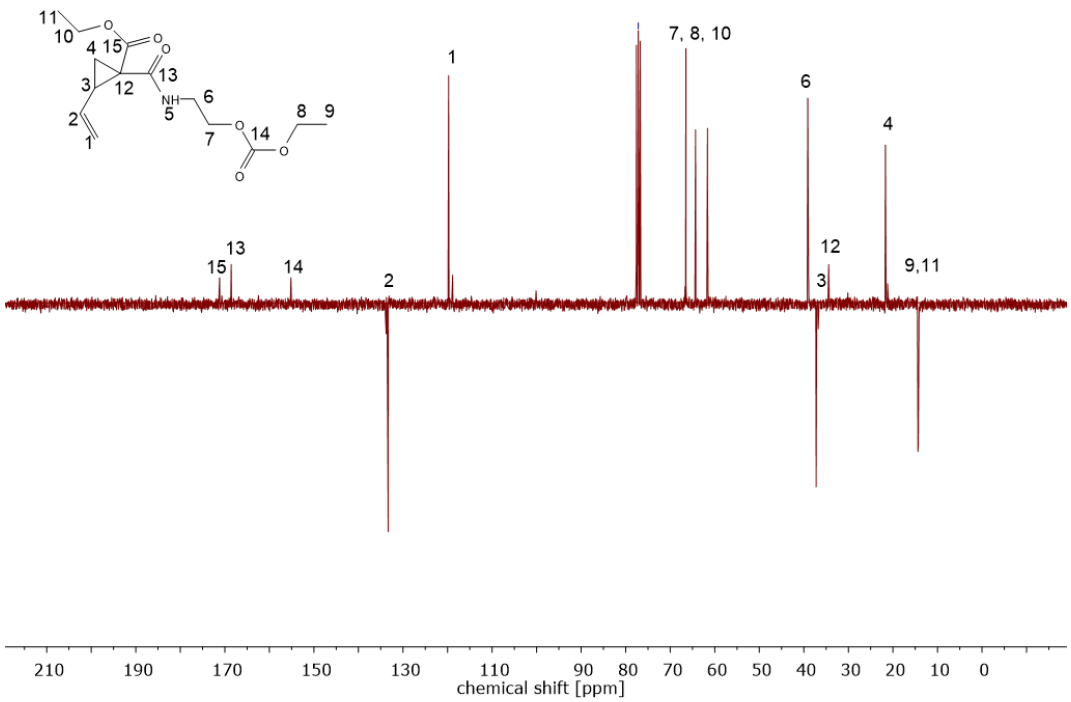

Figure 60: ^{13}C APT NMR of **5**.

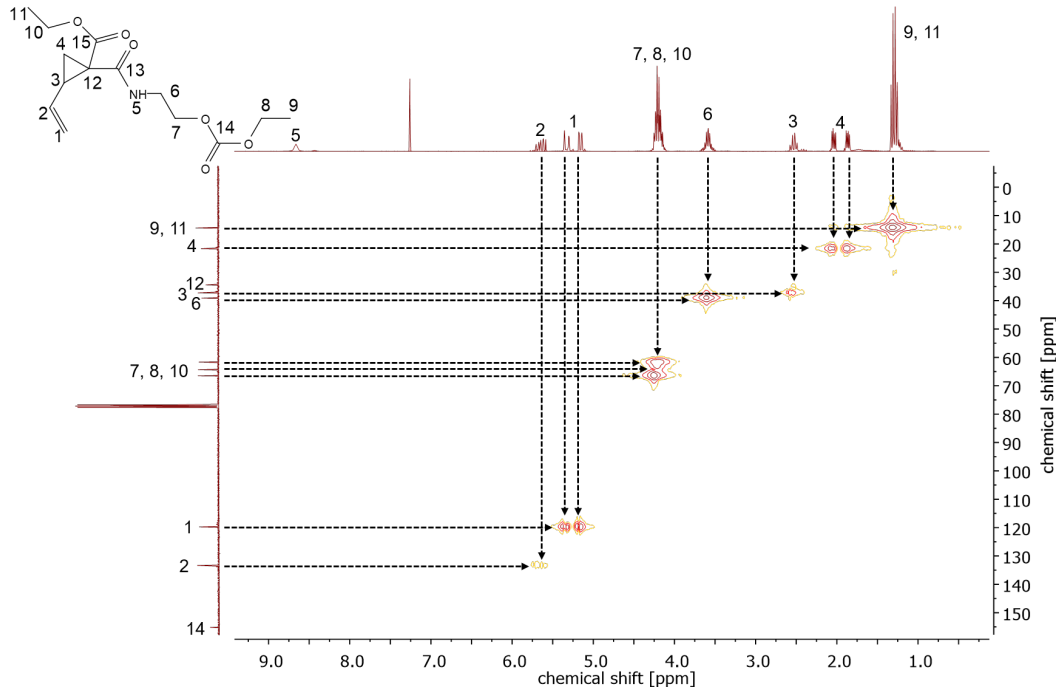

Figure 61: HSQC 2D NMR of **5**.

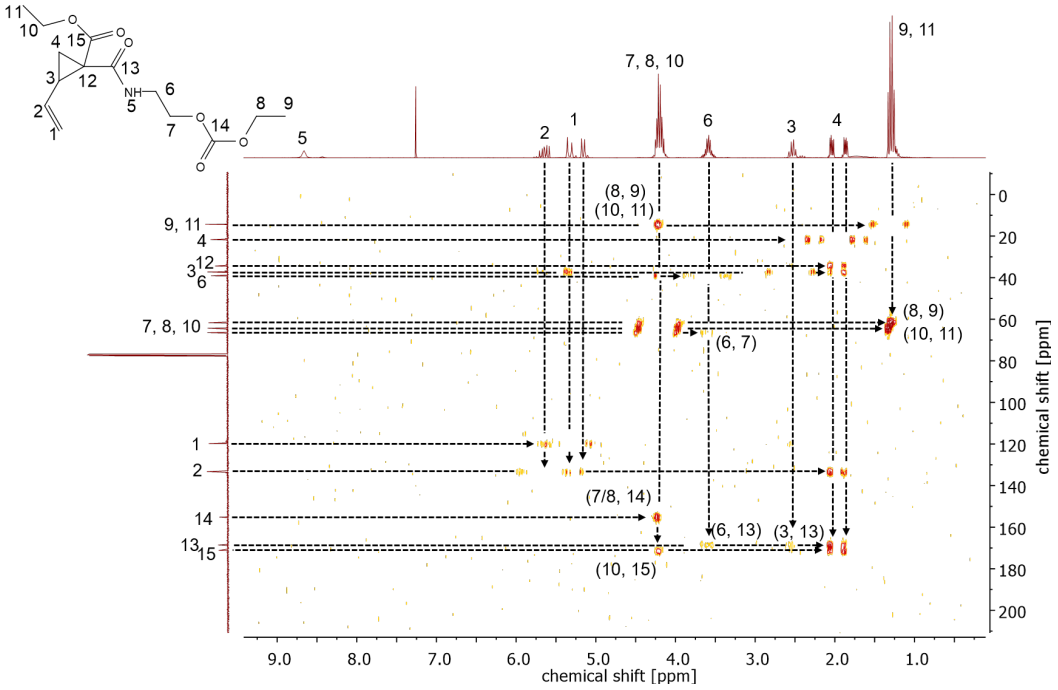

Figure 62: HMBC 2D NMR of **5**.

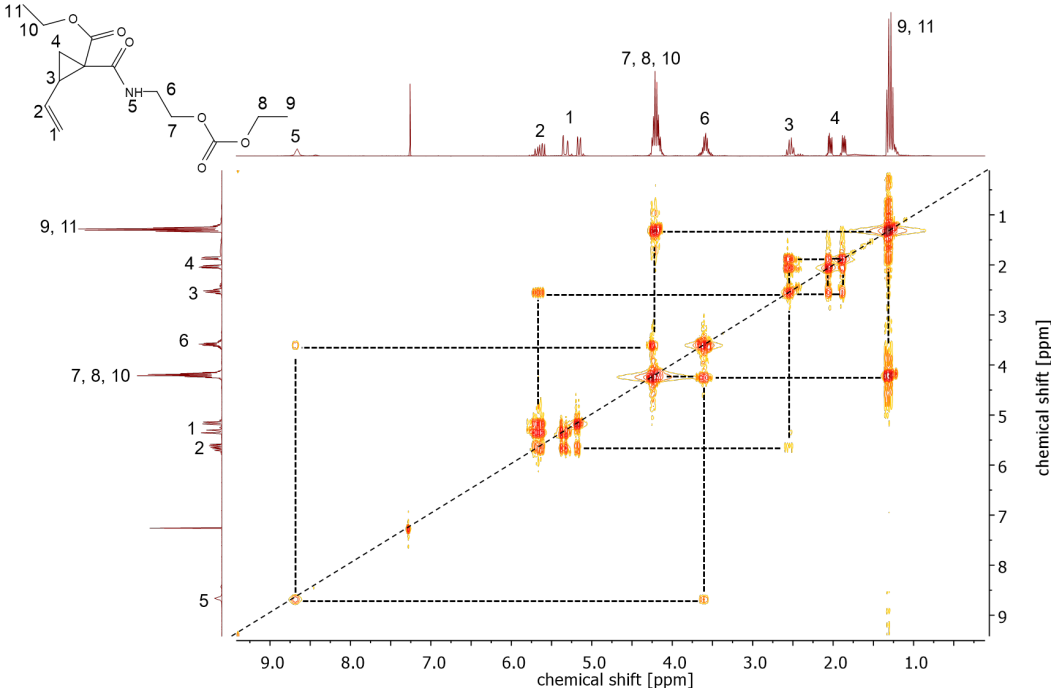

Figure 63: COSY 2D NMR of **5**.

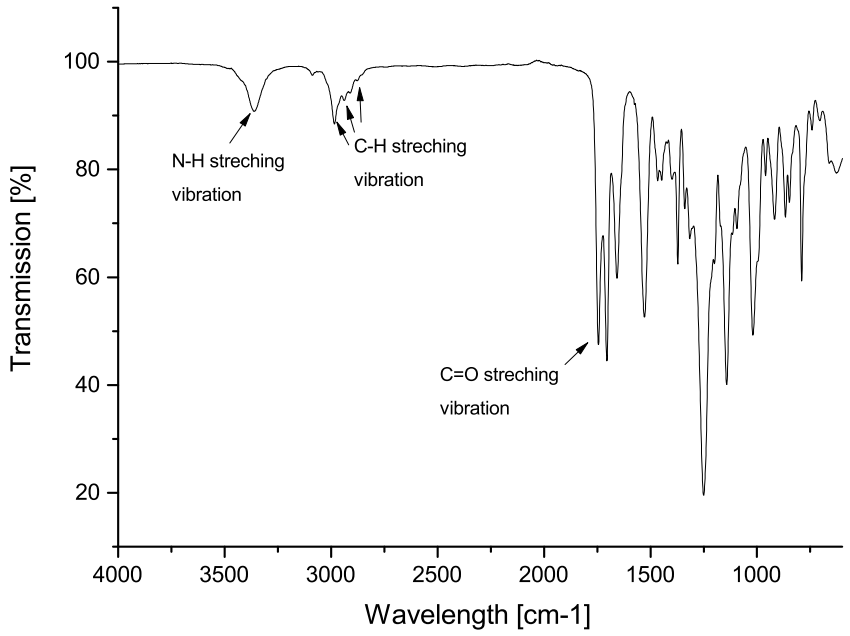

Figure 64: FT-IR of **5**.

Ethyl (2-aminoethyl)carbamate

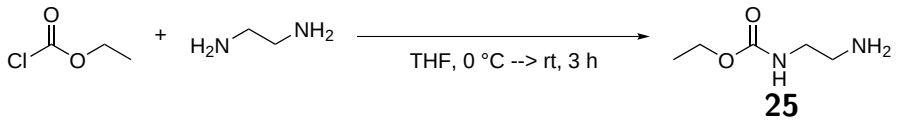

25

Under argon, at 0 °C , in 100 ml THF dissolved ethyl chloroformate (2.7 g, 25 mmol) was added slowly to a solution of ethylenediamine (10 eq, 15.0 g, 250 mmol), dissolved in 200 THF. The solution was stirred at room temperature for three hours. The organic phase was extracted using a HCl solution (pH=2) and saturated NaCl solution. The aqueous phase was basified to pH=12 and extracted with THF. The solvent was removed under reduced pressure and product **25** was obtained as a colourless oil in a yield of 33 % (1.09 g, 8.24 mmol). **^{1}H NMR (300 MHz, $CDCl_3$, 293K):**
δ [ppm] = 5.10 (s, 1H), 4.10 (q, J = 7.1 Hz, 2H), 3.23 (dd, J = 11.7, 5.9 Hz, 2H), 2.87 – 2.77 (m, 2H), 1.62 (s, 1H), 1.60 (s, 1H), 1.23 (t, J = 7.1 Hz, 3H).

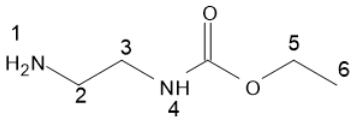

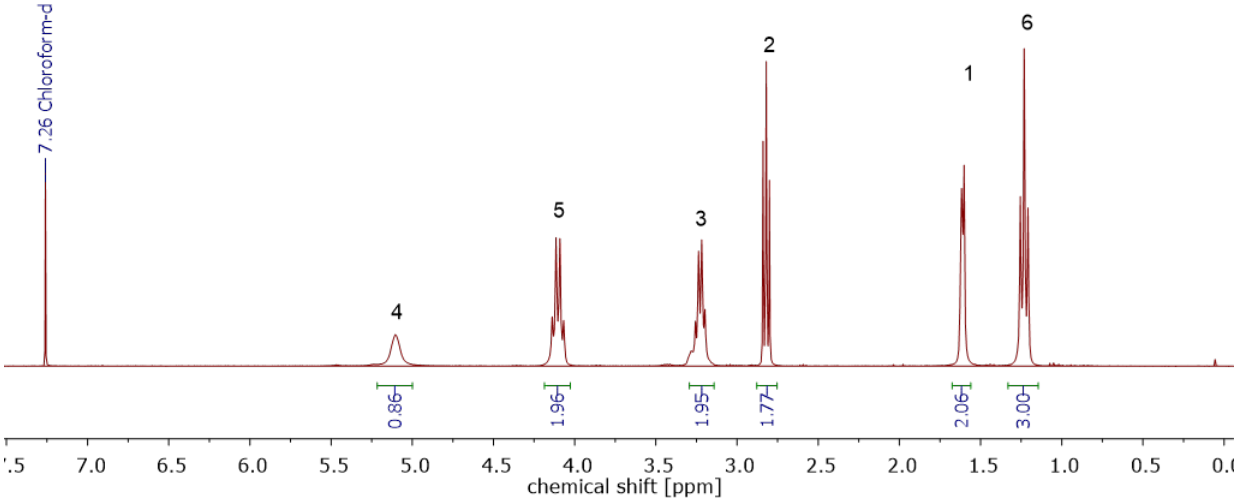

Figure 65: ^{1}H NMR of **25**.

1-ethyl 1-(2-propionamidoethyl) 2-vinyl cyclopropane-1,1-dicarboxylate

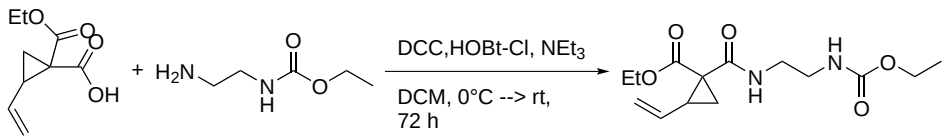

43 **25** **6**

Under argon, 1.45 g **43** (1.1 eq, 7.9 mmol), HOBt-Cl (1.25 eq, 1.41 g, 8.3 mmol), and **25** (950 mg g, 7.2 mmol) were dissolved in 20 ml dry DCM. At 0 °C , NEt_3 (2.1 eq, 1.60 g, 2.2 ml, 15.8 mmol) was added, and the reaction stirred for 15 min. At 0 °C in 10 dry DCM, dissolved DCC (1.05 eq, 1.63 g, 7.9 mmol) was slowly added. The reaction was stirred at 0 °C for one hour and at room temperature for 17 h. The reaction mixture was filtered, and the filtrate was washed three times with 0.5 M HCl, saturated $NaHCO_3$, and saturated NaCl solution, respectively. The organic phase was dried over $MgSO_4$, and the solvent was removed under reduced pressure. The product **6**

was obtained after purification using flash chromatography (Cylcohexane:EtOAc 100:0 → 8:2). White solid, yield 94 % (2.02 g, 6.8 mmol).

^{1}H NMR (300 MHz, $CDCl_3$, 293K):

δ [ppm] = 8.62 (s, 1H), 5.64 (ddd, J = 17.1, 10.2, 8.7 Hz, 1H), 5.37 – 5.28 (m, 1H), 5.16 (dd, J = 10.2, 1.1 Hz, 1H), 4.24 – 4.04 (m, 4H), 3.49 – 3.26 (m, 4H), 2.53 (dd, J = 17.1, 8.7 Hz, 1H), 2.03 (dt, J = 8.7, 4.3 Hz, 1H), 1.87 (dd, J = 8.0, 4.3 Hz, 1H), 1.31 – 1.18 (m, 7H).

^{13}C NMR (75 MHz, $CDCl_3$, 293K):

δ [ppm] = 171.3, 169.2, 157.0, 133.3, 119.8, 61.7, 61.0, 41.4, 40.1, 37.2, 34.4, 21.6, 14.8, 14.3 ppm.

FT-IR (ATR mode):

3326, 2981, 2929, 1716, 1691, 1641, 1531, 1479, 1450, 1373, 1344, 1314, 1258, 1239, 1146, 1030, 1018, 991, 971, 961, 915, 868, 838, 789, 738, 653 cm-1.

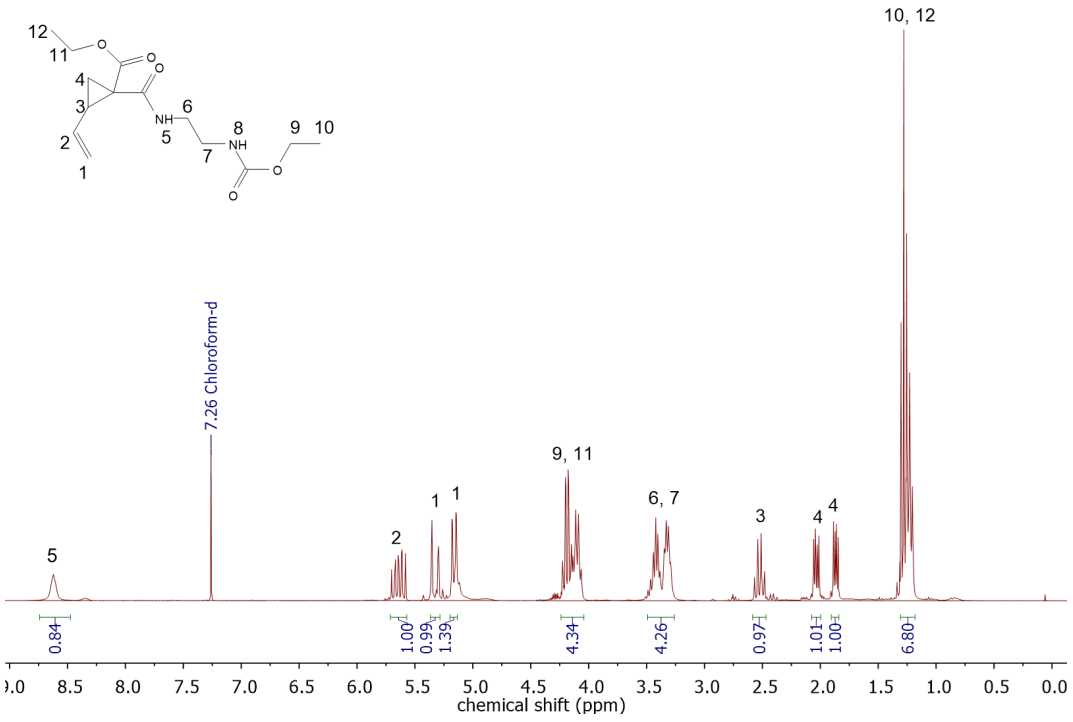

Figure 66: ^{1}H NMR of **6**.

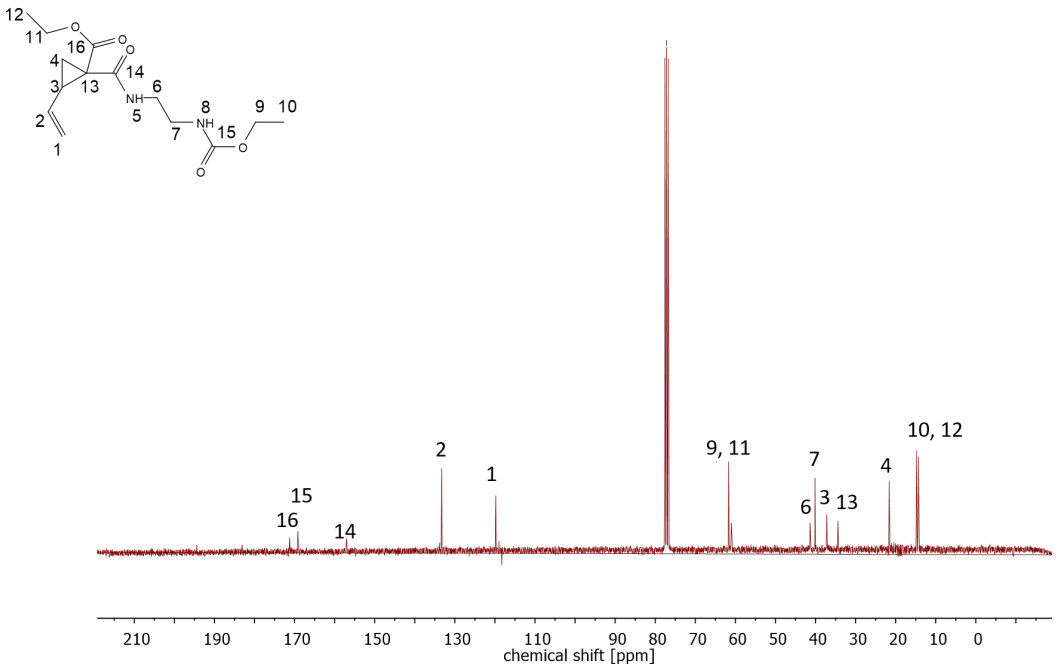

Figure 67: ^{13}C NMR of **6**.

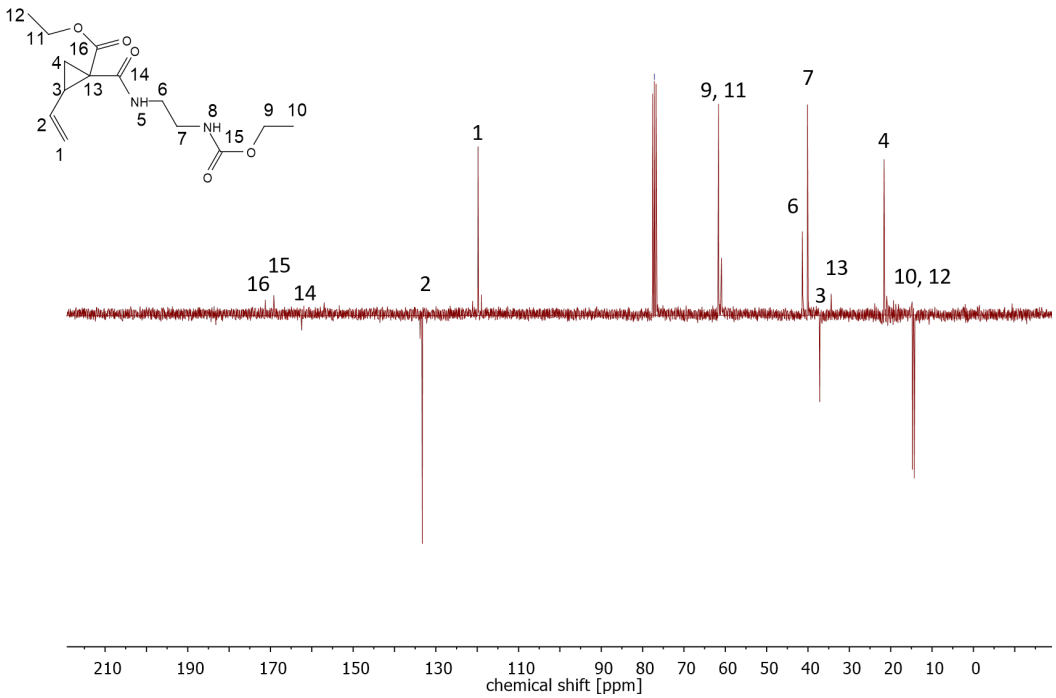

Figure 68: ^{13}C APT NMR of **6**.

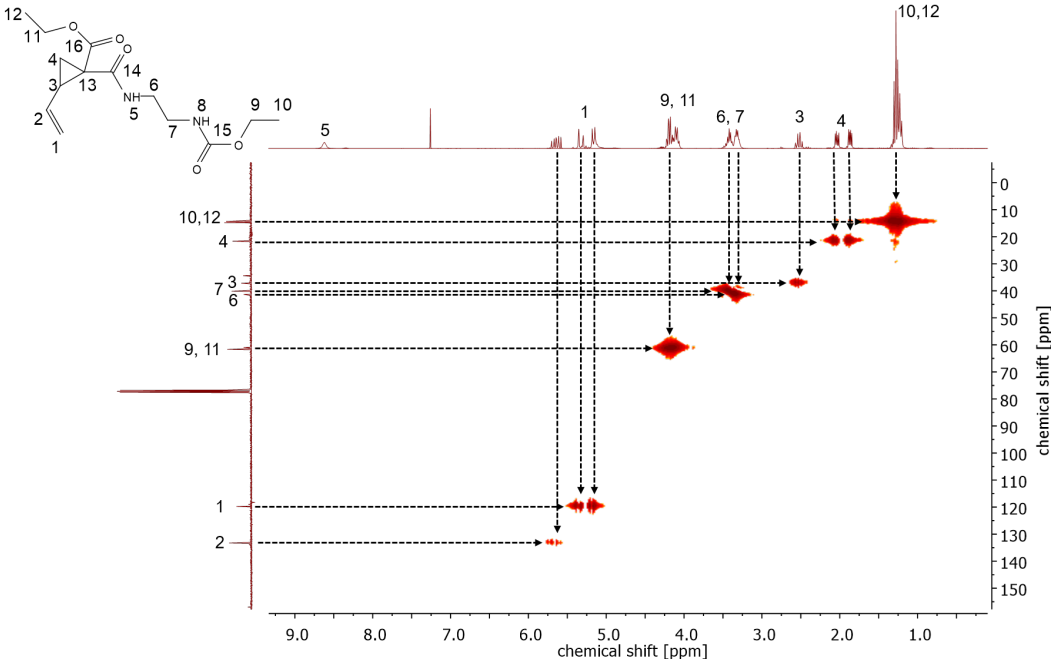

Figure 69: HSQC 2D NMR of **6**.

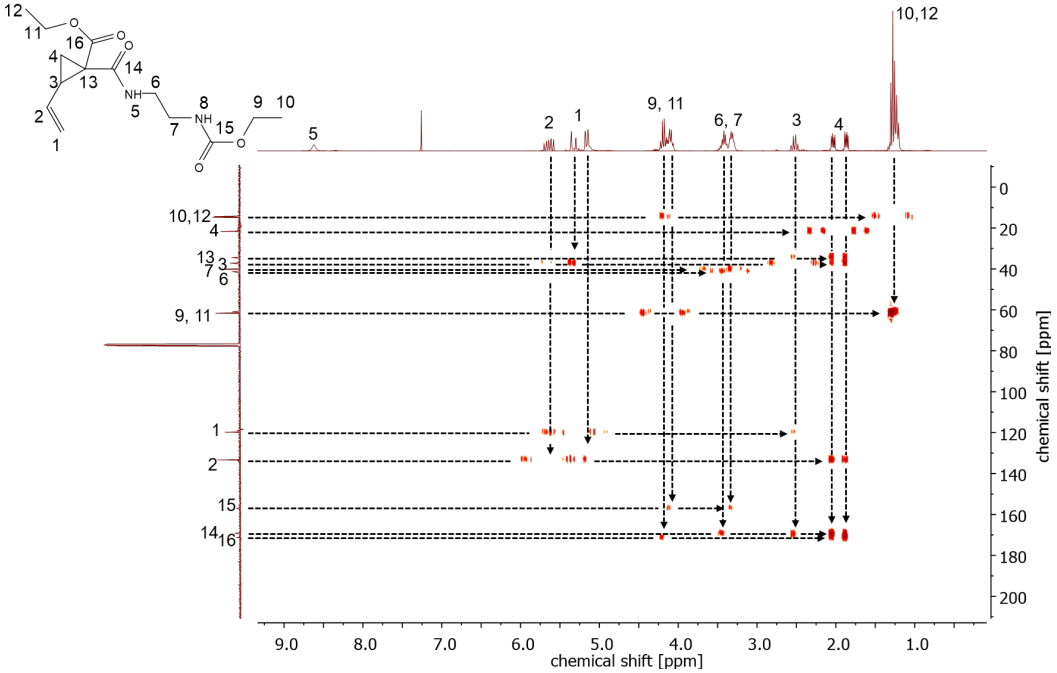

Figure 70: HMBC 2D NMR of **6**.

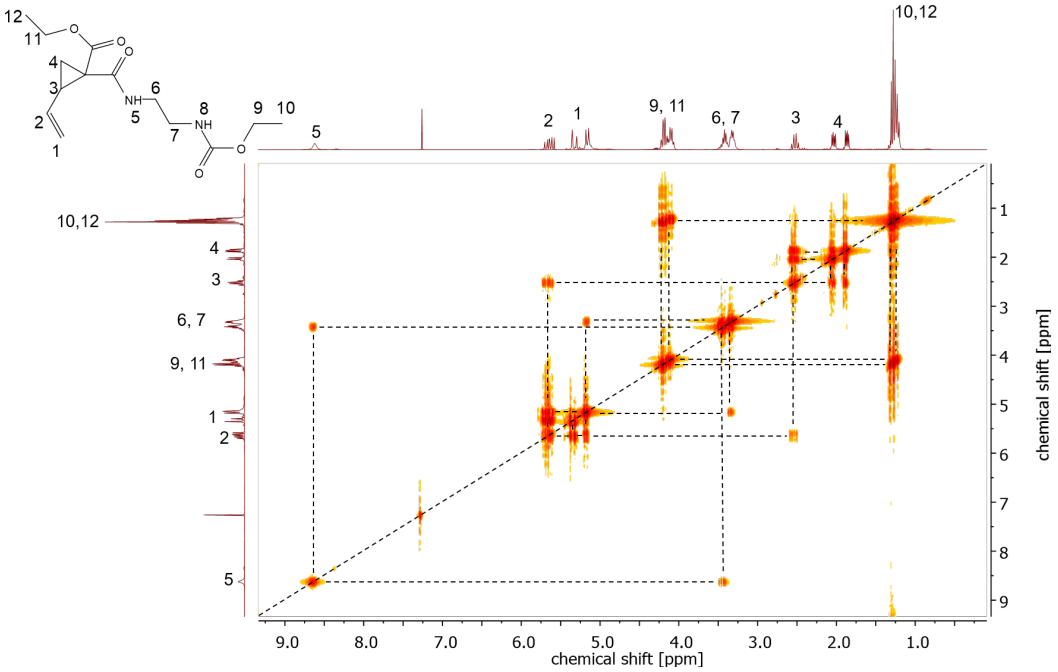

Figure 71: COSY 2D NMR of **6**.

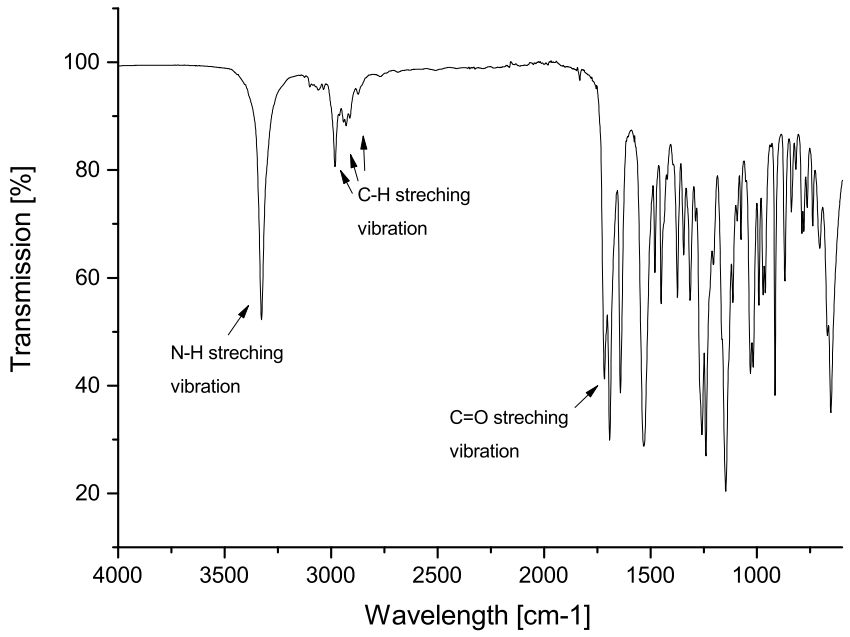

Figure 72: FT-IR of **6**.

Tert-butyl (2-aminoethyl)carbamate

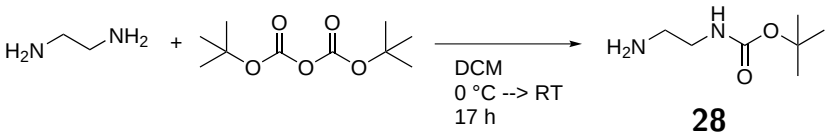

Ethylene diamine (10 eq, 60.1 g, 1000 mmol) was dissolved in 700 ml DCM. At 0°, in 500 ml DCM dissolved *tert*-butyl dicarbonate (21.8 g, 100 mmol) was added dropwise. The reaction mixture was stirred one hour at 0 °C and over night at room temperature. The solvent was removed, the reaction mixture dissolved in saturated $NaHCO_3$ solution and extracted with DCM. After evaporating the solvent, the product **28** was obtained as a slightly yellow liquid in a quantitative yield.

^{1}H NMR (300 MHz, $CDCl_3$, 293K):

δ [ppm] = 4.95 (s, 1H), 3.18 (dd, J = 11.7, 5.8 Hz, 2H), 2.81 (t, J = 5.9 Hz, 2H), 1.76 (s, 2H), 1.44 (s, 9H).

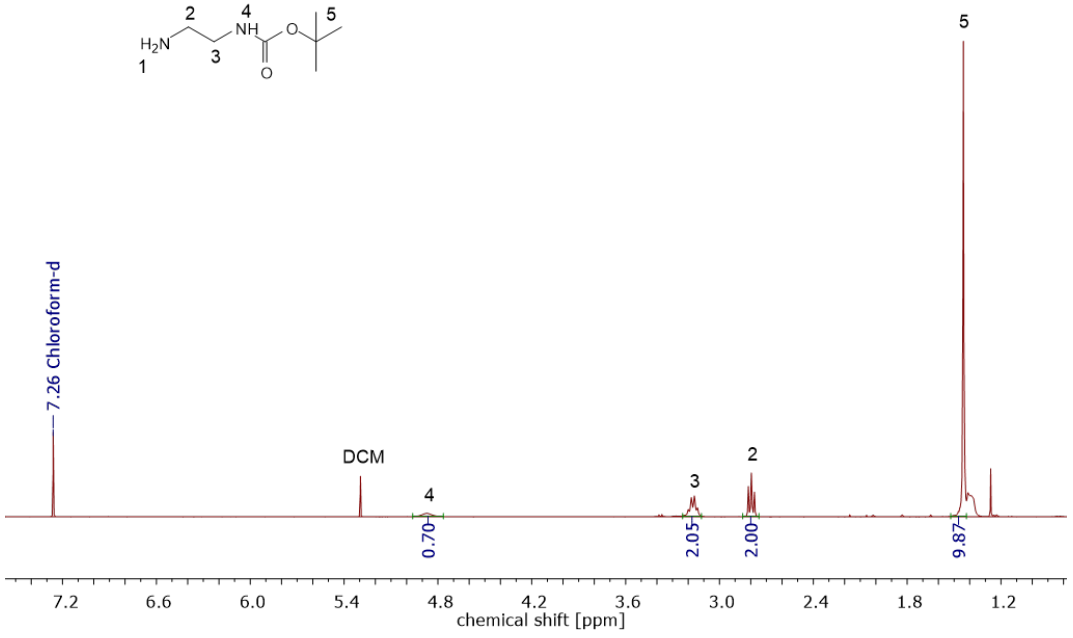

Figure 73: ^{1}H NMR of **28**.

1-(2-aminoethyl)-3-ethylurea

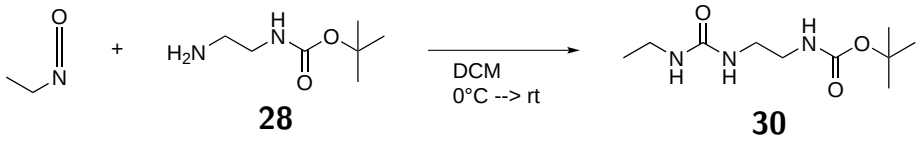

28 **30**

The protected diamine **28** (4.00 g, 25 mmol) was dissolved in 70 ml DCM. At 0 °C, in 25 ml DCM dissolved ethyl isocyanate (1 eq, 25 mmol 1.98 ml) was added. The reaction was stirred at 0 °C for one hour and at room temperature overnight. The formed solid was filtered and washed with hexane. The product **30** was obtained as a white solid in a yield of 83 % (4.81 g, 20.8 mmol).

^{1}H NMR (300 MHz, DMSO, 293K):

δ [ppm] = 6.78 (t, J = 5.0 Hz, 1H), 5.93 – 5.76 (m, 2H), 3.08 – 2.83 (m, 6H), 1.37 (s, 9H), 0.96 (t, J = 7.2 Hz, 3H).

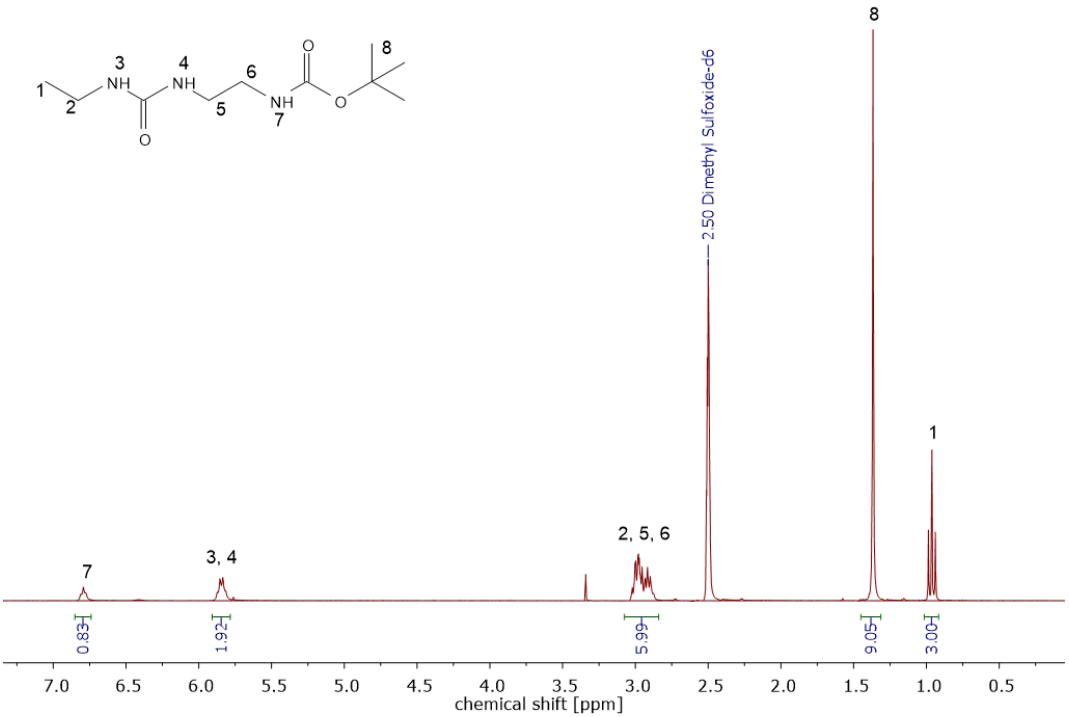

Figure 74: ^{1}H NMR of **30**.

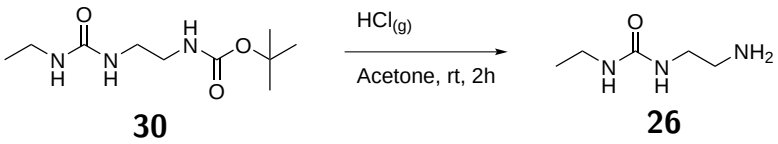

30 **26**

The protected Urea **30** (4.62 g, 18 mmol) was dissolved in 200 ml acetone. Over 1.5 h, freshly created HCl gas was bubbled through. The HCl gas was created by slowly adding concentrated H_2SO_4 to NH_4Cl. As soon the acetone solution is saturated with HCl, the solution becomes turbid and then a white solid is produced. After 1.5 h, the HCl flow was stopped and the solution was left for another hour. The product **26** was obtained as a white solid after filtration and washing with acetone.

^{1}H NMR (300 MHz, DMSO, 293K):

δ [ppm] = 8.11 (s, 2H), 3.20 (t, J = 6.2 Hz, 2H), 3.00 (q, J = 6.9 Hz, 2H), 2.78 (d, J = 5.2 Hz, 2H), 0.98 (t, J = 6.8 Hz, 3H).

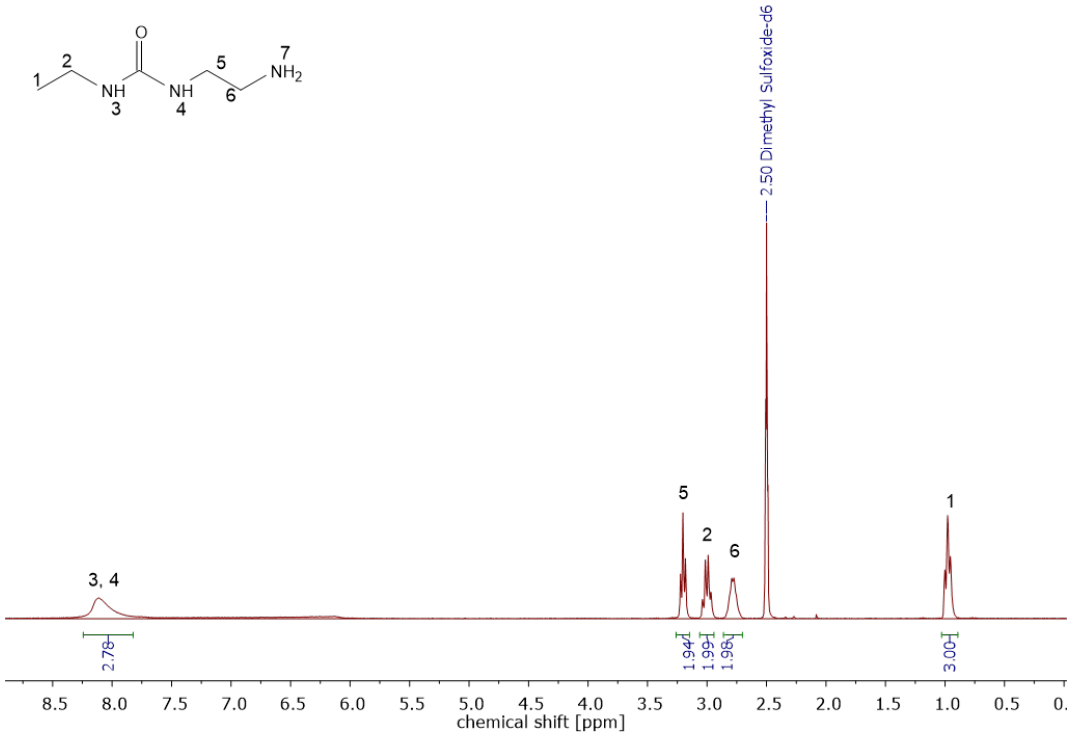

Figure 75: ^{1}H NMR of **26**.

1-ethyl 1-(2-(3-ethylureido)ethyl) 2-vinyl cyclopropane-1,1-dicarboxylate

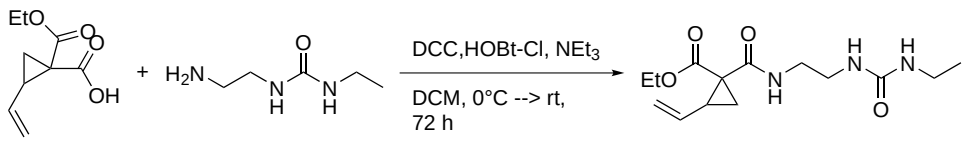

43 **26** **7**

Under argon, 3.0 g **43** (1.1 eq, 16.3 mmol), HOBt-Cl (1.25 eq, 2.89 g, 17.0 mmol), and **26** (1.94 g, 14.8 mmol) were dissolved in 45 ml dry DCM. At 0 °C , NEt_3 (2.1 eq, 3.30 g, 4.5 ml, 32.6 mmol) was added, and the reaction stirred for 15 min. At 0 °C in 20 dry DCM, dissolved DCC (1.05 eq, 3.36 g, 16.3 mmol) was slowly added. The reaction was stirred at 0 °C for one hour and at room temperature for 17 h. The reaction mixture was filtered, and the filtrate was washed three times with 0.5 M HCl, saturated $NaHCO_3$, and saturated NaCl solution, respectively. The organic phase was dried over $MgSO_4$, and the solvent was removed under reduced pressure. The product **7** was obtained after purification using flash chromatography (DCM:EtOAc 3:7 → 0:100). Light yellow highly viscous liquid, yield 19 % (847 mg, 2.85 mmol).

^{1}H NMR (300 MHz, $CDCl_3$, 293K):

δ [ppm] = 8.69 (s, 1H), 5.75 – 5.56 (m, 1H), 5.39 – 5.25 (m, 1H), 5.20 – 5.09 (m, 1H), 4.29 – 4.09 (m, 2H), 3.43 (ddt, J = 10.8, 8.3, 6.0 Hz, 2H), 3.36 – 3.26 (m, 2H), 3.18 (q, J = 7.2 Hz, 2H), 2.58 – 2.42 (m, 1H), 2.05 – 1.93 (m, 1H), 1.93 – 1.84 (m, 1H), 1.26 (dt, J = 6.0, 4.8 Hz, 4H), 1.12 (t, J = 7.2 Hz, 3H).

^{13}C NMR (75 MHz, $CDCl_3$, 293K):

δ [ppm] = 171.1, 169.7, 158.6, 133.2, 119.8, 61.7, 41.1, 40.5, 37.0, 35.5, 34.5, 21.6, 15.5, 14.3 ppm.

FT-IR (ATR mode):

3345, 2978, 2874, 1707, 1633, 1531, 1444, 1372, 1312,2 1242, 1142, 10462, 1020, 993, 959, 915, 864, 773, 632 cm-1.

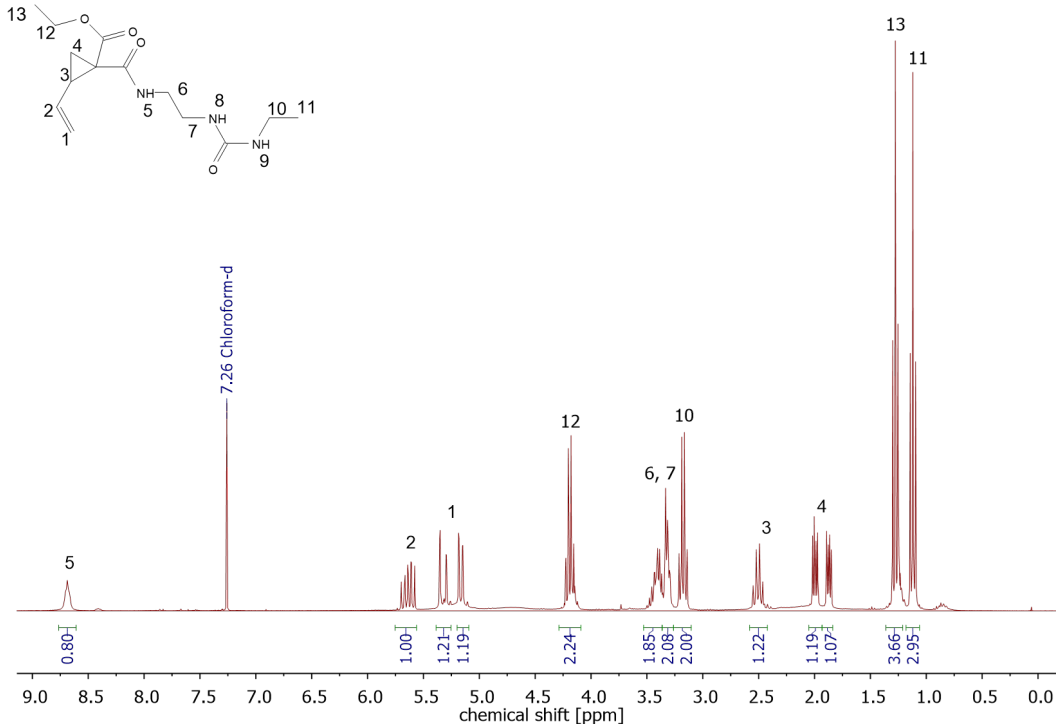

Figure 76: ^{1}H NMR of **7**.

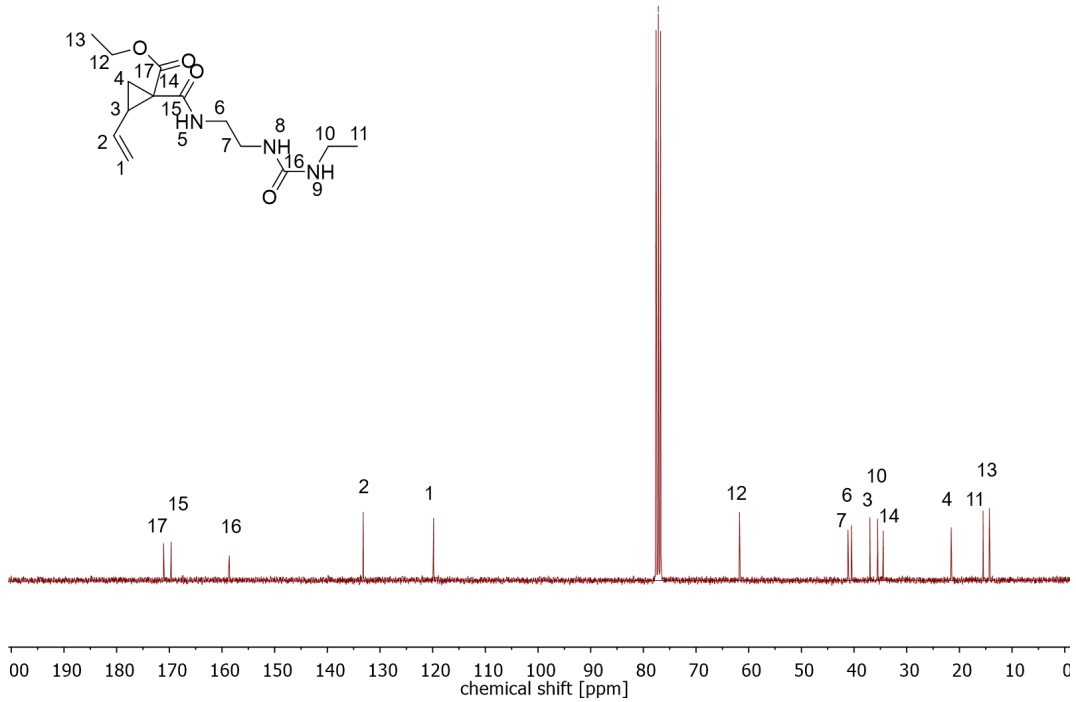

Figure 77: ^{13}C NMR of **7**.

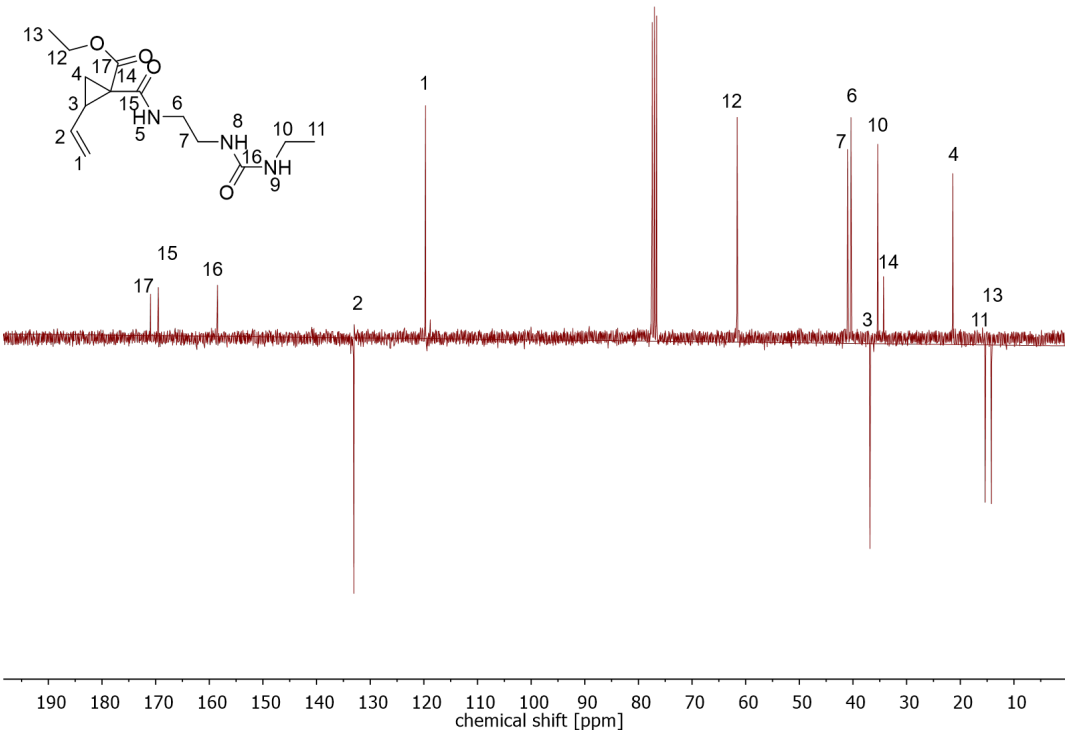

Figure 78: ^{13}C APT NMR of **7**.

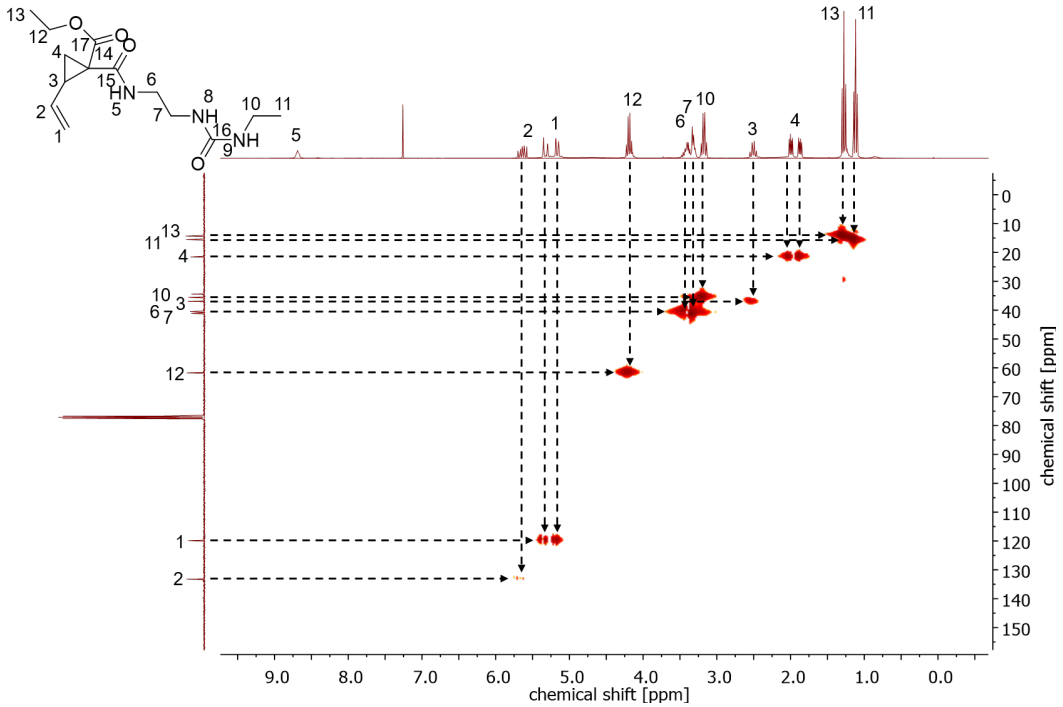

Figure 79: HSQC 2D NMR of **7**.

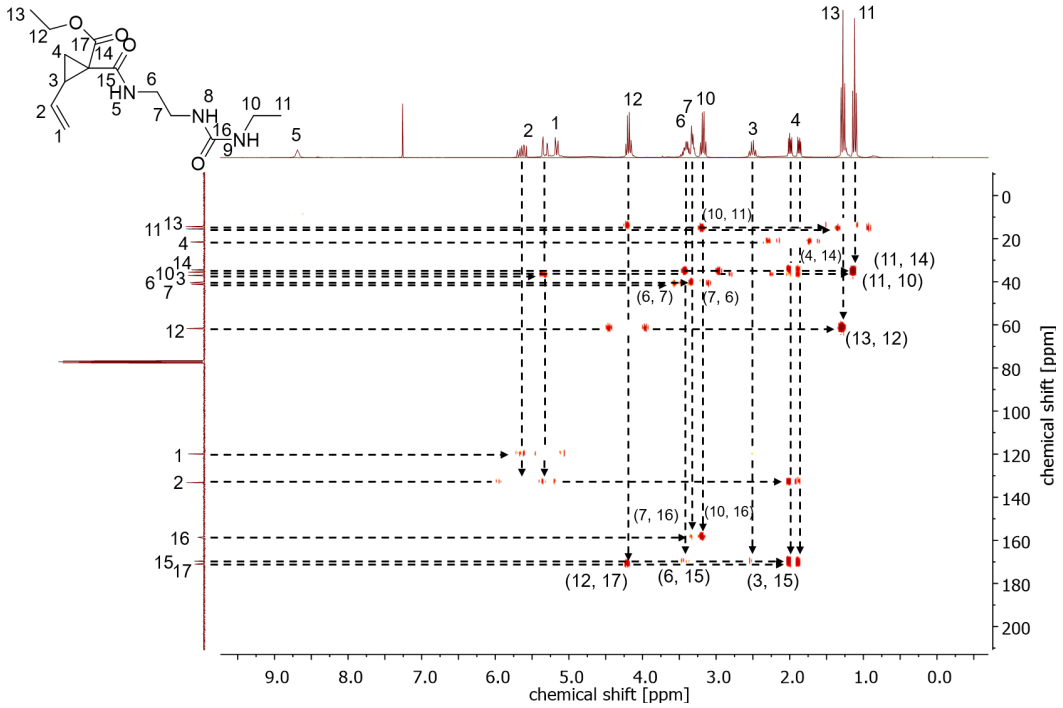

Figure 80: HMBC 2D NMR of **7**.

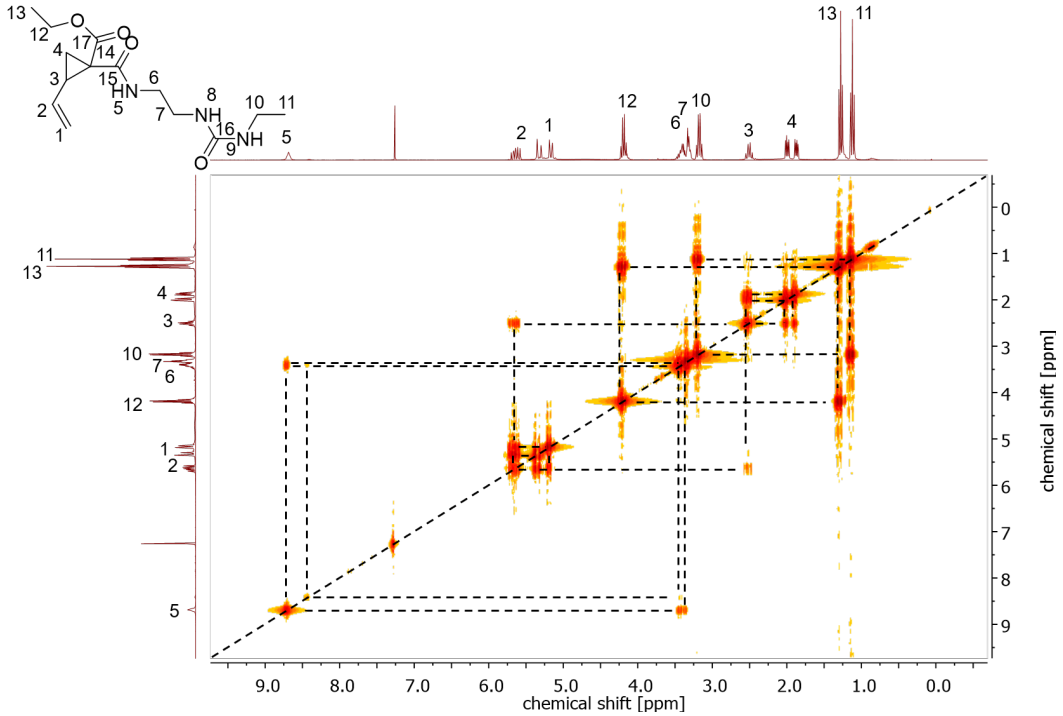

Figure 81: COSY 2D NMR of **6**.

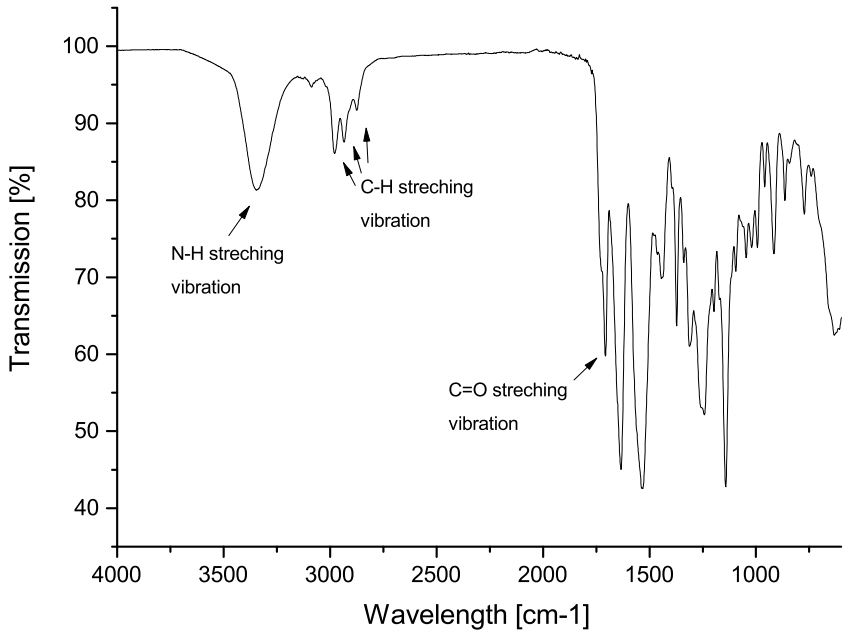

Figure 82: FT-IR of **6**.

N-(2-aminoethyl)propionamide

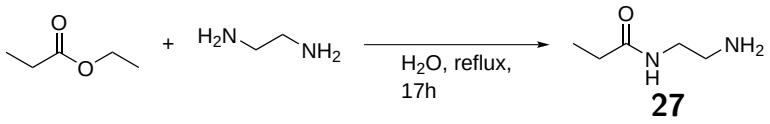

Under argon, ethylene diamine (24.0 g, 400mmol) and ethyl propionate (1 eq, 40.8 g, 400 mmol) were dissolved in 20 ml water. The mixture was stirred under reflux overnight. The solvent and unreacted compounds were removed under reduced pressure. The crude product **27** was used without further purification. **^{1}H NMR (300 MHz, $CDCl_3$, 293K):**

δ [ppm] = 6.10 (s, 1H), 3.32 (dd, J = 11.6, 5.8 Hz, 2H), 2.90 – 2.82 (m, 2H), 2.29 – 2.14 (m, 2H), 1.20 – 1.13 (m, 3H).

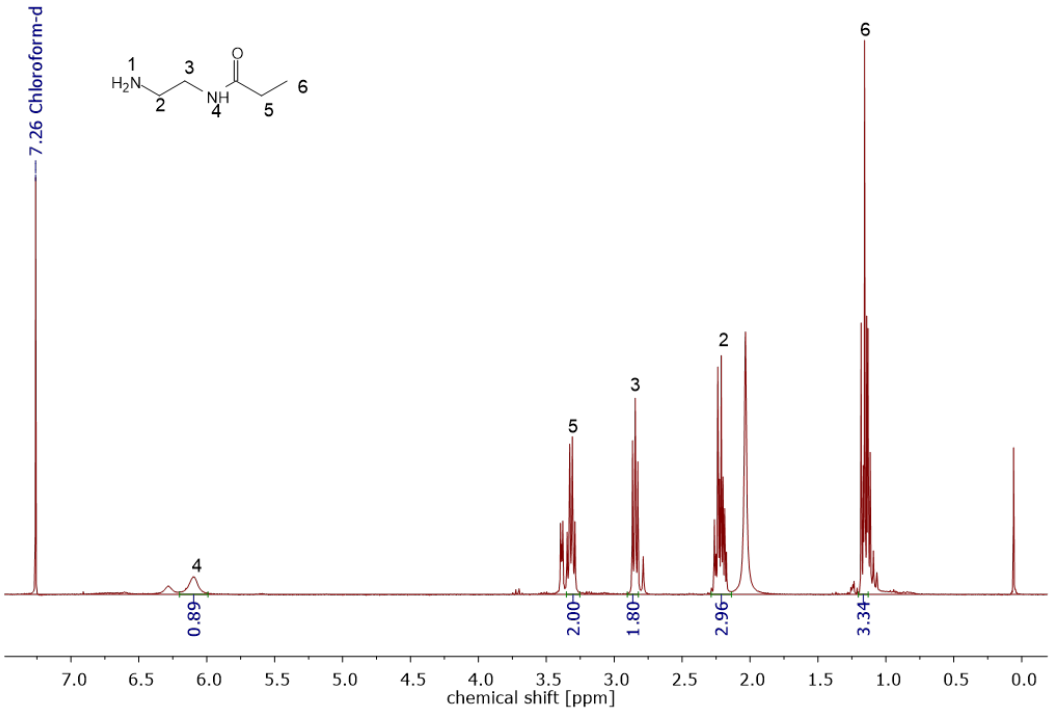

Figure 83: ^{1}H NMR of **27**.

1-(2-((ethoxycarbonyl)amino)ethyl) 1-ethyl 2-vinyl cyclopropane-1,1-dicarboxylate

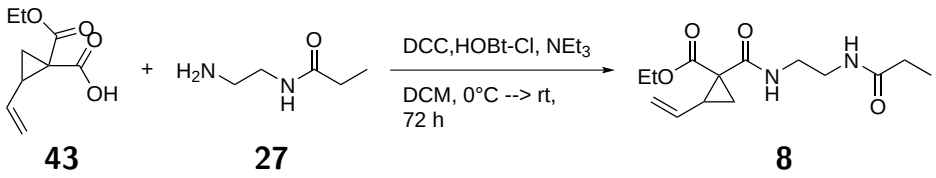

43 **27** **8**

Under argon, 6.8 g **43** (1.1 eq, 36.9 mmol), HOBt-Cl (1.25 eq, 6.68 g, 39.4 mmol), and **27** (3.98 g, 34.0 mmol) were dissolved in 15 ml dry DCM. At 0 °C, NEt_3 (2.1 eq, 7.64 g, 10.5 ml, 75.4 mmol) was added, and the reaction stirred for 15 min. At 0 °C in 40 dry DCM, dissolved DCC (1.05 eq, 5.47 g, 37.7 mmol) was slowly added. The reaction was stirred at 0 °C for one hour and at room temperature for 17 h. The reaction mixture was filtered, and the filtrate was washed three times with 0.5 M HCl, saturated $NaHCO_3$, and saturated NaCl solution, respectively. The organic phase was dried over $MgSO_4$, and the solvent was removed under reduced pressure. The product **8** was obtained after purification using flash chromatography (EtOAc: MeOH 100:0 →

9:1). Light yellow viscous liquid, yield 41 % (3.84 g, 13.7 mmol).

^{1}H NMR (300 MHz, $CDCl_3$, 293K):

δ [ppm] = 8.73 (s, 1H), 6.38 (s, 1H), 5.64 (ddd, J = 17.2, 10.1, 8.8 Hz, 1H), 5.39 – 5.25 (m, 1H), 5.17 (dd, J = 10.2, 1.4 Hz, 1H), 4.19 (q, J = 7.2 Hz, 2H), 3.55 – 3.30 (m, 4H), 2.51 (q, J = 8.7 Hz, 1H), 2.20 (q, J = 7.6 Hz, 2H), 2.02 (dd, J = 9.1, 4.3 Hz, 2H), 1.88 (dd, J = 8.0, 4.3 Hz, 1H), 1.28 (t, J = 7.1 Hz, 3H), 1.13 (t, J = 7.6 Hz, 3H).

^{13}C NMR (75 MHz, $CDCl_3$, 293K):

δ [ppm] = 174.5, 171.2, 169.9, 133.2, 119.9, 61.8, 41.0, 39.6, 37.3, 34.3, 29.8, 21.7, 14.3, 10.0.

FT-IR (ATR mode):

3317, 2981, 2939, 1707, 1642, 1529, 1464, 1434, 1372, 1339, 1238, 1143,1046, 959, 915, 863, 774, 634 cm 1.

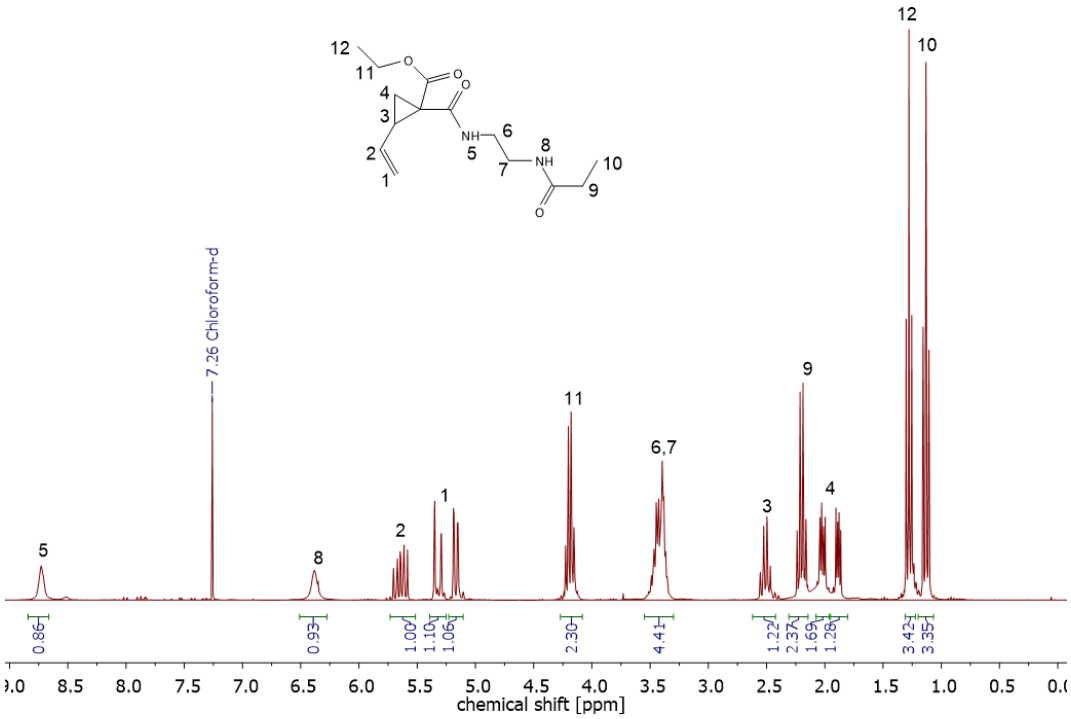

Figure 84: ^{1}H NMR of **8**.

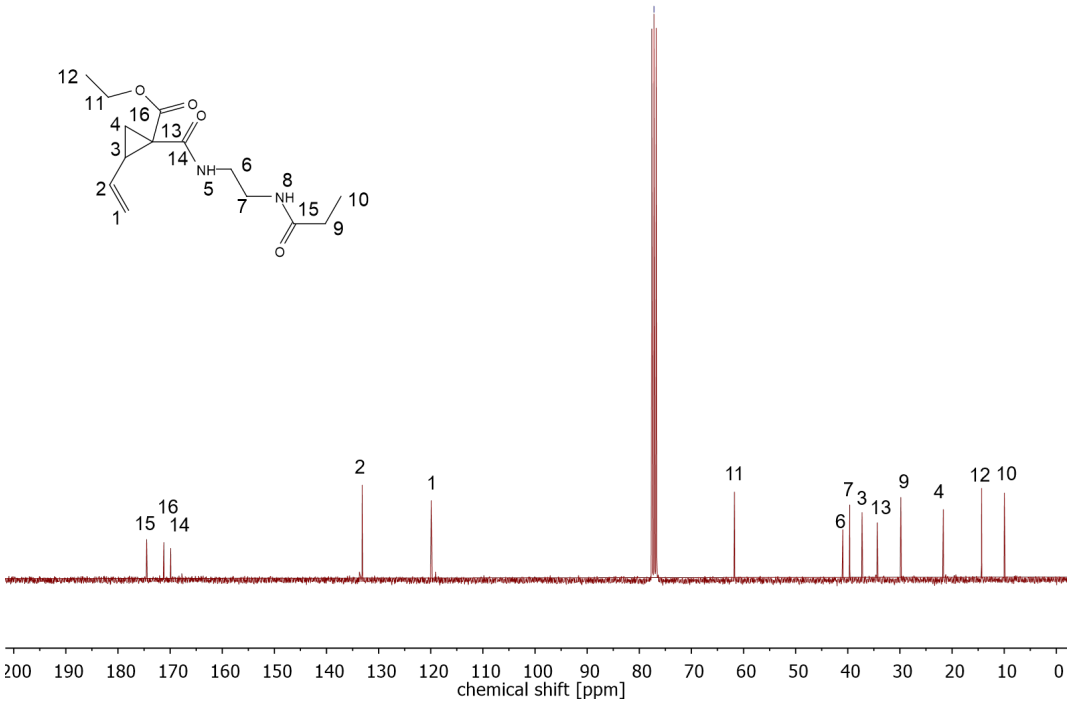

Figure 85: ^{13}C NMR of **8**.

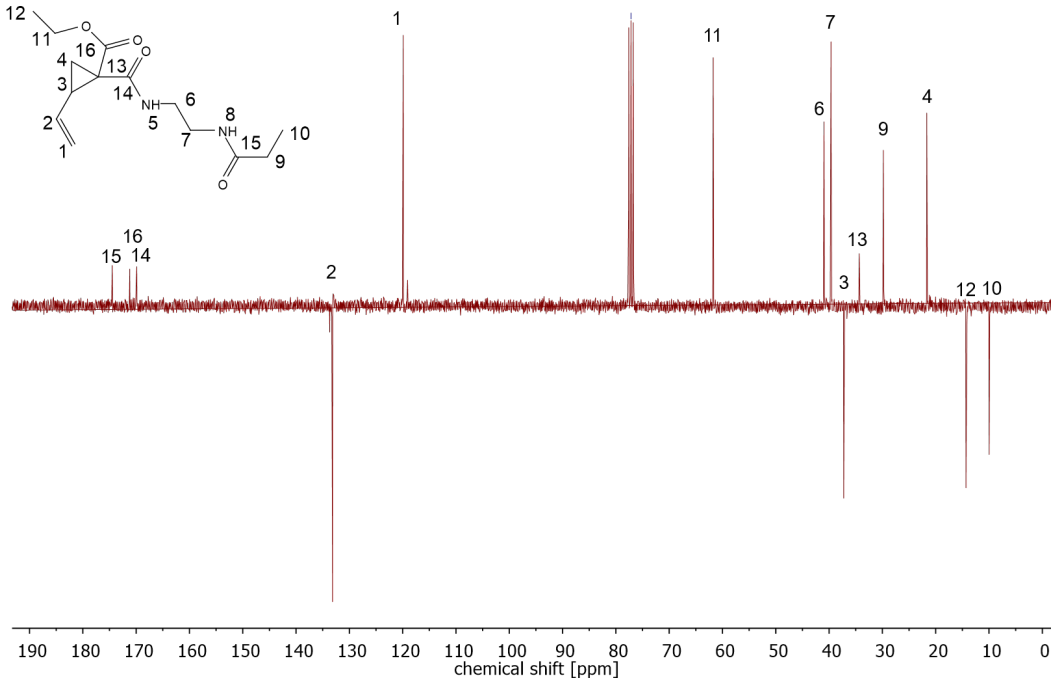

Figure 86: ^{13}C APTNMR of **8**.

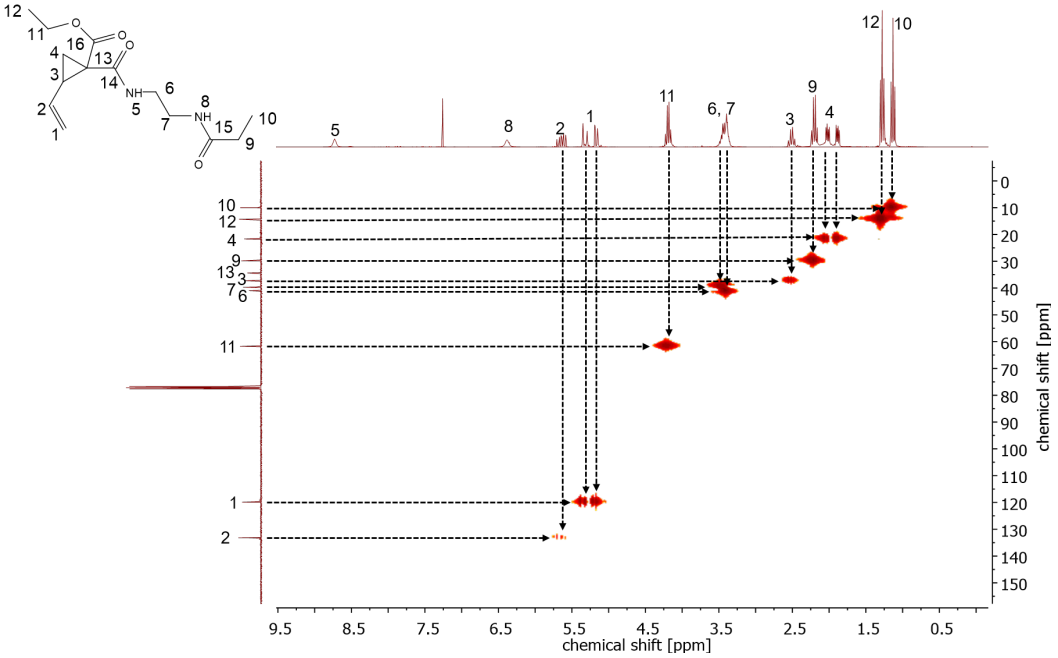

Figure 87: HSQC 2D NMR of **8**.

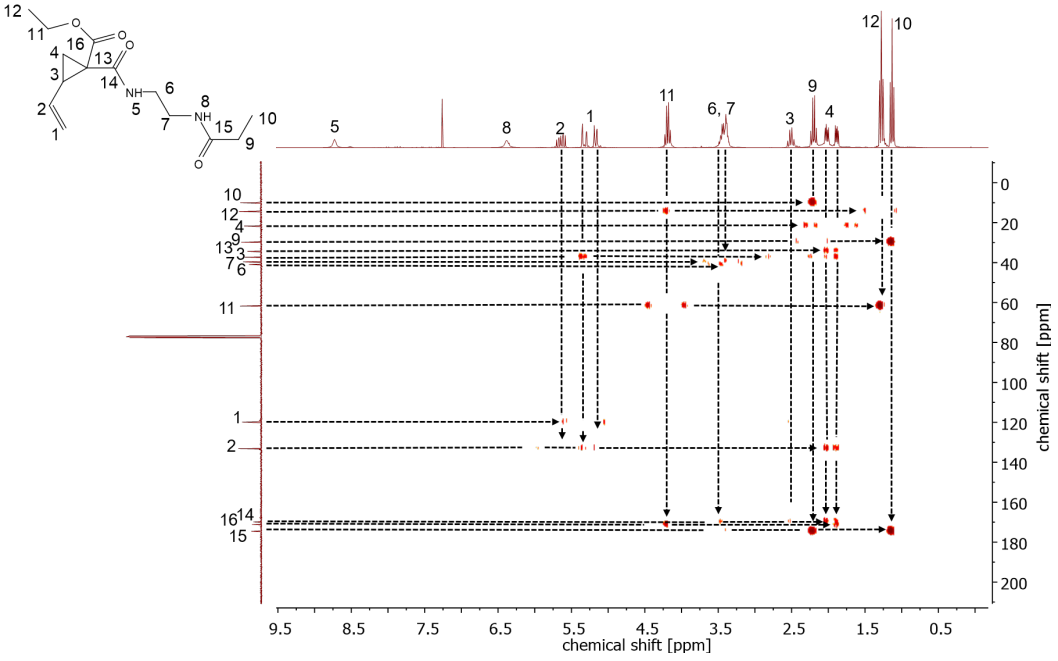

Figure 88: HMBC 2D NMR of **8**.

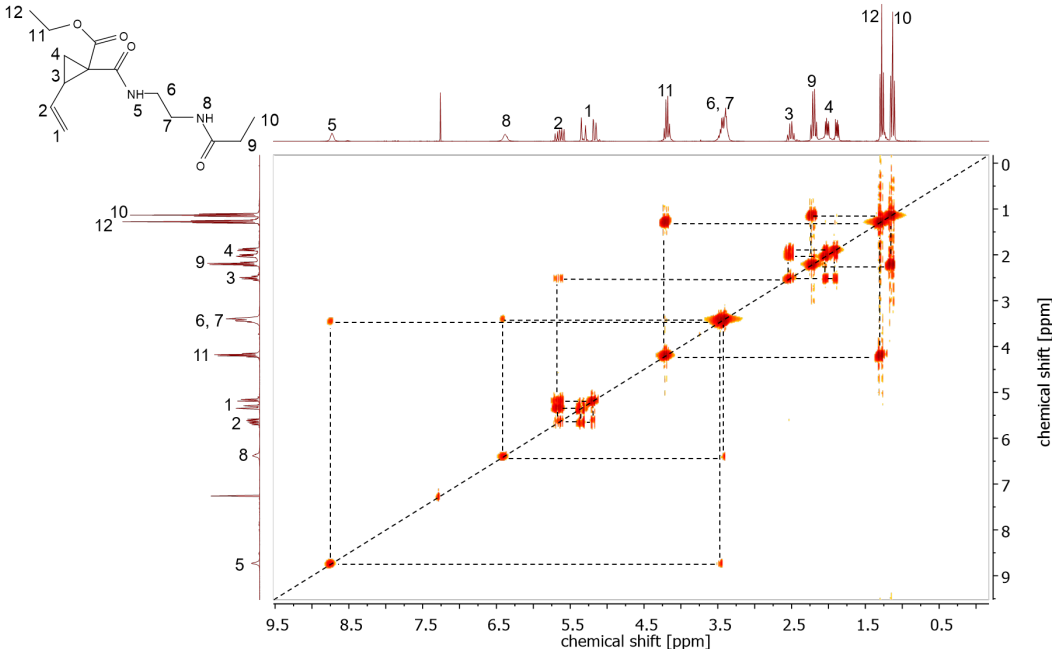

Figure 89: COSY 2D NMR of **8**.

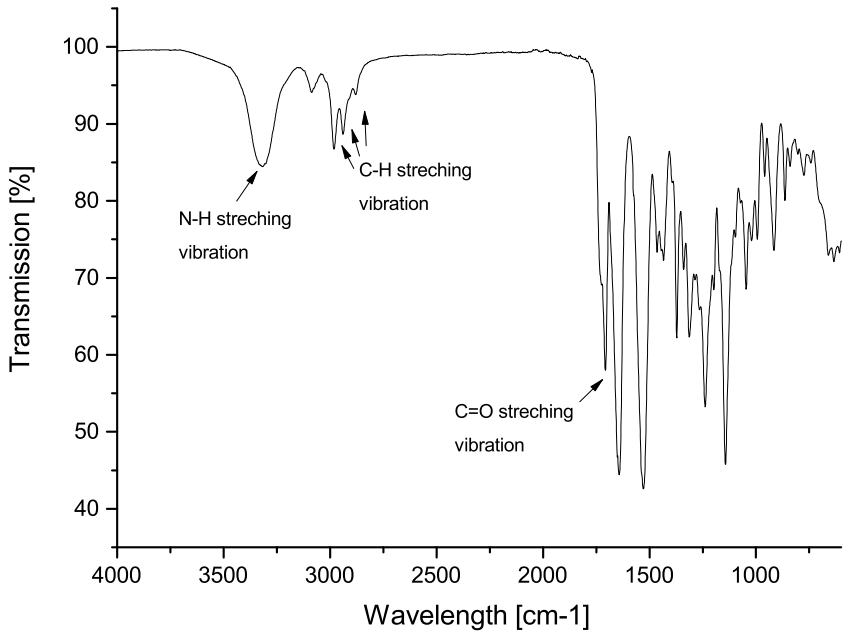

Figure 90: FT-IR of **8**.

4.2.5 Synthesis of Bifunctional VCPs

1,3-bis(2-aminoethyl)urea

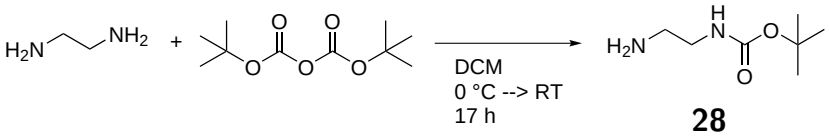

28

Synthesis of **28** was performed as described in section 4.2.4.

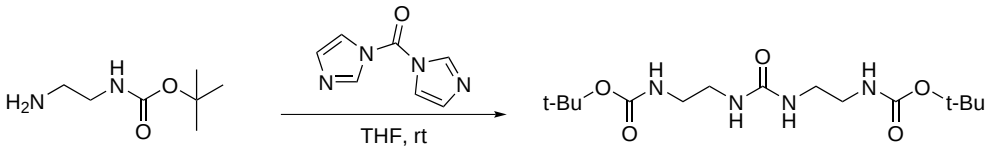

28 **36**

28 (2 eq, 7.9 g, 49.34 mmol) was dissolved in 100 ml of dry THF. At 0 °C CDI (4.0 g, 24.67 mmol) was added. The reaction mixture was stirred at room temperature over night. The reaction was quenched by adding water and extracted with EtOAc. The organic phase was dried over $MgSO_4$, and the solvent was reduced to a little amount. The product **36** starts to crystallize and can be obtained after filtration and washing with THF in a yield of 58 % (4.93 g, 14.3 mmol)

^{1}H NMR (300 MHz, DMSO, 293K):
δ [ppm] = 2.98 (t, J = 5.5 Hz, 2H), 2.92 (t, J = 5.3 Hz, 2H), 1.37 (s, 9H).

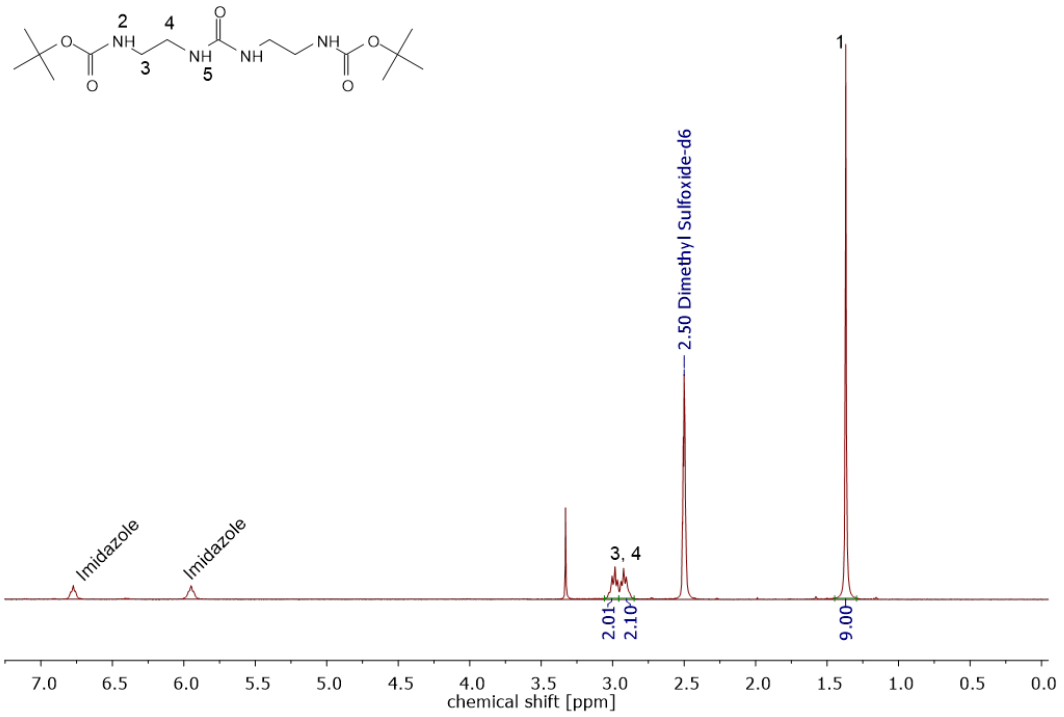

Figure 91: ^{1}H NMR of **36**.

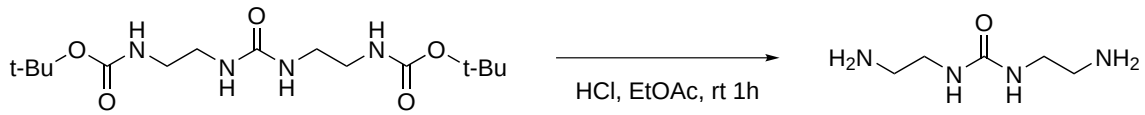

36 **35**

36 (2.0 g, 5.8 mmol) was added to 6 ml of a 6 molar (M) HCl in EtOAc solution. The mixture was stirred at room temperature (rt) for 2 h. After 1 h, 1 ml of concentrated HCl was added. The mixture was filtered and washed with EtOAc to obtain the product **35** as white solid.

^{1}H NMR (300 MHz, DMSO, 293K):

δ [ppm] = 3.31 – 3.18 (m, 4H), 2.81 (dd, J = 11.4, 5.7 Hz, 4H).

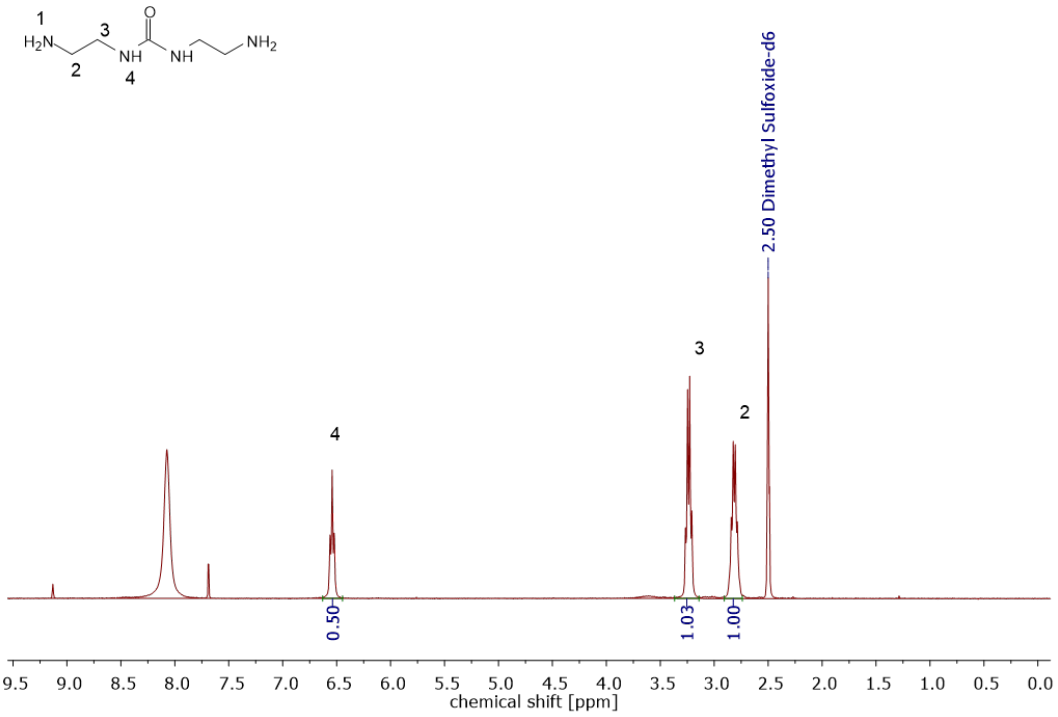

Figure 92: ^{1}H NMR of **35**.

Diethyl 1,1'-(6-oxo-2,5,7,10-tetraazaundecane-1,11-dioyl)bis(2-vinylcyclopropanecarboxylate)

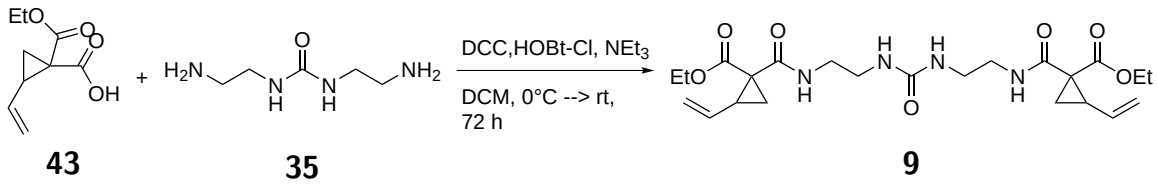

43 **35** **9**

Under an argon atmosphere, **35** (1.86g, 12.7 mmol), **9** (2.0 eq, 4.68 g, 25.4 mmol) and HOBt-Cl(2.1 eq, 4.5 g, 26.6 mmol) were dissolved in 20 ml dry DCM. At 0 °C NEt_3 (4.2 eq, 7.4 ml, 53.3 mmol) was added and in 30 ml dry DCM dissolved DCC (2.2 eq, 5.76 g, 27.9 mmol) was added dropwise. The reaction mixture was stirred at room temperature overnight. The mixture was filtrated, the solvent removed and the mixture purified via flash chromatography (EtOAc:MeOH 20:1 → 10:1) to obtain the product **9** in a yield of 4% (424 mg, 0.5 mmol).

^{1}H NMR (300 MHz, $CDCl_3$, 293K):

δ [ppm] = 5.70 – 5.54 (m, 2H), 5.31 (dd, J = 17.1, 1.1 Hz, 2H), 5.15 (dd, J = 10.3, 1.3 Hz, 2H), 4.16 (tdd, J = 7.2, 5.3, 1.9 Hz, 4H), 3.51 – 3.20 (m, 8H), 2.50 (dd, J = 17.1,

8.7 Hz, 2H), 1.98 (dd, J = 9.1, 4.3 Hz, 2H), 1.85 (dd, J = 8.0, 4.3 Hz, 2H), 1.26 (t, J = 7.1 Hz, 6H).

^{13}C NMR (75 MHz, $CDCl_3$, 293K):

δ [ppm] = 171.0, 169.3, 158.8, 133.2, 119.8, 61.7, 40.6, 36.9, 34.4, 21.5, 14.3.

FT-IR (ATR mode):

3335, 3087, 2983, 2935, 1705, 1634, 1530, 1467, 1435, 1395, 1340, 1313, 1264, 1197, 1142, 1095, 1073, 1019, 993, 959, 916, 863, 840, 805, 775, 712, 639,516

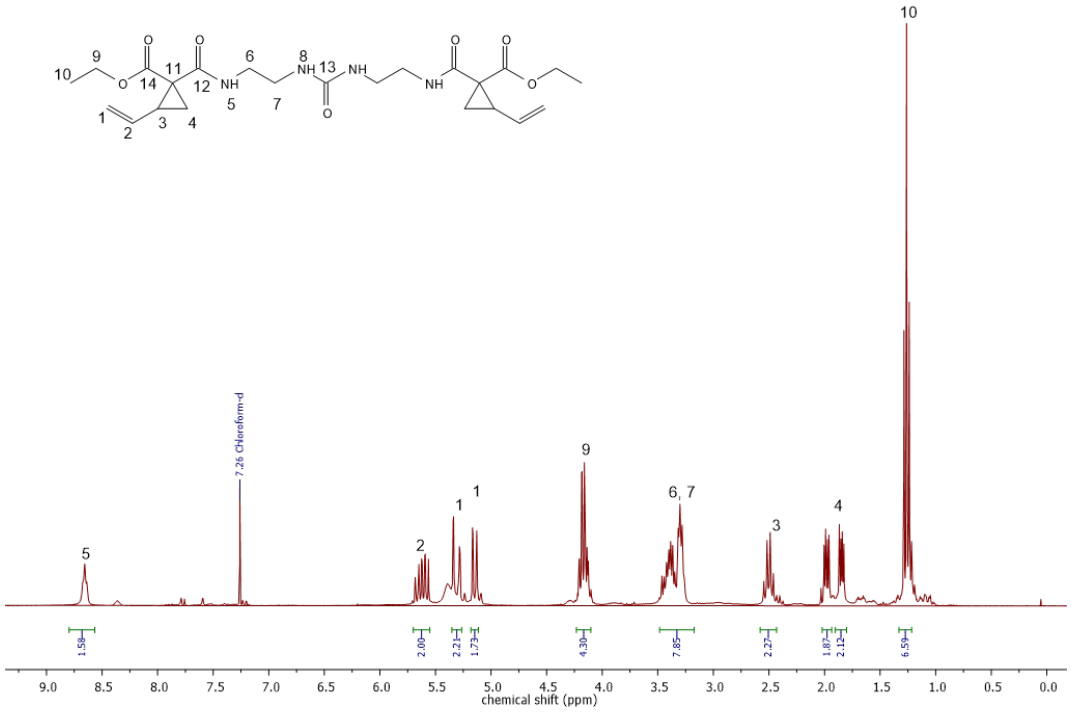

Figure 93: ^{1}H NMR of **9**.

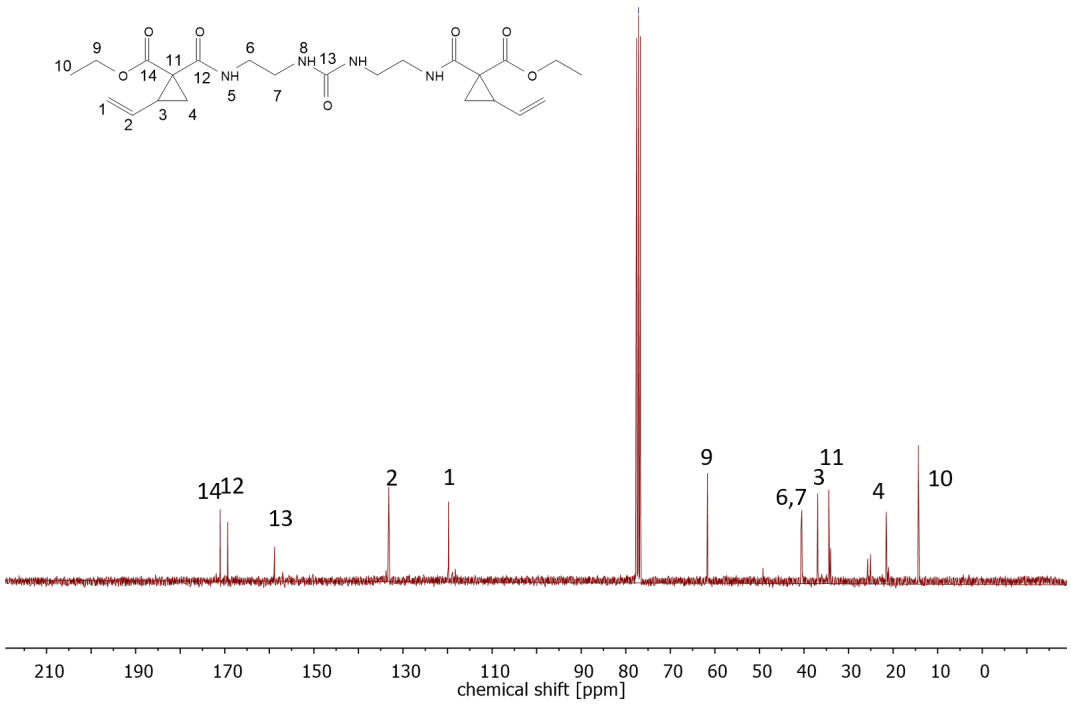

Figure 94: ^{13}C NMR of **9**.

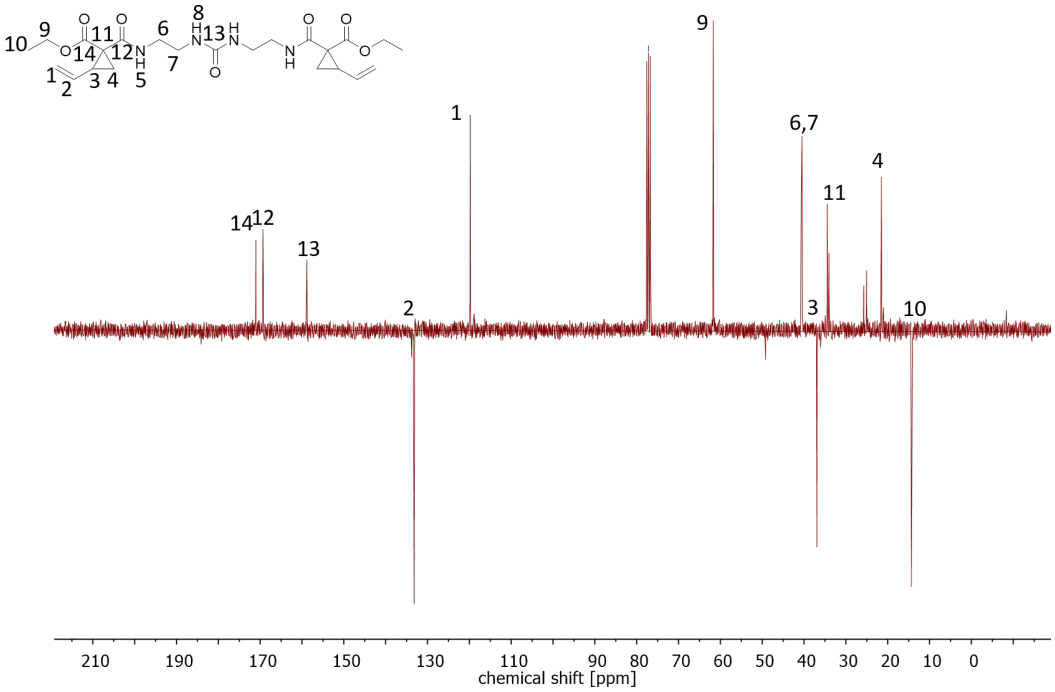

Figure 95: ^{13}C APT NMR of **9**.

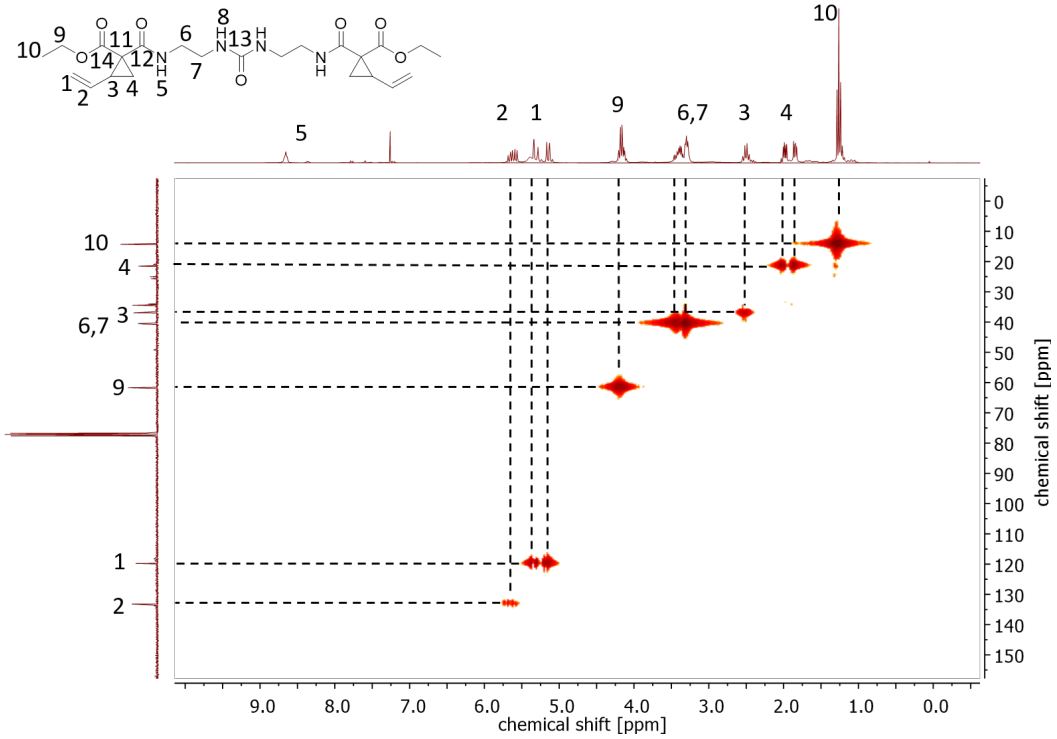

Figure 96: HSQC 2D NMR of **9**.

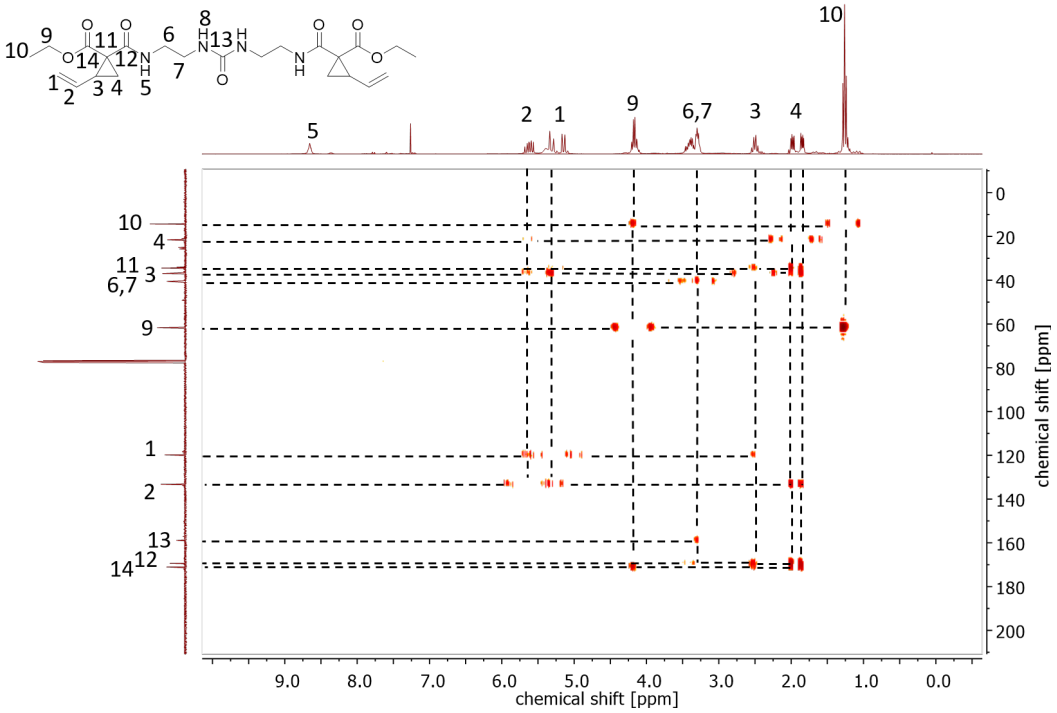

Figure 97: HMBC 2D NMR of **9**.

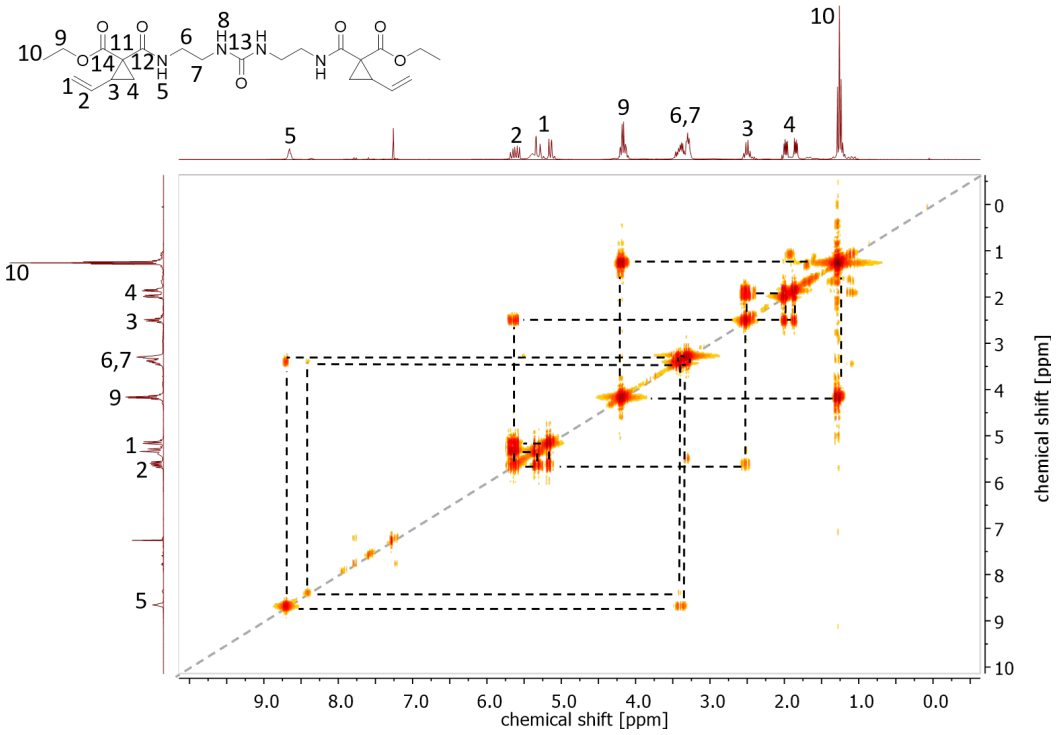

Figure 98: COSY 2D NMR of **9**.

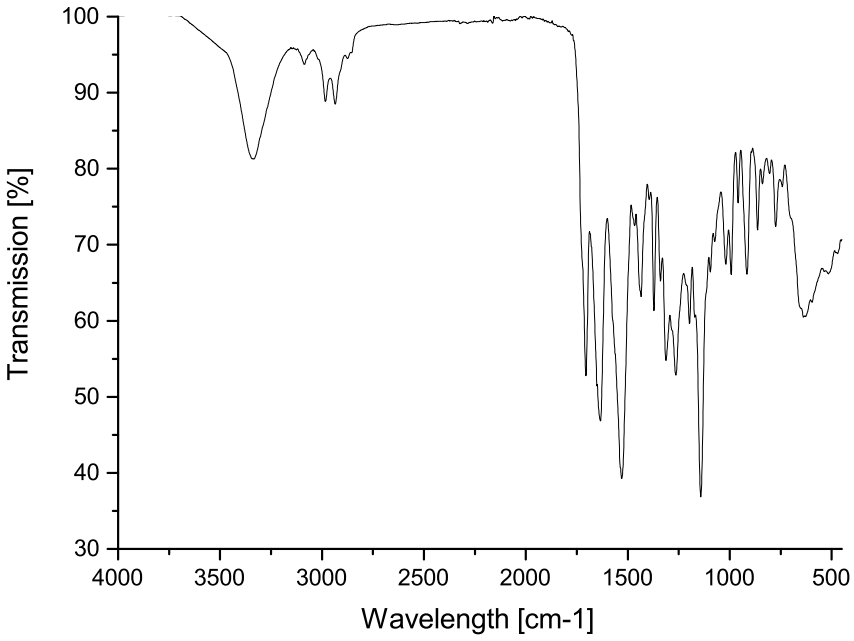

Figure 99: FT-IR of **9**.

1,3-bis(2-hydroxyethyl)urea

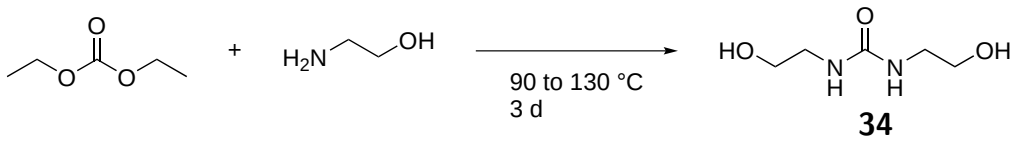

34

Diethylcarbonate (72.15 g, 610 mmol) and 2-aminoethan-1-ol (3 eq, 111.78 g, 1830 mmol) were stirred at 90 °C for one hour and at 130 °C for three days. The flask was attached to a distillation bridge to remove the built ethanol from the reaction. The mixture was put under reduced pressure till a solid was formed. The crude mixture was recrystallized in ethanol to yield the pure product **34** as white crystals.

^{1}H NMR (300 MHz, DMSO, 293K):

δ [ppm] = 5.98 (t, J = 5.6 Hz, 2H), 4.66 (t, J = 5.2 Hz, 2H), 3.33 (dt, J = 5.7 Hz, 4H), 3.03 (dt, J = 5.8 Hz, 5.7 Hz, 4H).

O'1,O1-((carbonylbis(azanediyl))bis(ethane-2,1-diyl)) 1-diethyl bis(2-vinylcyclopropane-1,1-dicarboxylate)

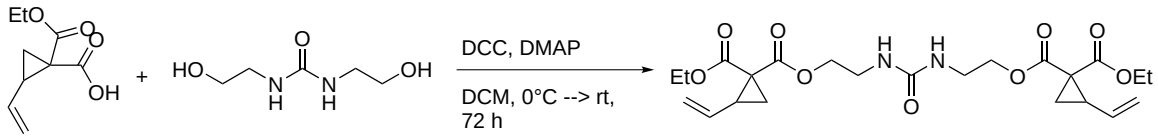

43 **34** **10**

Under argon **34** (1.48 g, 10.0 mmol), **43** (2.5 eq, 4.60 g, 25.0 mmol) and DMAP (0.1 eq, 122 mg, 1.00 mmol) were dissolved in 20 ml dry DCM. At 0°in 40 ml dry DCM dissolved DCC (2.4 eq, 4.95 g, 24.0 mmol) was added dropwise. The reaction was stirred at room temperature for 5 days and afterwards filtrated. The organic phase was washed once with 0.5 M HCl solution, once with saturated $NaHCO_3$ solution and twice with water. After drying over $MgSO_4$ the solvent was removed and the product **10** obtained after purification via flash chromatography (Cylcohexane:EtOAc 7:3 → 3:7 → 0:100) in a yield of 68% (3.26 g, 6.78 mmol).

^{1}H NMR (300 MHz, $CDCl_3$, 293K):

δ [ppm] = 5.52 – 5.38 (m, 2H), 5.31 (dd, J = 17.0, 1.8 Hz, 2H), 5.16 (dd, J = 10.0, 1.6 Hz, 2H), 4.36 – 4.08 (m, 8H), 3.48 (s, 4H), 2.61 (dd, J = 16.8, 7.9 Hz, 2H), 1.75 (dd, J = 7.6, 5.0 Hz, 2H), 1.59 (dd, J = 9.1, 4.9 Hz, 2H), 1.26 (t, J = 7.1 Hz, 6H).

^{13}C NMR (75 MHz, $CDCl_3$, 293K):

δ [ppm] = 169.7, 167.6, 157.8, 132.8, 119.1, 652, 61.7, 39.4, 35.8, 31.8, 20.9, 14.4.

FT-IR (ATR mode):

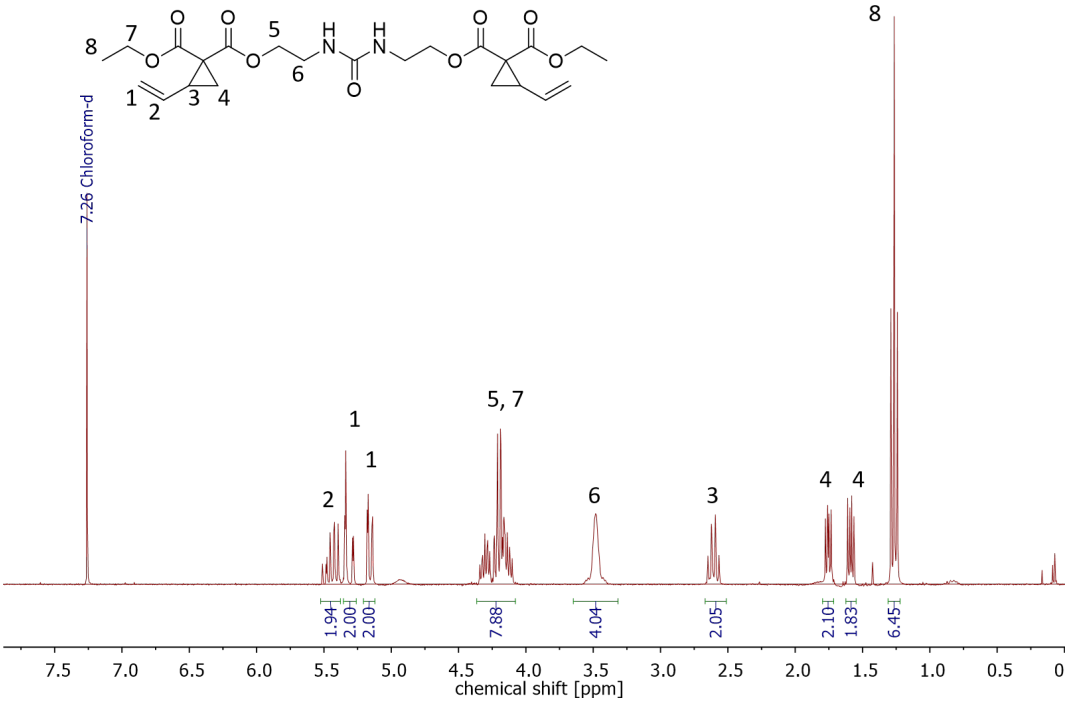

Figure 100: ^{1}H NMR of **10**.

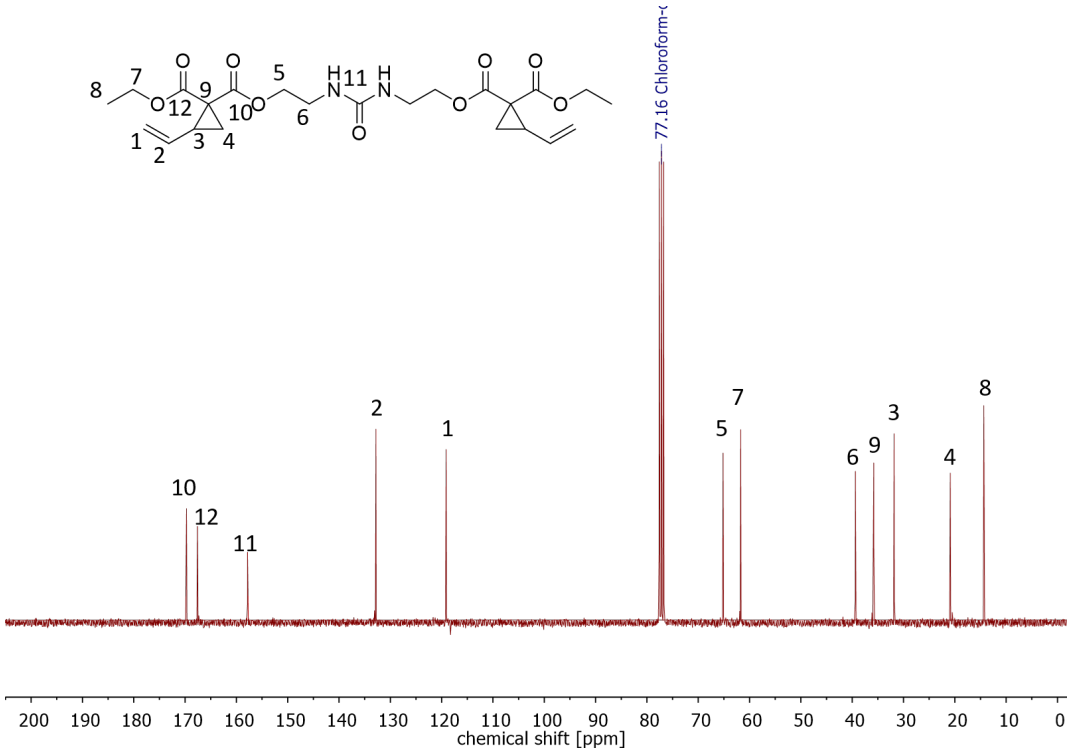

Figure 101: ^{13}C NMR of **10**.

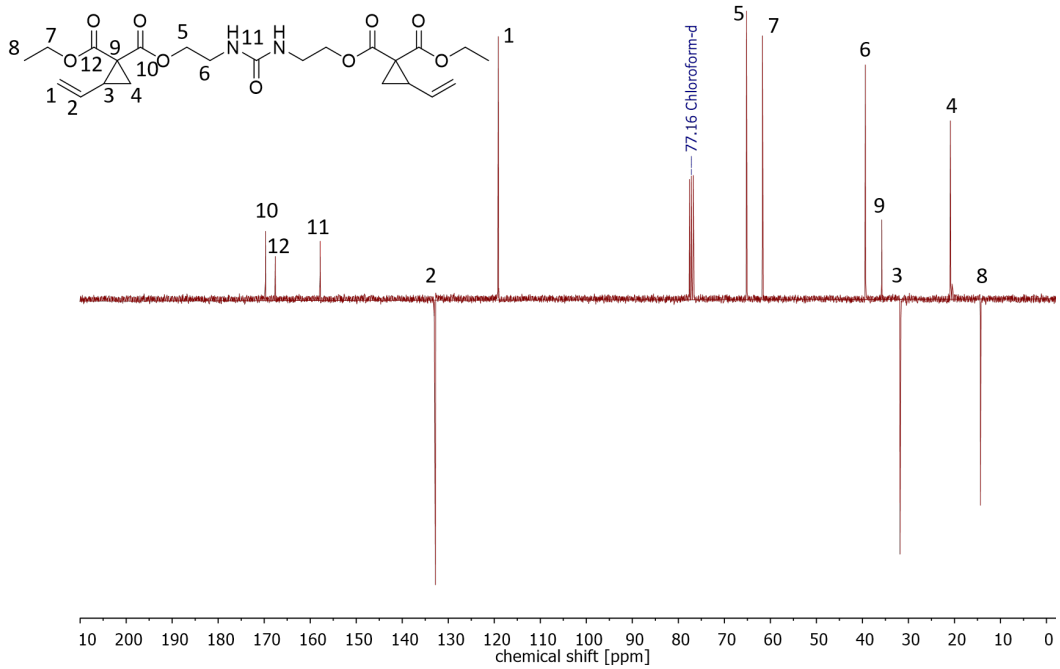

Figure 102: ^{13}C APT NMR of **10**.

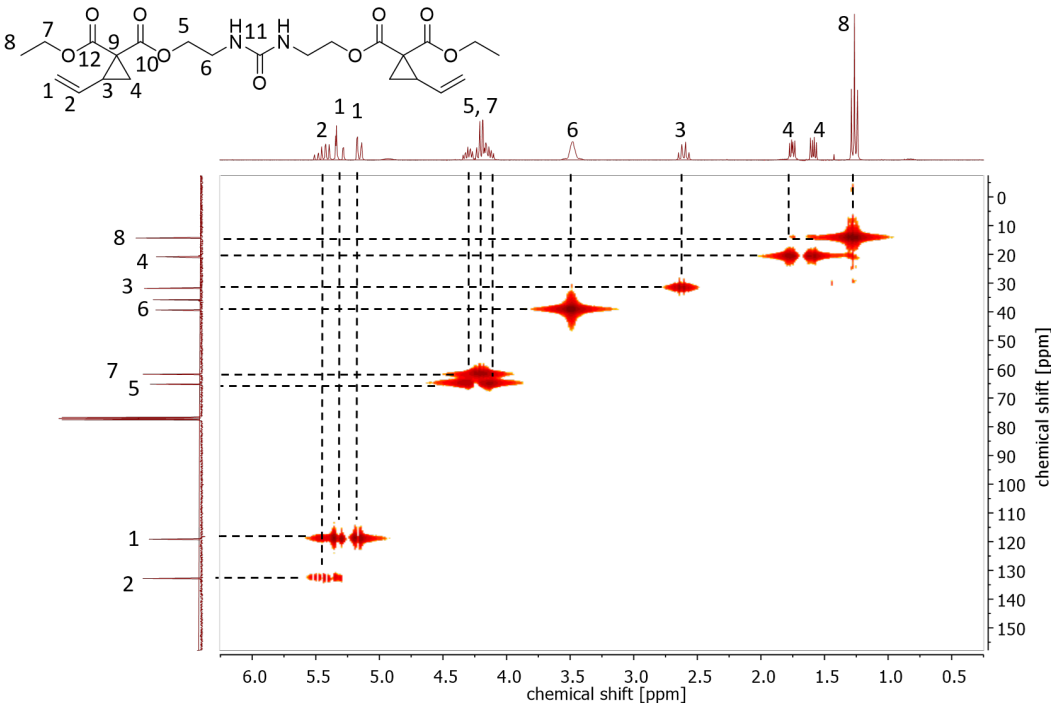

Figure 103: HSQC 2D NMR of **10**.

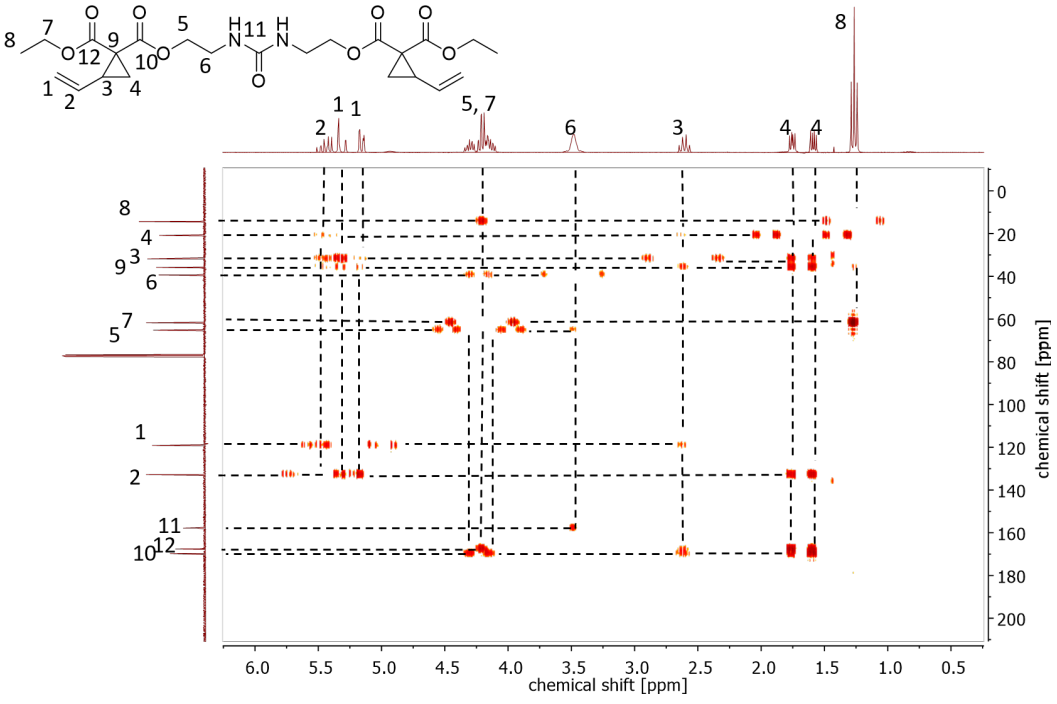

Figure 104: HMBC 2D NMR of **10**.

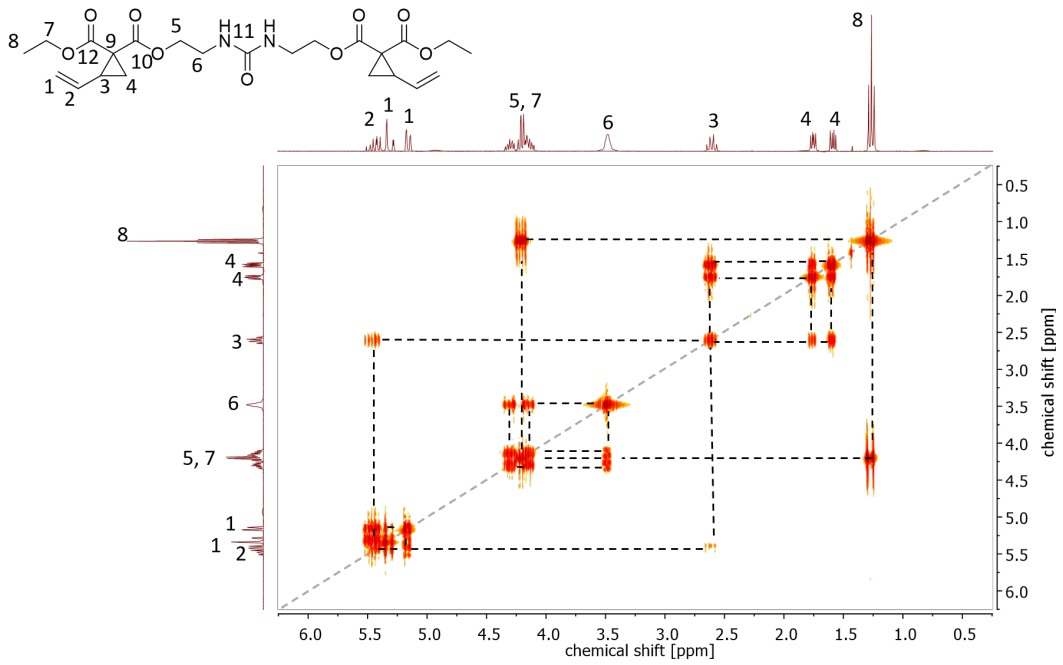

Figure 105: COSY 2D NMR of **10**.

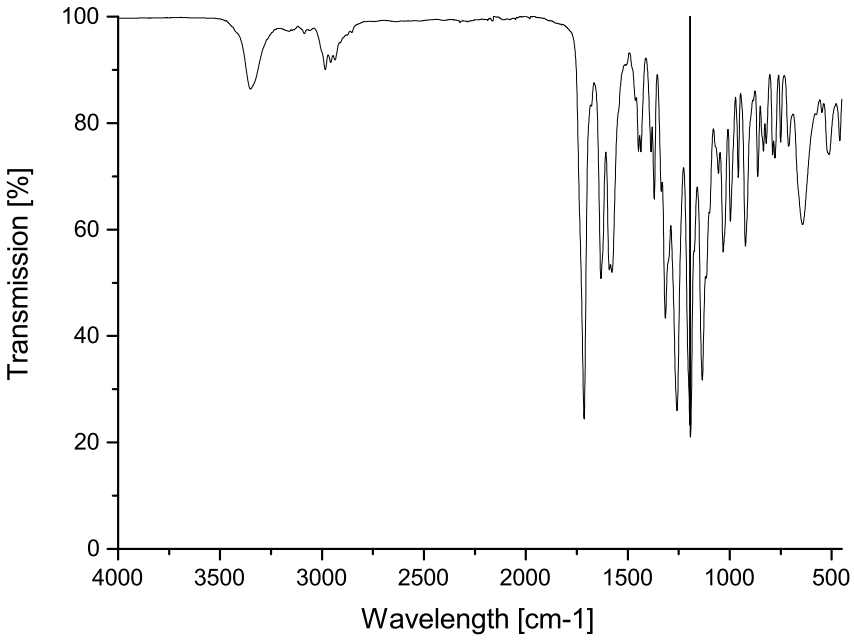

Figure 106: FT-IR of **10**.

Diethyl
1,1'-(((cyclohexane-1,3-diylbis(methylene))bis(azanediyl))bis(carbonyl))bis(2-vinylcyclopropane-1-carboxylate)

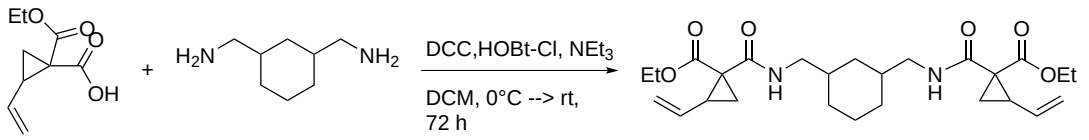

43 **11**

Under an argon atmosphere, 3.0 g **43** (2.1 eq, 16.3 mmol), DCC (2.1 eq, 3.36 g, 16.3 mmol) and HOBt-Cl(2.16 eq, 2.84 g, 16.75 mmol) were dissolved in 50 ml dry DCM. At 0°C NEt_3 (4.2 eq, 3.29 g, 4.54 ml, 32.56 mmol) was added and in 50 ml dry DCM dissolved cyclohexane-1,3-diyldimethanamine (1.10 g, 7.76 mmol) was added dropwise. The reaction mixture was stirred at room temperature for three days. The mixture was filtrated and the organic phase was washed once with 0.5 M HCl solution, once with saturated $NaHCO_3$ solution and twice with water. After drying over $MgSO_4$ the solvent was removed and the product **11** obtained after purification via flash chromatography (Cylcohexane:EtOAc 9:1 → 7:3) in a yield of 24% (866.15 mg, 1.83 mmol).

^{1}H NMR (300 MHz, $CDCl_3$, 293K):

δ [ppm] = 8.50 (t, J = 5.2 Hz, 1H), 5.65 (ddd, J = 17.2, 10.2, 8.8 Hz, 1H), 5.30 (dd, J = 8.9, 8.2 Hz, 1H), 5.15 (dd, J = 10.2, 1.3 Hz, 1H), 4.28 – 4.07 (m, 2H), 3.33 – 2.98 (m, 2H), 2.52 (q, J = 8.6 Hz, 1H), 2.13 – 1.97 (m, 1H), 1.84 (dd, J = 7.9, 4.2 Hz, 1H), 1.78 (d, J = 11.5 Hz, 2H), 1.67 – 1.45 (m, 1H), 1.28 (t, J = 7.1 Hz, 4H), 0.96 – 0.79 (m, 1H), 0.66 (q, J = 12.1 Hz, 1H).

^{13}C NMR (75 MHz, $CDCl_3$, 293K):

δ [ppm] = 171.6, 168.0, 133.5, 119.6, 61.5, 46.3, 37.6, 37.0, 35.3, 34.3, 30.8, 25.4, 21.5, 14.3.

FT-IR (ATR mode):

3357, 3086, 2983, 2922, 2854, 1703, 1650, 1531, 1463, 1446, 1395, 1371, 1338, 1313, 1286, 1265, 1197, 1137, 1096, 1074, 1019, 993, 959, 913, 772, 741, 705, 684, 628, 515, 458

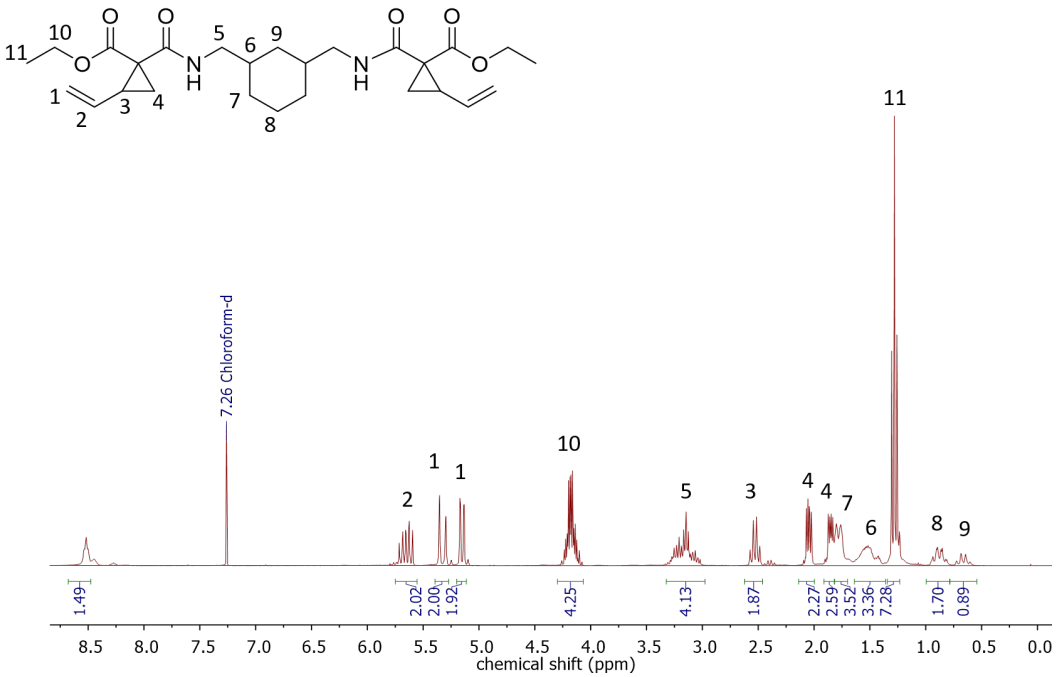

Figure 107: ^{1}H NMR of **11**.

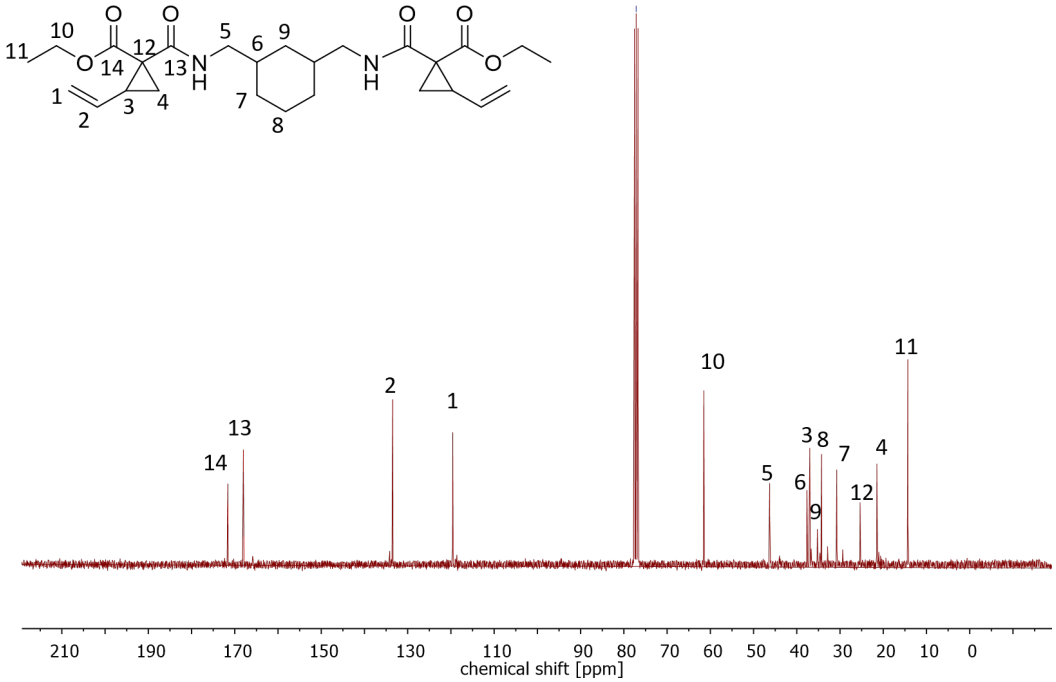

Figure 108: ^{13}C NMR of **11**.

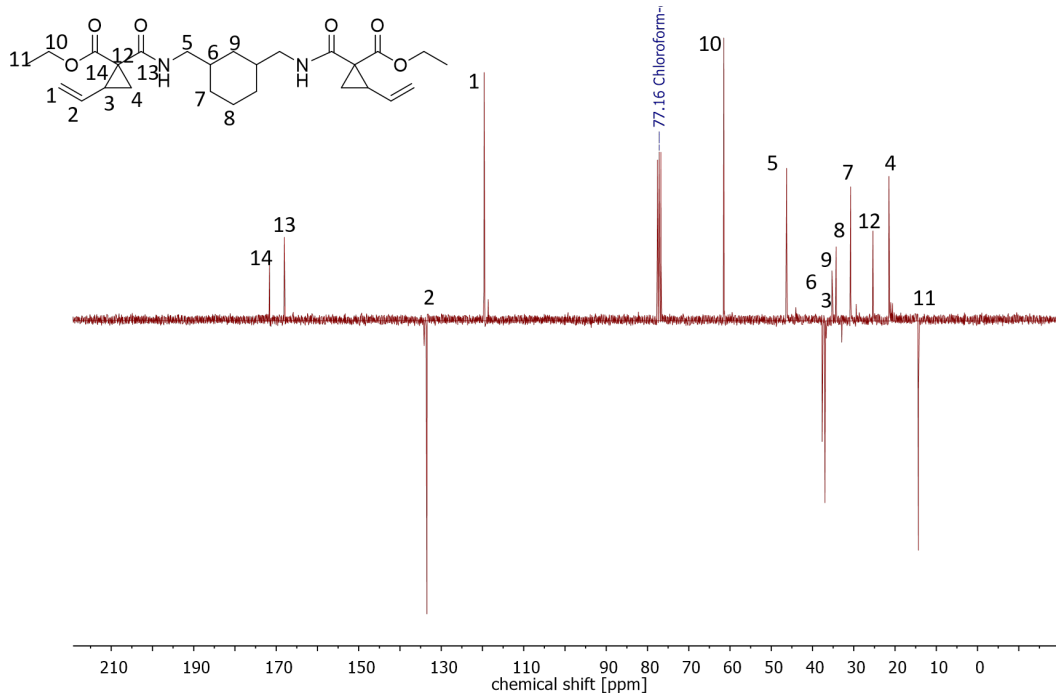

Figure 109: ^{31}C APT NMR of **11**.

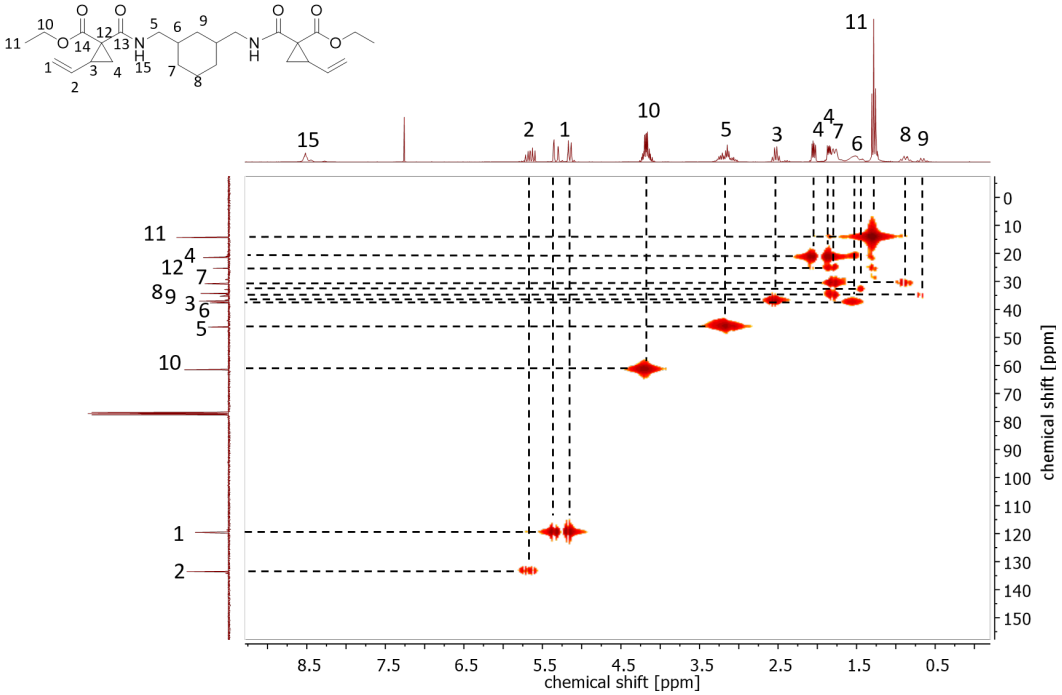

Figure 110: HSQC 2D NMR of **11**.

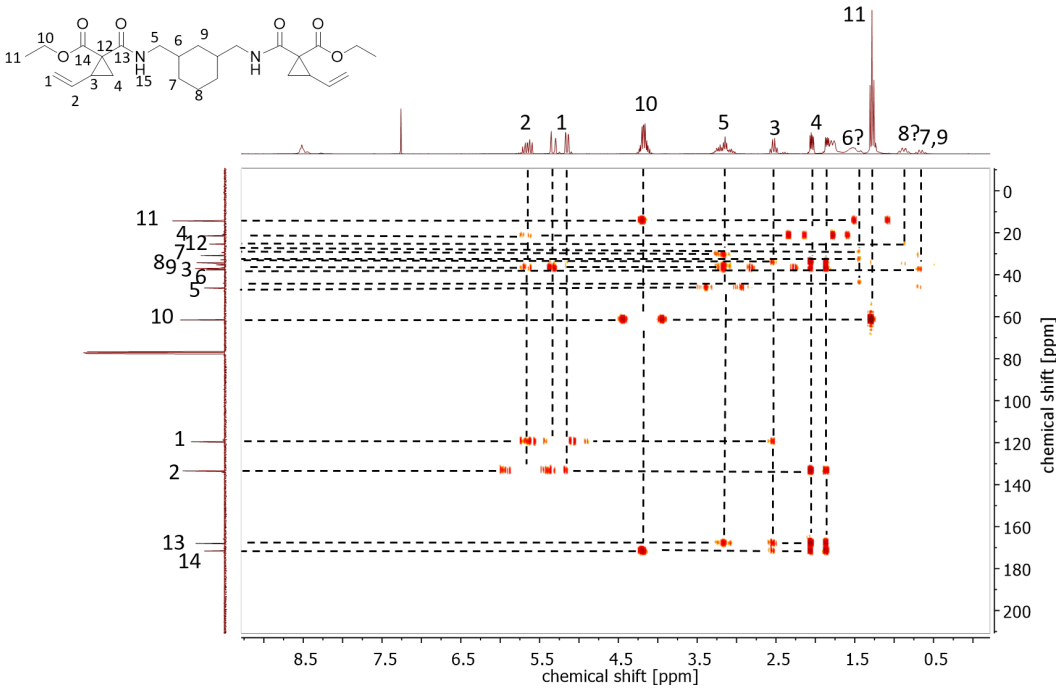

Figure 111: HMBC 2D NMR of **11**.

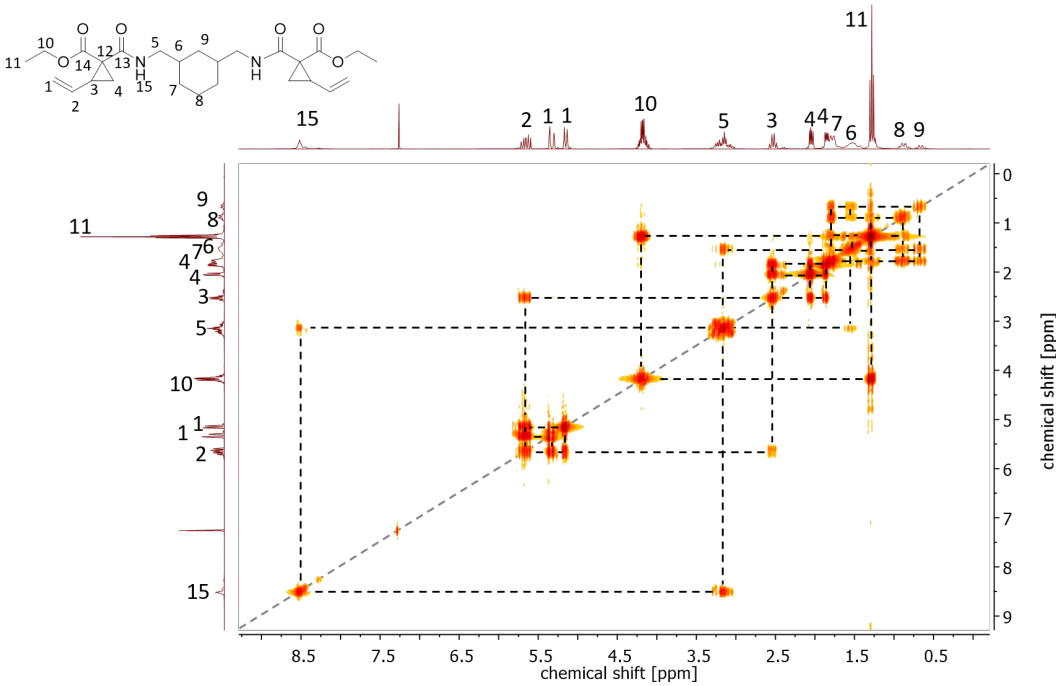

Figure 112: COSY 2D NMR of **11**.

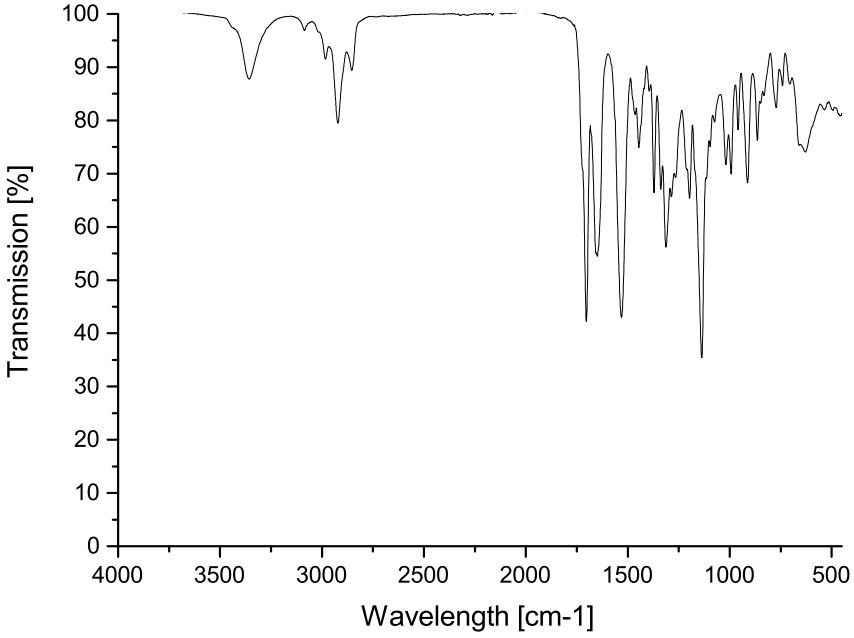

Figure 113: FT-IR of **11**.

Ethyl 1-(((5-(1-(ethoxycarbonyl)-2-vinylcyclopropane-1-carboxamido)-1,3,3-trimethylcyclohexyl)methyl)carbamoyl)-2-vinylcyclopropane-1-carboxylate

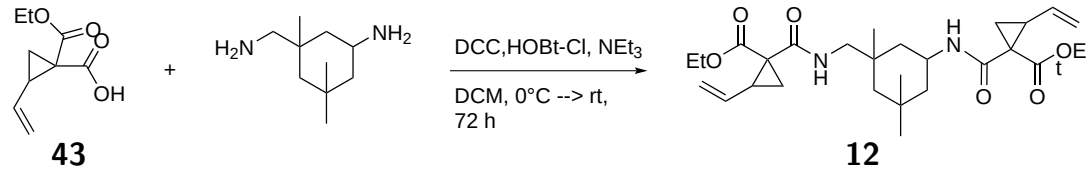

43 **12**

Under an argon atmosphere, 3.0 g **43** (2.1 eq, 16.3 mmol), DCC (2.1 eq, 3.36 g, 16.3 mmol) and HOBt-Cl(2.16 eq, 2.84 g, 16.75 mmol) were dissolved in 50 ml dry DCM. At 0°C NEt_3 (4.2 eq, 3.29 g, 4.54 ml, 32.56 mmol) was added and in 50 ml dry DCM dissolved isophorone diamine (IPDA) (1.32 g, 7.76 mmol) was added dropwise. The reaction mixture was stirred at room temperature for three days. The mixture was filtrated and the organic phase was washed once with 0.5 M HCl solution, once with saturated $NaHCO_3$ solution and twice with water. After drying over $MgSO_4$ the solvent was removed and the product **12** obtained after purification via flash chromatography (Cylcohexane:EtOAc 100:0 $\rightarrow$ 7:3) in a yield of 38% (1.70 g, 2.95 mmol).

^{1}H NMR (300 MHz, $CDCl_3$, 293K):

δ [ppm] = 8.58 (s, 1H), 8.25 (t, J = 8.4 Hz, 1H), 5.77 – 5.52 (m, 2H), 5.32 (dd, J = 21.2, 5.6 Hz, 2H), 5.22 – 5.07 (m, 2H), 4.35 – 3.98 (m, 5H), 3.25 – 2.90 (m, 2H), 2.67 – 2.43 (m, 2H), 2.17 – 1.95 (m, 2H), 1.95 – 1.81 (m, 2H), 1.74 (t, J = 12.2 Hz, 2H), 1.34 – 1.26 (m, 6H), 1.24 (dd, J = 7.1, 1.3 Hz, 2H), 1.10 (t, J = 3.1 Hz, 3H), 1.08 (d, J = 2.9 Hz, 3H), 1.04 – 0.97 (m, 2H), 0.91 (dd, J = 13.3, 5.8 Hz, 4H).

^{13}C NMR (75 MHz, $CDCl_3$, 293K):

δ [ppm] = 171.7, 168.3, 167.1, 133.5, 119.7, 61.6, 54.0, 47.6, 46.1, 43.5, 37.2, 36.3, 35.2, 34.3, 32.0, 27.7, 23.5, 21.5, 14.3.

FT-IR (ATR mode):

3354, 3086, 2983, 2955, 1703, 1651, 1528, 1463, 1447, 1371, 1338, 1313, 1286, 1265, 1198, 1139, 1096, 1075, 1017, 993, 959, 913, 865, 838, 773, 741, 710, 661, 628, 272

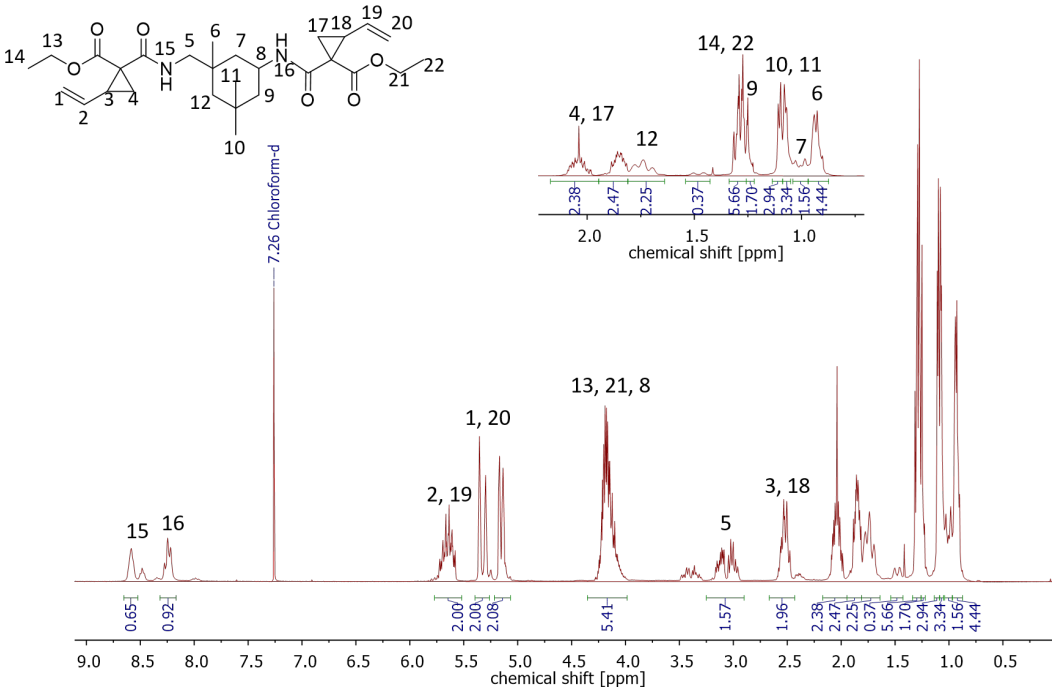

Figure 114: ^{1}H NMR of **12**.

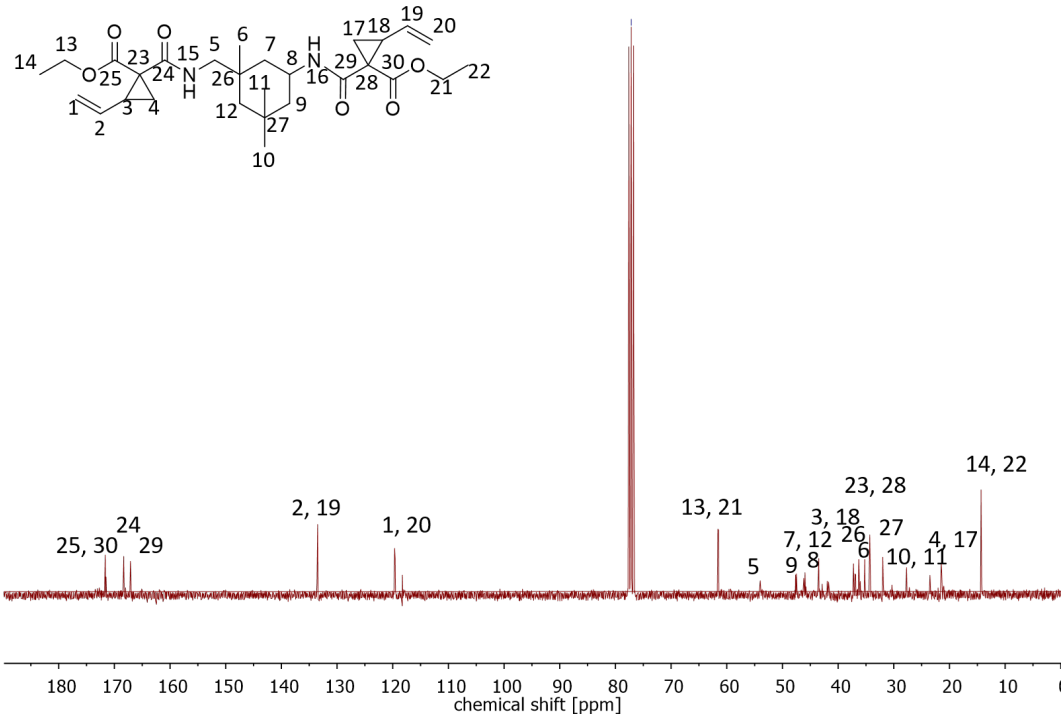

Figure 115: ^{13}C NMR of **12**.

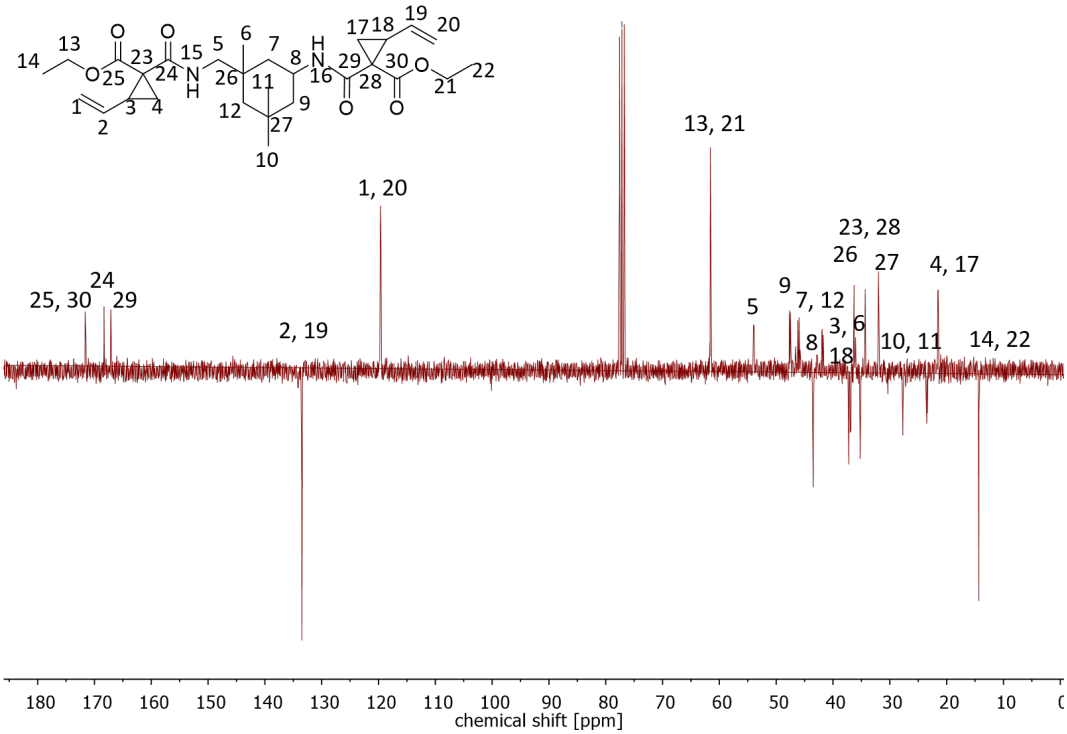

Figure 116: ^{13}C APT NMR of **12**.

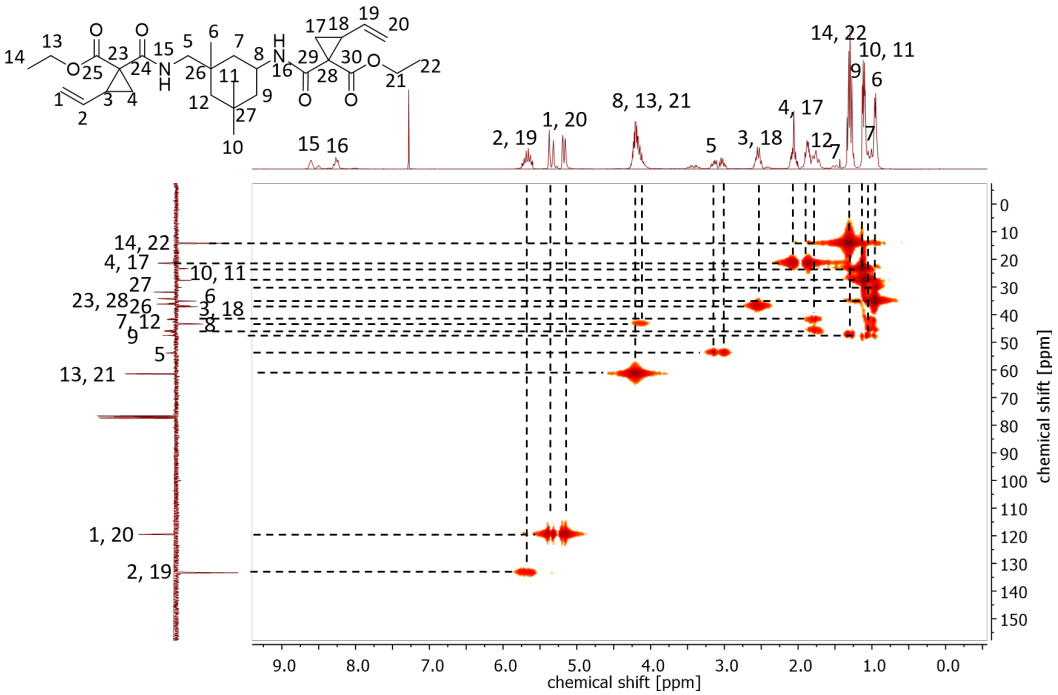

Figure 117: HSQC 2D NMR of **12**.

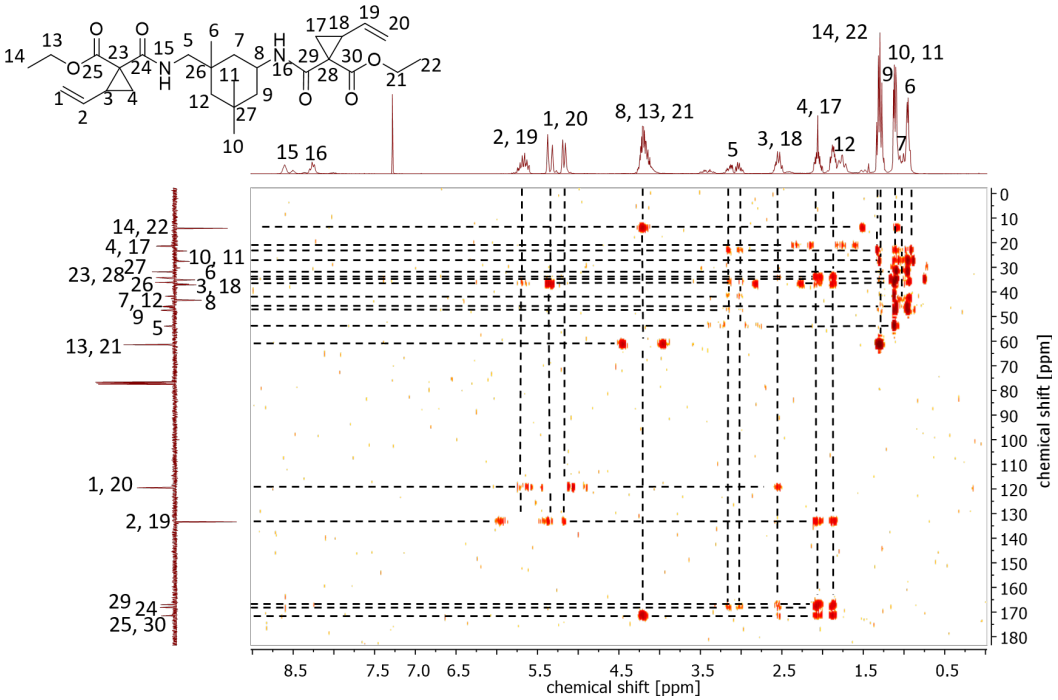

Figure 118: HMBC 2D NMR of **12**.

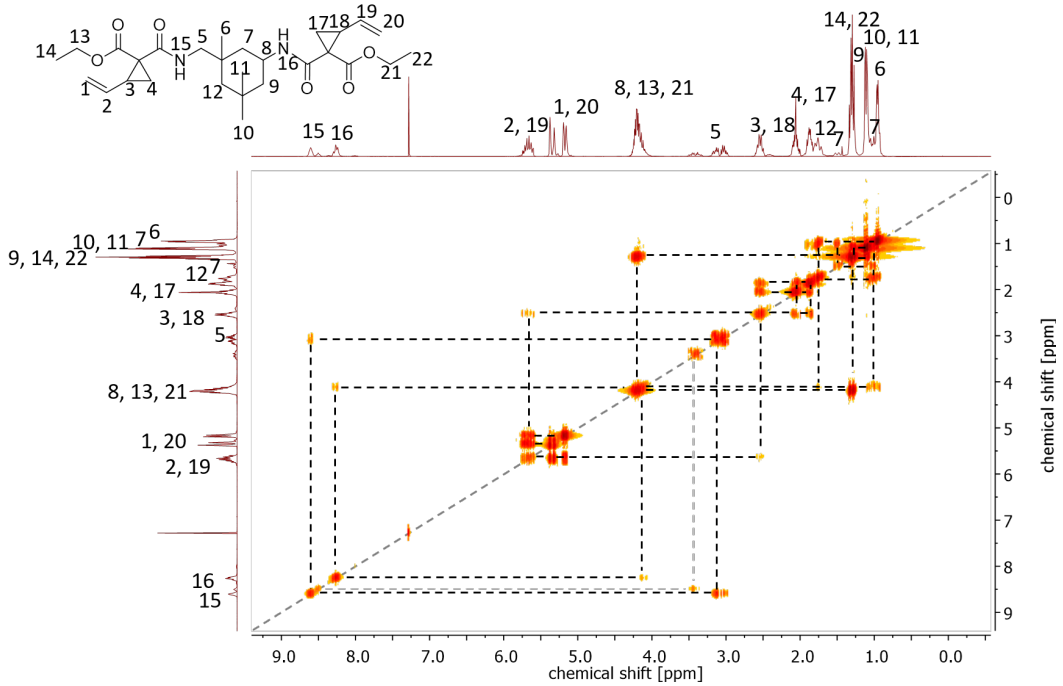

Figure 119: COSY 2D NMR of **12**.

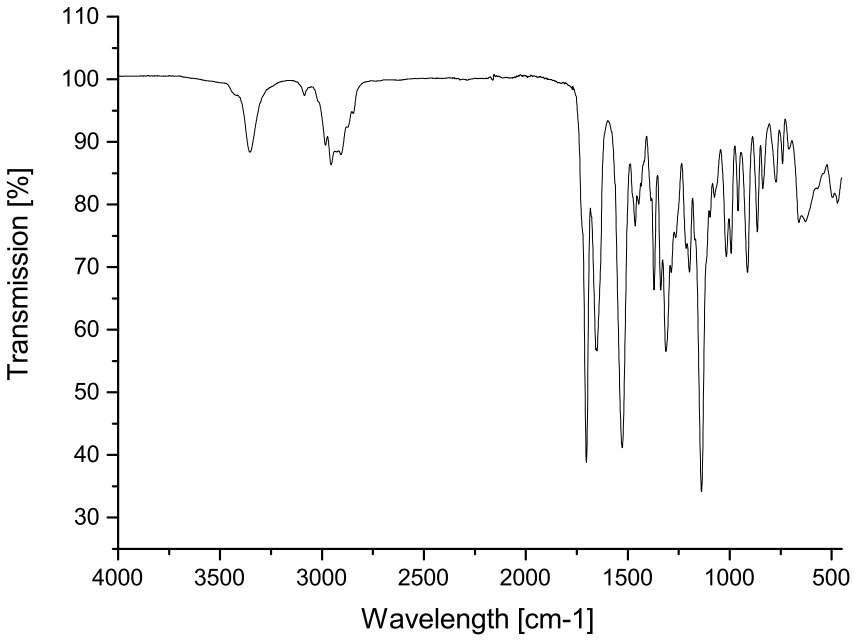

Figure 120: FT-IR of **12**.

Diethyl 1,1'-(((methylenebis(2-methylcyclohexane-3,1-diyl))bis(azanediyl))bis(carbonyl))bis(2-vinylcyclopropane-1-carboxylate)

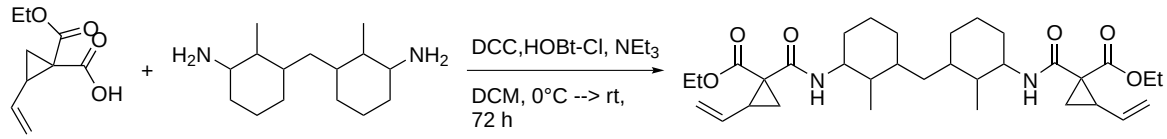

43 **13**

Under an argon atmosphere, 3.0 g **43** (2.1 eq, 16.3 mmol), DCC (2.1 eq, 3.36 g, 16.3 mmol) and HOBt-Cl(2.16 eq, 2.84 g, 16.75 mmol) were dissolved in 60 ml dry DCM. At 0°C NEt_3 (4.2 eq, 3.29 g, 4.54 ml, 32.56 mmol) was added and in 40 ml dry DCM dissolved 3,3'-methylenebis(2-methylcyclohexan-1-amine) (1.85 g, 7.76 mmol) was added dropwise. The reaction mixture was stirred at room temperature for three days. The mixture was filtrated and the organic phase was washed once with 0.5 M HCl solution, once with saturated $NaHCO_3$ solution and twice with water. After drying over $MgSO_4$ the solvent was removed and the product **13** obtained after purification via flash chromatography (Cylcohexane:EtOAc 9:1 → 7:3) in a yield of 68% (2.65 g, 5.27 mmol).

^{1}H NMR (300 MHz, $CDCl_3$, 293K):

δ [ppm] = 8.16 (dt, J = 8.3, 4.1 Hz, 1H), 5.75 – 5.58 (m, 1H), 5.38 – 5.27 (m, 1H), 5.19 – 5.10 (m, 1H), 4.30 – 4.03 (m, 2H), 3.46 (ddt, J = 15.1, 10.8, 5.9 Hz, 1H), 2.59 – 2.43 (m, 1H), 2.08 – 1.99 (m, 1H), 1.90 – 1.81 (m, 1H), 1.71 (d, J = 9.7 Hz, 2H), 1.60 – 1.46 (m, 1H), 1.46 – 1.33 (m, 2H), 1.33 – 1.24 (m, 3H), 1.18 (dd, J = 18.0, 5.2 Hz, 1H), 1.05 (dd, J = 12.9, 5.5 Hz, 1H), 0.99 – 0.81 (m, 4H), 0.80 – 0.66 (m, 1H).

^{13}C NMR (75 MHz, $CDCl_3$, 293K):

δ [ppm] = 171.6, 167.5, 133.6, 119.4, 61.5, 55.0, 41.5, 38.2, 36.9, 34.3, 33.4, 32.3, 31.2, 27.7, 21.4, 19.4, 19.0, 14.4.

FT-IR (ATR mode):

3348, 3086, 2918, 2849, 1703, 1651, 1528, 1446, 1372, 1340, 1313, 1197, 1138, 1068, 1018, 993, 959, 912, 865, 835, 781, 766, 740, 706, 630, 503, 470

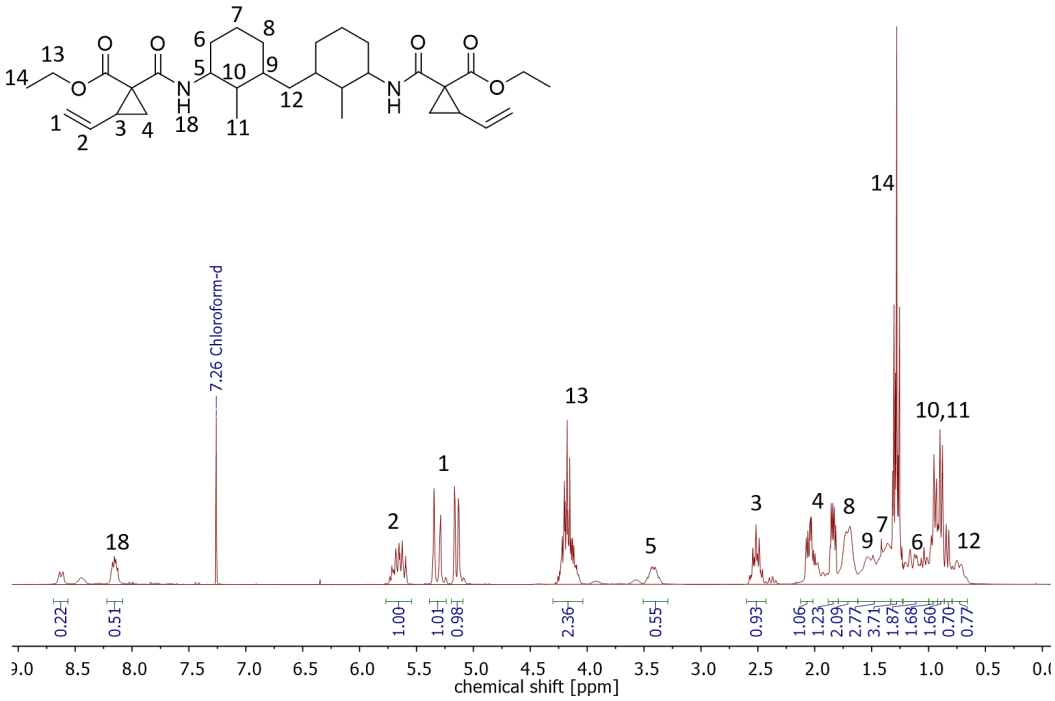

Figure 121: ^{1}H NMR of **13**.

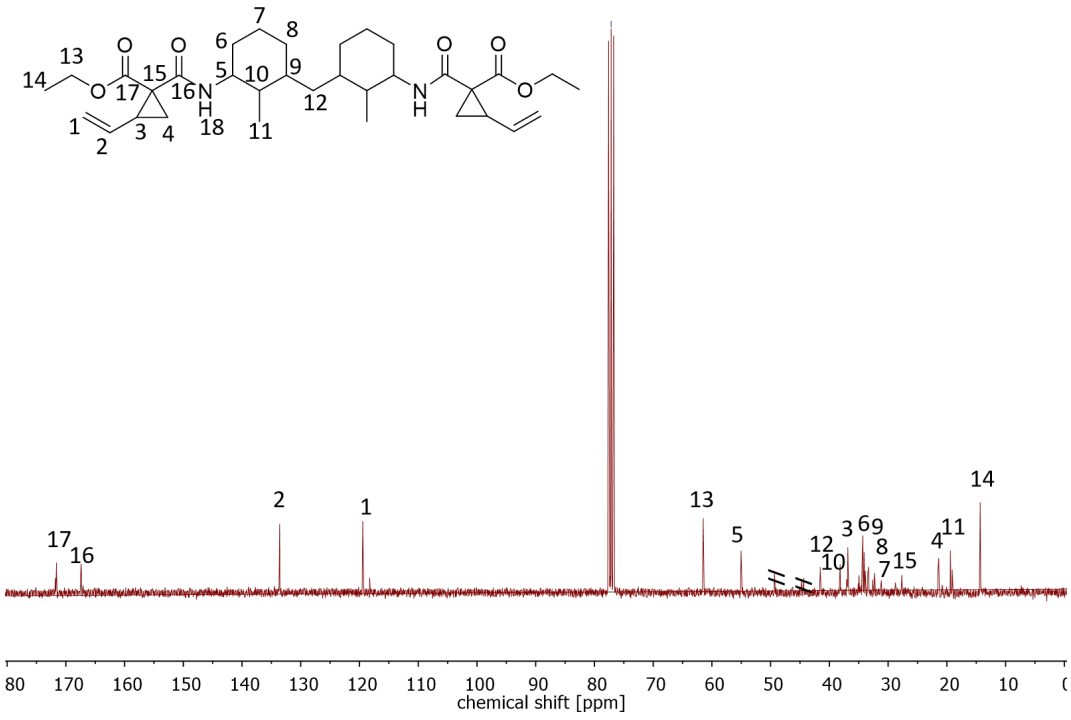

Figure 122: ^{13}C NMR of **13**.

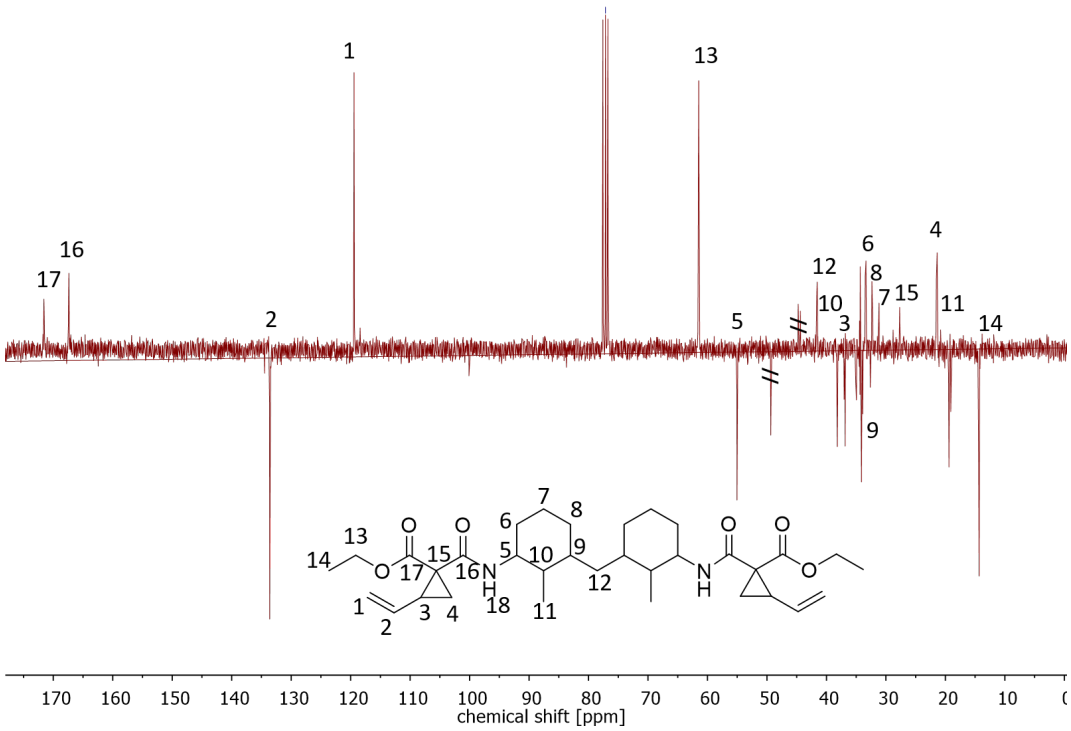

Figure 123: ^{13}C APT NMR of **13**.

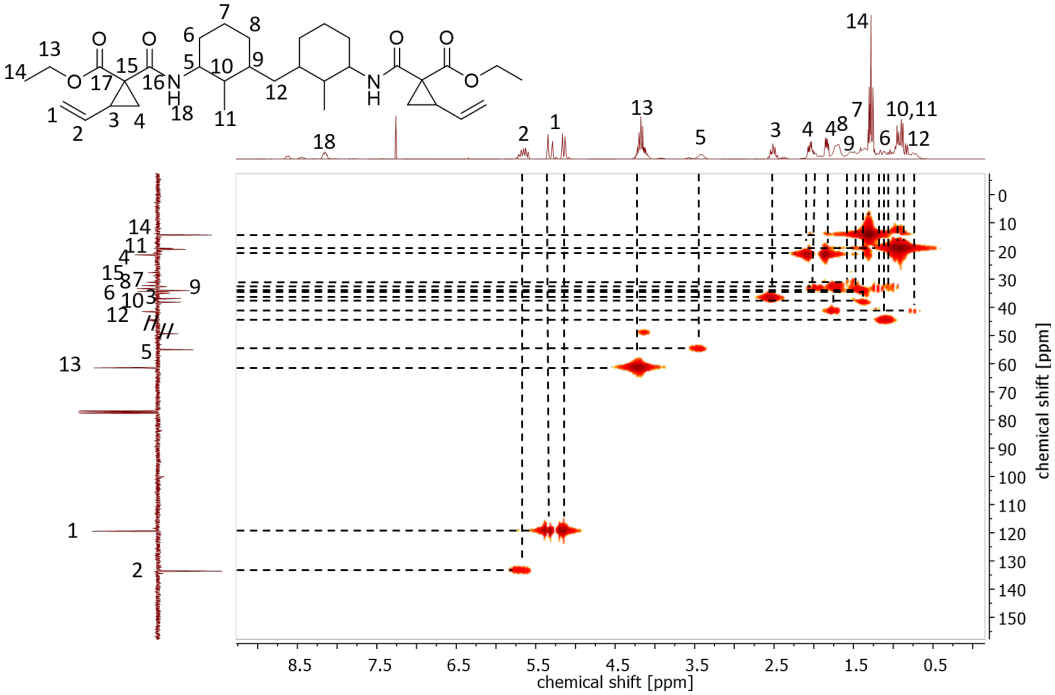

Figure 124: HSQC 2D NMR of **13**.

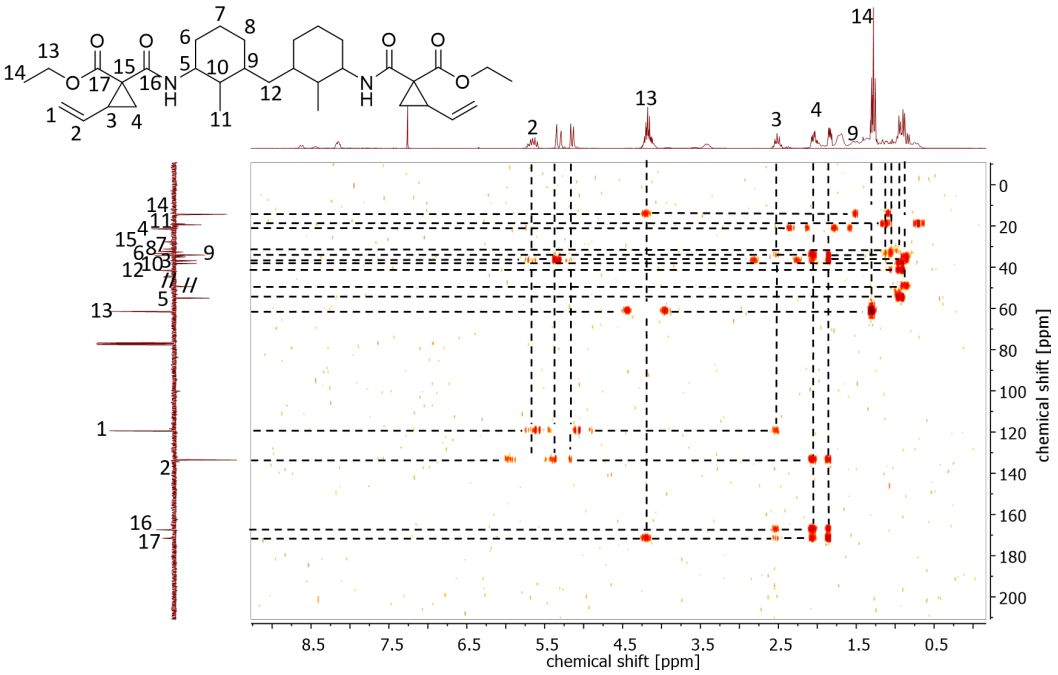

Figure 125: HMBC 2D NMR of **13**.

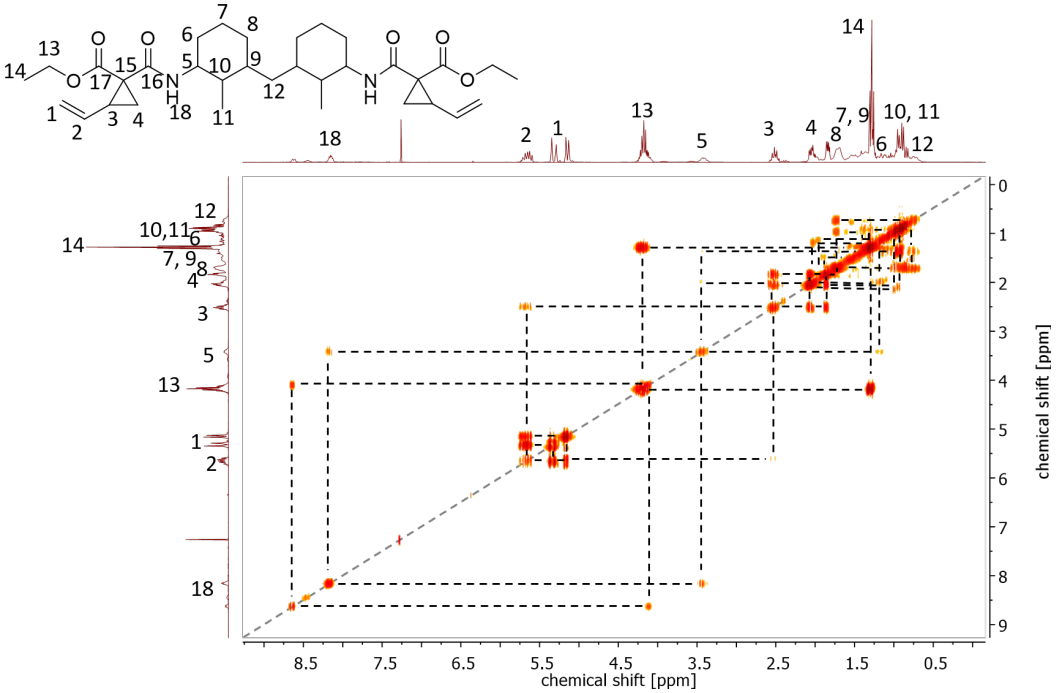

Figure 126: COSY 2D NMR of **13**.

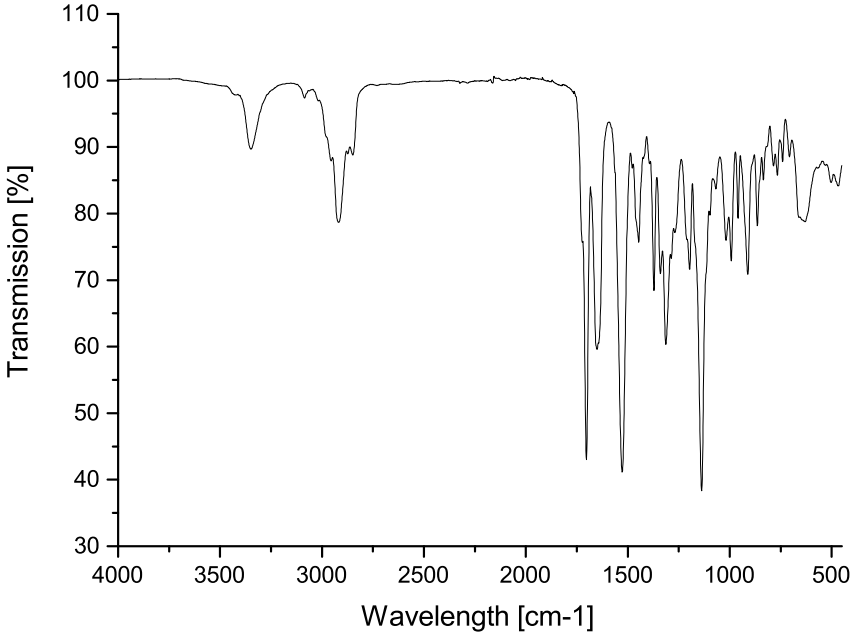

Figure 127: FT-IR of **13**.

Diethyl 1,1'-((propane-1,2-diylbis(azanediyl))bis(carbonyl))bis(2-vinylcyclopropane-1-carboxylate)

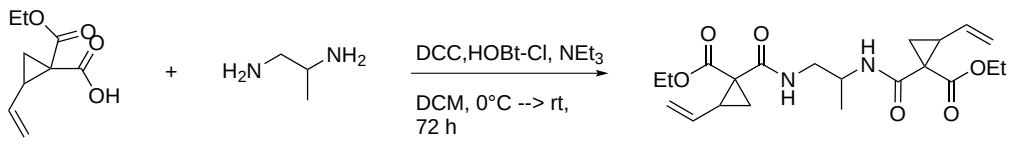

43 **14**

Under an argon atmosphere, 5.5 g **43** (2.2 eq, 29.9 mmol), DCC (2.2 eq, 6.17 g, 29.9 mmol) and HOBt-Cl(2.3 eq, 5.29 g, 31.2 mmol) were dissolved in 30 ml dry DCM. At 0°C NEt_3 (4.2 eq, 5.76 g, 7.95 ml, 57.0 mmol) was added and in 50 ml dry DCM dissolved propane-1,2-diamine (1.00 g, 13.6 mmol) was added dropwise. The reaction mixture was stirred at room temperature for three days. The mixture was filtrated and the organic phase was washed once with 0.5 M HCl solution, once with saturated $NaHCO_3$ solution and twice with water. After drying over $MgSO_4$ the solvent was removed and the product **14** obtained after purification via flash chromatography (Cylcohexane:EtOAc 7:3 $\rightarrow$ 1:1) in a yield of 15% (805 mg, 2.0 mmol).

^{1}H NMR (300 MHz, $CDCl_3$, 293K):

δ [ppm] = 8.64 – 8.46 (m, 1H), 8.44 – 8.25 (m, 1H), 5.74 – 5.52 (m, 2H), 5.39 – 5.25 (m, 2H), 5.18 – 5.10 (m, 2H), 4.28 – 4.01 (m, 6H), 3.62 – 3.15 (m, 2H), 2.64 – 2.41 (m, 2H), 2.10 – 1.90 (m, 3H), 1.90 – 1.76 (m, 2H), 1.31 – 1.23 (m, 7H), 1.23 – 1.15 (m, 4H).

^{13}C NMR (75 MHz, $CDCl_3$, 293K):

δ [ppm] = 171.1, 168.6, 168.0, 1335, 119.5, 61.5, 46.1, 45.4, 36.8, 34.5, 22.1, 18.5, 14.3.

FT-IR (ATR mode):

3346, 3087, 2982, 2936, 1704, 1651, 1523, 1463, 1447, 1372, 1339, 1313, 1287, 126, 1198, 1137, 1097, 1019, 993, 959, 913, 864, 834, 776, 742, 710, 627, 510, 466

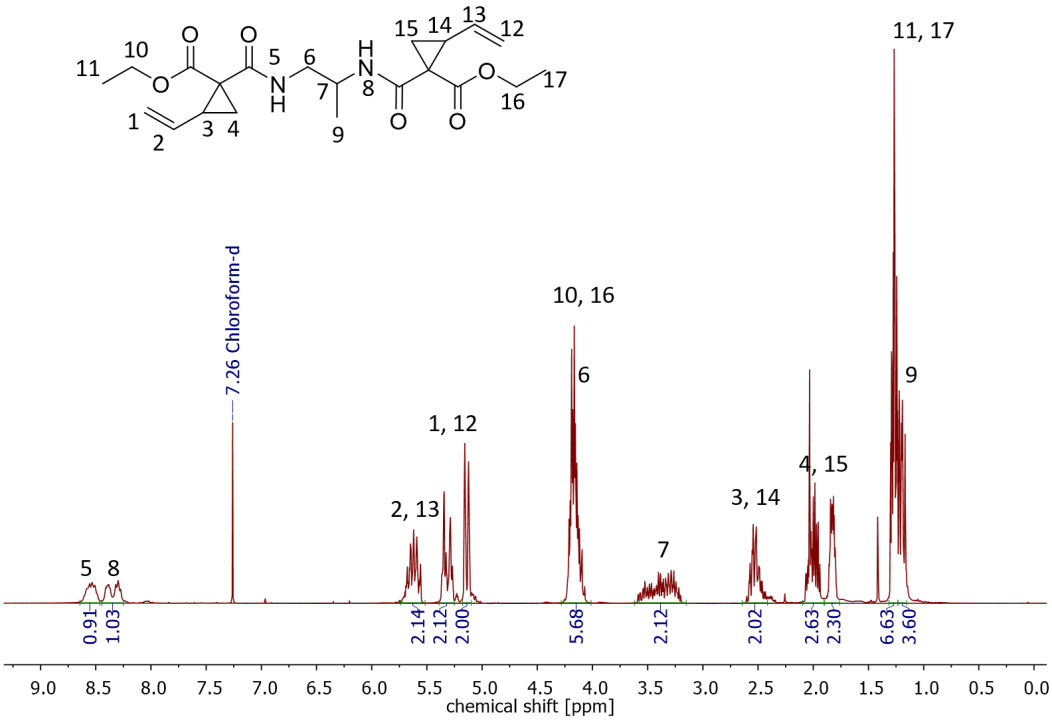

Figure 128: ^{1}H NMR of **14**.

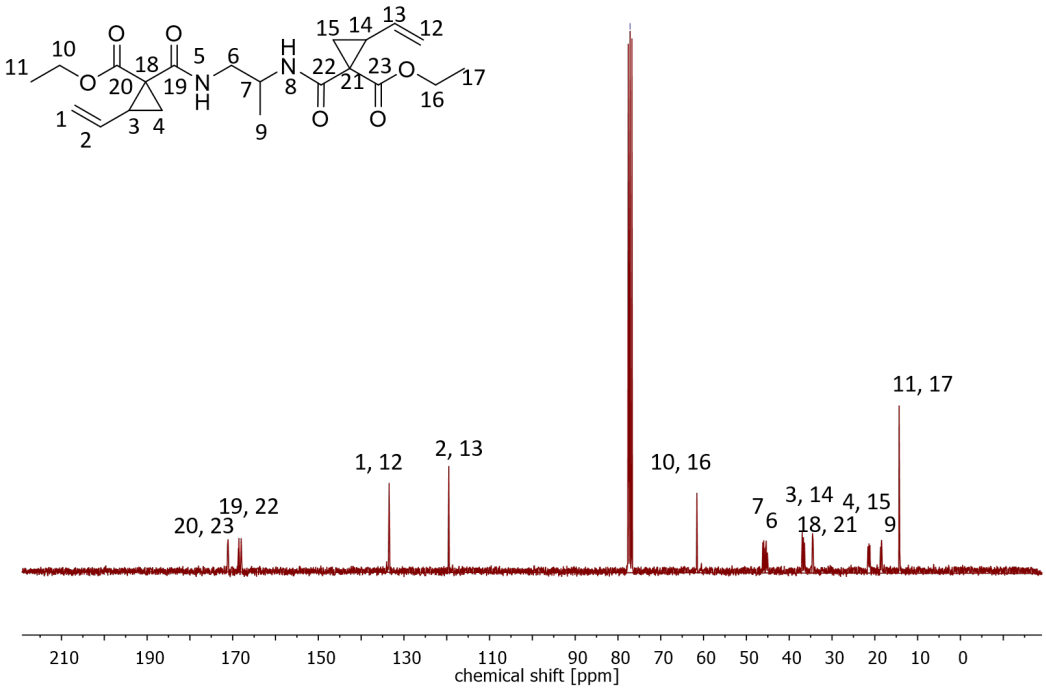

Figure 129: ^{13}C NMR of **14**.

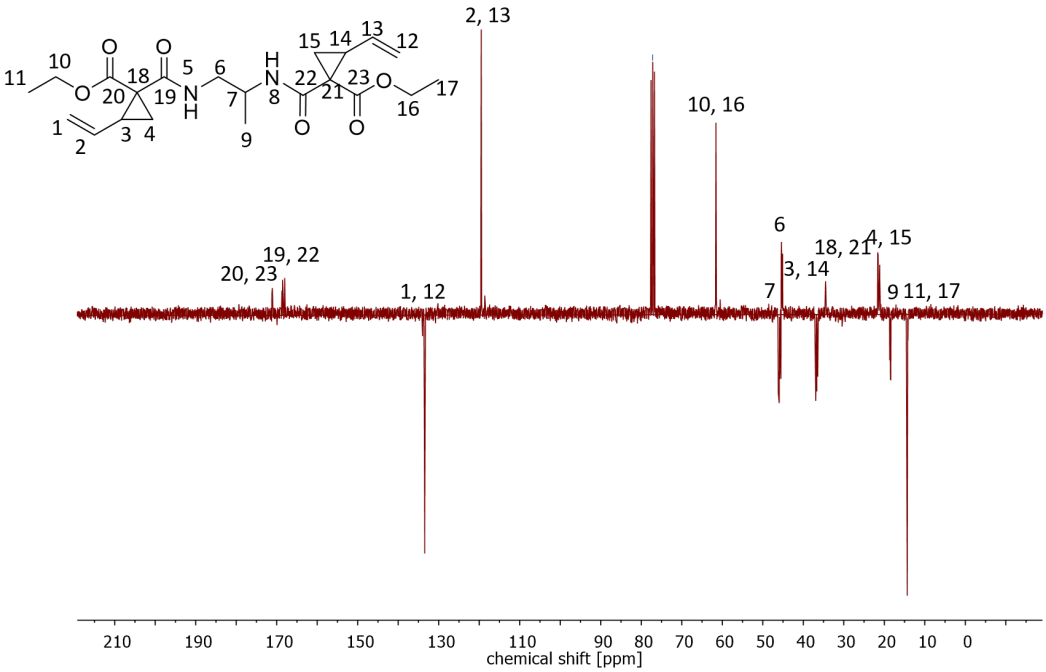

Figure 130: ^{13}C APT NMR of **14**.

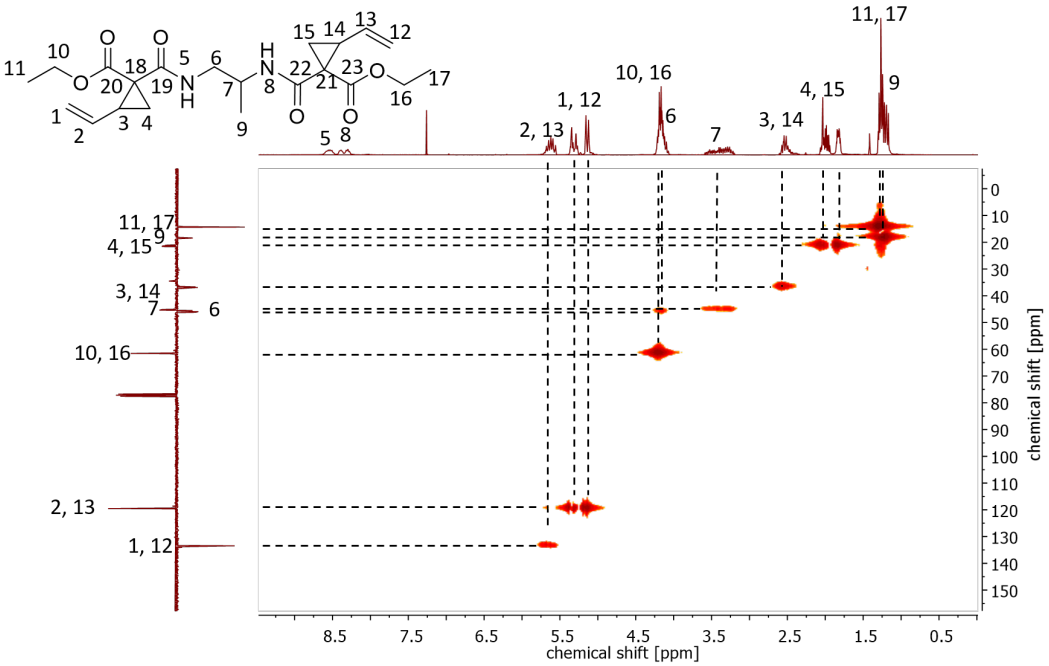

Figure 131: HSQC 2D NMR of **14**.

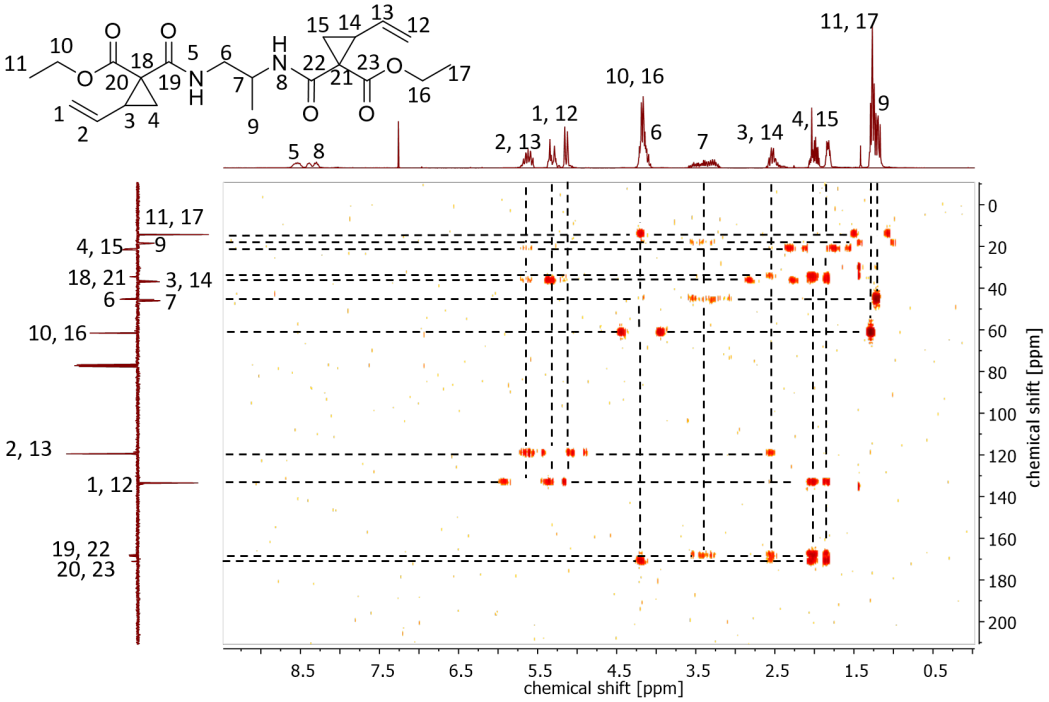

Figure 132: HMBC 2D NMR of **14**.

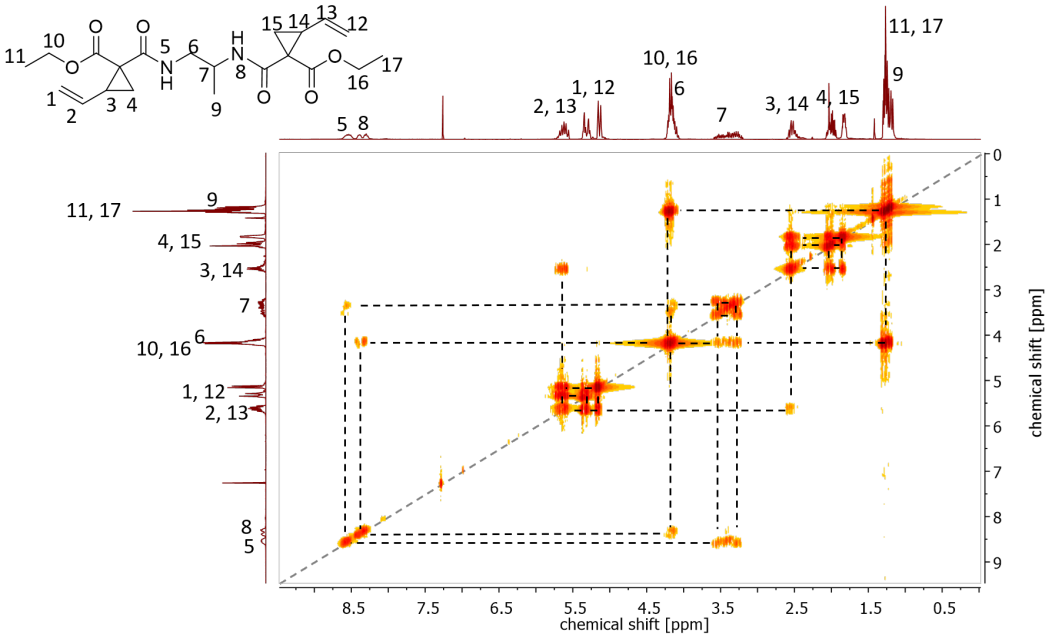

Figure 133: COSY 2D NMR of **14**.

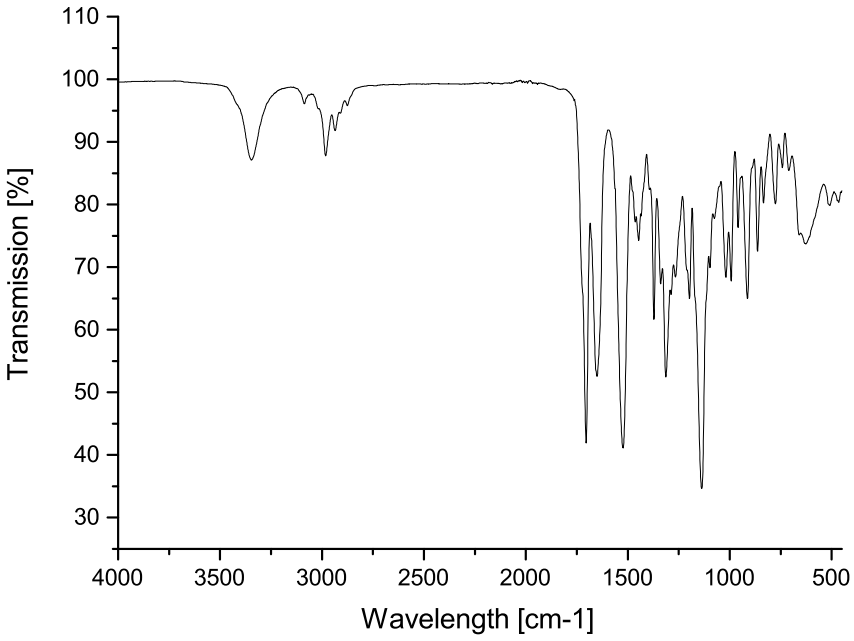

Figure 134: FT-IR of **14**.

Diethyl 1,1'-(((2,2-dimethylpropane-1,3-diyl)bis(azanediyl))bis(carbonyl))bis(2-vinylcyclopropane-1-carboxylate)

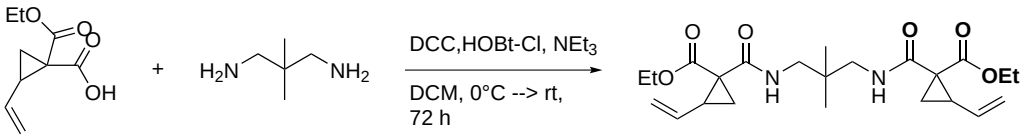

43 **15**

Under an argon atmosphere, 5.5 g **43** (2.2 eq, 29.9 mmol), DCC (2.2 eq, 6.17 g, 29.9 mmol) and HOBt-Cl(2.3 eq, 5.29 g, 31.2 mmol) were dissolved in 30 ml dry DCM. At 0°C NEt_3 (4.2 eq, 5.76 g, 7.95 ml, 57.0 mmol) was added and in 50 ml dry DCM dissolved 2,2-dimethylpropane-1,3-diamine (1.39 g, 13.6 mmol) was added dropwise. The reaction mixture was stirred at room temperature for three days. The mixture was filtrated and the organic phase was washed once with 0.5 M HCl solution, once with saturated $NaHCO_3$ solution and twice with water. After drying over $MgSO_4$ the solvent was removed and the product **15** obtained after purification via flash chromatography (Cylcohexane:EtOAc 100:0 $\rightarrow$ 7:3) in a yield of 24% (1.419 g, 3.27 mmol).

^{1}H NMR (300 MHz, $CDCl_3$, 293K):

δ [ppm] = 8.59 (t, J = 6.1 Hz, 1H), 5.71 – 5.57 (m, 1H), 5.36 – 5.27 (m, 1H), 5.18 – 5.10 (m, 1H), 4.27 – 4.15 (m, 2H), 3.26 – 2.97 (m, 2H), 2.60 – 2.44 (m, 1H), 2.02 – 1.93 (m, 1H), 1.82 (dt, J = 8.4, 4.2 Hz, 1H), 1.33 – 1.24 (m, 3H), 0.91 (d, J = 3.2 Hz, 3H).

^{13}C NMR (75 MHz, $CDCl_3$, 293K):

δ [ppm] = 171.0, 168.7, 133.6, 119.4, 61.6, 46.9, 36.7, 36.4, 34.8, 23.6, 21.4, 14.4.

FT-IR (ATR mode):

3350, 3087, 2963, 2933, 2873, 1704, 1651, 1531, 1472, 1446, 1393, 1371, 1338, 1308, 1198, 1178, 1139, 1096, 1063, 1021, 993, 959, 913, 863, 832, 775, 660, 569, 502, 472

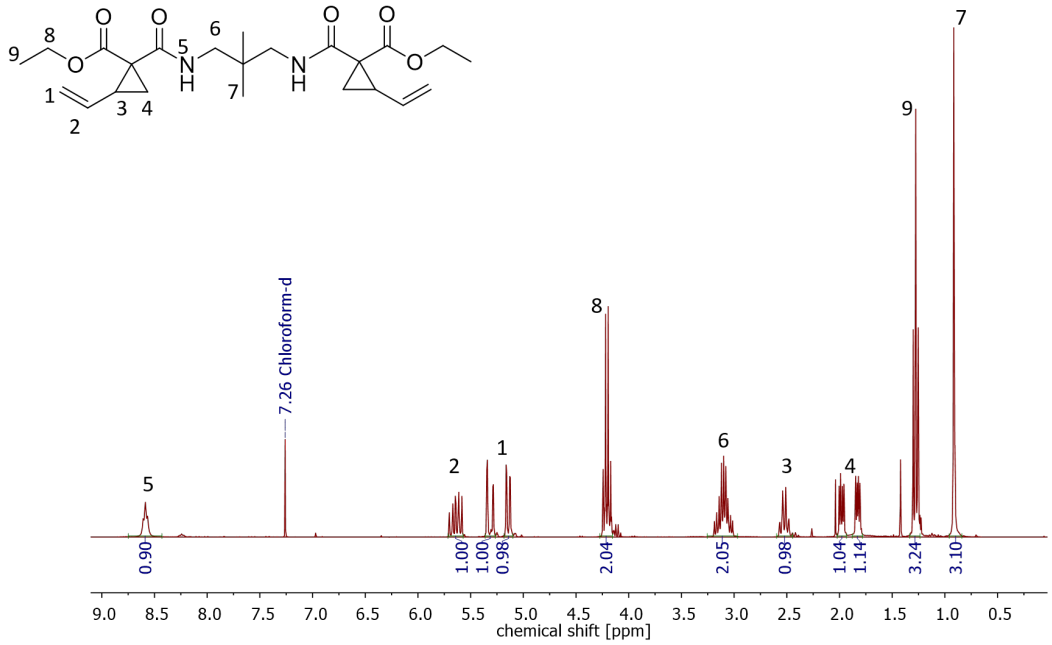

Figure 135: ^{1}H NMR of **15**.

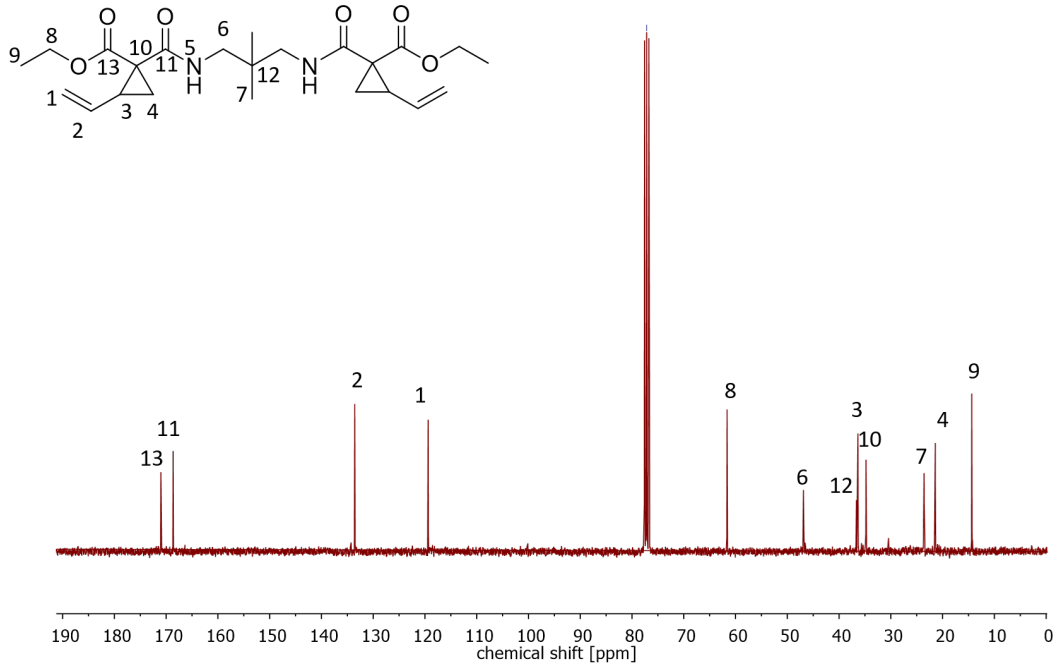

Figure 136: ^{13}C NMR of **15**.

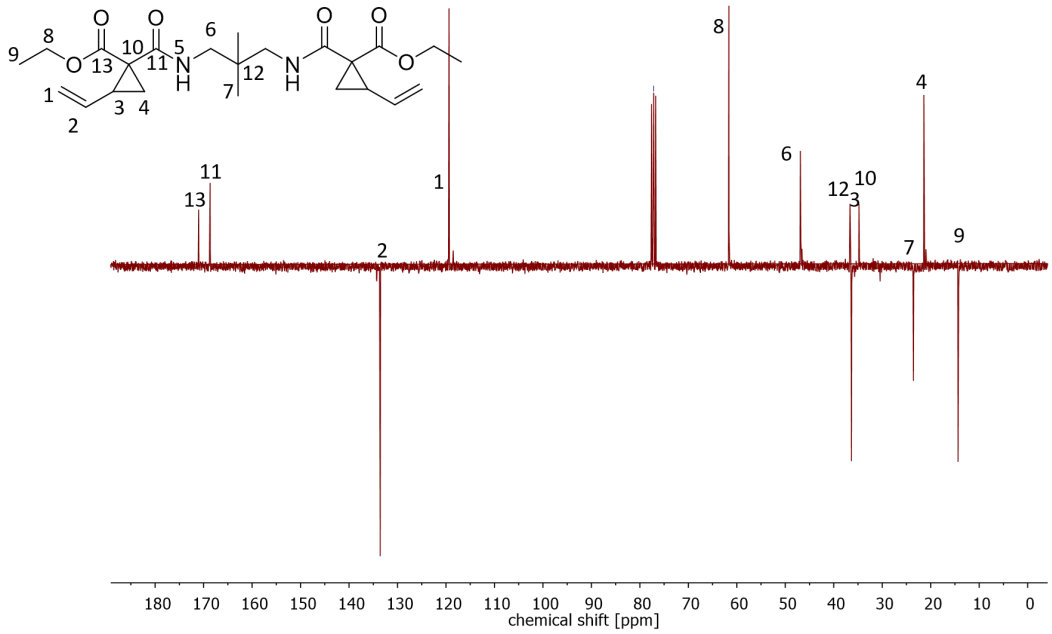

Figure 137: ^{13}C APT NMR of **15**.

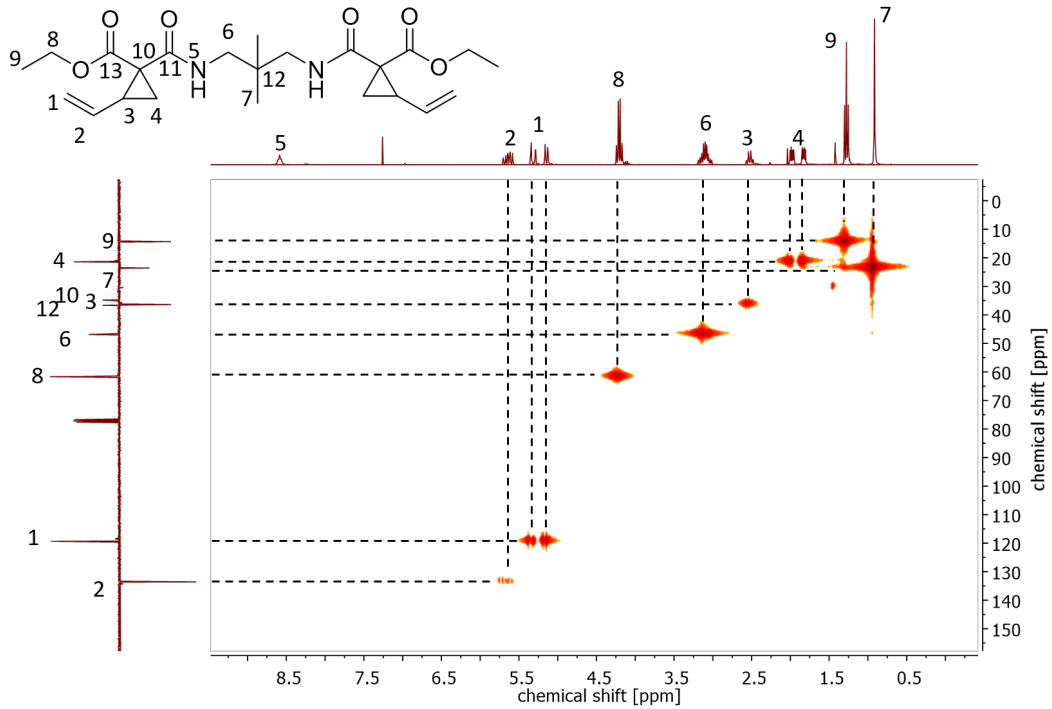

Figure 138: HSQC 2D NMR of **15**.

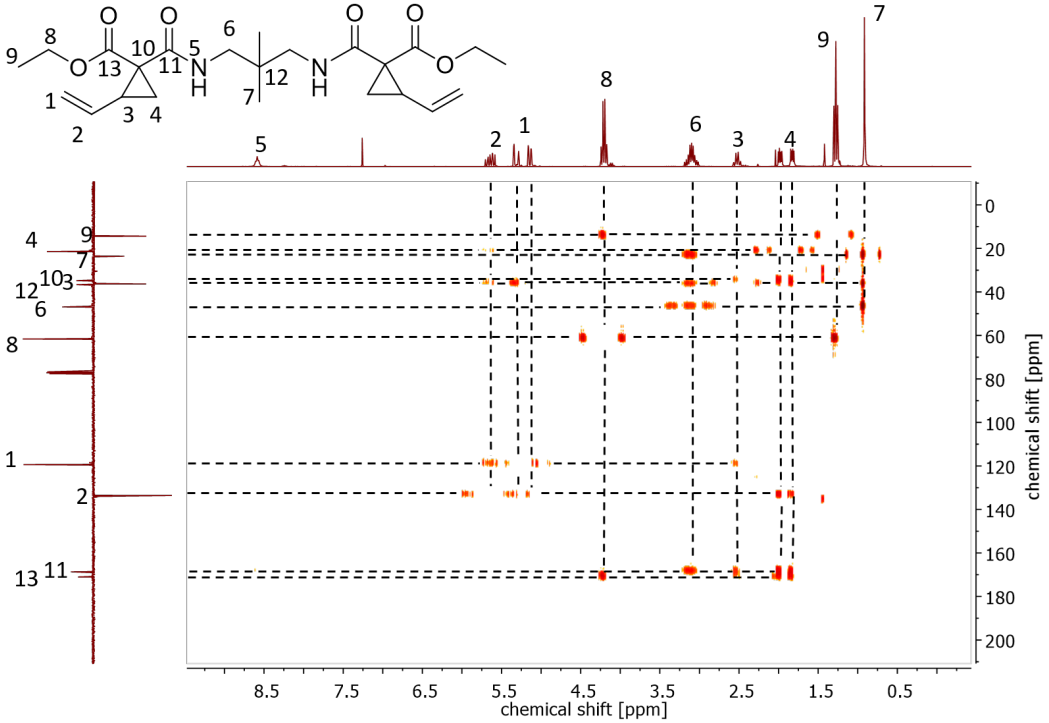

Figure 139: HMBC 2D NMR of **15**.

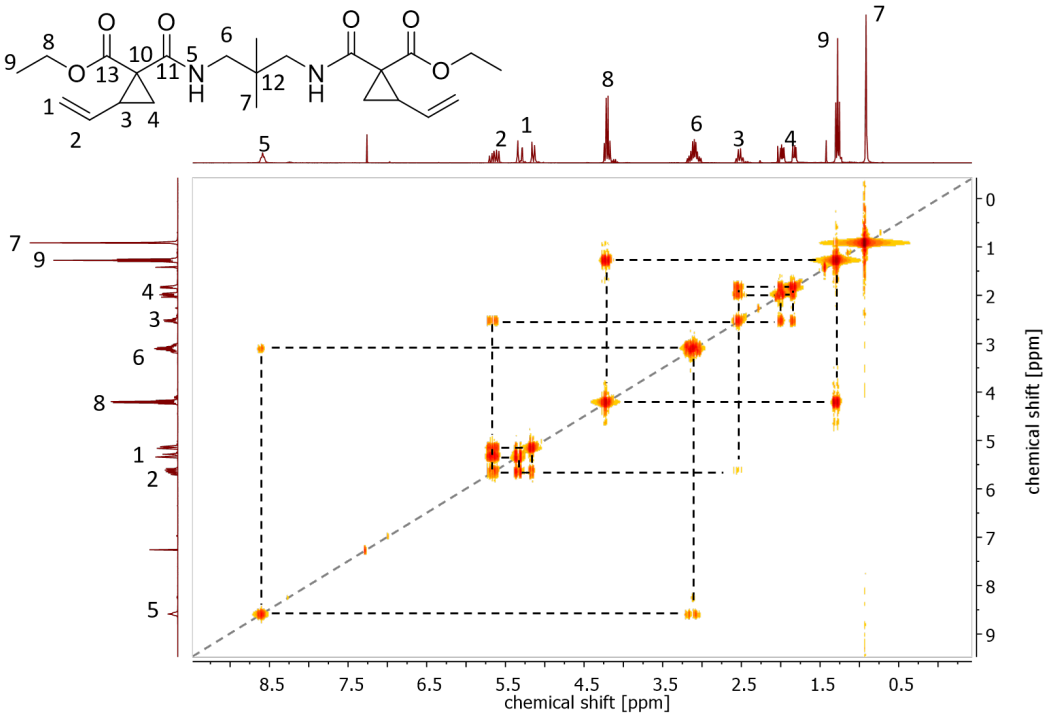

Figure 140: COSY 2D NMR of **15**.

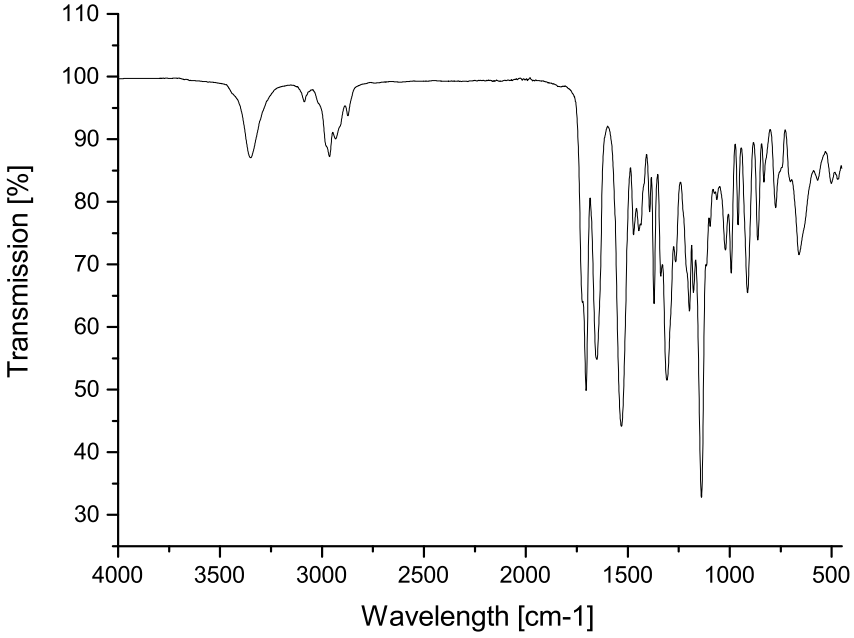

Figure 141: FT-IR of **15**.

4.2.6 Unsuccessful synthesis of new bi functional monomers

N^1,N^2-bis(2-aminoethyl)oxalamide

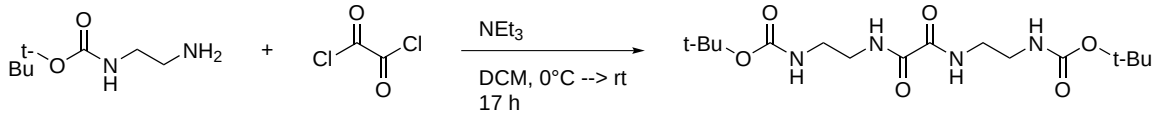

50 **37**

Under an argon atmosphere, **50** (2.0 eq, 15.0 g, 93.6 mmol) and NEt_3 (3.0 eq, 14.09 g, 19.3 ml, 13.9 mmol) were dissolved in 100 ml dry DCM. At 0 °, in 70 ml dry DCM dissolved oxalylchloride (5.90 g, 4.00 ml, 4.66 mmol) was added dropwise. The reaction was stirred at rt over night. The reaction was quenched by adding H_2O, stirred for another hour and filtrated. The filter cake was suspended in EtOAc, stirred for 30 min and centrifuged. The solvent was removed under reduced pressure to obtain the desired product **37** as white solid in a yield of 91 % (15.84 g, 4.23 mmol). **^{1}H NMR (300 MHz, DMSO, 293K):**

δ [ppm] = 8.72 (d, J = 5.4 Hz, 1H), 6.89 (s, 1H), 3.23 – 3.12 (m, 2H), 3.11 – 3.03 (m,

3H), 1.37 (s, 9H).

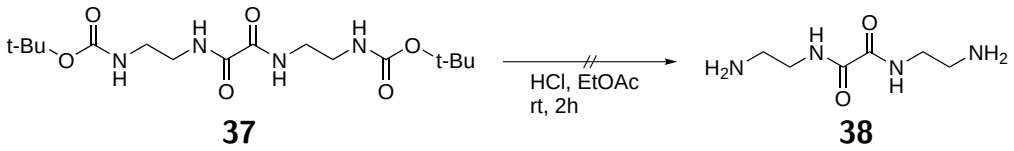

37 **38**

The, in 6 ml of a 4 molar solution of HCl in EtOAc, dissolved **37** was stirred at room temperature for 2 h. The solvent was removed under reduced pressure to obtain a brown solid. No analysis technique was possible for the obtained substance, since no solvent could be found in which the solid was solvable.

diethyl 1,1'-(4,8-dimethyl-6-oxo-2,5,7,10-tetraazaundecanedioyl)bis(2-vinylcyclopropane-1-carboxylate)

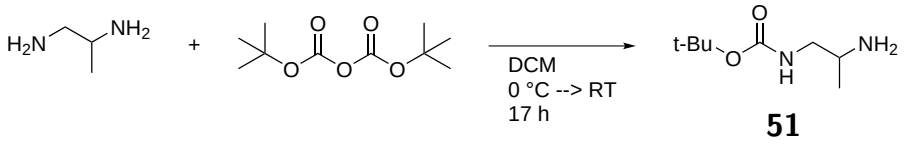

51

Propane-1,2-diamine (10 eq, 37.13 g, 500 mmol) was dissolved in 400 ml DCM. At 0 °C , in 200 ml DCM dissolved N-Boc decarbonate (11.7 g, 53.8 mmol) was added dropwise. The reaction mixture was stirred one hour at 0 °C and over night at room temperature. The reaction mixture was filtrated and washed with DCM. After evaporating the solvent, the product **51** was obtained as a slightly yellow liquid in a quantitative yield.
^{1}H NMR (300 MHz, $CDCl_3$, 293K):
δ [ppm] = 5.01 (s, 1H), 3.13 (dd, J = 11.3, 6.3 Hz, 1H), 3.07 – 2.93 (m, 1H), 2.93 – 2.79 (m, 1H), 1.42 (s, 9H), 1.06 (d, J = 6.3 Hz, 3H).

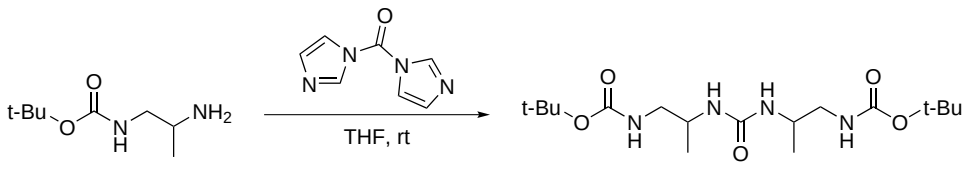

51 **52**

Under an argon atmosphere, 4.0 g CDI (24.87 mmol) was dissolved in 100 ml dry THF. At 0 °C , **51** (2.0 eq, 8.7 g, 50.0 mmol) was added. The reaction was stirred 20 min

at 0 °C and at rt over night. The solvent was removed under reduced pressure, the mixture dissolved in EtOAc and washed with H_2O. The solvent was removed under reduced pressure and the product **52** obtained as white solid in a yield of 90% (8.89 g, 23.7 mmol).

^{1}H NMR (300 MHz, $CDCl_3$, 293K):

δ [ppm] = 5.00 (s, 1H), 3.25 – 3.10 (m, 1H), 3.04 (dt, J = 10.6, 6.4 Hz, 1H), 2.98 – 2.85 (m, 1H), 1.51 – 1.36 (m, 9H), 1.10 (d, J = 6.3 Hz, 3H).

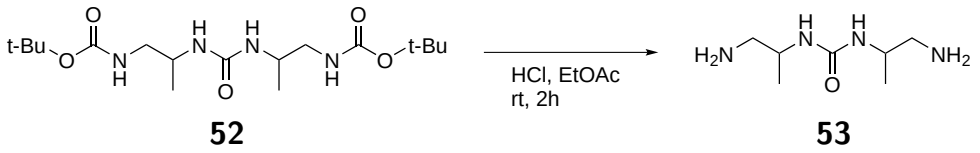

52 **53**

In a mixture of 4 ml concentrated HCl in 9.3 ml EtOAc, 8.89 g of **52** (23.7 mmol) was stirred at rt for 2 h. The reaction was quenched by adding a saturated $NaHCO_3$ solution and the organic phase washed with a saturated $NaHCO_3$ solution. The organic phase was filtered and the solvent removed under reduced pressure and the product used as such, without further purification.

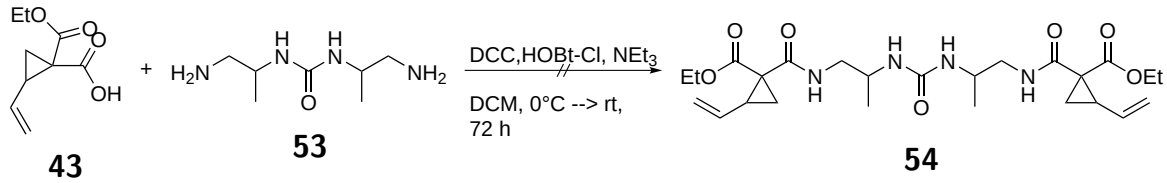

43 **53** **54**

Under an argon atmosphere, 6.19 g **43** (2.2 eq, 33.6 mmol), **53** (2.80 g, 16.0 mmol) and HOBt-Cl(2.3 eq, 5.869 g,34.6 mmol) were dissolved in 100 ml dry DCM. At 0°C NEt_3 (4.2 eq,6.80 g, 9.31 ml, 67.2 mmol) was added and in 90 ml dry DCM dissolved DCC (2.2 eq, 6.93 g, 33.6 mmol) was added drop wise. The reaction mixture was stirred at room temperature for three days. The mixture was filtrated and the organic phase was washed twice with 0.5 M HCl solution, once with saturated $NaHCO_3$ solution and twice with water. After drying over $MgSO_4$ the solvent was removed and the mixture purified via flash chromatography (Cylcohexane:EtOAc 50:50). The desired product couldn't be identified.

diethyl 1,1'-(4,8-diisopropyl-6-oxo-2,5,7,10-tetraazaundecanedioyl)bis(2-vinylcyclopropane-1-carboxylate)

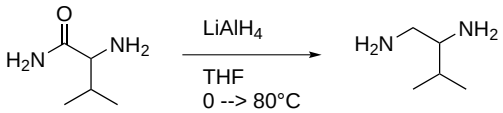

55

Compound **55** was synthesized as per published procedure[]. Under an argon atmosphere, 14.8 g of $LiAlH_4$ (2.2 eq, 390.4 mmol) was suspended in 200 ml dry THF. At 0 °C , 2-amino-3-methylbutanamide (19.86 g, 171 mmol) was added in small portions. The mixture was stirred at 80 °C over night. The reaction was quenched by carefully adding technical grade THF and extracted with cyclohexane. The solvent was removed under reduced pressure and the product **55** obtained as white solid and used without further purification.

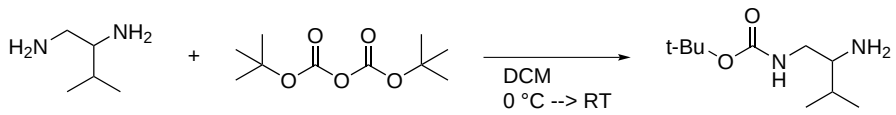

55 **56**

The previously obtained diamine **55** (1.2 eq, 9.95 g, 97.0 mmol) was dissolved in 20 ml dry THF. In 80 ml dry THF dissolved *tert*-butyl dicarbonate (7.9 g, 48.5 mmol) was added at 0 °C . The solution was stirred at rt for 3 days, the solvent removed and the mixture dissolved in DCM. After washing with water, the poduct **56** was obtained in a yield of 38 % (3.68 g, 18.2 mmol) whose presence was confirmed using liquid chromatography–mass spectrometry (LC-MS)

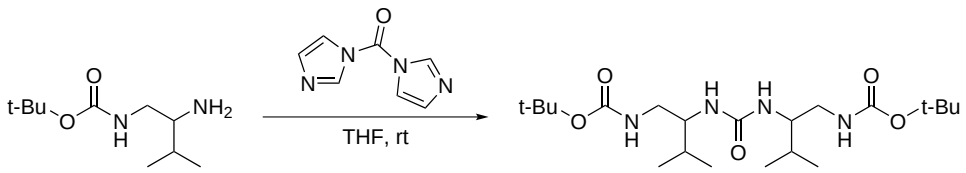

56 **57**

Under and argon atmosphere, 3.45 g **56** (2.0 eq, 17.0 mmol) was dissolved in 36 ml dry THF. At 0 °C , DCC (8.5 mmol, 1.38 g) was added and the mixture stirred at rt over night. The reaction was quenched by addition of H_2O and the mixture extracted with EtOAc. The organic phase was separated and washed with H_{20}. The organic

phase was dried over $MgSO_4$ and the solvent was removed to obtain the product **57** in a quantitative yield. **^{1}H NMR (300 MHz, $CDCl_3$, 293K):**
δ [ppm] = 6.74 (s, 1H), 4.88 – 4.49 (m, 1H), 3.97 – 3.41 (m, 1H), 3.17 (s, 1H), 1.68 (s, 1H), 1.43 (s, 9H), 1.03 – 0.85 (m, 6H).

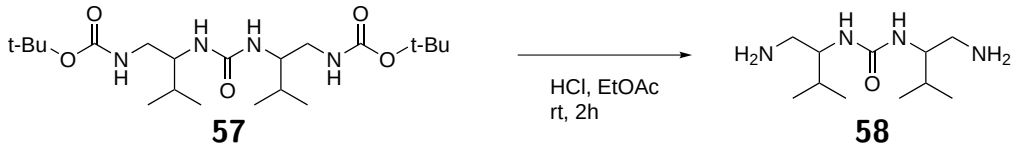

57 **58**

Deprotection was performed by the addition of 5 ml of a 12 molar HCl solution at 0 °C to 4.23 g of **57** (9.25 mmol). The mixture was stirred at rt for 2 h before the solvent was removed and the obtained mixture purified by flash cromatography. The product was obtained in a yield of 19% (410 mg, 1.78 mmol). **^{1}H NMR (300 MHz, $CDCl_3$, 293K):**
δ [ppm] = 3.62 – 3.44 (m, 2H), 3.31 – 3.10 (m, 1H), 1.79 – 1.58 (m, 1H), 0.94 (d, J = 6.7 Hz, 3H), 0.88 (d, J = 6.7 Hz, 3H).

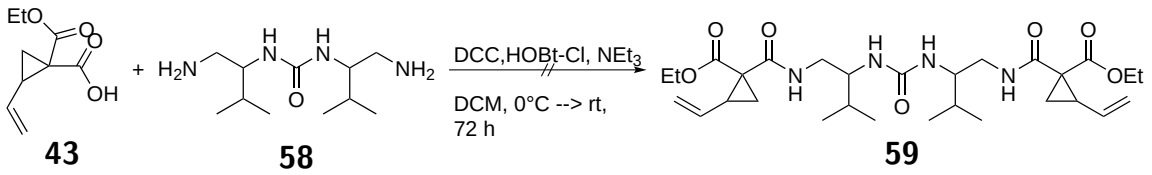

43 **58** **59**

Under an argon atmosphere, 722 mg **43** (2.2 eq, 3.92 mmol), DCC (2.2 eq, 808 mg, 3.92 mmol) were added to in 10 ml dry DCM dissolved **57** (410 mg, 1.78 mmol). At 0°C NEt_3 (4.2 eq, 756 mg, 1.0 ml, 7.48 mmol) was added to the mixture. HOBt-Cl(2.3 eq, 693 mg, 4.09 mmol) was dissolved in 10 ml dry DCM and added dropwise at 0 °C . The reaction mixture was stirred at room temperature for six days. The mixture was filtrated and analysed using LC-MS, where no product could be found.

1,3-bis(2-(aminomethyl)-3-methylbutyl)urea

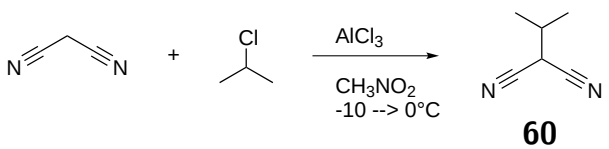

60

To at -10 °C in 240 ml nitromethane dissolved $AlCl_3$ (104 g,), in 60 ml nitromethane dissolved malononitrile (1.00 eq, 56.6 g, 856 mmol) was added drop wise. Secondly, 147.6 ml of pre-distilled isopropyl chloride (2.0 eq, 127.3 g, 1.62 mol), dissolved in 60 ml nitromethane was added drop wise. The mixture was stirred at 0 °C over night before 1 litre of a saturated $NaHCO_3$ solution was added drop wise, maintaining the temperature below 10 °C . The reaction mixture was charged with $NaHCO_3$ till no gas formation can be observed. The phases where separated and the aqueous phase washed with DCM. The combined organic phases were dried over $MgSO_4$ and the solvent was removed under reduced pressure. The mixture was was purified by water steam distillation. The desired product couldn't be obtained.

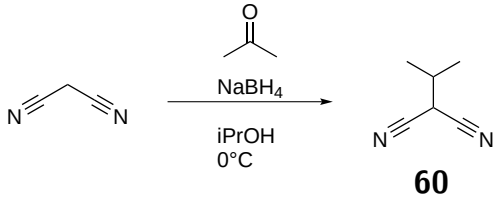

60

At 0 °C , 33.3 ml malononitril (39.64 g, 600 mmol) and acetone (2 eq, 69.69 g, 1.20 mol, 88.3 ml) were dissolved in 1.2 liter isopropanol. $NaBH_4$ (1 eq, 22.69 g, 600 mmol) was added and the mixture stirred at 0 °C for 2 h before another 11.9 q $NaBH_4$ (0.5 eq, 300 mmol) was added. The reaction was quenched by the addition of a 2 molar HCl solution until a pH of 1 is obtained. The product was extracted with DCM, dried over $MgSO_4$ and the solvent removed under reduced pressure. The product **60** was obtained after distillation and purification via flash chromatography as a yellow viscous liquid in a yield of 5% (3.31 g, 31.0 mmol).

^{1}H NMR (300 MHz, $CDCl_3$, 293K):

δ [ppm] = 3.36 (d, J = 5.4 Hz, 1H), 2.49 – 2.29 (m, 1H), 1.33 – 1.00 (m).

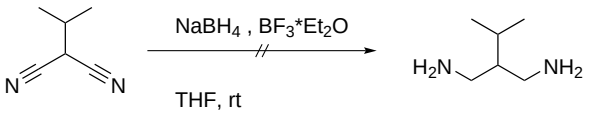

60 **61**

Under an argon atmosphere 3.0 g of **60** (27.76 mmol) and $NaBH_4$ (1.8 eq, 1.90 g, 50.30 mmol) were dissolved in 17 ml dry THF. In 5.5 ml dry THF dissolved $BF_3 \cdot Et_2O$ (2.2 eq, 9.46 g, 8.22 ml, 60.62 mmol) was added drop wise. The reaction was stirred at rt over night before it was quenched by the addition of 3.3 ml concentrated HCl. The solvent was removed under reduced pressure and the mixture neutralized by slow

addition of a 40% NaOH solution. The aqueous phase was extracted with Et_2O, the organic phase dried over $MgSO_4$ and the solvent removed under reduced pressure. No product could be found.

1,3-bis(2-(aminomethyl)-3,3-dimethylbutyl)urea

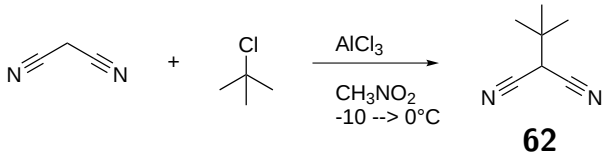

62

To at 0 °C in 200 ml nitromethane dissolved $AlCl_3$ (90.0 g, 674 mmol), in 50 ml nitromethane dissolved malononitrile (1.00 eq, 45.0 g, 682 mmol) was added drop wise. Secondly, 178.6 ml of *tert*-butyl chloride (2.0 eq, 150.0 g, 1.62 mol), dissolved in 50 ml nitromethane was added drop wise. The mixture was stirred at 0 °C over night before 1 litre of a saturated $NaHCO_3$ solution was added drop wise, maintaining the temperature below 10 °C . The phases where separated and the aqueous phase washed with DCM. The combined organic phases were dried over $MgSO_4$ and the solvent was removed under reduced pressure. The mixture was was purified by water steam distillation. The obtained solid was washed with Et_2O and purified via sublimation at 40 °C under reduced pressure to obtain the product **62** in a yield of 45% (33.3 g, 308 mmol).

^{1}H NMR (300 MHz, $CDCl_3$, 293K):

δ [ppm] = 3.45 (s, 1H), 1.27 (s, 9H).

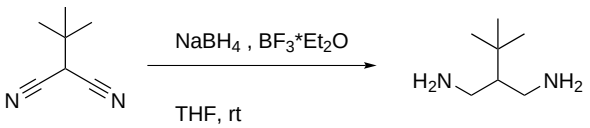

62 **63**

Under an argon atmosphere 33.3 g of **62** (308 mmol) and $NaBH_4$ (1.8 eq, 21.0 g, 555 mmol) were dissolved in 180 ml dry THF. In 70 ml dry THF dissolved $BF_3 \cdot Et_2O$ (2.4 eq, 105.0 g, 91.3 ml, 740 mmol) was added drop wise. The reaction was stirred at rt over night before it was quenched by the addition of 30 ml concentrated HCl. The solvent was removed under reduced pressure and the mixture neutralized by slow addition of 125 ml of a 40% NaOH solution. The mixture was stirred at 90 °C for 30

min, the aqueous phase was extracted with Et_2O, the organic phase dried over $MgSO_4$ and the solvent removed under reduced pressure. The product **63** was obtained after destillation in a yield of 25% (9.92 g, 76.2 mmol).

^{1}H NMR (300 MHz, $CDCl_3$, 293K):

δ [ppm] = 3.11 – 2.97 (m, 2H), 2.74 – 2.59 (m, 2H), 1.16 (dt, J = 5.8, 2.2 Hz, 1H), 0.91 (s, 9H).

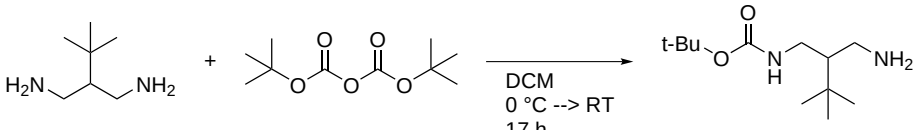

63 **64**

To in 100 ml dry DCM dissolved **63** (10 eq, 9.92 g, 76.2 mmol), at 0 °C , in 100 ml dry DCM dissolved *tert*-butyl dicarbonate (1.66 g, 7.6 mmol) was slowly added. The reaction mixture was stirred 1 hour (h) at 0 °C and at rt over night. The solvent was removed under reduced pressure, the crude product dissolved in saturated $NaHCO_3$ solution and extracted with DCM. No product could be found in any of the analyzed fractions

1,3-bis(3-amino-2,2-dimethylpropyl)urea

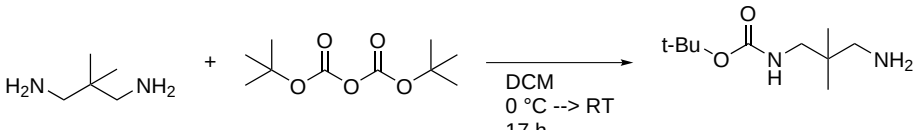

65

To in 200 ml dry DCM dissolved 2,2-dimethylpropane 1,3-diamine (20.0 g, 195.7 mmol), at 0 °C NEt_3 (19.8 g, 27.3 ml, 195.7 mmol) was added and in 100 ml dry DCM dissolved *tert*-butyl dicarbonate (0.7 eq, 41.82 g, 191.7 mmol) was slowly added. The reaction mixture was stirred at rt over night. The reaction mixture was filtrated and the aqueous phase extracted with DCM. After driying over $MgSO_4$ and removal of the solvent under reduced pressure, the product **65** was obtained without further purification.

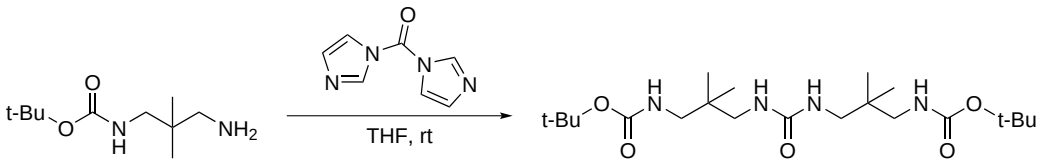

65 **66**

Under an argon atmosphere, 10.15 g **65** (50.2 mmol) was dissolved in 100 ml dry THF. At 0 °C , CDI (0.5 eq, 4.0 g, 24.67 mmol) was added. The reaction was stirred 1 h at 0 °C and for 3 days at rt. The reaction was quenched by adding water, extracted with EtOAc and dried over $MgSO_4$. The solvent was removed under reduced pressure but no product could be found.

1,3-bis((3-(aminomethyl)cyclohexyl)methyl)urea

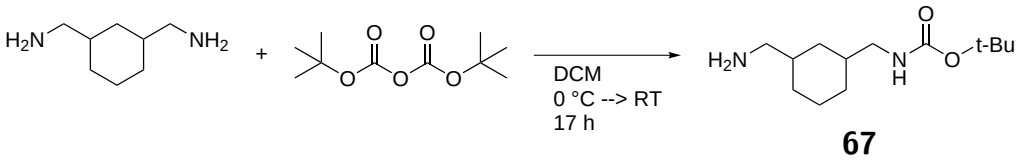

67

To in 200 ml dry DCM dissolved cyclohexane-1,3-diyldimethanamine (50 g, 351 mmol), at 0 °C NEt_3 (1.0 eq, 35.6 g, 52.6 ml, 351 mmol) was added and in 400 ml dry DCM dissolved *tert*-butyl dicarbonate (0.7 eq, 53.7 g, 246 mmol) was slowly added. The reaction mixture was stirred at rt over night. The reaction mixture was filtrated and the aqueous phase extracted with DCM. After drying over $MgSO_4$ and removal of the solvent under reduced pressure, the product **67** was obtained in a yield of 14% (12.1 g, 49.9 mmol)

^{1}H NMR (300 MHz, $CDCl_3$, 293K):

δ [ppm] = 4.64 (s, 1H), 3.13 – 2.85 (m, 2H), 2.58 – 2.46 (m, 3H), 1.88 – 1.64 (m, 4H), 1.40 (d, J = 13.3 Hz, 9H), 1.26 (dtdd, J = 17.0, 10.3, 6.4, 3.6 Hz, 3H), 0.79 (ddt, J = 16.1, 7.6, 4.2 Hz, 2H), 0.53 (qd, J = 12.0, 2.9 Hz, 1H).

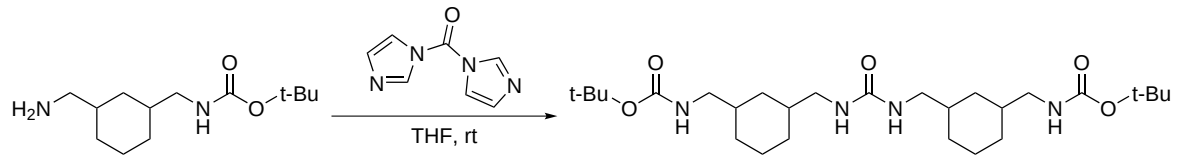

Under an argon atmosphere, 5.44 g **67** (22.46 mmol) was dissolved in 100 ml dry THF. At 0 °C , CDI (0.5 eq, 1.82 g, 11.23 mmol) was added. The reaction was stirred 1 h at 0 °and for 3 days at rt. The reaction was quenched by adding water, extracted with EtOAc and dried over $MgSO_4$. The solvent was removed under reduced pressure and the product **68** obtained in a yield of 28% (3.14 g, 6.15 mmol).

^{1}H NMR (300 MHz, $CDCl_3$, 293K):

δ [ppm] = 4.62 (d, J = 25.1 Hz, 1H), 2.96 (t, J = 5.7 Hz, 3H), 1.89 – 1.65 (m, 3H), 1.53 – 1.32 (m, 14H), 1.26 (ddt, J = 19.4, 14.0, 7.2 Hz, 1H), 0.91 – 0.69 (m, 1H), 0.70 – 0.48 (m, 1H).

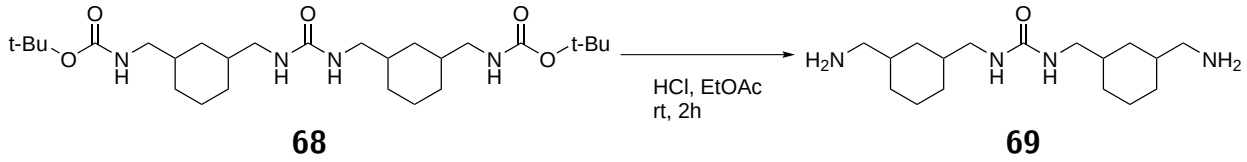

In a mixture of 4 ml concentrated HCl in 9.3 ml EtOAc, 3.14 g of **68** was stirred at rt for 4 days. The reaction was quenched by adding a saturated $NaHCO_3$ solution and the organic phase washed with a saturated $NaHCO_3$ solution. The organic phase was filtered and the solvent removed under reduced pressure not resulting in the desired product.

1,3-bis(3-((3-amino-2-methylcyclohexyl)methyl)-2-methylcyclohexyl)urea

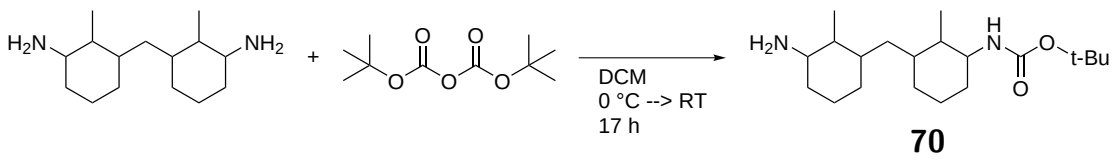

To in 40 ml dry MeOH dissolved 3,3'-methylenebis(2-methylcyclohexan-1-amine) (23.8 g, 25.1 ml, 100 mmol), at 0 °C 42 ml of a 8 molar HCl solution was added dropwise.

The reaction mixture was stirred at rt for 1 h and in 448 ml MeOH dissolved *tert*-butyl dicarbonate (1.0 eq, 21.8 g, 100 mmol) was slowly added. The reaction mixture was stirred at rt for 2 h and washed with Et_2O. The aqueous phase was neutralized by adding in 100 ml dissolved NaOH (1.0 eq, 4.0 g) and extracted with DCM. The combined organic phases were washed with a saturated NaCl solution, dried over $MgSO_4$ and the solvent was removed under reduced pressure. The product was obtained in a yield of 30% (10.1 g, 29.9 mmol) without further purification.

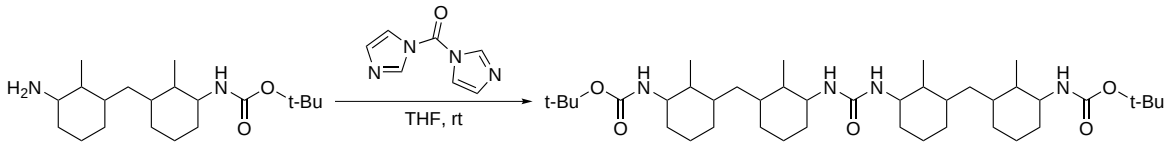

70 **71**

Under an argon atmosphere, 10.11 g **70** (29.9 mmol) was dissolved in 100 ml dry THF. At 0 °C , CDI (0.5 eq, 2.42 g, 14.95 mmol) was added. The reaction was stirred 1 h at 0 °C and for 4 days at rt. The solvent was removed under reduced pressure, the crude product was dissolved in water and extracted with ETOAc. No product could be detected in any of the phases.

4.3 Monomer characterization

4.3.1 nuclear magnetic resonance spectroscopy

For ^{1}H- NMR 5 mg and for ^{13}C-NMR 20 mg were dissolved in 0.7 ml of the respective deuterated solvent $CDCl_3$, CD_2Cl_2, d-DMSO or d-DMF.

4.3.2 temperature variable NMR

Temperature dependent solid state NMR was performed by the group of Prof. Dr. Senker (Inorganic Chemistry III)

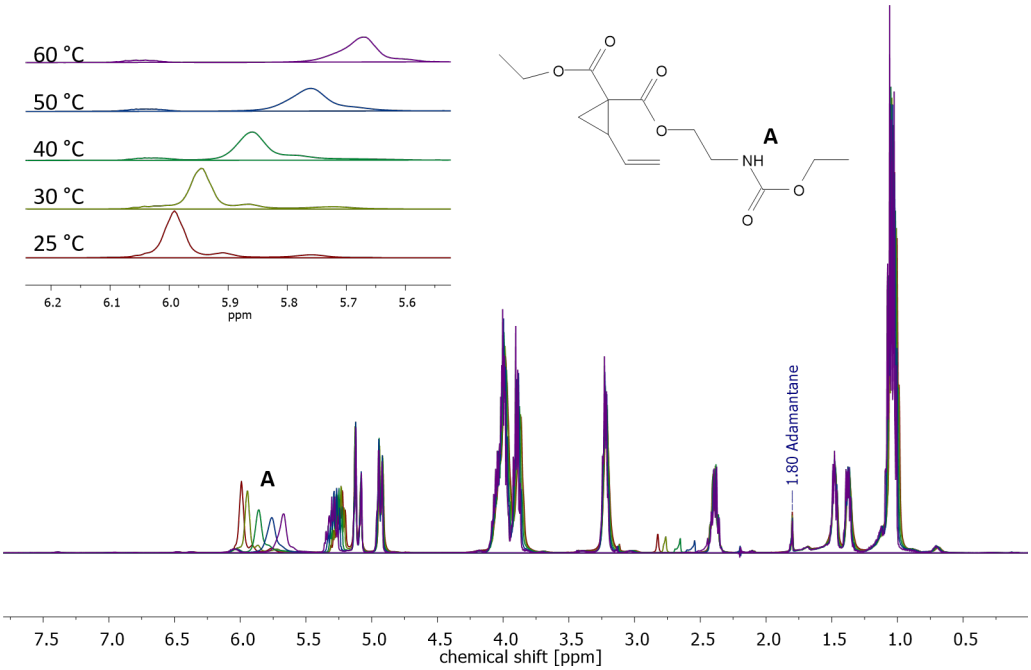

Figure 142: temperature dependent solid state NMR of monomer **2**

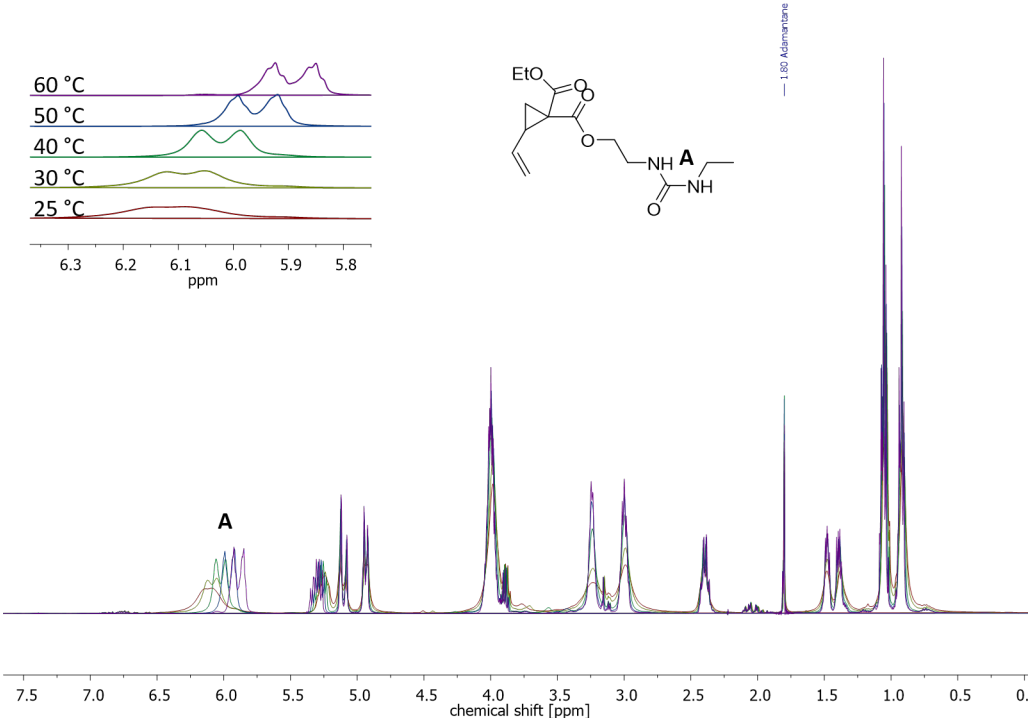

Figure 143: temperature dependent solid state NMR of monomer **4**

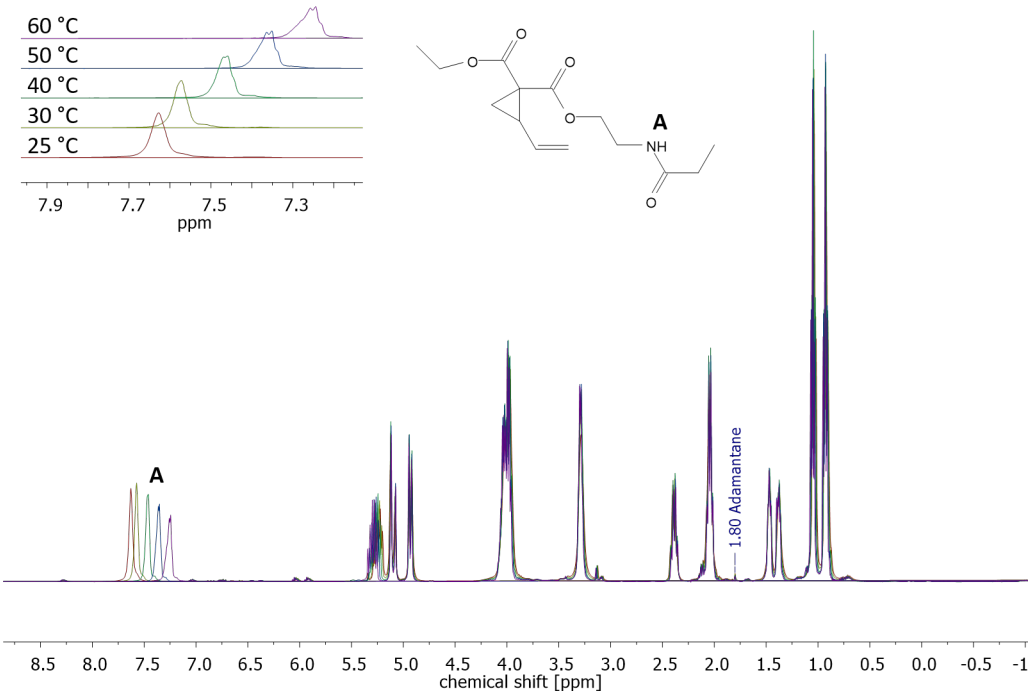

Figure 144: temperature dependent solid state NMR of monomer **22**

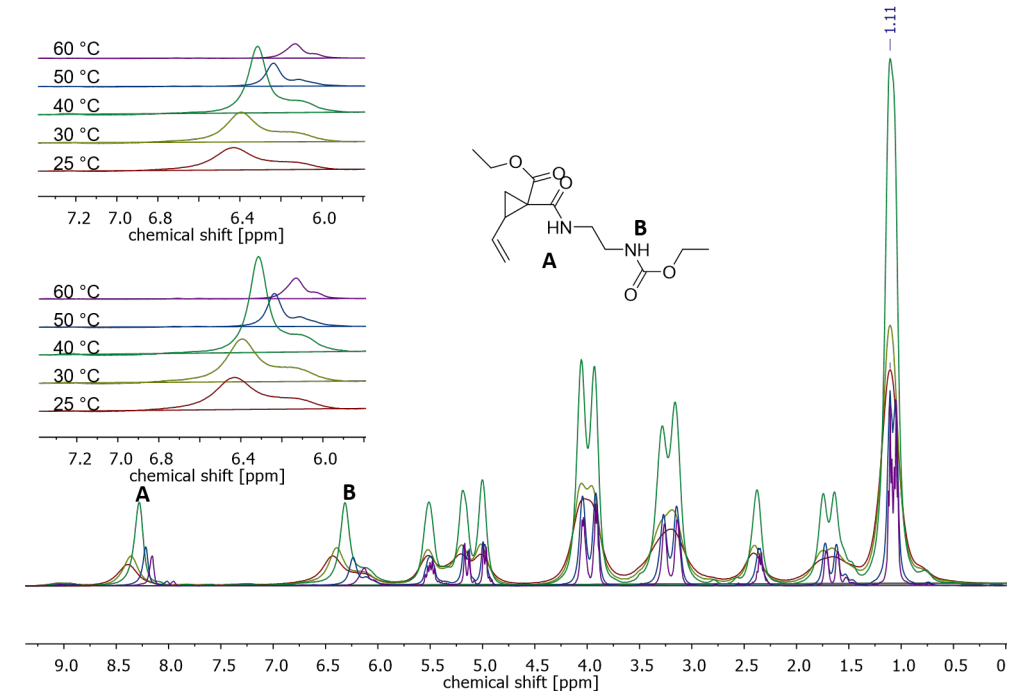

Figure 145: temperature dependent solid state NMR of monomer **6**

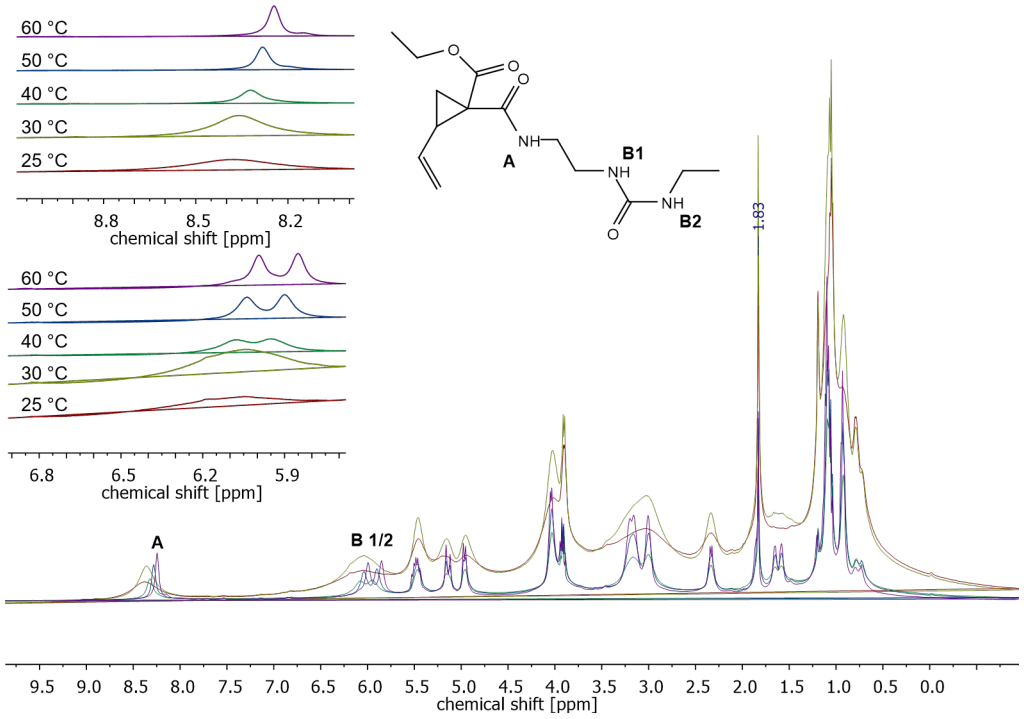

Figure 146: temperature dependent solid state NMR of monomer **7**

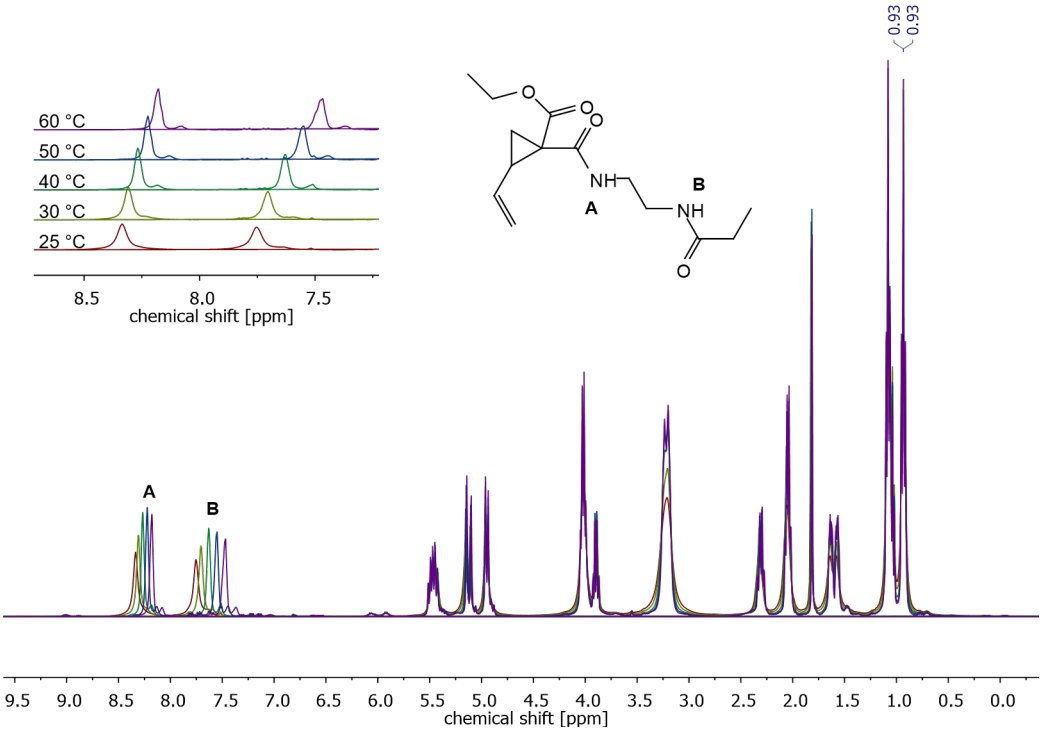

Figure 147: temperature dependent solid state NMR of monomer **8**

4.4 Photo-polymerization

4.4.1 Kinetic measurements

In a brow glass vial 1 mol% CQ as initiator and 2 mol% EDMAB as coinitiator were dissolved in the respective monomers **3**, **4** and **72**. In the abscence of light, 11 vials were prepared, each containing 10 μl of the solution. Each vial was degassed for 30 sec with argon. The solutions were irradiated with light with a maximum intensity of 800 W halogen equivalents (data as per the lamp manual provided by GSVITEC) primarily at 442 and 540 nm. After 1, 3, 5, 10, 15 and 30 min, 1, 2, 4, 8 and 24h a vial was removed and quenched by adding it to liquid nitrogen. To each vial, 1.5 ml Et_2O containing phenol in a concentration of 1 mg/ml was added and the residual monomer was extracted. The amount of unreacted monomer was analyzed via GC, using phenol as internal standard.

For monomers **7**, **8** and **73**, in a brown glass vial, the respective monomers as well as 1 mol % CQ as initiator and 2 mol% EDMAB as coinitiator were dissolved in anisol as a 2.5 M solution. In the abscence of light, 14 vials were prepared, each containing 20 μl of the solution. Each vial was degassed for 30 sec with argon. The solutions were irradiated with light with a maximum intensity at 442 nm and 540 nm. After 5, 10, 20, 30 and 45 s, 1, 3, 5, 10, 15 and 30 min, 1, 2 and 24h a vial was removed and quenched by adding it to liquid nitrogen. To each vial, 1.5 ml Et_2O in case of monomers **5** and **8** and toluene in case of monomers **6** and **7** containing phenol in a concentration of 1 mg/ml was added and the residual monomer was extracted. The amount of unreacted monomer was analyzed via GC, using phenol as internal standard.

For monomers **9**, **10**, **11**, **12**, **13**, **14** and **15**, in a brown glass vial, the respective monomers as well as 1 mol % CQ as initiator and 2 mol% EDMAB as coinitiator were dissolved in anisol as a 2.5 M solution. In the abscence of light, 6 vials were prepared, each containing 20 μl of the solution. Each vial was degassed for 30 sec with argon. The solutions were irradiated with light with a maximum intensityof 800 W halogen equivalents (data as per the lamp manual provided by GSVITEC) primarily at 442 and 540 nm. After 30s, 1, 3, 10 and 30 min and 17 h a vial was removed and quenched by adding it to liquid nitrogen. In the case of monomers **14** and **15**, the residual monomer was extracted using DCM, containing phenol in a concentration of 1 mg/ml and for monomers **9**, **10**, **11**, **12** and **13** the residual monomer was extracted using $CDCl_3$ and mesythylen as internal standard. The amount of unreacted monomer was determined using GC for monomers **14** and **15** and NMR for monomers **9**, **10**, **11**, **12** and **13**

4.4.2 Photo-Rheology

In a brow glass vial 1 mol % CQ as initiator and 2 mol% EDMAB as coinitiator were dissolved in the respective monomers **1**, **2**, **3** and **4**. Each monomer was degassed using argon. In a nitrogen atmosphere ca. 250 mg of each solution was placed on a class plate and a frequency sweep was performed. At the there determined frequency, the viscosity was measured over time, while the sample was irradiated with ultra violet (UV)-light at a intensity of 20 Wcm^{-1}. The viscosity was plotted in a logarithmic scale against the time of irradiation.

4.5 Polymer characterization

4.5.1 gel permeation chromatography

Polymer masses and dispersity were analyzed by gel permeation chromatography. The measurements were recorded using an SDV XL gel column (particle size=5 µm with a separation range of 100 - 3 000 000 Da) and a refractive index detector (1200 series, Agilent Technologies). Chloroform or DMF was used as the solvent and eluant with a flow rate of 0.5 ml min^{-1}.The calibration was performed with a narrowly distributed polystyrene homopolymer (PSS calibration kit). Before measurement, sample was dissolved in the respective solvent to a concentration of 10 mg/ml and filtered with a 0.22 µm PTFE filter. The injection volume was 20 µl. Toluene served as the internal standard.

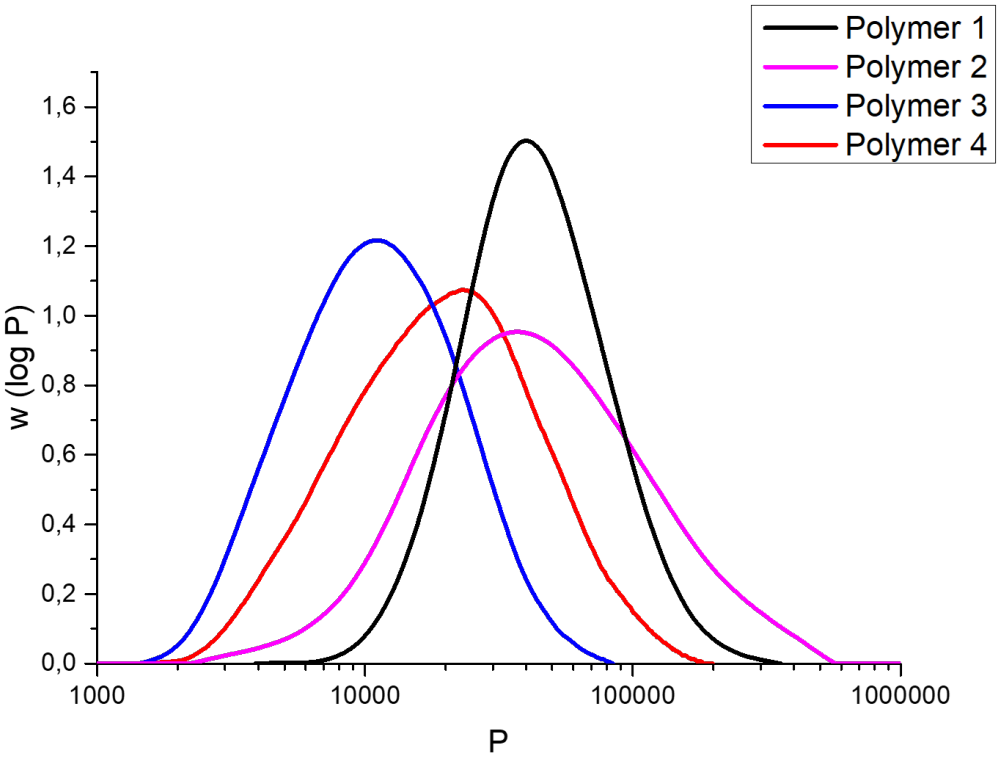

Figure 148: GPC curves of VCP-ester polymers **1 - 4**

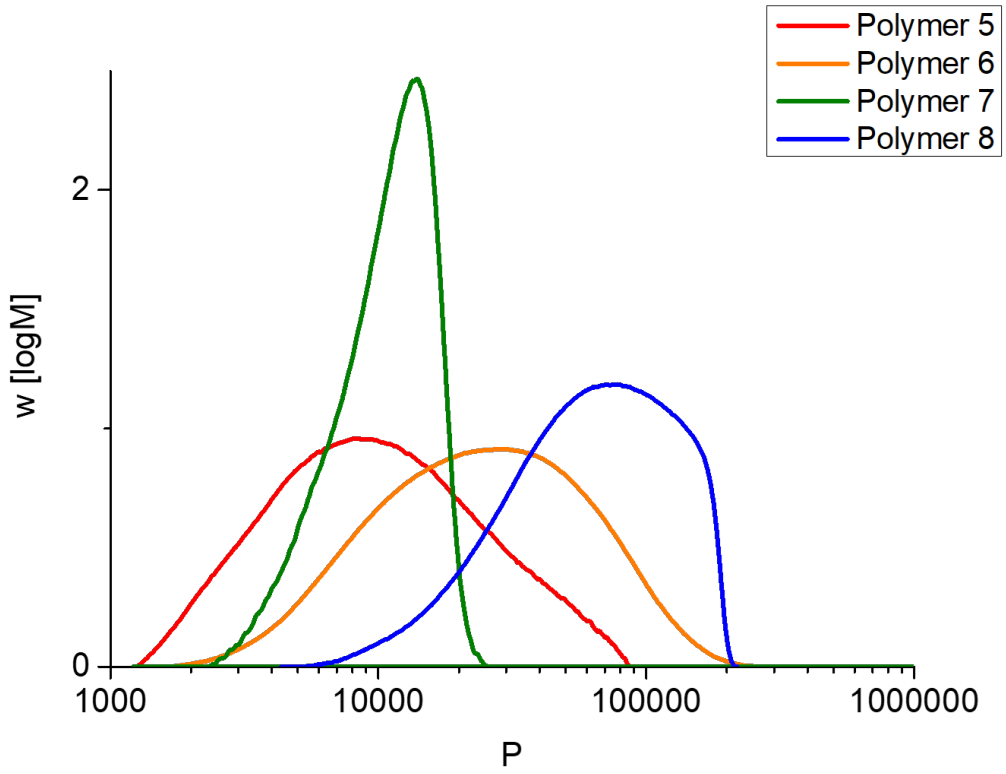

Figure 149: GPC curves of VCP-amide polymers **5 - 8**

4.5.2 differential scanning calorimetry

Thermal stability is measured by TGA in a NETZSCH 204 F1 Phoenix. measurement conditions were dependent on the sample and range where signals are expected. The upper range was conducted by the thermal stability, while the lower range was selected to be at least 50 K below the T_g. Standard heating rate was 10 K/min, while in cases where the T_g was hard to observe, a heating rate of 20 K/min was selected. For each sample about 5 mg were added to an aluminium pan, equipped with a pinned cap. Evaluation was done in the software provided by NETZSCH. In all cases, T_g of the second heating curve was evaluated.

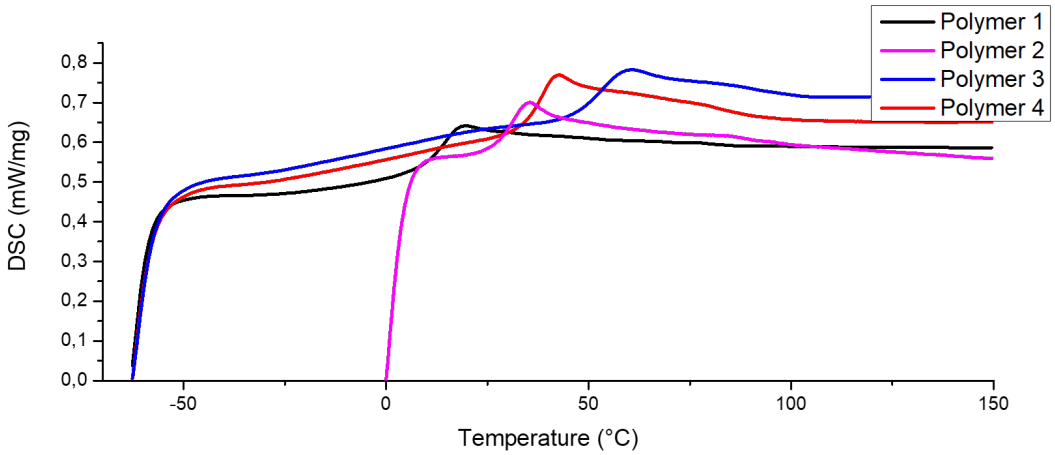

Figure 150: DSC curves of VCP-ester polymers **1 - 4**

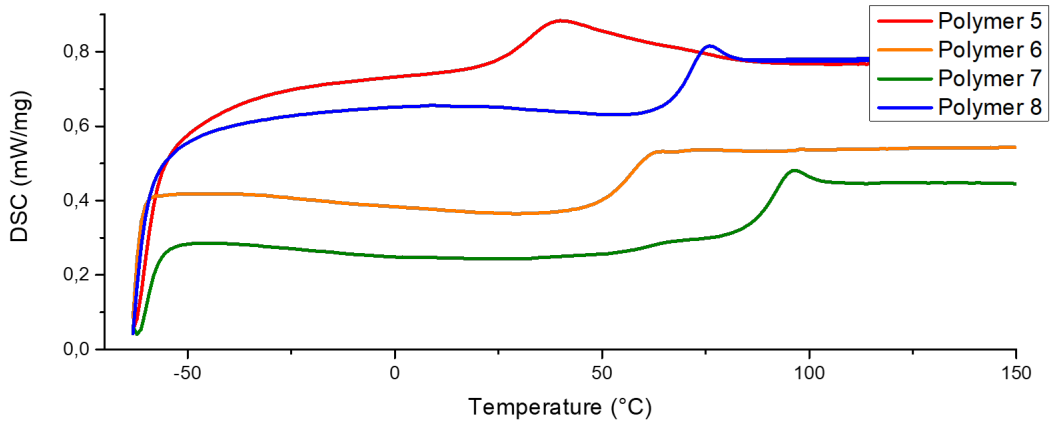

Figure 151: DSC curves of VCP-amide polymers **5 - 8**

4.5.3 Thermal stability

Thermal stability is measured by TGA in a NETZSCH Libra F1. Measurements were done under a nitrogen atmosphere with a flow of $20ml/min$ from 20 to 600 °C with a heating rate of 10 k/min. For each sample about 5 mg were added to an aluminium pan, equipped with a pinned cap. Evaluation was done in the software provided by NETZSCH

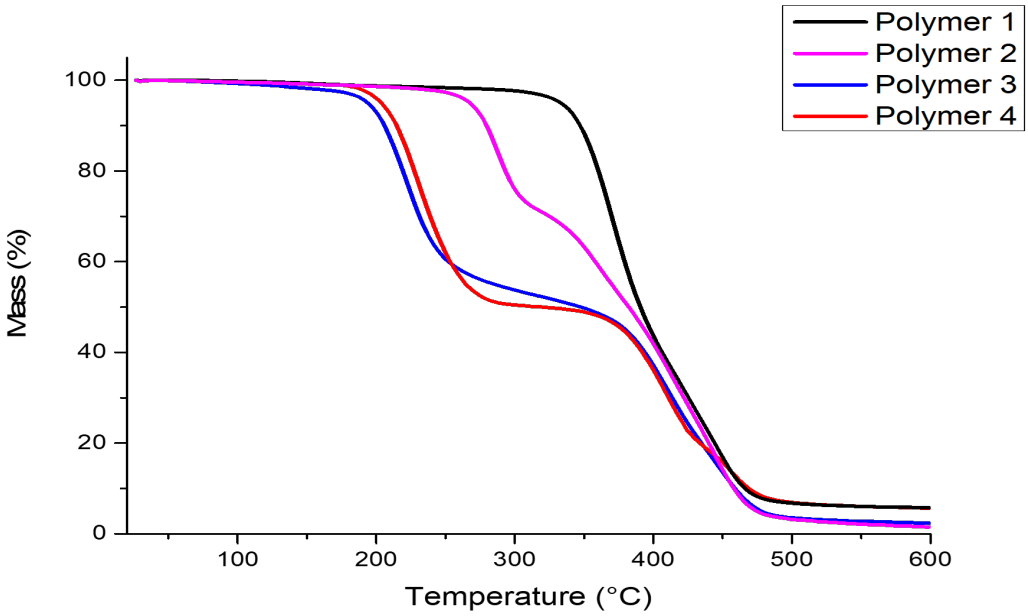

Figure 152: TGA curves of VCP-ester polymers **1 - 4**

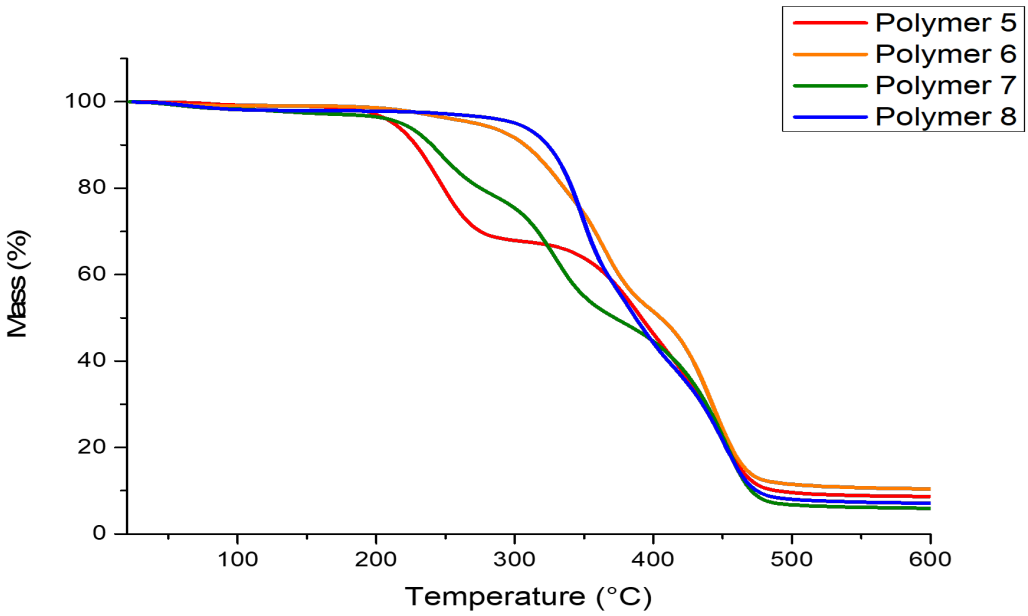

Figure 153: TGA curves of VCP-amide polymers **5 - 8**

4.5.4 Volume shrinkage

Volume shrinkage was determined by the change of density from monomer and polymer. Therefore, the density of monomers **9**, **10**, **11**, **12**, **13**, **14** and **15** was determined by gas pycnometry. The pycnometer was calibrated beforehand by the Prof. Moos chair. An empty glas vial was added into the chamber and the volume was measured to determine the free volume of the chamber. To this glass vial, ca. 1 g of a monomer was added and the weight was noted. The volume of the chamber was measured again. By the difference of these two volumes and the added weight monomer density can be obtained. For polymer density, the pure and dried polymer was weighted in the chamber and the free volume determined. Polymer density was determined by the alchimedes method. Here, around 100 mg of the resulting polymers were put on a balance, equipped with a beaker filled with water. The balance was set to zero and the polymers immersed in water. by the difference of weight and the known density of water at that temperature, the polymer density could be obtained.

Bibliography

[1] Schumacher, S.; Pantawane, S.; Gekle, S.; Agarwal, S. Theoretical and Experimental Study of Monofunctional Vinyl Cyclopropanes Bearing Hydrogen Bond Enabling Side Chains. *Macromolecules* **2021**, *54*, 11–21.

[2] Schumacher, S.; Pantawane, S.; Gekle, S.; Agarwal, S. The Effect of Hydrogen Bonding on Polymerization Behavior of Monofunctional Vinyl Cyclopropane-Amides with Different Side Chains. *Macromolecular Chemistry and Physics* **2022**, *223*, 2200155.

[3] Davidson, C.; De Gee, A. Relaxation of polymerization contraction stresses by flow in dental composites. *Journal of dental research* **1984**, *63*, 146–148.

[4] Feilzer, A. J.; De Gee, A. J.; Davidson, C. Setting stress in composite resin in relation to configuration of the restoration. *Journal of dental research* **1987**, *66*, 1636–1639.

[5] Yap, A.; Soh, M. Post-gel polymerization contraction of" low shrinkage" composite restoratives. *OPERATIVE DENTISTRY-UNIVERSITY OF WASHINGTON-* **2004**, *29*, 182–187.

[6] Altunbulak, M.; Klyachko, A. The Pauli principle revisited. *Communications in Mathematical Physics* **2008**, *282*, 287–322.

[7] Chandler, D.; Weeks, J. D.; Andersen, H. C. Van der Waals picture of liquids, solids, and phase transformations. *Science* **1983**, *220*, 787–794.

[8] Ewing, G. E. Intermolecular interactions: van der Waals Molecules. *Angewandte Chemie International Edition in English* **1972**, *11*, 486–495.

[9] Langbein, D. Theory of van der Waals Attraction. *Springer tracts in modern physics* **2006**, 1–139.

[10] Zefirov, Y. V.; Zorkii, P. Van der Waals radii and their application in chemistry. *Russian Chemical Reviews* **1989**, *58*, 421.

[11] Martinez, C. R.; Iverson, B. L. Rethinking the term "pi-stacking". *Chemical Science* **2012**, *3*, 2191–2201.

[12] Molčanov, K.; Kojić-Prodić, B. Towards understanding π-stacking interactions between non-aromatic rings. *IUCrJ* **2019**, *6*, 156–166.

[13] Weinhold, F.; Klein, R. A. What is a hydrogen bond? Mutually consistent theoretical and experimental criteria for characterizing H-bonding interactions. *Molecular Physics* **2012**, *110*, 565–579.

[14] Wojtulewski, S.; Grabowski, S. J. Different donors and acceptors for intramolecular hydrogen bonds. *Chemical physics letters* **2003**, *378*, 388–394.

[15] Fargher, H. A.; Sherbow, T. J.; Haley, M. M.; Johnson, D. W.; Pluth, M. D. C–H S hydrogen bonding interactions. *Chemical Society Reviews* **2022**,

[16] Roudaut, G.; Simatos, D.; Champion, D.; Contreras-Lopez, E.; Le Meste, M. Molecular mobility around the glass transition temperature: a mini review. *Innovative Food Science & Emerging Technologies* **2004**, *5*, 127–134.

[17] Wendorff, J.; Fischer, E. Thermal density fluctuations in amorphous polymers as revealed by small angle X-ray diffraction. *Kolloid-Zeitschrift und Zeitschrift für Polymere* **1973**, *251*, 876–883.

[18] Rathje, J.; Ruland, W. Density fluctuations in amorphous and semicrystalline polymers. Kristallinität und Fehlordnung: Charakterisierung und technologische Bedeutung: Vorträge der Frühjahrstagung des Fachausschusses Physik der Hochpolymeren im Rahmen der Frühjahrstagung des Arbeitskreises Festkörperphysik bei der Deutschen Physikalischen Gesellschaft in Münster vom 17. bis 22. März 1975. 1976; pp 230–242.

[19] Fetters, L.; Lohse, D.; Richter, D.; Witten, T.; Zirkel, A. Connection between polymer molecular weight, density, chain dimensions, and melt viscoelastic properties. *Macromolecules* **1994**, *27*, 4639–4647.

[20] Mavrikakis, M.; Doren, D.; Barteau, M. Density functional theory calculations for simple oxametallacycles: Trends across the periodic table. *The Journal of Physical Chemistry B* **1998**, *102*, 394–399.

[21] Grabowski, S. J. *Hydrogen bonding: new insights*; Springer, 2006; Vol. 3.

[22] Gilli, G.; Gilli, P. *The nature of the hydrogen bond: outline of a comprehensive hydrogen bond theory*; Oxford university press, 2009; Vol. 23.

[23] Ippolito, J. A.; Alexander, R. S.; Christianson, D. W. Hydrogen bond stereochemistry in protein structure and function. *Journal of molecular biology* **1990**, *215*, 457–471.

[24] Corradini, P.; Auriemma, F.; De Rosa, C. Crystals and crystallinity in polymeric materials. *Accounts of chemical research* **2006**, *39*, 314–323.

[25] Moszner, N.; Salz, U. New developments of polymeric dental composites. *Progress in polymer science* **2001**, *26*, 535–576.

[26] Srivastava, R.; Liu, J.; He, C.; Sun, Y. BisGMA analogues as monomers and diluents for dental restorative composite materials. *Materials Science and Engineering: C* **2018**, *88*, 25–31.

[27] Hu, Y.; Shang, Q.; Wang, C.; Feng, G.; Liu, C.; Xu, F.; Zhou, Y. Renewable epoxidized cardanol-based acrylate as a reactive diluent for UV-curable resins. *Polymers for Advanced Technologies* **2018**, *29*, 1852–1860.

[28] Sanda, F.; Endo, T. Radical ring-opening polymerization. *Journal of Polymer Science Part A: Polymer Chemistry* **2001**, *39*, 265–276.

[29] Dainton, F.; Devlin, T.; Small, P. The thermodynamics of polymerization of cyclic compounds by ring opening. *Transactions of the Faraday Society* **1955**, *51*, 1710–1720.

[30] Bailey, W. J.; SUN, R. L.; KATSUKI, H.; ENDO, T.; IWAMA, H.; TSUSHIMA, R.; SAIGOU, K.; BITRITTO, M. M. *Ring-opening polymerization with expansion in volume*; ACS Publications, 1977.

[31] Agarwal, S. Chemistry, chances and limitations of the radical ring-opening polymerization of cyclic ketene acetals for the synthesis of degradable polyesters. *Polymer Chemistry* **2010**, *1*, 953–964.

[32] Agarwal, S.; Ren, L.; Kissel, T.; Bege, N. Synthetic Route and Characterization of Main Chain Ester-Containing Hydrolytically Degradable Poly (N,

N-dimethylaminoethyl methacrylate)-Based Polycations. *Macromolecular Chemistry and Physics* **2010**, *211*, 905–915.

[33] Seema, A.; Liqun, R. Polycaprolactone-based novel degradable ionomers by radical ring-opening polymerization of 2-methylene-1, 3-dioxepane. *Macromolecules* **2009**, *42*, 1574–1579.

[34] Ferguson, L. N. Ring strain and reactivity of alicycles. *Journal of Chemical Education* **1970**, *47*, 46.

[35] Dubois, P.; Coulembier, O.; Raquez, J.-M. *Handbook of ring-opening polymerization*; John Wiley & Sons, 2009.

[36] Kubisa, P. Cationic polymerization of heterocyclics. *Plastics Engineering-New York* **1996**, *35*, 437–553.

[37] Handbook, P.; Brandrup, J.; Immergut, E. John Wiley & Sons. *New York* **1975**, *27*.

[38] Brunelle, D. J. Ring-Opening Polymerization. Mechanisms, Catalysis, Structure, Utility. *Hanser Publishers, 1993,* **1993**, 361.

[39] Hashimoto, K. Ring-opening polymerization of lactams. Living anionic polymerization and its applications. *Progress in polymer science* **2000**, *25*, 1411–1462.

[40] Sanda, F.; Takata, T.; Endo, T. Radical ring-opening polymerization of. alpha.-cyclopropylstyrenes. Polymerization behavior and mechanistic aspects of polymerization by the molecular orbital method. *Macromolecules* **1993**, *26*, 5748–5754.

[41] Moszner, N.; Zeuner, F.; Völkel, T.; Rheinberger, V. Synthesis and polymerization of vinylcyclopropanes. *Macromolecular Chemistry and Physics* **1999**, *200*, 2173–2187.

[42] Folini, J.; Murad, W.; Mehner, F.; Meier, W.; Gaitzsch, J. Updating radical ring-opening polymerisation of cyclic ketene acetals from synthesis to degradation. *European Polymer Journal* **2020**, *134*, 109851.

[43] Hill, M. R.; Kubo, T.; Goodrich, S. L.; Figg, C. A.; Sumerlin, B. S. Alternating radical ring-opening polymerization of cyclic ketene acetals: access to tunable and functional polyester copolymers. *Macromolecules* **2018**, *51*, 5079–5084.

[44] Takahashi, T. Polymerization of vinylcyclopropanes. II. *Journal of Polymer Science Part A-1: Polymer Chemistry* **1968**, *6*, 403–414.

[45] Nuyken, O.; Pask, S. D. Ring-opening polymerization—an introductory review. *Polymers* **2013**, *5*, 361–403.

[46] Ata, S.; Mal, D.; Singha, N. K. Copper catalyzed ring opening copolymerization of a vinyl cyclopropane and methyl methacrylate. *RSC advances* **2013**, *3*, 14486–14494.

[47] Takahashi, T. Polymerization of vinylcyclopropanes. IV. Radical copolymerization of 1, 1-dichloro-2-vinylcyclopropane with maleic anhydride. *Journal of Polymer Science Part A-1: Polymer Chemistry* **1970**, *8*, 617–627.

[48] Takahashi, T. Polymerization of vinylcyclopropanes. V. Radical copolymerization of 1, 1-dichloro-2-vinylcyclopropane with monosubstituted ethylenes. *Journal of Polymer Science Part A-1: Polymer Chemistry* **1970**, *8*, 739–749.

[49] Pesenti, T.; Zhu, C.; Gonzalez-Martinez, N.; Tomás, R. M.; Gibson, M. I.; Nicolas, J. Degradable Polyampholytes from Radical Ring-Opening Copolymerization Enhance Cellular Cryopreservation. *ACS Macro Letters* **2022**, *11*, 889–894.

[50] Sarker, P.; Ebdon, J. R.; Rimmer, S. Branched Oligovinylcyclopropane by Transfer to Allylic Carbonate Comonomers via Radical Ring-Opening Polymerization. *Macromolecular rapid communications* **2006**, *27*, 2007–2013.

[51] Gao, Y.; Fu, X.-F.; Yu, Z.-X. Transition Metal-Catalyzed Cycloadditions of Cyclopropanes for the Synthesis of Carbocycles: C–C Activation in Cyclopropanes. *CC Bond Activation* **2014**, 195–231.

[52] Neureiter, N. Pyrolysis of 1, 1-Dichloro-2-vinylcyclopropane Synthesis of2-Chlorocyclopentadiene. *The Journal of Organic Chemistry* **1959**, *24*, 2044–2046.

[53] Demjanow, N.; Dojarenko, M. Über Vinylcyclopropan, einige Derivate des Methyl-cyclopropyl-carbinols und die Isomerisation des Cyclopropan-Ringes. *Berichte der deutschen chemischen Gesellschaft (A and B Series)* **1922**, *55*, 2718–2727.

[54] Zhang, J.; Yang, X.; Yan, J.; Wang, Y.; Dang, W.; Chen, X.; Yan, Y.; He, H. Preparation method of 1-chloro-1-chloroacetyl cyclopropane. 2020; CN110963877A.

[55] Maré, G. R. D.; Deslauriers, H.; Collin, G. J. Isomerization of unsaturated radicals. VI. Isomerization of 3-cyclopenlenyl and pentamethylene radicals. *Research on chemical intermediates* **1990**, *14*, 133–159.

[56] Mizobuchi, Y.; Miller, L. L. RF plasma promoted di-. pi.-methane rearrangement of 3-phenylpropene. *The Journal of Organic Chemistry* **1985**, *50*, 318–321.

[57] Dass, C.; Peake, D. A.; Gross, M. L. Structures of gas phase C5H8 radical cations: A collisional ionization study. *Organic mass spectrometry* **1986**, *21*, 741–746.

[58] Charette, A. B.; Beauchemin, A. Simmons-Smith Cyclopropanation Reaction. *Organic Reactions* **2004**, *58*, 1–415.

[59] Yamaguchi, M.; Matsunaga, S.; Shibasaki, M.; Michelet, B.; Bour, C.; Gandon, V. Encyclopedia of reagents for organic synthesis. 2001.

[60] Rassadin, V. A.; Sokolov, V. V.; Khlebnikov, A. F.; Ulin, N. V.; Kozhushkov, S. I.; de Meijere, A. Convenient Synthesis of Ethenylcyclopropane and Some 2-Cyclopropylcyclopropane Derivatives. *Synthesis* **2012**, *44*, 372–376.

[61] Overberger, C.; Borchert, A. Ionic Polymerization. XVI. Reactions of 1-Cyclopropylethanol-Vinylcyclopropane1-3. *Journal of the American Chemical Society* **1960**, *82*, 4896–4899.

[62] Tsunoda, T.; Hudlicky, T. Practical Synthesis of Vinylcyclopropane. *Synlett* **1990**, *1990*, 322–322.

[63] Hubbs, J. C.; Barnette, T. S.; Boaz, N. W. Poly (3-cyclopropyl-3-hydroxypropionate) and processes for its preparation and derivatives thereof. 2003; US Patent 6,610,878.

[64] Desai, S. P.; Ye, J.; Zheng, J.; Ferrandon, M. S.; Webber, T. E.; Platero-Prats, A. E.; Duan, J.; Garcia-Holley, P.; Camaioni, D. M.; Chapman, K. W., et al. Well-defined rhodium–gallium catalytic sites in a metal–organic framework: promoter-controlled selectivity in alkyne semihydrogenation to E-alkenes. *Journal of the American Chemical Society* **2018**, *140*, 15309–15318.

[65] Bailey, W. F.; Tao, Y. Efficient Preparation of Vinylcyclopropane by SN' Cyclization of the Organolithium Derived from (E)-5-Iodo-1-methoxy-2-pentene. *Tetrahedron letters* **1997**, *38*, 6157–6158.

[66] Hioe, J.; Zipse, H. Radical stability and its role in synthesis and catalysis. *Organic & biomolecular chemistry* **2010**, *8*, 3609–3617.

[67] Wright, J. S.; Shadnia, H.; Chepelev, L. L. Stability of carbon-centered radicals: Effect of functional groups on the energetics of addition of molecular oxygen. *Journal of computational chemistry* **2009**, *30*, 1016–1026.

[68] Raskildina, G.; Borisova, Y. G.; Yakovenko, E.; Spirikhin, L.; Zlotskii, S. Condensation of CH-acids with cis-1, 4-dichlorobut-2-ene. *Russian Journal of General Chemistry* **2017**, *87*, 151–153.

[69] Aminova, E.; Kazakova, A.; Proskurnina, M.; Zlotskiy, S. Synthesis of cyclic acetals containing gem-dichlorocyclopropane fragment. *Izvestiya Vysshikh Uchebnykh Zavedenii. Seriya Khimiya i Khimicheskaya Tekhnologiya* **2013**, *56*.

[70] Huwyler, R.; Al-Dulayymi, A.; Neuenschwander, M. Synthesis of Functionalized Bi (cyclopropylidenes). *Helvetica Chimica Acta* **1999**, *83*, 2336.

[71] Seitz, E. P. Ring expansion reactions of alkoxides and their application toward synthesis of large ring hormone models. **1977**,

[72] Novikov, M.; Volchkov, N.; Lipkind, M.; Nefedov, O. CuCl-Catalyzed ring-opening isomerization of gem-chlorofluorocyclopropanes with the formation of chlorofluoroalkenes and chlorofluoroalkadienes. *Russian Chemical Bulletin* **2013**, *62*, 71–82.

[73] Cho, I.; Ahn, K.-D. Polymerizations of substituted cyclopropanes. I. Radical polymerization of 1, 1-disubstituted 2-vinylcyclopropanes. *Journal of Polymer Science: Polymer Chemistry Edition* **1979**, *17*, 3169–3182.

[74] Tomilov, Y. V.; Bordakov, V.; Dolgii, I.; Nefedov, O. Reaction of diazoalkanes with unsaturated compounds. 2. Cyclopropanation of olefins with diazomethane catalyzed by palladium compounds. *Chemischer Informationsdienst* **1984**, *15*, no–no.

[75] Rudashevskaya, T. Y.; Nesmeyanova, O. Synthesis of cyclopropane hydrocarbons on the basis of addition of Grignard reagents to the double bond of cyclopropenes. *Bulletin of the Academy of Sciences of the USSR, Division of chemical science* **1983**, *32*, 1647–1650.

[76] Tang, Y.; Huang, Y.-Z.; Dai, L.-X.; Chi, Z.-F.; Shi, L.-P. Cyclopropanation Reactions of Allylic Ylides with α, β-Unsaturated Esters and Amides: Tuning of Stereoselectivity and the Dramatic Effect of Lithium Salts. *The Journal of Organic Chemistry* **1996**, *61*, 5762–5769.

[77] Montesinos-Magraner, M.; Costantini, M.; Ramírez-Contreras, R.; Muratore, M. E.; Johansson, M. J.; Mendoza, A. General Cyclopropane Assembly by Enantioselective Transfer of a Redox-Active Carbene to Aliphatic Olefins. *Angewandte Chemie International Edition* **2019**, *58*, 5930–5935.

[78] Vogel, E. Kleine kohlenstoff-ringe. *Angewandte Chemie* **1960**, *72*, 4–26.

[79] Overberger, C.; Borchert, A. Novel thermal rearrangements accompanying acetate pyrolysis in small ring systems. *Journal of the American Chemical Society* **1960**, *82*, 1007–1008.

[80] Baldwin, J. E. Thermal rearrangements of vinylcyclopropanes to cyclopentenes. *Chemical reviews* **2003**, *103*, 1197–1212.

[81] Danheiser, R. C. Martinez-Davila, JM.. Morin. *J. Org. Chem* **1980**, *45*, 1341.

[82] Danheiser, R. L.; Bronson, J. J.; Okano, K. Carbanion-accelerated vinylcyclopropane rearrangement. Application in a general, stereocontrolled annulation approach to cyclopentene derivatives. *Journal of the American Chemical Society* **1985**, *107*, 4579–4581.

[83] Murray, C. K.; Yang, D. C.; Wulff, W. D. Cyclopropanation with acyloxy chromium carbene complexes. A synthesis of (.+-.)-prostaglandin E2 methyl ester. *Journal of the American Chemical Society* **1990**, *112*, 5660–5662.

[84] Zuo, G.; Louie, J. Highly active nickel catalysts for the isomerization of unactivated vinyl cyclopropanes to cyclopentenes. *Angewandte Chemie* **2004**, *116*, 2327–2329.

[85] Lingam, K. A. P.; Shanmugam, P.; Selvakumar, K. Stereoselective synthesis of geometrically strained, oxindole-appended vinyl cyclopropanes and highly substituted cyclopentenes via sulfur ylide cyclopropanation and vinyl cyclopropane rearrangement. *Synlett* **2012**, *2012*, 278–284.

[86] Khoury, P. R.; Goddard, J. D.; Tam, W. Ring strain energies: substituted rings, norbornanes, norbornenes and norbornadienes. *Tetrahedron* **2004**, *60*, 8103–8112.

[87] Schneider, T. F.; Kaschel, J.; Werz, D. B. A new golden age for donor–acceptor cyclopropanes. *Angewandte Chemie International Edition* **2014**, *53*, 5504–5523.

[88] Tomilov, Y. V.; Menchikov, L. G.; Novikov, R. A.; Ivanova, O. A.; Trushkov, I. V. Methods for the synthesis of donor-acceptor cyclopropanes. *Russian Chemical Reviews* **2018**, *87*, 201.

[89] Kim, H.; Kim, S.; Kim, J.; Son, J.-Y.; Baek, Y.; Um, K.; Lee, P. H. One-pot synthesis of indolizines via sequential rhodium-catalyzed [2+ 1]-cyclopropanation, palladium-catalyzed ring expansion, and oxidation reactions from pyridotriazoles and 1, 3-dienes. *Organic letters* **2017**, *19*, 5677–5680.

[90] Gai, S.; Lucas, N. T.; Hawkins, B. C. Benzannulated 6, 5-Spiroketals from Donor–Acceptor Cyclopropanes. *Organic letters* **2019**, *21*, 2872–2875.

[91] Taber, D. F.; Guo, P.; Guo, N. Intramolecular [1+ 4+ 1] cycloaddition: establishment of the method. *Journal of the American Chemical Society* **2010**, *132*, 11179–11182.

[92] Jiao, L.; Ye, S.; Yu, Z.-X. Rh (I)-catalyzed intramolecular [3+ 2] cycloaddition of trans-vinylcyclopropane-enes. *Journal of the American Chemical Society* **2008**, *130*, 7178–7179.

[93] Yu, Z.-X.; Wender, P. A.; Houk, K. On the mechanism of [Rh (CO) 2Cl] 2-catalyzed intermolecular (5+ 2) reactions between vinylcyclopropanes and alkynes. *Journal of the American Chemical Society* **2004**, *126*, 9154–9155.

[94] Liu, P.; Sirois, L. E.; Cheong, P. H.-Y.; Yu, Z.-X.; Hartung, I. V.; Rieck, H.; Wender, P. A.; Houk, K. Electronic and steric control of regioselectivities in Rh (I)-catalyzed (5+ 2) cycloadditions: experiment and theory. *Journal of the American Chemical Society* **2010**, *132*, 10127–10135.

[95] Hong, X.; Liu, P.; Houk, K. Mechanism and origins of ligand-controlled selectivities in [Ni (NHC)]-catalyzed intramolecular (5+ 2) cycloadditions and homo-ene reactions: a theoretical study. *Journal of the American Chemical Society* **2013**, *135*, 1456–1462.

[96] Fürstner, A.; Majima, K.; Martin, R.; Krause, H.; Kattnig, E.; Goddard, R.; Lehmann, C. W. A cheap metal for a "Noble" task: preparative and mechanistic

aspects of cycloisomerization and cycloaddition reactions catalyzed by low-valent iron complexes. *Journal of the American Chemical Society* **2008**, *130*, 1992–2004.

[97] Taber, D. F.; Sheth, R. B. A three-step route to a tricyclic steroid precursor. *The Journal of organic chemistry* **2008**, *73*, 8030–8032.

[98] Mustard, T. J.; Wender, P. A.; Cheong, P. H.-Y. Catalytic efficiency is a function of how rhodium (I)(5+ 2) catalysts accommodate a conserved substrate transition state geometry: induced fit model for explaining transition metal catalysis. *ACS catalysis* **2015**, *5*, 1758–1763.

[99] Jiao, L.; Lin, M.; Zhuo, L.-G.; Yu, Z.-X. Rh (I)-catalyzed [(3+ 2)+ 1] cycloaddition of 1-yne/ene-vinylcyclopropanes and CO: Homologous Pauson- Khand reaction and total synthesis of (±)-α-agarofuran. *Organic Letters* **2010**, *12*, 2528–2531.

[100] Goldberg, A. F.; Stoltz, B. M. A palladium-catalyzed vinylcyclopropane (3+ 2) cycloaddition approach to the Melodinus alkaloids. *Organic letters* **2011**, *13*, 4474–4476.

[101] Wang, J.; Blaszczyk, S. A.; Li, X.; Tang, W. Transition metal-catalyzed selective carbon–carbon bond cleavage of vinylcyclopropanes in cycloaddition reactions. *Chemical reviews* **2020**, *121*, 110–139.

[102] Sanda, F.; Takata, T.; Endo, T. Radical ring-opening polymerization of .alpha.-cyclopropylstyrenes. Polymerization behavior and mechanistic aspects of polymerization by the molecular orbital method. *Macromolecules* **1993**, *26*, 5748–5754.

[103] Sanda, F.; Takata, T.; Endo, T. Radical ring-opening polymerization of novel vinylcyclopropanes designed as low shrinkage monomers. Structure of the polymer, mechanism of the polymerization, and volume change on the polymerization. *Macromolecules* **1995**, *28*, 1346–1355.

[104] Zeuner, F.; Moszner, N.; Rheinberger, V. Polymerization of cyclic monomers, 2. Synthesis and radical polymerization of vinylcyclopropanes. *Macromolecular Chemistry and Physics* **1996**, *197*, 2745–2752.

[105] Moszner, N.; Zeuner, F.; Rheinberger, V. Polymerization of cyclic monomers, 4. Synthesis and radical polymerization of bi-and trifunctional 2-vinylcyclopropanes. *Macromolecular rapid communications* **1997**, *18*, 775–780.

[106] Takahashi, T.; Yamashita, I. 1, 5-Polymerization of vinylcyclopropane. *Journal of Polymer Science Part B: Polymer Letters* **1965**, *3*, 251–255.

[107] Overberger, C.; Halek, G. Synthesis and reactions of polyvinylcyclopropane. *Journal of Polymer Science Part A-1: Polymer Chemistry* **1970**, *8*, 359–376.

[108] Takahashi, T. Polymerization of vinylcyclopropanes. III. Cationic polymerization of stereoisomers of 1-halo-2-vinylcyclopropanes. *Journal of Polymer Science Part A-1: Polymer Chemistry* **1968**, *6*, 3327–3331.

[109] Cho, I. New ring-opening polymerizations for copolymers having controlled microstructures. *Progress in polymer science* **2000**, *25*, 1043–1087.

[110] Sanda, F.; Takata, T.; Endo, T. Radical polymerization behavior of 1, 1-disubstituted 2-vinylcyclopropanes. *Macromolecules* **1993**, *26*, 1818–1824.

[111] Sugiyama, J.-i.; Kayamori, N.; Shimada, S.-i. Free radical ring-opening polymerization of 1, 1-bis [(1-adamantyloxy) carbonyl]-2-vinylcyclopropane. *Macromolecules* **1996**, *29*, 1943–1950.

[112] Zhou, L.; Huang, R.; Lu, S.; Liu, B.; Gao, M.; Xu, B. Direct Nitration of Vinylcycles with Copper Nitrate. *Organic Letters* **2023**, *25*, 1415–1419.

[113] Moszner, N.; Catel, Y.; Fischer, U. K.; Tauscher, S. Dental materials based on monofunctional vinylcyclopropane derivatives. 2019; US Patent 10,512,593.

[114] Catel, Y.; Fässler, P.; Fischer, U.; Gorsche, C.; Schörpf, S.; Tauscher, S.; Liska, R.; Moszner, N. Evaluation of difunctional vinylcyclopropanes as reactive diluents for the development of low-shrinkage composites. *Macromolecular Materials and Engineering* **2017**, *302*, 1700021.

[115] Tauscher, S.; Catel, Y.; Fässler, P.; Fischer, U.; Moszner, N. Development of low-shrinkage composites based on novel crosslinking vinylcyclopropanes. *Journal of Applied Polymer Science* **2017**, *134*, 45577.

[116] Contreras, P. P.; Kuttner, C.; Fery, A.; Stahlschmidt, U.; Jérôme, V.; Freitag, R.; Agarwal, S. Renaissance for low shrinking resins: all-in-one solution by bi-functional vinylcyclopropane-amides. *Chemical Communications* **2015**, *51*, 11899–11902.

[117] Catel, Y.; Fässler, P.; Fischer, U.; Gorsche, C.; Liska, R.; Schörpf, S.; Tauscher, S.; Moszner, N. Synthesis and polymerization of vinylcyclopropanes bearing urethane groups for the development of low-shrinkage composites. *European Polymer Journal* **2018**, *98*, 439–447.

[118] Schörpf, S. Urethane based vinylcyclopropanes for low shrinkage dental composites. Ph.D. thesis, Wien, 2017.

[119] Takahashi, N.; Sudo, A.; Endo, T. Isolation of Epimers in the Synthesis of Vinylcyclopropane Bearing Two Alanine Moieties and Their Radical Ring-Opening Polymerization. *Macromolecules* **2017**, *50*, 5679–5686.

[120] Sangermano, M.; Razza, N.; Crivello, J. V. Cationic UV-curing: Technology and applications. *Macromolecular Materials and Engineering* **2014**, *299*, 775–793.

[121] Decker, C. Kinetic study and new applications of UV radiation curing. *Macromolecular Rapid Communications* **2002**, *23*, 1067–1093.

[122] Catel, Y.; Fischer, U.; Fässler, P.; Moszner, N. Bis (4-methoxybenzoyl) diethylgermane: A highly efficient photoinitiator for the polymerization of vinylcyclopropanes. *Macromolecular Chemistry and Physics* **2016**, *217*, 2686–2691.

[123] Temel, G.; Enginol, B.; Aydin, M.; Balta, D. K.; Arsu, N. Photopolymerization and photophysical properties of amine linked benzophenone photoinitiator for free radical polymerization. *Journal of Photochemistry and Photobiology A: Chemistry* **2011**, *219*, 26–31.

[124] Georg, H. C.; Coutinho, K.; Canuto, S. Solvent effects on the UV-visible absorption spectrum of benzophenone in water: A combined Monte Carlo quantum mechanics study including solute polarization. *The Journal of chemical physics* **2007**, *126*, 034507.

[125] Ledwith, A. Initiation of free-radical polymerization by photoinduced electron-transfer processes. *Polymer* **1973**, *14*, 521.

[126] Monroe, B. M.; Weiner, S. A. Mechanisms of photochemical reactions in solution. LVIII. Photoreduction of camphorquinone. *Journal of the American Chemical Society* **1969**, *91*, 450–456.

[127] Al-Doaiss, A. A.; Klemm, E.; Stadermann, D.; Moszner, N. Synthesis and Photoinitiated Cationic Polymerization of Substituted 2-Cyclopropyl-4-methylene-1, 3-dioxolanes. *Macromolecular Chemistry and Physics* **2001**, *202*, 270–275.

[128] Crivello, J. Cationic polymerization—iodonium and sulfonium salt photoinitiators. *Initiators—poly-reactions—optical activity* **2005**, 1–48.

[129] Sipani, V.; Scranton, A. B. Dark-cure studies of cationic photopolymerizations of epoxides: Characterization of the active center lifetime and kinetic rate constants. *Journal of Polymer Science Part A: Polymer Chemistry* **2003**, *41*, 2064–2072.

[130] Contreras, P. P.; Tyagi, P.; Agarwal, S. Low volume shrinkage of polymers by photopolymerization of 1, 1-bis (ethoxycarbonyl)-2-vinylcyclopropanes. *Polymer Chemistry* **2015**, *6*, 2297–2304.

[131] Crivello, J. V. Hybrid free radical/cationic frontal photopolymerizations. *Journal of Polymer Science Part A: Polymer Chemistry* **2007**, *45*, 4331–4340.

[132] Oxman, J. D.; Jacobs, D. W.; Trom, M. C.; Sipani, V.; Ficek, B.; Scranton, A. B. Evaluation of initiator systems for controlled and sequentially curable free-radical/cationic hybrid photopolymerizations. *Journal of Polymer Science Part A: Polymer Chemistry* **2005**, *43*, 1747–1756.

[133] Zhang, D.-Y.; Han, D.; Li, Y.; Chen, D.-F. Expanding monomer scope and enabling post-modification in photocontrolled radical ring-opening polymerization of vinylcyclopropanes by an iodine transfer strategy. *Polymer Chemistry* **2022**, *13*, 5691–5699.

[134] Luinstra, G. A.; Theato, P., et al. Post-polymerization modification of reactive polymers derived from vinylcyclopropane: 1. synthesis and thermo-responsive behaviour. *Polymer Chemistry* **2013**, *4*, 2724–2730.

[135] Ntoukam, D. H. S.; Jiworrawathanakul, S.; Hoven, V. P.; Luinstra, G. A.; Theato, P. 1, 1-Disubstituted-2-vinylcyclopropanes for the synthesis of amphiphilic polymers. *European Polymer Journal* **2015**, *66*, 319–327.

[136] Ntoukam, D. H. S.; Mutlu, H.; Theato, P. Post-polymerization modification of Poly (vinylcyclopropanes): A potential route to periodic copolymers. *European Polymer Journal* **2020**, *122*, 109319.

[137] Mahy, W.; Plucinski, P. K.; Frost, C. G. Copper-catalyzed one-pot synthesis of N-aryl oxazolidinones from amino alcohol carbamates. *Organic letters* **2014**, *16*, 5020–5023.

[138] Laxminarayan, B.; Seema, B. Cycloalkylmethylamines. 2014; US20140066500A1.

[139] Leonov, O.; Shcherbakov, V.; Devichensky, V.; Kryukova, L. Y.; Vorontsov, E.; Kuznetsov, S.; Kryukov, L. Synthesis of 1-Hydroxyalkyl-3-Substituted Ureas and Thioureas, Substrates for Alcohol Dehydrogenase. *Russian Journal of Bioorganic Chemistry* **2001**, *27*, 191–194.

[140] Guan, L.-P.; Zhao, D.-H.; Xiu, J.-H.; Sui, X.; Piao, H.-R.; Quan, Z.-S. Synthesis and Anticonvulsant Activity of N-(2-Hydroxy-ethyl) amide Derivatives. *Archiv der Pharmazie: An International Journal Pharmaceutical and Medicinal Chemistry* **2009**, *342*, 34–40.

[141] Yang, B.; Lang, H.; Liu, Z.; Wang, S.; Men, Z.; Sun, C. Three stages of hydrogen bonding network in DMF-water binary solution. *Journal of Molecular Liquids* **2021**, *324*, 114996.

[142] Solarova, H.; Cisarova, I.; Stepnicka, P. Synthesis, Structural Characterization, and Catalytic Evaluation of Phosphinoferrocene Ligands Bearing Extended Urea-Amide Substituents. *Organometallics* **2014**, *33*, 4131–4147.

[143] Fang, T.; Sun, C.; Xu, Y.; Yuan, J.; Wang, Y.; Xing, J. Synthesis, insecticidal activities and molecular docking studies on cis-nitenpyram analogues with a flexible amido segment anchored on tetrahydropyrimidine ring. *Chemical Research in Chinese Universities* **2014**, *30*, 931–936.

[144] Attenni, B.; Donghi, M.; Gardelli, C.; Meppen, M.; Narjes, F.; Pacini, B. Antiviral Agents. 2010; US Patent App. 12/601,002.

[145] Kenichi, I.; Yusuke, U.; Akaike, T. Aligning agent for liquid crystal, liquid crystal orientation film and liquid crystal cell and their manufacture method. 2016; CN106479519A.

[146] Mattia, J.; Painter, P. A Comparison of Hydrogen Bonding and Order in a Polyurethane and Poly (urethane- urea) and Their Blends with Poly (ethylene glycol). *Macromolecules* **2007**, *40*, 1546–1554.

[147] Lommerse, J. P.; Price, S. L.; Taylor, R. Hydrogen bonding of carbonyl, ether, and ester oxygen atoms with alkanol hydroxyl groups. *Journal of computational chemistry* **1997**, *18*, 757–774.

[148] Jansen, J. F.; Dias, A. A.; Dorschu, M.; Coussens, B. Fast monomers: factors affecting the inherent reactivity of acrylate monomers in photoinitiated acrylate polymerization. *Macromolecules* **2003**, *36*, 3861–3873.

[149] Oyama, T. Method for producing urea compound. 2006; JP2006143645.

[150] Kuroda, S.; Kawabe, K.; Ushiki, Y.; Ohta, H.; Uneuchi, F.; Shibata, T.; Tabuse, H.; Munetomo, E.; Chonan, S. Preparation of aryl-substituted phenyltetrahydroisoquinoline compounds with NHE3 inhibitory effect, and pharmaceuticals containing them. 2016; WO2016013657 A1.

[151] Austin, J. A relation between the molecular weights and melting points of organic compounds. *Journal of the American Chemical Society* **1930**, *52*, 1049–1053.

[152] Aminoroaya, A.; Esmaeely Neisiany, R.; Nouri Khorasani, S.; Panahi, P.; Das, O.; Ramakrishna, S. A review of dental composites: Methods of characterizations. *ACS Biomaterials Science & Engineering* **2020**, *6*, 3713–3744.

[153] Cramer, N.; Stansbury, J.; Bowman, C. Recent advances and developments in composite dental restorative materials. *Journal of dental research* **2011**, *90*, 402–416.

[154] Chiba, H.; Kitazume, K.; Yamada, S.; ENDO, T. Synthesis and radical ring-opening polymerization of adamantane-containing bifunctional vinylcyclopropane undergoing volume expansion on polymerization. *Journal of Polymer Science Part A: Polymer Chemistry* **2016**, *54*, 39–43.

[155] Horvath, J.; Horvath, J. A brief history of 3D printing. *Mastering 3D Printing* **2014**, 3–10.

[156] Low, Z.-X.; Chua, Y. T.; Ray, B. M.; Mattia, D.; Metcalfe, I. S.; Patterson, D. A. Perspective on 3D printing of separation membranes and comparison to related unconventional fabrication techniques. *Journal of membrane science* **2017**, *523*, 596–613.

[157] Yan, Q.; Dong, H.; Su, J.; Han, J.; Song, B.; Wei, Q.; Shi, Y. A review of 3D printing technology for medical applications. *Engineering* **2018**, *4*, 729–742.

[158] Müller, A.; Karevska, S.; Wienken, R.; Kilger, C. How will 3D printing make your company the strongest link in the value chain: EY's Global 3D printing Report 2016. *Ernst & Young GmbH* **2016**,

[159] Stevenson, A. C. Ammonolysis. *Industrial & Engineering Chemistry* **1948**, *40*, 1584–1589.

[160] Reznichenko, A. L.; Hultzsch, K. C. Hydroamination of alkenes. *Organic Reactions* **2004**, *88*, 1–554.

[161] Jang, W. D.; Kim, G. B.; Lee, S. Y. An interactive metabolic map of bio-based chemicals. *Trends in Biotechnology* **2022**,

[162] Mora, A.-S.; Tayouo, R.; Boutevin, B.; David, G.; Caillol, S. Vanillin-derived amines for bio-based thermosets. *Green Chemistry* **2018**, *20*, 4075–4084.

[163] Froidevaux, V.; Negrell, C.; Caillol, S.; Pascault, J.-P.; Boutevin, B. Biobased amines: from synthesis to polymers; present and future. *Chemical Reviews* **2016**, *116*, 14181–14224.

[164] Pelckmans, M.; Renders, T.; Van de Vyver, S.; Sels, B. Bio-based amines through sustainable heterogeneous catalysis. *Green Chemistry* **2017**, *19*, 5303–5331.

[165] Mori, Y.; Noda, S.; Shirai, T.; Kondo, A. Direct 1, 3-butadiene biosynthesis in Escherichia coli via a tailored ferulic acid decarboxylase mutant. *Nature Communications* **2021**, *12*, 2195.

[166] Song, D. Kinetic model development for dehydration of 2, 3-butanediol to 1, 3-butadiene and methyl ethyl ketone over an amorphous calcium phosphate catalyst. *Industrial & Engineering Chemistry Research* **2016**, *55*, 11664–11671.

[167] Song, C. W.; Kim, J. W.; Cho, I. J.; Lee, S. Y. Metabolic engineering of Escherichia coli for the production of 3-hydroxypropionic acid and malonic acid through β-alanine route. *ACS synthetic biology* **2016**, *5*, 1256–1263.

[168] Choi, S.; Song, C. W.; Shin, J. H.; Lee, S. Y. Biorefineries for the production of top building block chemicals and their derivatives. *Metabolic engineering* **2015**, *28*, 223–239.

[169] Bentley, L. Occurrence of malonic acid in plants. *Nature* **1952**, *170*, 847–848.

[170] Kim, Y.-S. Malonate metabolism: biochemistry, molecular biology, physiology, and industrial application. *BMB Reports* **2002**, *35*, 443–451.

[171] Sabuzi, F.; Pomarico, G.; Floris, B.; Valentini, F.; Galloni, P.; Conte, V. Sustainable bromination of organic compounds: A critical review. *Coordination Chemistry Reviews* **2019**, *385*, 100–136.

[172] Zhang, R.; Yao, W.-Z.; Qian, L.; Sang, W.; Yuan, Y.; Du, M.-C.; Cheng, H.; Chen, C.; Qin, X. A practical and sustainable protocol for direct amidation of unactivated esters under transition-metal-free and solvent-free conditions. *Green Chemistry* **2021**, *23*, 3972–3982.

[173] Santos, A. S.; Silva, A. M.; Marques, M. M. B. Sustainable amidation reactions–recent advances. *European Journal of Organic Chemistry* **2020**, *2020*, 2501–2516.

5 Acknowledgment

First and far-most, I'd like to deeply thank Prof. Seema Agarwal for the opportunity to work on this nice and interesting topic, which let me get a good insight into the, beforehand unknown field, of polymer science. Her supervision and openness to had a big contribution to the success of this work. I'd also like to thank her for all the discussions and the freedom to develop and pursue my own ideas and the support during the time of lack of success.
I would also like to thank Prof. Andreas Greiner for his mentoring and support.

I acknowledge the University of Bayreuth Graduate School and the BayNAT for financial support and training courses. Thereby, I thank Prof. Peter Strohriegel and Prof. Matthias Breuning for being my BayNAT mentors.

My huge thanks go to my research students Chen Yuchen, Marius Luik and Denise Schweser as well to student trainee Carina Riecken on their effort and contribution to different aspects of my research, even though some of it was finally not included in this thesis. I wish you all the best for your future careers.
Furthermore, I'd like to give my huge thanks to Sanwardhini Pantawane and Prof. Stephan Gekle from the faculty of therotical physics for the great collaboration which led to a deeper understanding of the topic, acknowledged with two joint publications.

I would like to thank my colleagues and friends from the MC II chair for all the tips, help, discussions and suggestions. Among them I want to thank Dr. Julia Kronawitt, Dr. Ann-Kathrin Müller, Dr. Mina Heidari, Dr. Mahsa Mafi, Dr. Martin Pretscher, Dr. Simon Neumann, Dr. Felix Bretzschneider, Sophie Fritzsche, Dr. Marcel Höferth, Lisa Leitner, Dr. Nikola Majstorovic, Tasmai Paul, Benedict Petran, Marius Schmidt, Tobias Schmitt, Hendrik Volz, and all other current and former members of MC II respectively.
Special thanks to my labmates Dr. Elmar Sehl, Sagar Joshi and Dr. Chenzhang Xu, who accompanied me almost during my whole PhD and made every day even more

enjoyable. Special thanks also to Dr. Elmar Sehl, Dr. Adrian Wambach and Dr .Maximilian Rist for the countless scientific discussions.

I want to thank our academic councilor Dr. Holger Schmalz for important scientific discussions and input, and our technicians Rika Schneider and Annette Krökel for their contributions concerning installation and repair of analytical instruments and measurements. Thank you for your help and for the nice work together.
I thank also the technical support from Dr. Matthias Völkl and Dr. Reneé Siegel, all from other departments of the University of Bayreuth, as well as from Dr. Stefan Schmölzer (Netzsch Company).

Many thanks to Gaby Rösner-Oliver, Christina Lindörfer and Ramona Lechner our chair secretaries for their support and guidance during my thesis and for being the good soul of this chair.

I'd like to deeply thank my family, my mother Andrea and my father Jürgen for always being there for me, teaching me and helping me to achieve all my dreams.

I'd like to thank my colleagues, Dr. Anja Langstoer, Dr. Patrik Fuchs and Dr. Hubert Theil for the support and council during the time of writing down my work.

And last but not least I'd like to thank my friends Anh, Basti, Hanna, Ilona, Jonas, Katha, Lisa, Maren, Maxi, Tania, and Viktor for their friendship for so many years, their support during my studies but also my PhD, even though we're now spread over whole world. I feel blessed to call you all my friends and happy for all the great times in the past but also what will await us in the future.

6 Eidesstattliche Erklärung

(§ 9 Satz 2 Nr. 3 PromO BayNAT)
Hiermit versichere ich eidesstattlich, dass ich die Arbeit selbstständig verfasst und keine anderen als die von mir angegebenen Quellen und Hilfsmittel benutzt habe (vgl. Art. 97 Abs. 1 Satz 8 BayHIG).

(§ 9 Satz 2 Nr. 3 PromO BayNAT)
Hiermit erkläre ich, dass ich die Dissertation nicht bereits zur Erlangung eines akademischen Grades eingereicht habe und dass ich nicht bereits diese oder eine gleichartige Doktorprüfung endgültig nicht bestanden habe.

(§ 9 Satz 2 Nr. 4 PromO BayNAT)
Hiermit erkläre ich, dass ich Hilfe von gewerblichen Promotionsberatern bzw. -vermittlern oder ähnlichen Dienstleistern weder bisher in Anspruch genommen habe noch künftig in Anspruch nehmen werde.

(§ 9 Satz 2 Nr. 7 PromO BayNAT)
Hiermit erkläre ich mein Einverständnis, dass die elektronische Fassung meiner Dissertation unter Wahrung meiner Urheberrechte und des Datenschutzes einer gesonderten Überprüfung unterzogen werden kann.

(§ 9 Satz 2 Nr. 8 PromO BayNAT)
Hiermit erkläre ich mein Einverständnis, dass bei Verdacht wissenschaftlichen Fehlverhaltens Ermittlungen durch universitätsinterne Organe der wissenschaftlichen Selbstkontrolle stattfinden können.

Ort, Datum

Sören Schumacher